



**UNIVERSIDADE DE LISBOA  
INSTITUTO SUPERIOR TÉCNICO**

**Understanding Flow Dynamics in Drinking Water  
Storage Tanks**

**Alexandre da Silva Pinheiro**

**Supervisor: Doctor Dília Isabel Cameira Covas**

**Co-Supervisors: Doctor Maria do Céu de Sousa Teixeira de Almeida**

**Doctor Laura Sofia Pereira Pinto Monteiro**

**Thesis approved in public session to obtain the PhD Degree in  
Civil Engineering**

**Jury final classification: Pass with Distinction**

**2022**



**UNIVERSIDADE DE LISBOA**  
**INSTITUTO SUPERIOR TÉCNICO**

**Understanding Flow Dynamics in Drinking Water  
Storage Tanks**

**Alexandre da Silva Pinheiro**

**Supervisor: Doctor Dídia Isabel Cameira Covas**

**Co-Supervisors: Doctor Maria do Céu de Sousa Teixeira de Almeida**  
**Doctor Laura Sofia Pereira Pinto Monteiro**

**Thesis approved in public session to obtain the PhD Degree in  
Civil Engineering**

**Jury final classification: Pass with Distinction**

**Jury**

**Chairperson:** Doctor António Heleno Cardoso, Instituto Superior Técnico, Universidade de Lisboa

**Members of the Committee:**

Doctor Pedro L. Iglesias Rey, Universitat Politècnica de València, Espanha  
Doctor António Alberto do Nascimento Pinheiro, Instituto Superior Técnico, Universidade de Lisboa  
Doctor Dídia Isabel Cameira Covas, Instituto Superior Técnico, Universidade de Lisboa  
Doctor António Jorge Silva Guerreiro Monteiro, Instituto Superior Técnico, Universidade de Lisboa  
Doctor Rui Manuel Carvalho Viegas, Laboratório Nacional de Engenharia Civil  
Doctor Ana Margarida da Costa Ricardo, Instituto Superior Técnico, Universidade de Lisboa

**Funding Institution**

**Fundação para a Ciência e Tecnologia**

**2022**



## **Abstract**

Drinking water storage tanks are essential components of water supply systems to store water, to level off pressure in networks and to meet emergency storage. They are also frequent sources of deterioration of drinking water quality and safety owing to inadequate tank design and operation. Mostly, existing tanks design, dimensions and operation do not account for water mixing and renewal.

The current research aims to understand the flow dynamics inside water storage tanks to find practicable solutions to improve their design and rehabilitation and to support their operation to improve water mixing and to reduce water ageing. The methodology is based on experimental tests carried out in laboratory small-scale tanks, specially assembled for this research, as well as, on field tests in full-scale tanks. Three sets of experimental tests are carried out: traditional tracer tests to determine water residence time distribution and to calculate mixing, renewal, and plug-flow indexes; dye tracer tests to provide a qualitative understanding of the preferential flow paths; and Particle Image Velocimetry (PIV) tests to determine velocity fields and to assess turbulence intensity. Structural and operational characteristics, such as, tank cross-section shape, inlet and outlet pipe location, inlet pipe diameter, number of inlet pipes, inclusion and size of baffles, jet inflow, fluctuation of stored water, are experimentally analysed for assessing their effectiveness in water mixing and renewal. Full-scale tests operated under fill-and-draw mode provide complementary information on water mixing and residence time.

The main outcomes of this research are: (i) the characterization of water storage tanks in Portugal, focusing on the main physical characteristics and operational conditions; (ii) the study of mixing conditions and water ageing in small-scale circular and rectangular cross-section storage tanks; (iii) the analysis of the effect of the fill-and-draw cycles on the water mixing and renewal in small-scale and full-scale conditions; (iv) the proposal of a new empirical formula for estimating the turnover time in circular cross-section tanks operated at a constant level; (v) the study of flow dynamics conditions using PIV technology; (vi) the analyses of several improvement measures of water mixing and renewal and the identification of the most adequate

measures for different circular cross-section tanks; and (vii) the proposal of two water mixing models and the prediction of chlorine decay inside water tanks.

**Keywords:** water storage tanks; drinking water safety; residence time distribution; particle image velocimetry; chlorine decay.

## Resumo

Os reservatórios de água são componentes essenciais dos sistemas de abastecimento, quer para equilibrar a pressão na rede de distribuição, quer para garantir reservas de emergência. No entanto, os reservatórios são também frequentemente locais de deterioração da qualidade da água pondo em risco a segurança da água para consumo humano, devido a inadequado dimensionamento e exploração. Tipicamente os reservatórios não são projetados e operados de forma a garantir a mistura e a renovação da água no seu interior, sendo comum o estabelecimento de zonas de estagnação com elevados tempos de residência.

A presente investigação contribui para o avanço do estado do conhecimento em reservatórios de abastecimento de água e para a conceção de soluções viáveis que permitam melhorar o projeto de novos reservatórios e apoiar a reabilitação e operação dos já existentes, de modo a melhorar as condições de mistura e reduzir o tempo de permanência da água no interior destas estruturas de armazenamento. A metodologia baseia-se em ensaios experimentais realizados em modelos de reservatórios construídos à escala reduzida, especialmente concebidos para a presente investigação, bem como em ensaios de campo realizados em reservatórios reais. O trabalho inclui três tipos de testes experimentais: testes tradicionais de traçador para determinar a distribuição do tempo de residência da água e calcular os índices de mistura, renovação e caminhos preferenciais; testes de traçador com corante para permitir uma melhor visualização dos caminhos preferenciais e a identificação de zonas de estagnação; e testes recorrendo à técnica da velocimetria por imagem de partículas (PIV) para medição dos campos de velocidade e para a avaliação da intensidade da turbulência dentro dos reservatórios. As características estruturais e operacionais, como a forma da secção transversal do reservatório, a localização das condutas de entrada e de saída, o diâmetro e número de condutas de entrada, a inclusão e dimensão de septos, o fluxo de quantidade de movimento do jato de entrada, a flutuação do nível da água armazenada, são aspetos analisados experimentalmente para avaliar sua eficácia nas condições de mistura e de renovação da água. Os testes realizados em reservatórios à escala real e operados em modo de enchimento e esvaziamento fornecem informações complementares sobre as condições de mistura da água e de renovação.

Os principais resultados desta investigação são: (i) a caracterização dos reservatórios de abastecimento de água em Portugal, com especial foco nas principais suas características físicas e condições operacionais; (ii) o estudo das condições de mistura e tempo de permanência da

água em modelos de reservatórios à escala reduzida com secção circular e retangular; (iii) a análise do efeito dos ciclos de enchimento e esvaziamento nas condições de mistura e renovação da água em laboratório e à escala real; (iv) a proposta de uma nova fórmula empírica para estimar o tempo de renovação da água em reservatórios de secção circular operados com nível da água constante; (v) o estudo da dinâmica do escoamento dentro dos reservatórios utilizando a tecnologia PIV; (vi) a análise de diversas medidas de melhoria das condições de mistura e renovação da água e a identificação das medidas mais adequadas para diferentes reservatórios de secção circular; e (vii) a proposta de dois modelos de mistura da água e de previsão do decaimento do cloro em reservatórios de abastecimento de água.

**Palavras-chave:** reservatórios de abastecimento de água; segurança da água; distribuição dos tempos de residência; velocimetria por imagem de partículas; decaimento do cloro.



## **Acknowledgements**

I would like to thank my supervisor at IST, Professor Doctor Dídía Covas, for the continuous guidance, sharing of scientific knowledge and spirit of investigation with unparalleled humility. Your constant support and positive thinking were a driving force to finish this PhD.

I would like to thank my supervisor at LNEC, Doctor Maria do Céu Almeida, for the support, scientific rigour and all the contributions throughout the development of the research that led to this document. To my co-supervisor, Doctor Laura Monteiro, special thank for her continuous support and encouragement through these years.

This work was possible thanks to the Doctoral Programme H2Doc - Environmental Hydraulics and Hydrology, funded by the Fundação para a Ciência e Tecnologia, under the PhD Grant PD/BD/135214/2017. This research was also supported by the FCT funded project IMiST – Improving Mixing in Storage Tanks for safer water supply (PTDC/ECI-EGC/32102/2017).

I am grateful to the Laboratório Nacional de Engenharia Civil (LNEC) and to the Civil Engineering Research and Innovation for Sustainability (CERIS) research unit at the Instituto Superior Técnico, for the resources made available and for the support of all the people directly or indirectly involved in my research work.

A special thanks to Ana Margarida Ricardo for the availability and support in the laboratory and in the data processing. In addition to the support in the development of the scientific work, I thank you for your friendship.

I gratefully acknowledge the Portuguese water utilities that provide infrastructure data, as well as that allowed the inspection of water storage tanks. A special thanks to Águas do Algarve and SIMAS Oeiras e Amadora.

I want to express my gratitude to my colleagues for the constant support and the strong friendships developed – Joana Baltazar, Joana Carneiro, Joana Costa, João Nuno, João Paulo Ferreira, Luis Angel, Marta Cabral, Sofia Vaz and Soraia Teixeira.

Thanks to all the friends, the new friends whom I had the honour to meet over these 4 years, the colleagues that became friends, and everyone that supported me during the good and bad

times. For the fun between study periods, for all the experiences and good times we had together, your support was unparalleled.

Lastly, I want to thank my family for all the unconditional support, for never doubting my abilities and making me believe I can achieve anything I put my mind to. The biggest thanks go to my family, and still, it is not enough.

Thank you all.

*Para a minha família e amigos*



## Table of contents

Abstract .....	i
Resumo.....	iii
Acknowledgements .....	v
Table of contents .....	ix
List of figures .....	xiii
List of tables.....	xviii
List of acronyms.....	xix
List of symbols.....	xx
List of publications.....	xxii
1 Introduction.....	1
1.1 Research context.....	2
1.2 Thesis objectives .....	2
1.3 Methodological approaches.....	3
1.4 Thesis organization.....	4
2 Literature review .....	7
2.1 Introduction .....	8
2.2 Water storage tanks .....	8
2.3 Problems in drinking water storage tanks .....	10
2.4 Water quality regulations .....	11
2.5 Influencing factors of mixing and water retention time .....	11
2.5.1 General remarks .....	11
2.5.2 Thermal stratification .....	12
2.5.3 Tank design and operation.....	13
2.6 Modelling mixing in water storage tanks .....	20
2.6.1 Tank mixing models.....	20
2.6.2 Computational Fluid Dynamics models .....	21
2.6.3 Small-scale models.....	25
2.6.4 Field testing models.....	25
2.7 Residence time distribution .....	26
2.8 Modelling disinfectant decay .....	28
2.9 Gaps of knowledge.....	29
3 Water storage tanks characterization in Portugal .....	31

3.1	Introduction .....	32
3.2	Tank general characterization .....	32
3.3	Operational and structural characterization.....	33
3.4	Buried, semi-buried and supported tanks .....	34
3.5	Elevated tanks.....	36
3.6	Mixing time .....	37
3.7	Renewal volume fraction.....	38
3.8	Relevant results for the research.....	39
4	Water mixing and renewal in circular cross-section storage tanks .....	41
4.1	Introduction .....	42
4.2	Materials and methods.....	42
4.2.1	Experimental facility .....	42
4.2.2	Experimental procedure.....	44
4.2.3	Data treatment and analysis.....	45
4.3	Results .....	50
4.3.1	Qualitative assessment of preferential flow paths .....	50
4.3.2	Mixing at steady-state conditions .....	51
4.3.3	Mixing at variable water levels .....	58
4.4	Discussion .....	64
4.5	Conclusions .....	65
5	Rectangular storage tanks: small-scale and field tests tanks .....	67
5.1	Introduction .....	68
5.2	Materials and methods.....	68
5.2.1	Small-scale tests .....	68
5.2.2	Full-scale tests .....	70
5.2.3	Data treatment and analysis.....	71
5.3	Results and discussion.....	72
5.3.1	Laboratory results.....	72
5.3.2	Field results .....	80
5.4	Discussion of water mixing and renewal conditions .....	83
5.4.1	Morrill index.....	84
5.4.2	Dispersion index.....	85
5.4.3	Short-circuiting index.....	86
5.5	Conclusions .....	87
6	Flow dynamics in storage tanks using particle image velocimetry .....	89
6.1	Introduction .....	90

6.2	Particle image velocimetry .....	90
6.3	Data collection and analysis .....	91
6.3.1	Experimental setup description .....	91
6.3.2	Data processing .....	95
6.4	Experimental results .....	98
6.4.1	PIV velocity maps .....	98
6.4.2	Turbulence analysis .....	102
6.5	Discussion .....	104
6.6	Conclusions .....	105
7	Water mixing improvement measures .....	107
7.1	Introduction .....	108
7.2	Review of existing measures .....	108
7.3	Materials and methods .....	113
7.3.1	Experimental tests .....	113
7.3.2	Tested structural measures .....	113
7.3.3	Tested operational measures .....	116
7.4	Analysis of the results .....	117
7.4.1	Effects of the inlet pipe diameter .....	117
7.4.2	Effect of inlet pipe nozzles .....	119
7.4.3	Effect of baffle structures .....	122
7.4.4	Effects of operational measures .....	124
7.5	Discussion .....	126
7.6	Conclusions .....	130
8	Modelling chlorine decay in water storage tanks .....	133
8.1	Introduction .....	134
8.2	Residence time distribution models .....	134
8.3	Experimental data .....	135
8.4	Model development .....	136
8.5	Chlorine decay in storage tanks .....	140
8.6	Conclusions .....	141
9	Conclusions and further research .....	143
9.1	Research overview .....	144
9.2	Main scientific findings .....	144
9.3	Recommendations for future work .....	147
	References .....	151
	Appendix A .....	159

Appendix B ..... 163  
Appendix C ..... 167



## List of figures

Figure 2.1 – Types of water storage tanks: a) buried tank; b) partially-buried tank; c) ground-level tanks; d) elevated tank; e) standpipe tank.....	9
Figure 2.2 – Water stratification created from buoyant jets: a) positive; b) negative buoyant jets (Adapted from Grayman et al., 2004).....	13
Figure 2.3 – Inlet pipes in water storage tanks.....	14
Figure 2.4 – Baffles in rectangular cross-section water storage tanks: a) simplified plant; b) interior view. ....	16
Figure 2.5 – Flow patterns: a) original tank; b-f) different baffle configurations (Zhang et al. 2012)..	17
Figure 2.6 – RTD measurements for a pulse injection (top) and step injection (bottom) (adapted from Fogler, 2016).....	27
Figure 3.1 – The relative frequency of tanks per year of construction.....	33
Figure 3.2 – Examples of tank typologies: a) frustoconical water tower; b) circular cross-section half-buried tank; c) rectangular cross-section tank.....	33
Figure 3.3 – Distribution of tanks with baffles for different types of cross-sections: a) circular; b) rectangular; c) quadrangular.....	34
Figure 3.4 – Circular, rectangular and quadrangular tank type distribution in terms of: a) volume; b) $H/D$ ratio. ....	35
Figure 3.5 – Variation of the $H/D$ ratio with the volume for buried, semi-buried and supported tanks. ....	36
Figure 3.6 – Mixing time distribution for tanks with circular cross-section. ....	37
Figure 3.7 – Relationship between mixing time, inlet flow and volume in circular cross-section tanks. ....	38
Figure 3.8 – Relationship between mixing time, inlet flow and volume in circular cross-section tanks. ....	39
Figure 4.1 – Schematic of the experimental facility.....	43
Figure 4.2 – Tested small-scale tanks: a) Configuration A; b) Configuration B; c) Configuration C. .	43
Figure 4.3 – Daily water consumption profile.....	45
Figure 4.4 – Data treatment sequence: a) electric conductivity measured at the outflow pipe; b) cumulative distribution curves for all tests and median curve; c) obtained residence time distribution curve. Presented results are for Configuration A at Mode 1 and $Q3$ .....	50
Figure 4.5 – Rhodamine dispersion within the three configurations at 1, 5, and 10 min after injection (constant water level, flow rate $Q3$ ): a) Configuration A; b) Configuration B; c) Configuration C.....	51

Figure 4.6 – Normalized cumulative distribution and residence time distribution for the three storage tank configurations at steady-state conditions and flow rate: (a and b) $Q1$ ; (c and d) $Q2$ ; (e and f) $Q3$ ; (g and h) $Q4$ . Plots (a,c,e, and g) show the normalized cumulative distribution, and plots (b,d,f, and h) show the residence time distribution. ....	53
Figure 4.7 – Normalized residence time distribution for each configuration and different flow rates tested: (a and b) Configuration A; (c and d) Configuration B; (e and f) Configuration C. Plots (a, c, and e) show the small-scale tanks plan view, and plots (b, d, and f) show the normalized residence time distribution. ....	55
Figure 4.8 – Fit of Rossman and Grayman formula for turnover time for each configuration. ....	58
Figure 4.9 – Results of tracer tests at variable water level: (a, c, and e) water level and outflow rate variations; (b, d, and f) cumulative distribution curves. ....	60
Figure 4.10 – Cumulative distribution curves obtain for each configuration operated at variable water level: a) Configuration A; Configuration B; c) Configuration C. ....	61
Figure 4.11 – Turnover time for each configuration and volume variation. ....	63
Figure 5.1 – Small-scale tanks tested: a) Configuration A; b) Configuration B. ....	69
Figure 5.2 – Tracer tests facility pictures: a) deionized and tracer solution tanks; b) small-scale tank; c) conductivity probe, hydropneumatic tank and peristaltic pumps. ....	69
Figure 5.3 – Full-scale tank: a) layout and location of monitoring equipment; b) inlet pipe upper view. ....	71
Figure 5.4 – Rhodamine dispersion within the two configurations at 0.5, 2, 10 and 15 min after injection (constant water level, flow rate $9.1 \text{ Lh}^{-1}$ ): a) Configuration A; b) Configuration B. ....	73
Figure 5.5 – $F(t)$ and $E(t)$ for the two configurations at steady-state conditions and for three flow rates: (a,c) Configuration A; (b,d) Configuration B. ....	74
Figure 5.6 – Inflow and outflow rate variations at mode 2: a) 20%; b) 50%; and c) 80%. ....	77
Figure 5.7 – Variable water level results: a) cumulative distribution curves; b) water level variations. ....	78
Figure 5.8 – $F(t)$ curves obtain for each configuration and the respective volume variation: a) Configuration A; b) Configuration B. ....	79
Figure 5.9 – Collected field data: a) flow rate; b) water level. ....	81
Figure 5.10 – Full-scale results: a) electric conductivity measured at the three sampling sites; b) cumulative distributions curves for the intermediate and outlet sampling sites. ....	82
Figure 5.11 – Normalized turnover time as a function of volume variation and according to two approaches: a) the ratio between the average volume and average flow rate; b) the ratio between the maximum volume and the flow rate. ....	83
Figure 5.12 – Schematics for circular and rectangular small-scale tanks. ....	84

Figure 5.13 – Assessment of mixing and renewal conditions in storage tanks for: a) steady-state; b) fill-and-draw conditions. Normalized turnover time vs Morrill index. ....	85
Figure 5.14 – Assessment of mixing and renewal conditions in storage tanks for steady-state. Normalized turnover time vs dispersion index. ....	86
Figure 5.15 – Assessment of short-circuiting and renewal conditions in storage tanks for: a) steady-state; b) fill-and-draw conditions. Normalized turnover time vs Normalized short-circuiting time. ....	86
Figure 6.1 – Tested small-scale tanks: a) Configuration A; b) Configuration B; c) Configuration C. .	92
Figure 6.2 – Schematic representation of the experimental flow circuit. ....	92
Figure 6.3 – Schematic representation of the PIV instrumentation. ....	93
Figure 6.4 – Schematic view of the experimental facility: a) lateral view; b) axonometric view. ....	94
Figure 6.5 – Seeding particles illuminated and recorded from a section of the water storage tank: a) acquired (original) image; b) treated image. ....	97
Figure 6.6 – Time-averaged velocity maps at each configuration and horizontal plane. The colormap represents the velocity magnitude and the arrow is the scale of the vector plot. ....	99
Figure 6.7 – Flow streamlines for each tank configuration and horizontal plane. The grey colour represents low velocity regions. ....	101
Figure 6.8 – Spatial distribution of time-averaged velocity (absolute velocity) values for: a) Configuration A; b) Configuration B; c) Configuration C. ....	102
Figure 6.9 –Longitudinal ( $u'u'$ ), lateral ( $v'v'$ ) and Reynold's shear stresses distributions for the three configurations. ....	103
Figure 6.10 –Longitudinal ( $u'u'$ ) and lateral ( $v'v'$ ) stresses and time-averaged shear stress ( $u'v'$ ) for each horizontal plane in Configuration A. ....	104
Figure 7.1 – Inlet pipe with several flexible nozzles. ....	110
Figure 7.2 – Examples of water storage tanks with baffles in Portugal with: a) circular cross-section; b) rectangular cross-section. ....	112
Figure 7.3 – Baffle influence: a) baffle with 75% of tank diameter (Configuration C); b) baffle with 50% of tank diameter. ....	114
Figure 7.4 – Several views of the tested inlet pipe nozzles for tank: a) Configuration A; b) Configuration B. ....	115
Figure 7.5 – Inlet diffusers locations: a) Configuration A; b) Configuration B. ....	116
Figure 7.6 – Tracer tests with inlet diffusers: a) Configuration A; b) Configuration B. ....	116
Figure 7.7 – Hydraulic indexes for the three configurations in steady-state conditions with different inlet pipe diameter: (a-c) Configuration A; (d-f) Configuration B; (g-i) Configuration C. The dashed line corresponds to the Morrill index value for a CSTR. ....	118

Figure 7.8 – Rhodamine dispersion within Configuration A at 1, 5, and 10 min after injection (constant water level, flow rate Q3): a) A1; b) A2; c) A3.....	120
Figure 7.9 – Rhodamine dispersion within Configuration B at 1, 5, and 10 min after injection (constant water level, flow rate Q3): a) B1; b) B2; c) B3.....	121
Figure 7.10 – Morrill index, dispersion index and normalized short-circuiting time vs normalized turnover time: (a-c) Configuration A and inlet nozzles solutions; (d-f) Configuration B and inlet nozzles solutions. The dashed line corresponds to the Morrill index value for a CSTR. ....	122
Figure 7.11 – Rhodamine dispersion within the two baffled configurations at 1, 5, and 10 min after injection (constant water level, flow rate Q3): a) baffle 50% tank diameter; b) baffle 75% tank diameter (Configuration C).....	123
Figure 7.12 – Morrill index, dispersion index and normalized short-circuiting time vs normalized turnover time: (a-c) baffle with 50% of the tank diameter; (d-f) baffle with 75% of the tank diameter (Configuration C). The dashed line corresponds to the Morrill index value for a CSTR and the dotted line corresponds to a PFR.....	124
Figure 7.13 – Hydraulic indexes for the three configurations in variable water level operation: a) Morrill index vs normalized turnover time; b) normalized short-circuiting time vs normalized turnover time. The dashed line corresponds to the Morrill index value for a CSTR, and the dotted line corresponds to a PFR. ....	126
Figure 8.1 – Cumulative distribution functions, $F(t)$ for the two storage tank configurations: a) Configuration A; b) Configuration C.....	135
Figure 8.2 – Cumulative distribution functions, $F(t)$ . Comparison between the ideal CSTR model and experimental data for Configurations A and C. ....	137
Figure 8.3 – Schematic representation of the Model 1 developed for Configuration A. ....	138
Figure 8.4 – Cumulative distribution functions, $F(t)$ . Comparison between experimental data and results of Model 1 developed for Configuration A. ....	138
Figure 8.5 – Schematic representation of the Model 2 developed for Configuration C.....	139
Figure 8.6 – Cumulative distribution functions, $F(t)$ . Comparison between experimental data and results calculated by Model 2 developed for Configuration C.....	139
Figure 8.7 – Predicting the behaviour of the model obtained for the total segregation method: a) Configuration A; b) Configuration C.....	141

## Appendix A

Figure A.1 – Experimental facility designed for developing tracer tests in small-scale storage tanks and determining the water residence time distribution. Tracer tests facility pictures: a) deionized water system; b) tracer solution and deionized auxiliary tanks; c) tracer solution and deionized feeder tanks (above) and small-scale tank (below); d) control valves; e) small-scale tank; (f,g) conductivity probe, hydropneumatic vessel and peristaltic pumps; h) conductivity datalogger; i) controlling software. .... 160

Figure A.2 – Experimental facility designed for developing the particle image velocimetry technique in small-scale storage tanks: a) facility overview; b) part of the outflow system that includes the hydropneumatic vessel, pumps and auxiliary tank; c) digital camera; d) circular acrylic sheet with quadrangular grid; e) laser and camera calibration process; f) velocity fields. 161

## Appendix B

Figure B.1 – The time-averaged turbulent intensity maps ( $\mathbf{u}'\mathbf{u}'$ ) and ( $\mathbf{v}'\mathbf{v}'$ ) and the time-averaged shear stress map ( $\mathbf{u}'\mathbf{v}'$ ) for Configurations B. .... 164

Figure B.2 – The time-averaged turbulent intensity maps ( $\mathbf{u}'\mathbf{u}'$ ) and ( $\mathbf{v}'\mathbf{v}'$ ) and the time-averaged shear stress map ( $\mathbf{u}'\mathbf{v}'$ ) for Configurations C. .... 165

## List of tables

Table 3.1 – Characterization of circular, rectangular and quadrangular tank types. ....	35
Table 3.2 – Characterization of elevated tanks typology. ....	36
Table 4.1 – Operational conditions tested. ....	45
Table 4.2 – Hydraulic indexes for the three configurations in steady-state conditions. ....	57
Table 4.3 – Estimated dimensionless constant ( $k$ ) for each configuration. ....	58
Table 4.4 – Hydraulic indexes for the three configurations at variable water level. ....	62
Table 5.1 – Operational conditions tested in laboratory. ....	70
Table 5.2 – Hydraulic indexes for the two configurations at steady-state conditions. ....	75
Table 5.3 – Comparison of hydraulic indexes between circular cross-section (Pineiro et al. 2021) and rectangular cross-section tank (Configuration A) for steady-state conditions. ....	76
Table 5.4 – Hydraulic indexes for the three configurations at variable water level. ....	79
Table 5.5 – Comparison of hydraulic indexes between circular cross-section (Pineiro et al. 2021) and rectangular cross-section tank (Configuration A) for variable water level conditions. ....	80
Table 5.6 – Hydraulic indexes for intermediate and outlet sampling sites. ....	82
Table 7.1 – Structural improvement measures tested for Configuration A and the corresponding hydraulic indexes. ....	127
Table 7.2 – Structural improvement measures tested for Configuration B and the corresponding hydraulic indexes. ....	128
Table 7.3 – Structural improvement measures tested for Configuration C and the corresponding hydraulic indexes. ....	129
Table 7.4 – Operational measures tested and the corresponding hydraulic indexes. ....	130
Table 8.1 – Calibrated parameters for Model 1 developed for Configuration A. ....	138
Table 8.2 – Calibrated parameters for the Model 2 developed for Configuration C. ....	139

## List of acronyms

The following acronyms are used in this document.

<b>Acronym</b>	<b>Description</b>
CCD	Charge-coupled devise
CFD	Computational Fluid Dynamics
CSTR	Continuous Stirred Tank Reactor
WDS	Water Distribution System
EPANET	Environmental Protection Agency network model
ERSAR	Entidade Reguladora dos Serviços de Água e Resíduos
IA	Interrogation Area
IST	Instituto Superior Técnico
PFR	Plug Flow Reactor
PIV	Particle Image Velocimetry
RTD	Residence Time Distribution
RMSE	Root Mean Square Deviation
USEPA	United States Environmental Protection Agency
WHO	World Health Organization

## List of symbols

The following symbols are used in this document.

### Latin letters

Symbol	Description	Dimension
$C^*$	chlorine concentration	$M L^{-3}$
$C$	tracer concentration	$M L^{-3}$
$C_0$	inflow tracer concentration	$M L^{-3}$
$C_a$	outflow chlorine concentration	$M L^{-3}$
$C_e$	inflow chlorine concentration	$M L^{-3}$
$C_{out}$	inflow chlorine concentration	$M L^{-3}$
$C(t)$	measured tracer concentration	$M L^{-3}$
$D$	tank diameter	L
$d$	inlet pipe diameter	L
$E(t)$	residence time distribution function (RTD)	$T^{-1}$
$E(\theta)$	normalized residence time distribution function or dimensionless RTD	-
$F(t)$	cumulative distribution function	-
$F(\theta)$	normalized cumulative distribution function	-
$H$	water depth	L
$H_{max}$	maximum water depth	L
$H_{min}$	minimum water depth	L
$k$	dimensionless constant	-
$M$	inlet jet momentum flux	$L^4 T^{-2}$
$Mo$	Morrill index	-
$p$	percentage of tank area	%
$Q$	volumetric flow rate	$L^3 T^{-1}$
$Q_{out}$	outlet volumetric flow rate	$L^3 T^{-1}$
$Re$	Reynolds number	-
$R^2$	coefficient of determination	-
$t$	Time; time elapsed since the beginning of the experiment	T
$t'$	mean residence time	T
$t_m$	mixing time	T
$t_T$	turnover time	T
$t_{10}$	time needed for 10% of the injected tracer particles leave the tank	T
$t_{90}$	time needed for 90% of the injected tracer particles leave the tank	T
$t_{95}$	time needed for 95% of the injected tracer particles leave the tank	T
$u$	velocity; longitudinal velocity component – x direction	$L T^{-1}$



$u_i$	$i^{\text{th}}$ component of the velocity field	$L T^{-1}$
$\bar{u}$	time-averaged longitudinal velocity	$L T^{-1}$
$u'$	turbulent fluctuations of longitudinal velocity	$L T^{-1}$
$ \bar{u} $	absolute velocity	$L T^{-1}$
$\overline{u'u'}$	longitudinal turbulent normal stresses	$L^2 T^{-2}$
$\overline{u'v'}$	turbulent shear stresses	$L^2 T^{-2}$
$v$	lateral velocity component – y direction	$L T^{-1}$
$v_i$	$i^{\text{th}}$ component of the velocity field	$L T^{-1}$
$\bar{v}$	time-averaged lateral velocity	$L T^{-1}$
$v'$	turbulent fluctuations of lateral velocity	$L T^{-1}$
$V$	mean value of velocity;	$L T^{-1}$
	volume	$L^3$
$\overline{v'v'}$	lateral turbulent normal shear stresses	$L^2 T^{-2}$
$xyz$	cartesian coordinate system	

#### Greek letters

<b>Symbol</b>	<b>Description</b>	<b>Dimension</b>
$\alpha$	constant; turnover coefficient	-
$\Delta d_x$	particle's mean displacement in the x direction	L
$\Delta d_y$	particle's mean displacement in the y direction	L
$\Delta t$	time interval between two consecutive images	T
$\theta$	mean residence time;	T
	normalized time ( $t/\tau$ )	-
$\theta_{CSTR}$	mean residence time in the CSTR	T
$\theta_{PFR}$	mean residence time in the PFR	T
$\sigma^2$	variance of the RTD function	$T^2$
$\bar{\sigma}$	dispersion index	-
$\tau$	theoretical residence time	T

## List of publications

Several papers have been published and submitted in ISI indexed journals and peer-reviewed international or national conference proceedings during the development of this research work. These papers are listed by author and by chronological order as follows:

### National and international peer-reviewed journals:

- (i) Monteiro, L., **Pinheiro, A.**, Carneiro, J., Covas, D. (2021). Caracterização dos reservatórios de água para consumo humano em Portugal. *Ingeniería del Agua*, 25 (1), 49–58.
- (ii) **Pinheiro, A.**, Monteiro, L., Carneiro, J., Almeida, M.C., Covas, D. (2021). Water mixing and renewal in circular cross-section storage tanks as influenced by configuration and operational conditions. *Journal of Hydraulic Engineering* 147(12).
- (iii) **Pinheiro, A.**, Monteiro, L., Almeida, M.C., Covas, D. Water mixing in rectangular storage tanks: small-scale versus field tests. *Journal of Hydraulic Research* (*submitted in September 2021*).
- (iv) **Pinheiro, A.**, Ricardo, A., Monteiro, L., Almeida, M.C., Covas, D. Understanding flow dynamics in storage tanks using particle image velocimetry. *Journal of Experiments in Fluids* (*submitted in February 2022*).

### National and international peer-reviewed conferences:

- (i) **Pinheiro, A.**, Monteiro, L., Almeida, M.C., Covas, D. (2018). Hidrodinâmica de reservatórios de água para consumo humano. 18.º ENASB / 18.º SILUBESA, 10-12 October, Porto, Portugal.
- (ii) **Pinheiro, A.**, Monteiro, L., Almeida, M.C., Covas, D. (2019). Modelling flow Dynamics in drinking water storage tanks. 3<sup>rd</sup> Doctoral Congress in Engineering, 27 June, FEUP, Porto, Portugal.
- (iii) Monteiro, L., **Pinheiro, A.**, Carneiro, J., Covas, D. (2019). Caracterização dos reservatórios de água para consumo humano em Portugal. XVI Seminário Ibero-Americano sobre Sistemas de Abastecimento e Drenagem, 15-17 July, IST, Lisboa, Portugal.

- (iv) **Pinheiro, A.**, Carneiro, J., Monteiro, L., Almeida, M.C., Covas, D. (2019). Small-scale models of water storage tanks. 17<sup>th</sup> CCWI – International Computing & Control for the Water Industry Conference, 1-4 September, Exeter, United Kingdom.
- (v) Covas, D., **Pinheiro, A.**, Vaz, S., Monteiro, L., Martins, N., Ricardo, A. (2022). Modelling water mixing and renewal in storage tanks. 2<sup>nd</sup> International Joint Conference in Water Distribution Systems Analysis & Computing and Control in the Water Industry 18-22 July, Valencia, Spain.



# Chapter 1

---

## **Introduction**

## **1.1 Research context**

Drinking water storage tanks are traditionally designed and operated to meet the storage volume requirements of the distribution systems, while providing emergency storage and equalizing pressure, without considering changes in stored water quality. Yet, drinking water quality often deteriorates in storage tanks, because of the long residence times and of poor mixing. Inadequate tank design and operation facilitate microbial regrowth, exacerbate the formation of disinfection by-products (DBP), that are regulated owing to their toxicity and carcinogenicity, and increase the accumulation of deposits. Hence, water utilities often have to deal with unnecessary public health risks, increased difficulties in complying with regulated minute-concentrations of disinfection by-products and inconveniences and costs of storage tank cleaning and disinfection. Deficits in professional awareness of design engineers and water utility operators, together with knowledge gaps about storage tanks flow dynamics, methods, and tools for their study, persist as the main reasons that perpetuate these circumstances. Design and operation of storage tanks can influence mixing and contribute to water ageing.

With this respect, filling the gaps of knowledge that still hinder the development of guidelines to improving water quality in storage tanks with structural and operational characteristics similar to those found in real tanks is of fundamental importance. Therefore, it is important to identify the factors influencing the residence time and the path of the water inside the tanks and to identify the appropriate measures to promote mixing and renewal of water.

This doctoral thesis was developed at the Civil Engineering Research and Innovation for Sustainability (CERIS) at Instituto Superior Técnico (IST) and Urban Water Unit of the Portuguese National Civil Engineering Laboratory (LNEC), within the aim of the R&D project IMiST: Improving mixing in storage tanks for safer water supply.

## **1.2 Thesis objectives**

The present work aims to understand the factors influencing flow dynamics in drinking water storage tanks through an extensive data collection programme under controlled laboratory conditions for several tank configurations and operational conditions. The thesis is mainly experimental and includes innovative technologies for image recording

and velocity field measurements in small-scale tanks with advanced instrumentation, namely particle image velocimetry (PIV).

In this sense, the thesis specific objectives are:

- (i) To contribute to knowledge on governing factors on water mixing and on water ageing inside the storage tanks (e.g., location and number of inlets/outlets pipes, jet inflow(s), outflow effect, fluctuating stored water volume, tank geometry and demand profiles).
- (ii) To develop a database of tanks' typical structural and operational characteristics in Portugal.
- (iii) To develop a method to assess mixing conditions and renewal in full-scale storage tanks.
- (iv) To identify effective single or combined measures (structural or operational) to improve water mixing, suitable for implementation in the design of new storage tanks as well and in the operation and rehabilitation of existing tanks.
- (v) To assess the performance and compare existing tank mixing models (e.g., mixed, plug-flow) for predicting water residence time within the tanks.
- (vi) To propose recommendations for the design, rehabilitation and operation of storage tanks in order to improve water mixing and to reduce water ageing.

### **1.3 Methodological approaches**

The doctoral project is based on experimental tests carried out in laboratory small-scale tanks and on field tests in full-scale tanks.

To support the proposed objectives, the experimental tests were carried out in laboratory facilities, especially designed and built for this research, at the Laboratory of Hydraulics and Environment of Instituto Superior Técnico (IST) in Lisbon.

A large set of tests was carried out in small-scale storage tanks and three sets of experimental tests were carried out using different instrumentation to collect complementary data. First, traditional tracer tests were carried out; these tests consist of injecting a conservative compound (sodium chloride) at a certain location (typically, an inlet section) and the monitoring of this compound concentration evolution in time at selected locations of the system. An experimental procedure was developed for running

these tests. Collected data were used to determine the water residence time distribution (RTD) and to extract other hydraulic indexes used to assess short-circuiting, mixing and renewal time. Additionally, dye tracer tests were also carried out to provide a general qualitative understanding of the preferential flow paths within the small-scale tanks. Finally, Particle Image Velocimetry (PIV) technology were used to analyse the flow dynamics inside in the small-scale tanks. This technique allows the measurement of velocity fields at different water levels (in horizontal planes defined by the laser sheet) and the assessment of the water flow paths by measuring the displacement of seeding particles in the flow. A completely new experimental and data analysis procedures were developed to apply this technique in storage tanks.

Two tank geometries with circular and rectangular cross-section were tested. Dimensions and configurations of the tanks were determined by downscaling predominant dimensions of existing full-scale tanks in Portugal. The small-scale tanks, made of unreactive materials, allowed to test different structural configurations (i.e., tank shape, the number, location, orientation and diameter of inlet/outlet pipes, internal structures like baffles) and operating conditions (i.e., flow rates, fill-and-draw cycles).

Field research was also carried out, providing the chance to test a methodology for assessing mixing and renewal conditions in full-scale storage tanks, from a water transmission system, based on temperature and conductivity measurements at several water depths and locations inside the tank.

The prediction of bulk disinfectant decay was also studied based on models developed for the tanks with the tested configurations. These models were developed and calibrated with experimental data.

#### **1.4 Thesis organization**

The present thesis is organised into nine chapters and two appendices. The most relevant research carried out in this thesis is presented in Chapters 3 to 8. Some of these chapters are adapted versions of papers that have been submitted or published in peer-reviewed ISI Web of Science indexed journals.

In Chapter 1, the current chapter, the context, and motivation of this research are presented, as well as the main thesis objectives and the research methodology.



Chapter 2 presents the state-of-the-art review of the main areas of relevance to this research in water storage tanks. The main knowledge and achievements on mixing and water ageing found in the literature are explained. The major gaps in related knowledge are identified.

In Chapter 3, the characterization of water storage tanks in Portugal is presented, focusing on the tanks' physical and operational characteristics that influence their performance regarding mixing and water renewal. This chapter contents were presented at the Ibero-american conference, *SEREA 2019 – Seminário Ibero-Americano sobre Sistemas de Abastecimento e Drenagem*, held in Lisbon and was published in *Ingeniería del Agua* in 2021.

Chapters 4 and 5 present the experimental research carried out in circular and rectangular cross-section small-scale tanks, to study the effect of structural and operational characteristics on water mixing and renewal through traditional tracer techniques. Experimental studies carried out at IST on the influence of steady-state and fill-and-draw conditions in water residence time distribution are described. Chapter 5 also presents a case study in a Portuguese water utility, Águas do Algarve S.A., where a field test programme was developed for assessing mixing and renewal conditions in a full-scale tank. Outcomes from chapter 4 were published in the paper *Water mixing and renewal in circular cross-section storage tanks as influenced by configuration and operational conditions*, in the *Journal of Hydraulic Engineering*. Results from chapter 5 were summarised in a research paper, submitted to the *Journal of Hydraulic Research* for publication in 2021, entitled *Water mixing in rectangular storage tanks: small-scale versus field tests*.

Chapter 6 describes the experimental research with the particle image velocimetry (PIV) technique, which focuses on the analysis of the effect of water flow velocity on the formation of low-velocity regions (stagnation zones) and the analysis of turbulent intensities inside small-scale tanks for steady-state conditions. Results were presented in a research paper, to be submitted for publication in *Experiments in Fluids* in February of 2022, entitled *Understanding flow dynamics in storage tanks using particle image velocimetry*.

In Chapter 7, structural changes on the three most common water storage tank configurations of circular cross-section tanks in Portugal were tested for improving water mixing and renewal conditions. Tested conditions are thoroughly described, and the results achieved for different structural and operational measures are discussed. The most adequate improvement measures to avoid problems in water ageing and mixing are identified and discussed for each configuration type.

Chapter 8 presents the application of mixing models used for chemical reactors to describe the behaviour of residence time distribution in two small-scale water storage tanks, using experimental data for parameterization of the model. The simple and combined mixing models were tested by fitting the respective cumulative distribution curve to the experimental data and the quality of fit was assessed by the root-mean-square error. This chapter also describes the models developed to predict bulk chlorine decay as a first-order reaction.

In Chapter 9, the main conclusions of this research work and the recommendations for further developments are presented. A summary of the developed work is presented, and the main achievements and original contributions of this research are outlined.

Additional photographs of the experimental facilities are presented in Appendix A and additional information related to Chapter 6 about the velocity field maps obtained for other tanks configurations is presented in Appendix B. Complementary equations explaining the water mixing models for the circular-cross section small-scale tanks, proposed in Chapter 8, are presented in Appendix C.

# Chapter 2

---

## Literature review

## **2.1 Introduction**

This chapter presents a state-of-the-art review of research on water mixing and water ageing in the storage tanks using experimental and numerical approaches. First, a brief review of the importance of storage tanks characteristics, together with the problems that can arise because of the structural and operational conditions of these facilities, is presented. The effect of thermal stratification, tank design and operation on the water mixing and ageing are described. High water retention times in the storage tanks have important water quality implications, for instance, in storage tanks supplying areas where water demand is low are more prone to poor mixing conditions and higher water retention times. Another situation where retention times are increased is when mixing is poor, with the formation of dead zones where the water remains for substantial time. The same problem can result from dead zones created by temperature differences between the water entering the tank and the water volume retained in the tank. These situations can result from inadequate design and operation practices in storage tanks. Design characteristics as the height to diameter ratio, the inlet pipe size, location, and orientation, together with internal structures, are examples of factors influencing water retention. Daily operation of the tank, such as daily water level and volume variation during the filling and emptying cycles, are also relevant. In a second part of the literature review, methods of predicting mixing are summarized. Mixing in a storage tank and disinfectant residuals can be simulated by using tank mixing models, computation fluid dynamics or small and full-scale models.

This background review is essential to assess the state-of-the-art in this research area and to identify the gaps of knowledge that support the definition of the objectives of this research work.

## **2.2 Water storage tanks**

In water distribution systems, there are several types of tanks, such as water storage tanks, hydro-pneumatic or pressure tanks, backwash tanks, contact chambers, and other types. Drinking water storage tanks, the focus of this work, are essential components of water distribution systems. This asset is designed and operated to store treated water, to blend different water sources, to give contact time for disinfectants, to equalize supply and water demand in the distribution systems, to minimize pressure variations during periods of

high consumption, to maintain pressure in the system and to provide emergency storage for firefighting, power outages and loss of pumping capacity.

The main types of tanks include ground-level tanks, water towers and standpipes (Figure 2.1). A ground-level tank consists of a storage structure fully/partially buried or built below ground (Figure 2.1a-c), typically made of reinforced concrete or a prefabricated material, in which the ratio between width or diameter is typically higher than the height. Water towers or elevated tanks comprise tanks supported by a steel or concrete tower that is not part of the storage volume (Figure 2.1d). Elevated tanks' primary function is to provide adequate and constant pressure to the distribution networks. These tanks have limited water volumes to face emergency demands, such as firefighting; however, they minimize pumping requirements. A standpipe is a high cylindrical tank, typically built above the ground surface, with a height significantly higher than the diameter (Figure 2.1e). These tanks are generally located on high ground or near a groundwater source. Water in the upper portion of the tank is used for peak flow balancing; the remaining volume is for fire and emergency storage. Pressure levels in distribution systems vary with the water level in the tanks.

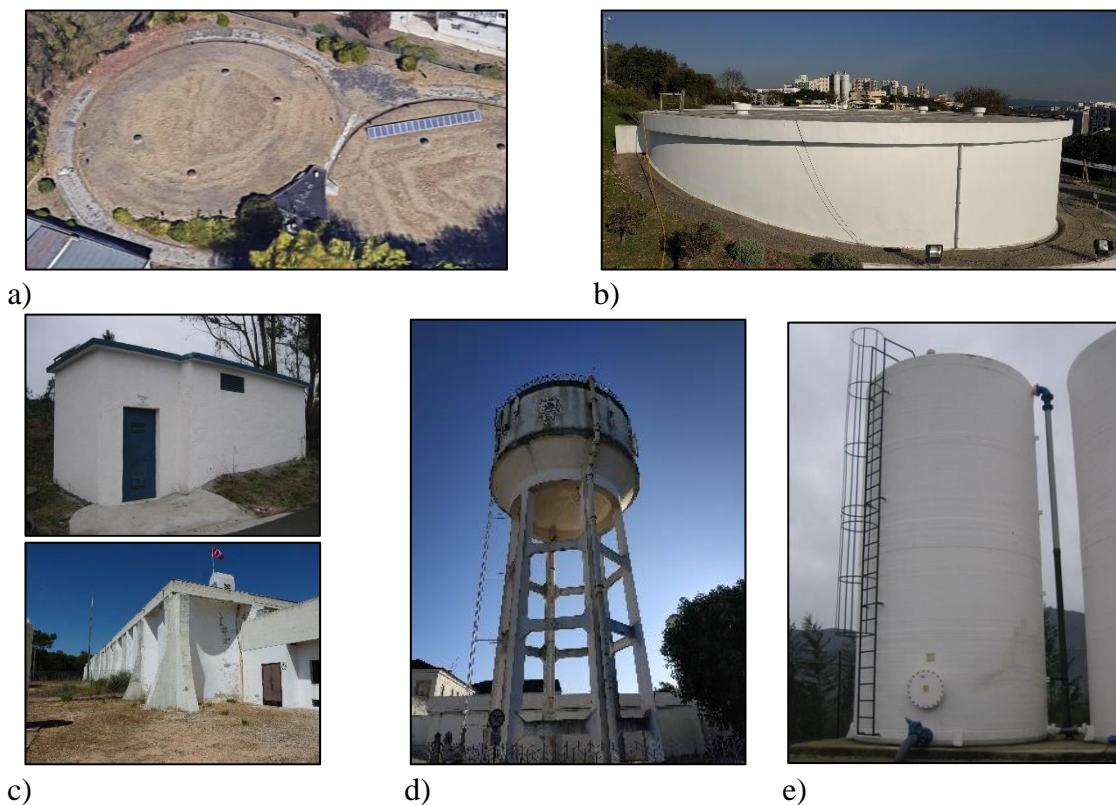


Figure 2.1 – Types of water storage tanks: a) buried tank; b) partially-buried tank; c) ground-level tanks; d) elevated tank; e) standpipe tank.

### 2.3 Problems in drinking water storage tanks

The principal goal of operating a water storage tank is to deliver the required water quantity with adequate pressure and quality to consumers. Excessive water retention time is the most important factor related to water quality deterioration in storage tanks.

The common practice in tank design and operation does not consider any requirements for adequate mixing and renewal of stored water (Grayman et al. 2004). By operating the tanks nearly full, water utilities increase system reliability, but also increase the water residence time in the storage facilities (USEPA 2002). Poor water mixing and stagnation zones with long residence times make storage tanks potential sites for deterioration of water quality, increasing the risk of drinking water contamination (Grayman et al. 2004; Martel et al. 2002). Disinfectant residuals in water usually have acceptable levels at the tank inlet; however, at the tank outlet to the drinking network, residual disinfectant levels can be low, showing large uncertainty (AWWA 2006). The location of the tank in the distribution system can exacerbate this problem. Depending on the mixing conditions promoted by the tank configuration and operation, the water can have or not sufficient levels of disinfectant.

In addition, high water residence time not only causes the depletion of residual disinfectant but results in the increasing formation of disinfection by-products, which are chemical compounds formed by the reaction of a water disinfectant and natural organic matter (Singer 2006). These products are undesirable in drinking water since there are potentially carcinogenic (Richardson et al. 2007). Evidence shows that long-term exposure cause health risks (Simard et al. 2011). The main disinfection by-products of concern are total trihalomethanes and haloacetic acids, formed when chlorine and chloramine are used in disinfection; these two products are frequently the disinfectant of choice used to maintain the water quality in distribution systems. While minimizing disinfection by-products is important, the risks of not disinfecting water far outweigh those created by disinfection by-products (AWWA 2002).

Excessive residence time can also lead to the increase in microbial cells associated with biofilm growth in the inner surface walls of storage tanks (Van Der Merwe et al. 2013) and to the accumulation of sediments (Ho et al. 2016). Water quality in the distribution system can be considerably compromised (Martel et al. 2002). The excessive water

retention time in the tank is enhanced by the water volume for emergencies, which is a portion of the volume that acts as inactive water stored in the tank. If tanks are kept full yet underutilized, the stored water ages and the water quality degrades (AWWA 2002). Tanks can also be over-designed with an excessive capacity to comply with increasing future population and industrial demands or to meet seasonal demand variation; often, these tanks do not guarantee the proper mixing and renewal of the water inside, leading to the formation of stagnant areas with long water residence times (Grayman et al. 2004). Another reason tanks are operated close to full is to be better prepared to respond to emergencies. Thus, the deficient mixing and renewal of water inside the tanks results in frequent supply disruptions for tank cleaning and disinfection, together with additional re-chlorination, resulting in higher operation and maintenance costs (Chambers et al. 2004).

## **2.4 Water quality regulations**

The tank inspection, cleaning and sanitizing process is crucial in the management of water quality since the surface walls and floor of a tank in service is in contact with the treated water. This contact can promote the formation of a biological layer resulting from the presence of non-biodegradable materials, microorganisms and sediment deposition at the bottom of the tank. Tanks must be subjected to regular cleaning actions, at a frequency adequate to the characteristics of the water supply system, typically yearly or biennially. ERSAR (2018) presents a recommendation indicating the most relevant aspects to be considered in the inspection, cleaning and sanitizing processes of tanks. In public water supply systems, it is usual to establish an annual periodicity for cleaning and sanitizing the tanks, however this can be tightened or extended depending on the characteristics of water quality, the type of tank and the physical condition. In Portugal, the Decree-Law n° 306/2007 establishes the required quality levels for drinking water.

## **2.5 Influencing factors of mixing and water retention time**

### **2.5.1 General remarks**

Hydrodynamics in storage tanks results from design characteristics, such as the shape of the tank (e.g., circular, rectangular or square cross-sections), the number, location and orientation of inlet and outlet pipes, the existence of baffles (Moncho-Esteve et al. 2015; Xavier and Janzen 2017) and operating modes. Active mixing devices (e.g., impellers)

are not common in water storage tanks, which rely only on the energy of the inflowing water jet during filling for the water movement inside the tank (Grayman et al. 2004). Completely mixed water is usually not achievable because of the large tanks dimensions and limited energy from the inflow momentum to promote mixing (Zhang et al., 2013b). The formation of water pockets or volumes not well mobilised by the flow in the tanks results in stagnant zones where the water retention time can be considerably higher than the average for the stored water (Grayman et al. 1996). In addition, due to temperature differences between the stored and the inflowing water, vertical thermal stratification can occur, resulting in water layers of different densities (Fisher et al. 2009; Grayman et al. 2004; Nordblom and Bergdahl 2004). The most relevant factors influencing mixing conditions are further explained in the following sections.

### **2.5.2 Thermal stratification**

Thermal stratification in storage tanks occurs when the density of the stored water differs from the density of the inflow water. Since water density depends on temperature, stratification can develop when the inflow water temperature contrasts significantly from the stored water. The inflow jet (submerged or above water) is the only mechanism that promotes mixing in storage tanks in most cases. Even if the inflow momentum increases the water mixture in the tank, the temperature or density differences can cause stratification (Grayman et al. 2004). The type of buoyancy (positive or negative) influences the flow dynamics inside the tank (Figure 2.2). A positive buoyancy jet is created, when the inflow is warmer than the water in the tank and the newer water rises to the top of the tank. Negative buoyancy occurs with an inflow colder than the water stored, promoting the permanence of the most recent water in the tank's bottom. As a result, the water at the bottom mixes better, but the water in the upper part of the tank does not mix and gets hotter each consecutive day. This leads to a localized increase in water retention time inside the tank. Even with an opposing outlet pipe, thermal stratification persists.



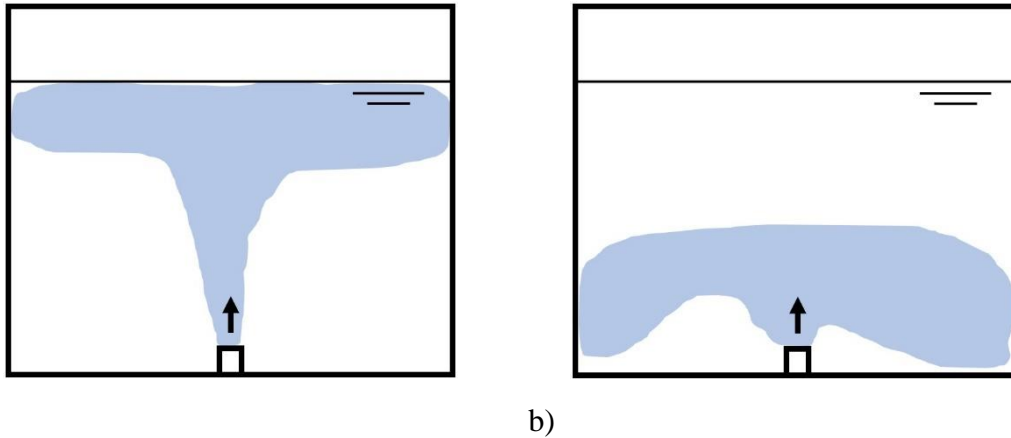


Figure 2.2 – Water stratification created from buoyant jets: a) positive; b) negative buoyant jets (Adapted from Grayman et al., 2004).

Computational fluid dynamics (CFD) numerical modelling was used to predict mixing in standpipes with a 1° C difference between the inflow jet (cooler) and the water inside the tank (warmer). Results showed the importance of studying buoyancy effects in storage tanks since a 1° C difference suffices to cause stratification (Mahmood et al., 2005).

Tian et al. (2008a) tested different inlet configurations on ground-level rectangular tanks considering the effects of temperature differences between the inlet and the water stored simulated by changing the density with the addition of NaCl to the inlet water. In these experiments, negatively buoyant inflows were used with density differences equivalent to 1.4, 2.8 and 5.6°C of temperature differences. Results showed that stratification with negatively buoyant jets can be minimised using horizontal inlets near the water surface or vertical inlets at the bottom of the tank (Tian et al. 2008b).

Water stratification promotes zones where the water stagnates or moves slower, leading to a degradation of the quality of the stored water (e.g., in what concerns disinfectant decay, microbial growth and by-product formation) (Grayman et al., 2004; WHO, 2004).

### 2.5.3 Tank design and operation

The design of water storage tanks has a dominant effect on water mixing conditions. The most relevant design characteristics are the height-to-width ratio ( $H/D$ ) and the inlet pipe characteristics, as explained in the following paragraphs.

### 2.5.3.1 Effect of inlet and outlet conditions

Storage tanks are operated without mixing devices and the inflow jet momentum is the only source of energy for water mixing during the filling cycle. The inlet and outlet pipes characteristics, such as pipe orientation, location, and diameter, can have a major impact on the operation of the tank. Mixing of the water in the storage tank and the momentum are related to the jet mean velocity, which depends on the inlet diameter and the flow rate. The proper tank mixing time is a function of the inflow momentum, geometry, and volume of water.

As pointed out, the number, position and orientation of the inlets are important factors that alter the degree of mixing inside the tank. Figure 2.3 depicts some examples of inlet pipes of storage tanks in Portugal, typically composed of one pipe, perpendicular to the wall and above the maximum water level.



Figure 2.3 – Inlet pipes in water storage tanks.

According to Grayman et al. (2004) and Lemke and Deboer (2013), the inlet pipes must be positioned to avoid stagnant regions inside the tank. The inflow jet will promote water mixing and can have enough momentum to promote the effective circulation of the stored water, depending on the flow rate variations. Turbulent flows promote better mixing than laminar flows (Grayman et al. 2004). Some studies show the effect of the position and orientation of the inlet pipe on mixing effectiveness (Grayman et al. 2004; Okita and Oyama 1963; Tian and Roberts 2008; Zhang et al. 2014). Okita and Oyama (1963) show that jets are useful devices for mixing water within the confined geometry of storage tanks. This is the case, for instance, when a vertical jet reaches the free surface within a tank or when a horizontal jet reaches the opposite wall and the water reverses direction. Grayman et al. (2004) tested several inlet configurations and the experimental results showed that some of them can cause poor mixing conditions inside circular cross-section tanks, namely: tangential inlet can lead to swirling flow, which can generate a dead area

in centre of the tank; inlet pipe directed to the wall does not allow the complete development of the jet, which can cause incomplete mixing or lengthy mixing times; deflectors not allowing the jet development, which can cause incomplete mixing or lengthy mixing times; and large diameter inlets can lead to low inlet velocities and low momentum values, increasing mixing time.

Tian and Roberts (2008a) carried out tracer and 3D laser-induced fluorescence experiments in rectangular cross-section tanks to study the influence of different inlet configurations on mixing conditions, considering only the tank filling cycle. These authors combined the quantity, location, and direction of the jet in their experiments. The results show that a higher number of jets is usually better when considering the same direction and horizontal jets showed better results than vertical or 45° angled jets.

Both Grayman et al. (2004) and Tian and Roberts (2008a) studied the influence of inflowing water jet on the mixing conditions but with submerged jets, and it is not clear how the influence of a jet would be on the surface of the stored water volume, nor the flow patterns resulting from this phenomenon.

The location of the outlet pipe relative to the inlet pipe can also influence the mixing inside the tank. The existence of an outlet close to the inlet pipe can promote a short-circuiting phenomenon, leading to newer water leaving the tank without mobilising the water already stored. This leads to the formation of older water pockets inside the tank. Studies considering simultaneously inflow and outflow and filling and drawing cycles are scarce (Zhang et al., 2013b).

According to Mahmood et al. (2005b) the inlet pipe diameter and orientation must provide adequate mixing within the filling period.

Zhang et al. (2013b) applied CFD to simulate the flow patterns and water age distributions of a rectangular cross-section tank considering a fill-and-draw cycle condition. The results showed that, depending on the cycle phase, the flow patterns change. This means that it is important to consider both the inlet and outlet pipes positions. The same study only examined the submerged inflow. Completely mixed flows are usually not achievable and stagnant zones tend to be created because of the large dimensions of the tanks and limited mixing energy provided by the inflow momentum (Grayman et al., 1996).

One way to provide a higher inlet momentum, assuming that the operating conditions can be changed, by is increasing the flow rate. Another way to increase the inlet momentum is to decrease the inlet pipe diameter. The reduction in the diameter of the inlet pipe causes an increase in the flow velocity and the jet momentum.

Based on the experiments of scaled cylindrical tanks, other researchers (Rossman and Grayman 1999; Tian and Roberts 2008) reported that the mixing time was inversely proportional to the square root of inflow momentum. Reducing the nozzle cross sectional area by half will, theoretically, reduce the mixing time by up to 50%.

### 2.5.3.2 Effect of internal structures (baffles)

The construction of internal structures, like walls (baffles), aims to direct the water flow inside the tank (Figure 2.4). These structures are commonly used in water treatment plants (contact tanks) since they promote plug-flow regimes needed to ensure the long contact time between the water and the disinfectant, e.g., ozone or chlorine in primary disinfection (Liu 2012; Rauen et al. 2012; Taylor et al. 2015). The baffles can improve the mechanical mixing efficiency (passive mixing) and reduce the short-circuiting, thus contributing to the adequate mixing of water and disinfectant (Mahmood et al. 2005b). Improving the mixing efficiency in the tank can reduce the quantity of disinfectant to treat the same volume of water (Chambers 2004; Kizilaslan et al. 2019).

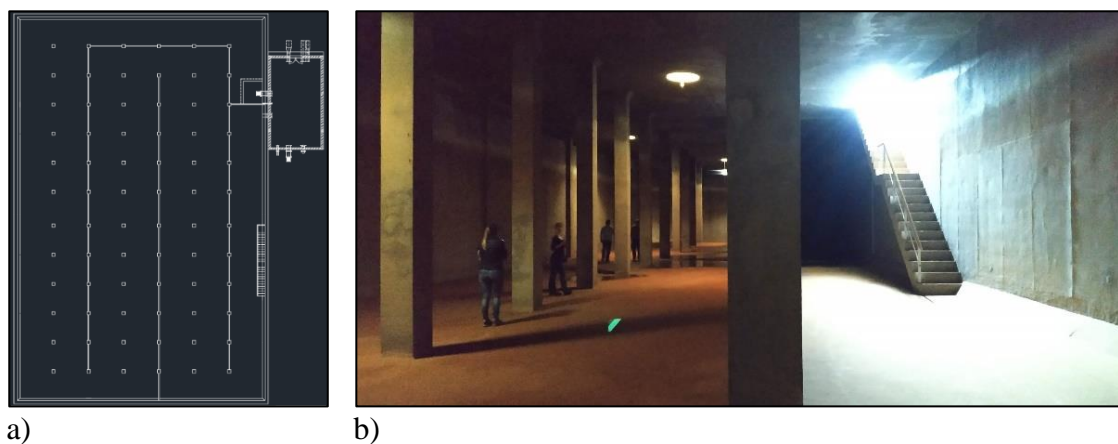


Figure 2.4 – Baffles in rectangular cross-section water storage tanks: a) simplified plant; b) interior view.

The inflow to water storage tanks contains a residual concentration of a disinfectant (typically, chlorine in Portugal) necessary to prevent the deterioration of the stored water. To avoid the loss of this disinfectant residual, regimes close to complete mixing operation

are preferable (i.e., the water enters the tank and is mixed with the existing water). In a plug-flow, like the one promoted in a tank with baffles, the disinfectant concentration is higher at the inlet region and lower at the outlet region, which can be a problem depending on the tank operation.

Some authors do not recommend using baffles in water storage tanks since they lead to poorer mixing conditions (Grayman et al., 2004; Zhang et al., 2012; Gualtieri, 2009; WHO, 2004). Using baffle structures is still an issue without consensus within the technical and scientific communities.

Zhang et al. (2012) applied CFD models to test different baffle configurations. The results show that the fluid velocity is lower after the baffle leading to worse mixing conditions (Figure 2.5).

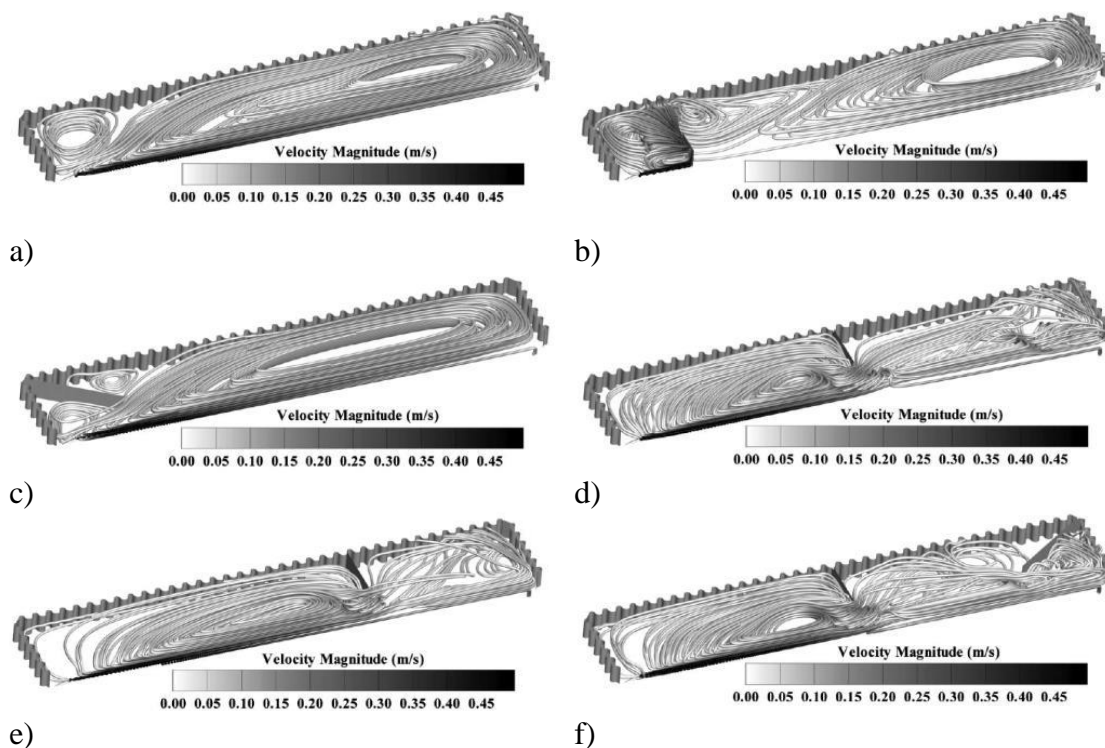


Figure 2.5 – Flow patterns: a) original tank; b-f) different baffle configurations (Zhang et al. 2012).

### 2.5.3.3 Effect of tank geometry

The design of the water storage tanks is not governed by standard guidelines and there is a wide variety of water storage tanks of different types (e.g., elevated, standpipes or ground-level), sizes and shapes (i.e., circular, quadrangular and rectangular cross-section)

and inlet and outlet pipes configurations. Tank geometry is one of the relevant physical characteristics for water mixing.

Kennedy et al. (1993) used full-scale tracer studies to describe the effect of tank geometry on water mixing conditions. Standpipes were found to be the most susceptible to stratification; because of the high height to diameter ratios, inflow water cannot reach the upper zone (dead zone) of the tank, causing poor mixing and stagnant water in the upper zone.

#### 2.5.3.4 Effect of tank operation

The operation of water storage tanks keeps these facilities nearly full to maximize the system's reliability. The fillings and emptying cycles are set and little attention is given to how the tank is operating. However, in the past decade, awareness of the relevance of water storage tank operation to the distribution system hydraulics and to the water quality has increased. Various operational strategies have been devised to deal with some of the identified issues. The basic operation of a water storage tank entails being able to maintain a balance between providing fire and emergency flows, maintaining elevation for optimum pressure delivery, and maintaining water quality.

The way a water utility operates a storage tank influences the water in the storage tank. In pioneering studies, mixing time was defined as the time needed for an added tracer to reach a specific degree of homogeneity inside a vessel (Okita and Oyama 1963). Later, Rossman and Grayman (1999) proposed an equation to estimate mixing time in cylindrical tanks with height-to-width ratio ( $H/D$ ) less than one, in which the inflow water has the same density as the stored water, given by Eq. 2.1:

$$t_m = \frac{kV^{2/3}}{M^{1/2}} \quad \text{Eq. 2.1}$$

where  $t_m$  is the mixing time (s),  $k$  is the dimensionless mixing time constant ( $k = 10.2$ ),  $V$  is the tank volume ( $\text{m}^3$ ) and  $M$  is the inflow momentum flux ( $\text{m}^4\text{s}^{-2}$ ) obtained by multiplying the inflow flow rate,  $Q$ , and velocity,  $u$ .

Both Rossman and Grayman (1999) and, later on, Tian and Roberts (2008), monitored the tracer concentration inside small-scale tanks during the filling period only. In their tests, there was no simultaneous outflow. Despite most mixing occurring during the filling

period (Grayman et al. 2004), caused by the inflowing water jet, the existence of a simultaneous outflow is likely to change the circulation patterns inside the tanks, thus influencing the water mixing (Tian and Roberts 2008) and the mixing time (Jayanti 2001). The few studies carried out with simultaneous inflow and outflow suggest that the mixing time is longer when compared to the no outflow situation (Roberts et al. 2006).

The work developed by Rossman and Grayman (1999) was used by Roberts et al. (2006) to include standpipes. A three-dimensional laser-induced fluorescence system was used to analyse tank mixing in the tracer studies performed by Roberts et al. (2006). A more accurate description of water movement was determined from the laser system than by the submerged probes used in the tracer study completed by Rossman and Grayman (1999). Roberts et al (2006) used Eq. 2.1; however, the mixing time was modified to be a function of the  $H/D$  ratio:

$$t_m = \begin{cases} 10.0 & \text{for } \frac{H}{D} \leq 1.0 \\ 10.0 + 3.5 \left( \frac{H}{D} - 1 \right) & \text{for } \frac{H}{D} > 1.0 \end{cases} \quad \text{Eq. 2.2}$$

In the operation of water tanks, effective mixing of the incoming water with the existing water can be guaranteed if the filling time is greater than the mixing time,  $t_m$ . In this way, it is possible to prevent the formation of water pockets with different residence times, thus with different ages and chemical and microbiological characteristics, along with continuous filling and emptying cycles (Rossman and Grayman, 1999). Since the filling time is given by  $\Delta V/Q$ , where  $\Delta V$  is the volume added to the tank in a filling cycle and  $Q$  is the inflow rate, to guarantee the desirable mixing the relationship expressed in Eq. 2.3 must be verified, or, equivalently, by Eq. 2.4

$$\frac{\Delta V}{Q} > \frac{t_m V_{min}^{2/3}}{M^{1/2}} \quad \text{Eq. 2.3}$$

$$\frac{\Delta V}{V_{min}} = \frac{9d}{V_{min}^{1/3}} \quad \text{Eq. 2.4}$$

where  $V_{min}$  is the volume of water corresponding to the minimum operating height during a filling cycle. This expression allows determining the fraction of tank volume ( $\Delta V/V_{min}$ ) that needs to be renewed in each filling cycle to ensure the mixing of the incoming water with the existing one. This fraction depends on the minimum volume stored in the tank and on the diameter of the inlet pipe,  $d$ , but not on the inlet flow rate.

## **2.6 Modelling mixing in water storage tanks**

Several models can be used to describe water residence time, mixing conditions, or disinfectant residuals in tanks namely, tank mixing models, computational fluid dynamic models, or small or full-scale models. Tank mixing models describe the water mixing phenomenon through the mass balance. Computational fluid dynamic model numerically solves the mass balance and momentum equations to predict the water movement within the tanks. Small-scale modelling uses dimensional analysis to scale tank sizes, such that they can be studied in a laboratory setting; and full-scale testing refers to experiments carried out in an actual system. Regardless of the method used, it is important to calibrate and verify the model results with field data.

### **2.6.1 Tank mixing models**

Network models are numerical models that can simulate the hydraulic and water quality behaviour of water distribution networks over time. If well developed and calibrated, these models can simulate the network behaviour for different operating conditions of the network. Any model that examines water quality in a distribution system requires modelling of hydraulic components first and the establishment of a pre-defined set of assumptions (Rossman 2000). In distribution system modelling, the tank is one of network components. The distribution system model will show the user how the tank is operating, but also how the tank operation is influencing the behaviour of the flow in other components in the system (e.g., pipes, pumps, valves). Information, such as the tank elevation, dimensions, maximum and minimum water levels, initial water level and the tank mixing model, is required for modelling a tank in a distribution system.

There are several tank mixing models to simulate flow characteristics in storage tanks within a distribution network model available in EPANET (e.g., Completely Mixed, Two-Compartment Mixing, Plug Flow, Stacked Plug Flow). Mau et al. (1996) carried out a study to describe different tank mixing models. Several parameters were assumed, including constant inflow and outflow rates, similar flow rates between zones and uni-directional flow. Clark et al. (1996) expanded the work of Mau et al. (1996) by studying time-varying flow rates using polynomials. Olson (2011) summarized the different tank mixing models from previous studies.



The mixed flow model assumes that immediately after water entering the tank, the water in the tank is completely mixed. Thus, any portion of the water stored will have identical residence time and quality. This tank corresponds to the continuous stirred tank reactor (CSTR). The plug flow (PF) model assumes no mixing when the water travels a path from the inlet to the outlet, with older being near the outlet. This model is known as the first in-first out (or last in-last out), The last in/first out (LIFO) model is like the PF model, but with a connected or adjacent inlet and outlet pipes, where it is assumed that does not exist water mixing, and the water drawn from the tank is always the youngest in the tank. The multi-compartment model is used to simulate more complex tanks that have non-uniform behaviour by dividing the tank in different zones, such as two-compartment model, three-compartment model, stratified three-compartment model and four-compartment model, as described by Mau et al. (1996), and three-and-one half model compartment model, presented by Grayman et al. (1996).

According to Grayman et al. (2000), the simplification of these models requires data to calibrate them and the best way to proceed with the calibration is to compare experimental data (laboratory or field) with the models results. The most effective method of calibration is to make a tracer study and to adjust the model parameters to fit results to the experimental data (Olson and Deboer 2008). If no data is available, the effectiveness of the model depends on the user experience and knowledge (Grayman et al. 2000).

### **2.6.2 Computational Fluid Dynamics models**

Computational fluid dynamic (CFD) modelling uses numerical methods and algorithms to solve and analyse problems that involve fluid flow. CFD models solve the dynamic behaviour of fluids in two or three-dimensions (using Navier-Stokes based solvers) based on the fundamental laws of mass, momentum, and energy conservation.

CFD modelling has been widely applied in the mechanical engineering and aeronautical industry for being a valuable tool, not only to understand the fluid dynamics but also to reduce associated costs (Laín and Aliod, 2000). This tool has gained acceptance also in environmental and civil engineering, specifically in the water supply industry, where CFD is applied for the assessment and optimization of disinfection processes in reactors commonly at the end of the water treatment train (Angeloudis et al., 2014; Zhang et al., 2014a).

Recent research on mixing in drinking water storage tanks relies almost only on numerical simulation using CFD models (Moncho-Esteve et al. 2015; Xavier and Janzen 2017; Zhang et al. 2013c).

CFD modelling has enabled the simulation of the effect of tank design options (e.g., baffling, inlet pipe diameter) in water mixing in order to reduce stagnation and the associated deterioration of stored water quality (Mahmood et al. 2005b; Zhang et al. 2013a). In those simulations, steady-state conditions are often considered, that is water mixing is assessed at constant inflow and outflow rates (Moncho-Esteve et al. 2015; Xavier and Janzen 2017). Zhang et al. (2013b) simulated the water mixing in a tank at variable water levels, but there was only either inflow or outflow at a particular instant. Zhang et al. (2019) found that the steady flow assumption often made in numerical models might lead to the incorrect characterization of the hydraulic performances. Hence, water mixing in storage tanks operated at variable water levels and simultaneous outflow, as in full-scale conditions, still requires further research.

Grayman et al. (1996) compared the results of the physical modelling, systems modelling and CFD with experimental data from a tracer test in a circular cross-section tank with simultaneous inlet and outlet flows. They found a suitable agreement between field data and modelled results. These authors also simulated a tracer test for 33.5 hours and found higher concentrations in the external ring of the tank compared with experimental measurements and a non-symmetric pattern in the tank cross-section, which was not experimentally recognized because of limited sampling points. Additionally, the experimental work identified a significant increase of the tracer in the upper region of the centre of the tank, which was not observed in the numerical modelling, likely caused by the non-consideration of the thermal effects over the flow pattern (Grayman et al., 1996).

Van der Walt (2002) research included CFD simulations of several scenarios of free residual chlorine decay in a storage tank. The author concluded that chlorine concentration at the tank outlet is not representative of that of the interior and specified that the minimum permissible limit of residual chlorine should be the criterion to choose a physical modification or an operational change in a tank to improve the quality of stored water.

Duer (2003) simulated 10 tank configurations by CFD, applying variations in the inlet configuration and water temperature (incoming and stored). The model showed that the studied tank had inefficient mixing and short circuits because of temperature differences between the stored and incoming water.

Mahmood et al. (2005) studied three tanks using temperature and residual chlorine measurements and CFD modelling of the tracer injection. From the CFD modelling results, they recommended the use of an inlet with a lower diameter to increase the momentum and to avoid the incoming water jet hitting the tank walls, for improving water mixing. Those modifications, made in an actual scale tank, and after the analysis of collected data, showed that water had appropriate mixing.

Stamou (2008) studied nine disinfection tanks. Two configurations in the tank geometry and several physical modifications in the tanks were simulated by CFD models. In the initial geometry, the flow was characterized by high levels of short-circuiting, large recirculation regions and low mixing degree, while, in the physical modifications, the use of baffles created flow fields with significant volumes of plug flow that reduced short circuits, recirculation zones and increased mixing.

Although CFD simulations for storage tanks have been carried out for constant water level and a specific inlet in most cases, Nordblom (2004) investigated the influence of a denser inflow to a cylindrical tank in transitory mixing processes, using dynamic mesh and grid deformation models to represent fill-and-drain periods in two tanks. After many simulations under critical conditions of mixing, a range of ratios between water level and tank diameter ( $H/D$ ) that resulted in adequate mixing were identified. Those simulations showed that the standard  $k-\varepsilon$  turbulence model suffices to represent the mixing characteristics in the tanks and that CFD modelling could replace more expensive scale model tests and field measurements.

Zhang et al. (2011) also applied volume-of-fluid (VOF) multiphase analysis and dynamic mesh as strategies for tracking water-level in a rectangular service tank, with separate inlet and outlet pipes and operating with drain cycles or fill-and-drain cycles. Hence, a dynamic mesh was used in further numerical simulations since it significantly saved computational time and storage. Results showed that the flow in the studied service tank presented short-circuiting and poor lateral and vertical mixing. The chlorine distribution

in the tank was not uniform, and a lower concentration was found in the recirculation regions. Later, Zhang et al. (2013) evaluated the effect of baffle structures in the same tank. They concluded that this option is not advisable since it may lead to a lower chlorine concentration at the tank outlet pipe because of lower flow velocities near interior walls, resulting in an increase in residence time. The same research team applied a dynamic mesh to assess the influence of tank shape on velocity and water age (Zhang et al., 2014b). The authors concluded that a rectangular shape tank is the best option to be considered by designers when the inlet and outlet are separated and at opposite sites (circular and quadrangular cross-section shapes were also evaluated). However, this study did not assess the effect of thermal stratification, inlet–outlet layout, turnover, and  $H/D$  ratio on water mixing and age distributions.

Most CFD studies in drinking water distribution systems have focused on comparisons of numerical results with data collected in experimental tracer tests. Further application of CFD modelling of the decay of free residual chlorine has been done in chlorine contact chambers, which are reactors characterized by small retention times (few minutes) and higher decay rates in comparison with storage tanks. Thus, the application of models representing water variations and free residual chlorine decay in CFD modelling of storage tanks in WDS is still required. The works of Nordblom (2004) and Zhang et al. (2013) represent an improvement in this area.

Montoya-Pachongo et al. (2016) evaluate the influence of the inlet configuration change in the flow pattern, mixing conditions and free residual chlorine decay in a service tank of a WDS. This was done by applying CFD in steady-state simulations for solving, in the first place, the flow pattern with constant water levels; then, this “frozen” flow field was used to simulate separately the behaviour of tracer transport and chlorine decay over time. The results of this study allow to conclude that increasing momentum at the inlet improves mixing and promotes flow patterns governed by complete mixing, which is advisable for drinking water tanks to maintain chlorine concentrations.

Mahmood et al. (2005) used CFD model to compare negatively buoyant jets and isothermal conditions in standpipe tanks with a vertical inlet. For the tested conditions, the colder inflow only promoted the water mixing in the first one-third of the tank. Under isothermal conditions, the water jet could reach the top of the standpipe and completely mix inside the tank. These results do not consider the influence of outflow; however, these

allow to understand the effect of minor changes in temperature between the filling and stored water in the water mixing inside the tanks.

### **2.6.3 Small-scale models**

Small-scale physical models provide a relatively simple means for studying the influence of tank configuration and operation on the flow dynamics and mixing phenomena (Clark et al. 1996). These models are based on dimensionless analysis to simulate real-life conditions. They are suitable for both qualitative and quantitative experiments. Rossman and Grayman (1999) used small-scale models to develop equations for predicting the mixing time and the occurrence of stratification in tanks. Roberts et al. (2006) used laser-induced fluorescence to provide detailed measurements of fluid flow in tanks. These measurements were used to develop dimensionless mixing times functions for several tank geometries, inlet configurations, and stratified conditions.

### **2.6.4 Field testing models**

Full-scale tanks have been studied by using systematic models, CFD or small-scale models and by comparing experimental results with collected field data (Angeloudis et al. 2014; Codina et al. 2015; Mahmood et al. 2005b). Water quality, temperature and tracer tests are the most common types of tests performed. Although sampling can be carried out at the inlet, outlet, or inside of the tank. For meaningful results, sampling should be carried out in as many locations as possible, including the three locations referred. These types of studies are useful in identifying mixing and water quality issues (Kennedy et al. 1993; Lemke and Deboer 2013; Olson and Deboer 2008).

Interior sampling (i.e., sampling inside the tank) is an effective method to determine a storage tank mixing and water quality characteristics. Grayman et al. (2000) described two different ways to carry out the sampling inside the tank. Taps can be installed at varying depths of the storage tank, or a sampling apparatus could be constructed and lowered into the storage tank with sampling locations at varying depths. The data from interior sampling studies can identify problems in particular areas of a storage tank. Mahmood et al. (2005) used an apparatus to measure temperature inside full-scale tanks to confirm the results of the developed CFD models. The temperature apparatus used by Mahmood et al. (2005) comprised temperature sensors attached to a chain at varying depths of the tank. The apparatus was weighted to ensure the chain remained straight

throughout the study. A data logger was used to store the temperature data by connecting the temperature sensors to the data logger.

Exterior sampling (i.e., sampling at the inlet or outlet sections) does not allow the identification of critical areas in storage tanks; monitoring the inflow and the outflow tracer concentration does not allow the accurate description of the storage tank mixing characteristics throughout the interior regions of the tank. Issues such as water stratification and short-circuiting can cause a difference in water quality between the bottom and the upper zone of the tank.

## **2.7 Residence time distribution**

The residence time distribution (RTD) and the associated hydraulic indexes are determined to diagnose mixing, short-circuiting and stagnation within the tanks (Teixeira and Siqueira 2008; Wilson and Venayagamoorthy 2010). Comparison of the RTD curves and associated indexes with those of ideal reactors (completely mixed and plug flow) have been carried out in contact tanks to assess similarities (Rauen et al. 2012). Similar studies in storage tanks were not found. For the latter, complete mixing conditions are often assumed in WDS modelling (Hua et al. 2018; Mau et al. 1996), despite the short-circuiting and the existence of poorly mixed zones that have been observed (Boulos et al. 1996; Fard and Barkdoll 2018; Kennedy et al. 1993). This assumption can lead to underestimating water age (Kennedy et al. 1993) and is likely to result in inaccurate predictions of disinfectant concentration.

Residence time analysis is typically carried out for different substances in reactors in chemical engineering. When the water flow passes the inlet of the reactor in a steady-state, the various fractions of the stream do not pass through the outlet section of the reactor at the same time, reflecting the fact that there is a distribution of the residence times in the reactor. This phenomenon can be represented by a residence time distribution, well known as RTD (Danckwerts 1953).

Determination of RTD can be carried out by a tracer-test method (also called the tracing method) that is used in a wide variety of industrial systems or in a small-scale model. The tracer test starts with the injection of a tracer into the feed stream at time  $t = 0$  and the simultaneous measurement of the tracer concentration  $C$  at a downstream location of the stream (typically, the stream end section) over time (Fogler 2016). The tracer should be

an inert chemical, molecule or atom and should have similar physical properties to the bulk fluid particles and be completely soluble in the bulk fluid. The tracer should also not be adsorbed by the surfaces of the reactor.

The pulse input and step input are the most common and simplest tracer injection techniques. In a pulse input, an amount of tracer is suddenly injected into the unit operation in a short time interval. The outlet concentration is then measured as a function of time. Typical concentration curves for a step input and pulse input are given in Figure 2.6.

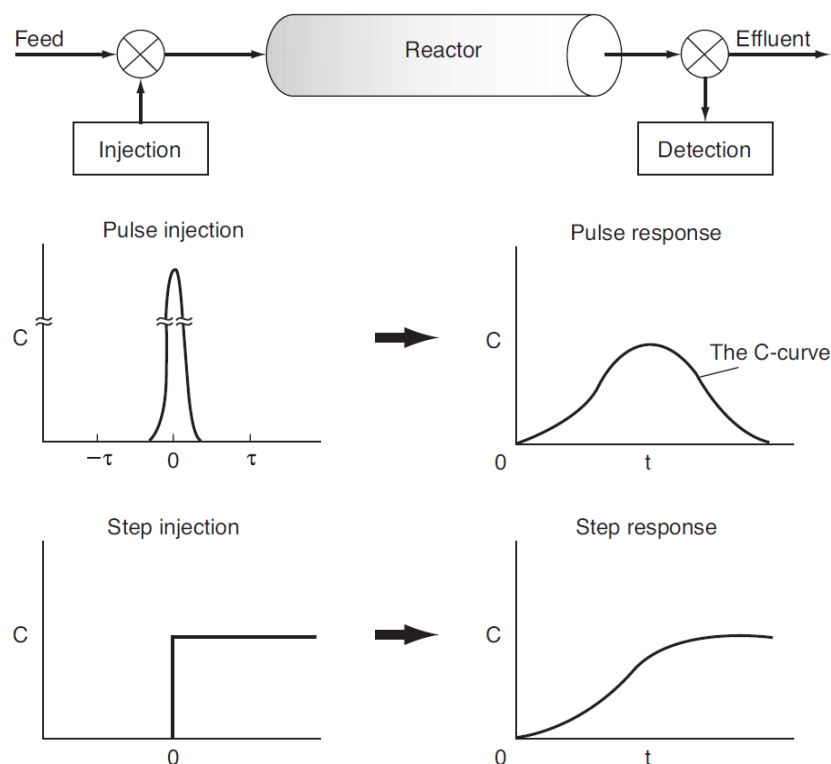


Figure 2.6 – RTD measurements for a pulse injection (top) and step injection (bottom) (adapted from Fogler, 2016).

In the stepped input tracer injection technique, the total amount of tracer must be known in the input stream over the experimental time. The step pulse is sometimes complicated to maintain at a constant tracer concentration in the input stream. Another drawback of this tracer injection technique is that the RTD involves differentiation of the data, leading to large errors. In a step input method, the tracer concentration in the outlet pipe  $C_{out}$  is normalized to calculate the non-dimensional cumulative distribution function  $F(t)$  (Eq. 2.5), where  $C_e$  is the tracer concentration in the inlet pipe. The residence time distribution function,  $E(t)$ , is found by differentiating  $F(t)$  (Eq. 2.6).

$$F(t) = \left[ \frac{C_{out}}{C_e} \right]_{step} = \int_0^t E(t') dt' \quad \text{Eq. 2.5}$$

$$E(t) = \frac{dF(t)}{dt} \quad \text{Eq. 2.6}$$

## 2.8 Modelling disinfectant decay

Controlling chlorine residual concentrations is an issue of the utmost importance for water quality management in drinking water systems. While excessive chlorine residual concentrations can lead to taste and odour related complaints and the increased formation of disinfection by-products, concentrations below 0.2 mg L<sup>-1</sup> may not be enough for counteracting microbial regrowth (Graham 2011). In addition, chlorine is a very strong disinfectant and reacts with many chemical species in drinking water and the residual concentration decreases over time (Deborde and von Gunten 2008). Chlorine disinfection presents the advantages of efficiency and durability.

Modelling chlorine decay can be a very useful tool for managing water distribution systems, supporting the decision on the injection of disinfectant doses and the most adequate location of chlorination stations. Such models are currently used for dosage optimization, chlorination facilities location and prediction of critical places where chlorine decays to ineffective levels. Although many efforts have been made in the last decades (Rossman et al. 1994; Shang et al. 2008), the modelling of chlorine residuals is still complex, as it relies on the accuracy of hydraulic models to describe flows and flow velocities (Blokker et al. 2008; Pasha and Lansley 2010) and on the adequacy of chlorine decay kinetic models (Fisher et al. 2011). The  $n^{th}$  order bulk decay kinetic model with respect to chlorine is described by Eq. 2.7.

$$\frac{dC^*}{dt} = -K_b C_0^n \quad \text{Eq. 2.7}$$

where  $C_0$  is initial chlorine concentration,  $K_b$  is the bulk decay rate coefficient and  $n$  is the order of the reaction with respect to chlorine. First-order bulk decay is a particular case of  $n^{th}$  order kinetics for chlorine. It has been extensively used in the simulation of chlorine decay in water supply systems (Monteiro et al. 2015, 2020, 2017; Rossman et al. 1994).



Considering a first-order bulk reaction, the conversion in the model will be independent of the degree of micromixing. The prediction of behaviour can then be carried out by assuming the total segregation at the microscopic level, without loss of precision. In a first-order process, conversion is determined by the time spent by individual fluid reactant elements in the reactor, not by their environment in the reactor.

The disinfectant concentration at the outflow is calculated from the parcels of all residence times in the right proportion dictated by the residence time distribution function and can be expressed as (Lemos et al. 2014):

$$C_a(t) = \int_0^t C^*(t). E(t) dt \quad \text{Eq. 2.8}$$

where  $C^*(t)$  is the concentration of disinfectant in a batch reactor initially fed with a defined concentration, as a function of the reaction time, and  $E(t)$  the residence time distribution resulting from the model. Alternatively, this concentration can be determined using the mass balance equations.

The application of the principle of total segregation requires the calculation of the chlorine concentration in a reactor charged with a reagent solution equal to that which enters the continuous reactor given by:

$$C^*(t) = C_0 e^{(-k_b t)} \quad \text{Eq. 2.9}$$

## 2.9 Gaps of knowledge

The large variety of existing tanks sizes, shapes, and configurations resulted in only a small number of conditions that have been studied. Most studies focused on a single factor (e.g., inlet flow location, tank shape) not integrating other critical and overlooked variables (e.g., varying stored volumes, tank filling, discharging flows, operating rules), nor testing single or combined mixing improvement measures. In addition, most CFD models lack experimental calibration and validation.

In summary, the major gaps of knowledge in drinking water storage tanks that have motivated the present work are:

- (i) The lack of understanding of the dependence of the flow dynamics in storage tanks on several factors, such as tank characteristics (e.g., cross-section geometry, number, and position of inlets and outlets, inflow momentum, baffle structures), operation mode, demand profiles and required storage volumes.
- (ii) The lack of criteria and knowledge-based guidelines for best practices on water tanks' design, operation, and rehabilitation to avoid water stagnation and water quality deterioration.
- (iii) The lack of knowledge on the effect of flow dynamics on both water mixing and renewal conditions in storage tanks.

# Chapter 3

---

## Water storage tanks characterization in Portugal

This chapter is based on a conference paper presented in SEREA 2019 that was selected for publication in a peer-review journal:

Monteiro, L., **Pinheiro, A.**, Carneiro, J., Covas, D. (2021). Characterization of drinking water storage tanks in Portugal. *Ingeniería del agua*, 25(1), 49-58. doi: 10.4995/Ia.2021.13659.

### 3.1 Introduction

This chapter presents a characterization of water storage tanks in Portugal, focusing on the main physical characteristics and operational conditions that mostly affect their performance regarding water mixing and renewal. The study is based on a survey developed in 11 water utilities in Portugal. These utilities were asked to record, for each tank, the type of water system (i.e., distribution network, bulk water system or combined system), the number of cells and for each cell, the shape of the cross-section of the tank (circular, rectangular or quadrangular), the tank type (buried, semi-buried, ground-level, water tower), the main dimensions (diameter and height), the capacity, interior structures (e.g. baffles or active mixing devices), the number of inlet and outlet pipes and their respective diameters and locations, and operational conditions, such as water levels (minimum and maximum) and flow rate values (minimum and maximum). Each cell was characterized by the height/diameter ratio,  $H/D$ , and for rectangular or square-shaped cells, the equivalent diameter,  $D_{eq}$ , was calculated based on the equivalent cross-sectional area,  $A$  (Rossman 2000).

Collected data were treated and statistical analysis was carried out to analyse these data. Several cohorts of pipes have been identified and organized by year of construction, capacity and ratio  $H/D$ . Statistics calculated include the maximum, the minimum and the median values for each cohort.

Eq. 2.1 was applied to determine the mixing times at each cell with an equivalent circular shape and Eq. 2.2 was used to calculate the respective dimensionless mixing times. The fraction of renewal volume that guarantees an adequate degree of mixing during filling was estimated by Eq. 2.4

### 3.2 Tank general characterization

A purpose-made database was assembled to compile survey results. The sample comprises 372 water storage tanks. Each tank was characterised in terms of the main physical and operational characteristics. The tanks are part of water distribution systems (42%), bulk water systems (28%) or combined distribution-bulk water systems (30%). About 49% of the tanks have only one cell, 45% have two cells and 6% have three or more cells. Since a tank can be composed of cells with different shapes and operating conditions, the results presented are for the cells as the unit of analysis. The total number

of cells is 593. The sample includes tanks built from 1882 to 2017. For 27% of the tanks, the year of construction was unknown. About half of the tanks with known construction date were built after the year 2000, i.e., have up to 20 years of operation (Figure 3.1).

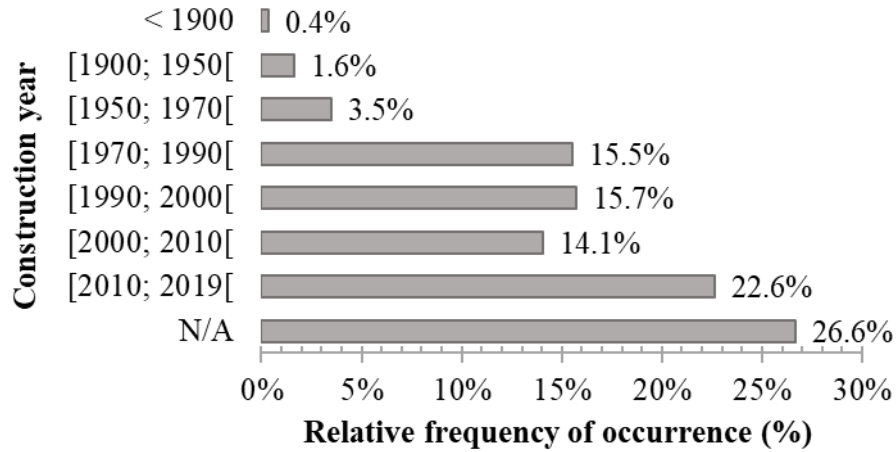


Figure 3.1 – The relative frequency of tanks per year of construction.

### 3.3 Operational and structural characterization

The circular cross-section tanks' geometry is predominant (74%), followed by rectangular (14%), frustoconical (8%) and quadrangular (4%) cross-section. Most of the tanks are located on the ground (50%), about 39% are partially below nominal surface of the ground, 10% are elevated (water tank supported by a steel or concrete tower), and 1% are buried. Figure 3.2 presents examples of the most common tank types in Portugal.



Figure 3.2 – Examples of tank typologies: a) frustoconical water tower; b) circular cross-section half-buried tank; c) rectangular cross-section tank.

Baffles are more frequent in tanks with a rectangular cross-section than in other geometries (Figure 3.3). These structures promote a “piston-type” water flow (plug-flow) inside the tank. The water is forced to follow a specific path from the inlet to the outlet.

This plug-flow minimizes the mixing of the stored water with the fresh water during the filling phase. None of the tanks from the sample have active mixing devices, such as stirrers.

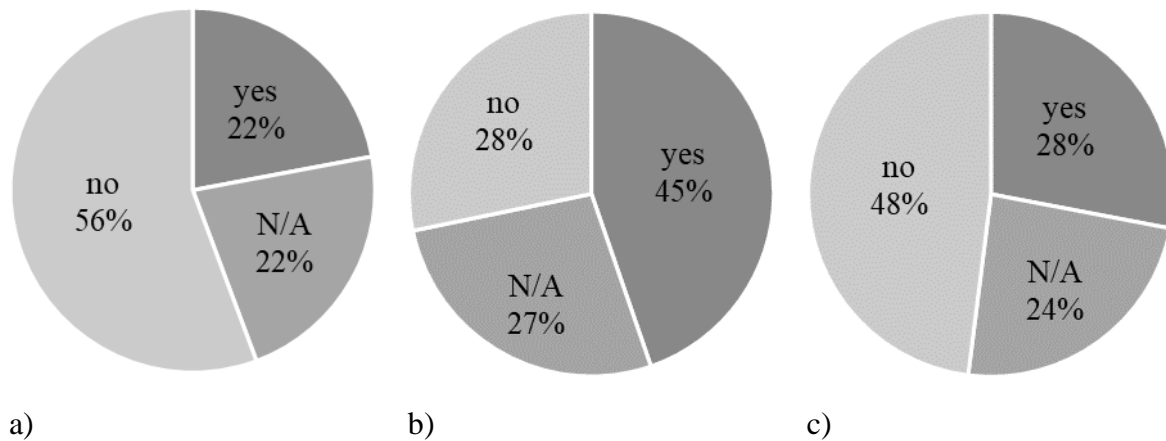


Figure 3.3 – Distribution of tanks with baffles for different types of cross-sections: a) circular; b) rectangular; c) quadrangular.

Concerning the inlet pipes, about 92% of the tanks in the database have only one inlet pipe, 5% have two inlet pipes and 3% of the tanks did not have this information available. The inlet pipe position is usually from above the water level (80%). In 7% of the tanks the position of the inlet pipe(s) is not known. Only 2% of tanks have the water inlets around half of the height of the tank. The diameters of the inlet pipes vary between 50 and 1 200 mm, with a median value of 300 mm.

### 3.4 Buried, semi-buried and supported tanks

Storage tanks with rectangular and quadrangular cross-sections have the highest storage capacities, ranging between 40 and 10 000 m<sup>3</sup>, with a median of 2 350 and 3 000 m<sup>3</sup>, respectively. Circular tanks are usually smaller, with a median of 500 m<sup>3</sup>. However, circular tanks with large capacities were also found, with volumes up to a maximum of 13 350 m<sup>3</sup> (Table 3.1 and Figure 3.4a).

The tanks have median values for the height/diameter ratio (or height/equivalent diameter) from 0.17 to 0.29, respectively, for the rectangular and the circular cross-section tanks (Figure 3.4b), the diameter much larger than the height, giving the tanks a flattened appearance. In circular tanks, this ratio varies between 0.04 and 1.85. The *H/D* ratios decrease with tank volume, with values higher than 1.0 in tanks with a capacity

lower than 200 m<sup>3</sup> (Figure 3.5). In tanks with volumes over 3 000 m<sup>3</sup>, the *H/D* ratio reaches the lowest values, below 0.2.

Table 3.1 – Characterization of circular, rectangular and quadrangular tank types.

Cross-section	Number of elements	Volume (m <sup>3</sup> )	<i>H/D</i> ratio (-)	<i>H<sub>min</sub>/H<sub>max</sub></i> ratio (%)
		[min max] (median)	[min max] (median)	[min max] (median)
circular	425	[15; 13 350] (500)	[0,04; 1,85] (0,29)	[7; 100] (60)
rectangular	85	[50; 10 000] (2 350)	[0,06; 1,02] (0,17)	[26; 97] (70)
quadrangular	22	[40; 7 865] (3 000)	[0,10; 0,85] (0,20)	[46; 89] (72)

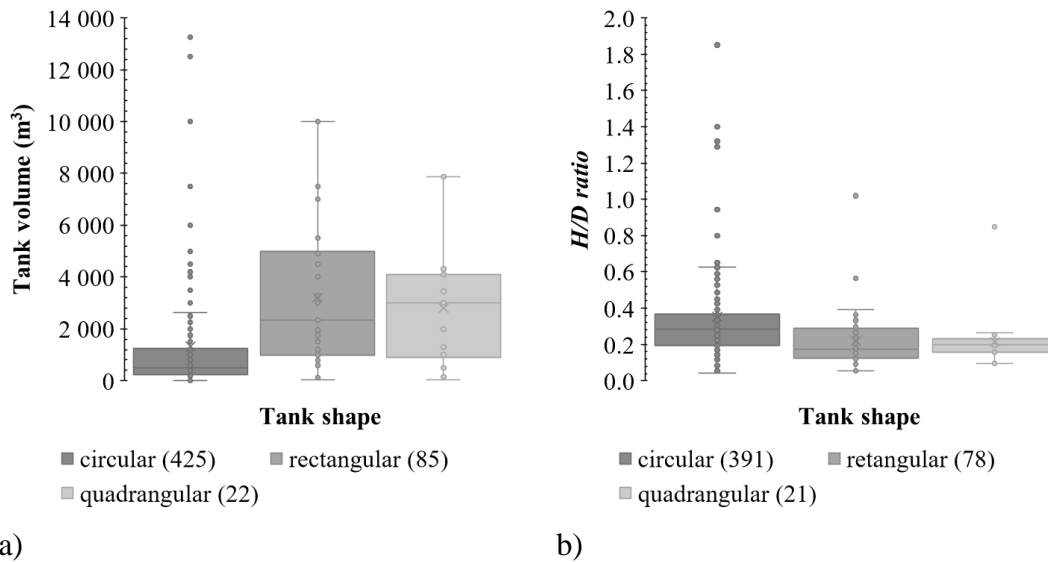


Figure 3.4 – Circular, rectangular and quadrangular tank type distribution in terms of: a) volume; b) *H/D* ratio.

Unlike the *H/D* ratio, which is a parameter for evaluating the relative dimensions of the infrastructure, the *H<sub>min</sub>/H<sub>max</sub>* ratio, defined as the ratio of the minimum and maximum tank operation water heights, allows evaluation of how they are operated. Results show this ratio has wide variations in circular cross-section tanks and lower variations in rectangular ones (Table 3.1). However, as median values of this ratio reveal minimum levels are 60% to 72% of the maximum levels, the tanks are operated predominantly close to full capacity to ensure higher system reliability.

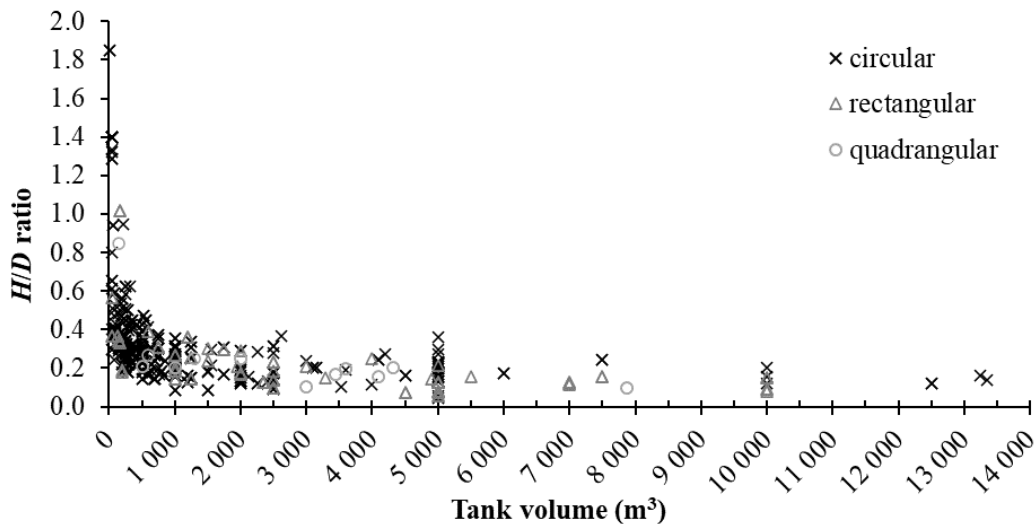


Figure 3.5 – Variation of the  $H/D$  ratio with the volume for buried, semi-buried and supported tanks.

### 3.5 Elevated tanks

The number of elevated tanks (61) is much smaller than others positioned at ground-level, buried and half-buried tanks (532). Elevated tanks have lower capacity and are predominantly of frustoconical shape (Table 3.2). Storage capacities vary between 50 and 769 m<sup>3</sup>, with median values of 300 to 405 m<sup>3</sup> for circular and frustoconical tanks, respectively. The  $H/D$  ratio for elevated tanks varies between 0.26 and 1.12, with a median of 0.39 and 0.57 for circular and quadrangular cross-sections, respectively. These median values, higher than those found in ground-level, buried and semi-buried tanks, are because their smaller storage volumes.

The  $H_{min}/H_{max}$  ratio was not calculated for all tanks because of lack of data. However, the estimated median value of 38% shows higher variability in water levels in these tanks than in the other types.

Table 3.2 – Characterization of elevated tanks typology.

Cross-section	Number of elements	Volume (m <sup>3</sup> ) [min max] (median)	$H/D$ ratio (-) [min max] (median)	$H_{min}/H_{max}$ ratio (%) [min max] (median)
circular	15	[100; 600] (300)	[0,26; 1,12] (0,39)	[19; 79] (38)
quadrangular	3	[50; 405] (405)	[0,30; 0,57] (0,57)	N/A
frustoconical	43	[150; 769] (313)	-	N/A



### 3.6 Mixing time

The mixing time (Eq. 2.1) was estimated for the 244 circular cross-section tanks with all necessary data available (Figure 3.6). Results show that the mixing time varies between 0.3 and 51 h, prevailing the mixing times between 1 and 2 h (25%). In only 1.2% of cases, mixing time longer than one day was estimated. It should be noted that to guarantee the mixing between the inflow and the stored water, the filling time should be longer than the mixing time, which, in practice, is not workable for most cases.

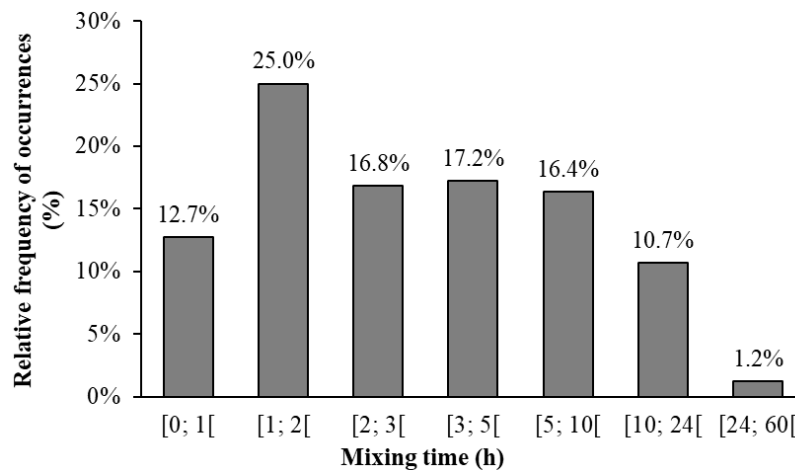


Figure 3.6 – Mixing time distribution for tanks with circular cross-section.

In tanks with smaller volumes, the increase in inlet flow leads to shorter mixing times (Figure 3.7). Longer mixing times are observed in tanks with higher volumes ( $>7\,000\text{ m}^3$ ) supplied by low inlet flows ( $<100\text{ m}^3\text{ h}^{-1}$ ). Also, the longest mixing time occurs in tanks with relatively large diameter inlet pipes (500 to 800 mm), which results in inlet water jets with low flow momentum. These tanks, with higher volumes, low inlet flow and large inlet pipe diameter, have the most unfavourable conditions for water mixing.

In this study, the mixing times correspond to the time it takes for a tracer to reach a homogeneous concentration inside the tank, as described by Eq. 2.1. This formula does not consider the effect that the location and position of the inlet/outlet pipes can have on the dispersion of the tracer. However, the calculated mixing time can be used as an indicator of how good mixing might be in these tanks, given their dimensions and the flow of momentum of the incoming jet.

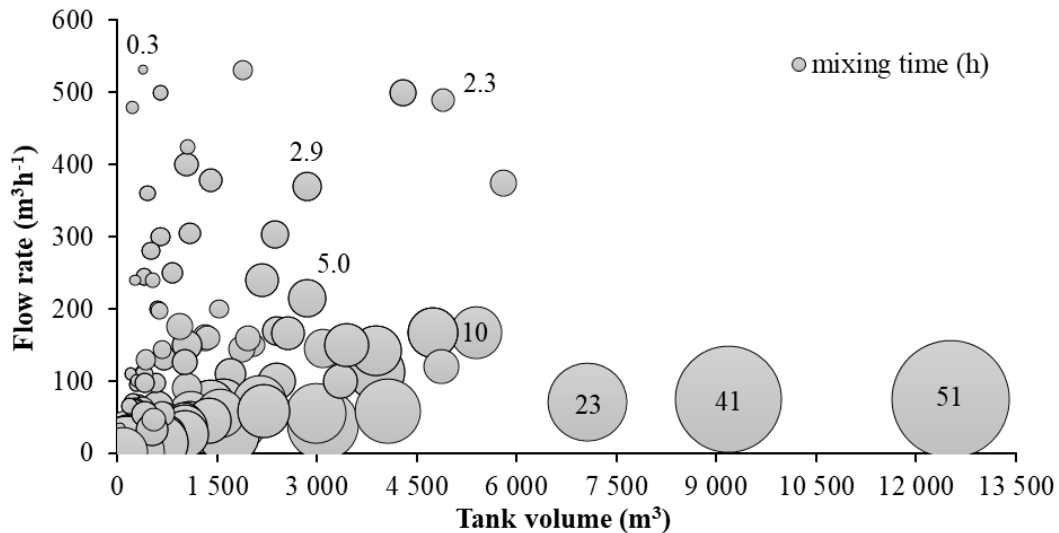


Figure 3.7 – Relationship between mixing time, inlet flow and volume in circular cross-section tanks.

### 3.7 Renewal volume fraction

Unlike mixing time, the turnover volume fraction ( $\Delta V/V_{min}$ ), calculated for circular cross-section tanks, can be compared with the theoretical values once the operating levels and inlet pipe diameter are known (Figure 3.8). It allows assessing whether the current operating conditions promote the complete mixing of the water that enters, in each filling cycle, with that existing in the tank. In 74% of cases, the operating conditions allow the volume of water that enters each filling cycle to mix with the existing water. These results assume that the water level inside the tank varies between the minimum and the maximum operational levels in each filling cycle reported by the water utility. In practice, it is common to observe minor variations in the level over time, depending on downstream water consumption and storage needs.

The  $H_{min}/H_{max}$  ratio is, on average, 49% in tanks where the complete mixing is reached and varies between 70% and 96%, with a value average of 84%, in tanks where complete mixing is not achieved. These results show that the variation in the water level in the tank significantly contributes to the water mixing conditions.

Mixing is achieved in almost all circular cross-section tanks with inlet pipes of 200 mm since the calculated fractional exchange of tank volume is higher than the minimum to ensure well-mixed conditions (Figure 3.8). The same is not true for tanks with larger inlet diameters (500 mm), whose renewal volume fractions are lower than the minimum necessary in 59% of cases.

In these cases, the flow momentum of the jet is smaller, and it is necessary to increase the fraction of the volume of renewal in each cycle to guarantee the well-mixed conditions for the same initial volume. These results show that tanks with the largest inlet pipe diameters have the worst performances because the operating conditions do not allow the mixing and promote the formation of stagnation zones with longer water residence times. Reducing the diameter of the inlet pipes could be a simple practical measure with significant benefits for the water mixture and, consequently, for the quality of the water.

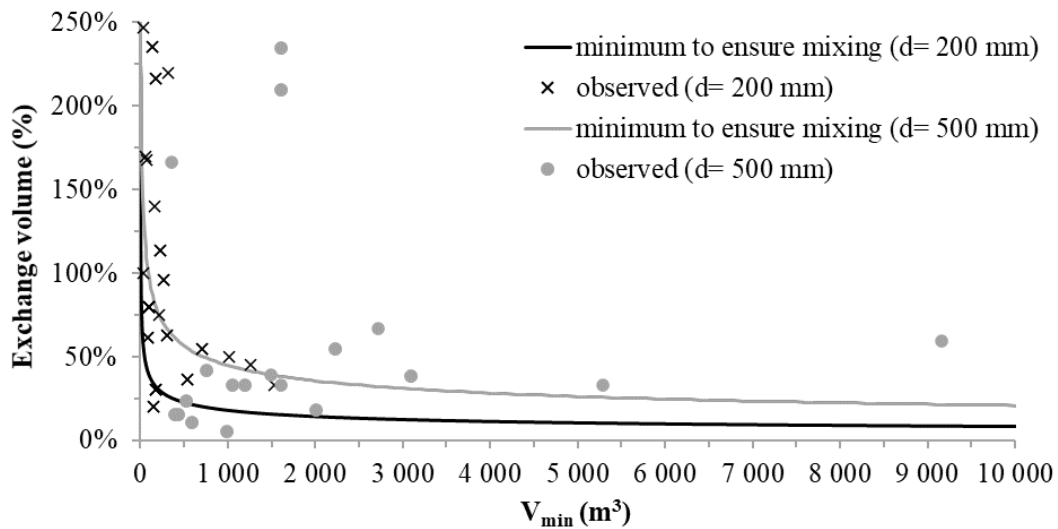


Figure 3.8 – Relationship between mixing time, inlet flow and volume in circular cross-section tanks.

### 3.8 Relevant results for the research

Existing drinking water storage tanks in Portugal have several configurations and dimensions. Tanks with rectangular and quadrangular cross-sections are more frequent in tanks with larger volumes, and circular cross-section shapes are often used for smaller to medium tank volumes. The tanks are operated almost full, being the level variation in a filling/drawing cycle small, with  $H_{min}/H_{max}$  ratio between 60% and 70%. The mixing times were, for the first time, estimated for tanks in Portugal, predominantly varying between 1 to 2 h (27%). In over 70% of the tanks, the volume of water entering the tank in each filling cycle suffices to mix completely the incoming water with that already stored. However, in many of these tanks, this mixing is only possible when the water level varies between the minimum and the maximum operational level in a single filling cycle. The study also shows that some water utilities are unaware of the structural and operational characteristics of their tanks, which emphasizes the need to create and maintain up-to-date databases with records of the main tank characteristics.



# Chapter 4

---

## Water mixing and renewal in circular cross-section storage tanks

This chapter is based on the following scientific publication in a peer-review journal:

**Pinheiro, A.,** Monteiro, L., Carneiro, J., Almeida, M.C., Covas, D. (2021) Water mixing and renewal in circular cross-section storage tanks as influenced by configuration and operational conditions. *Journal of Hydraulic Engineering* 147(12).

## 4.1 Introduction

The current chapter aims at analysing the effect of the tank configuration and the operating mode on water mixing and renewal processes in cylindrical (i.e., circular cross-section) storage tanks of typical configurations in Portugal, operated at steady-state and at variable water-level conditions, similar to the practice in water distribution systems. In particular, the study aims to show how the relative location of the inlet and outlet pipes, the flow rates, and the fraction of volume exchange in each fill-and-draw cycle affect water mixing and renewal. Additionally, the chapter presents an analysis to evaluate how much the degree of mixing in the tanks studied deviates from the fully mixed conditions to identify in which configurations and operational conditions the complete mixing assumption can be valid.

This chapter innovatively presents: i) the experimental study of mixing conditions in small-scale circular cross-section storage tanks for three tank configurations; ii) the analysis of the effect of the fill-and-draw cycles on the water mixing and renewal; and iii) a new empirical formula for estimating the turnover time in circular cross-section tanks operated at a constant level.

## 4.2 Materials and methods

### 4.2.1 Experimental facility

Experiments were carried out in a laboratory facility designed for developing tracer tests in small-scale storage tanks (Figure 4.1) and determining the water residence time distribution (RTD). The tank was gravity fed, either with deionized water (conductivity  $< 2 \mu\text{Scm}^{-1}$ ) or with a tracer solution from two secondary tanks positioned at a higher level. These tanks had a free inflow and an overflow weir, thus maintaining a relatively constant hydrostatic head. This layout allowed for step input tracer tests to be conducted, which consisted of continuously injecting a NaCl solution ( $0.05 \text{ gL}^{-1}$ ) at the inlet of the tank and of monitoring the tracer concentration at its outlet. A control valve located immediately upstream of the tank was manually operated to regulate the inflow rate. The outflow was controlled by three peristaltic pumps in parallel (FWT Model VPER Type 4-3). Conductivity probes were installed at the inlet (YSI, 556 MPS) and outlet (YSI, Pro 30) pipes. A small hydropneumatic vessel (0.8 L), was used to dampen the pulsation of

pumps in the sensor compartment. Flow rates were measured using a graduated cylinder. Further photos of the experimental facility are presented in Figure A.1 in Appendix A.

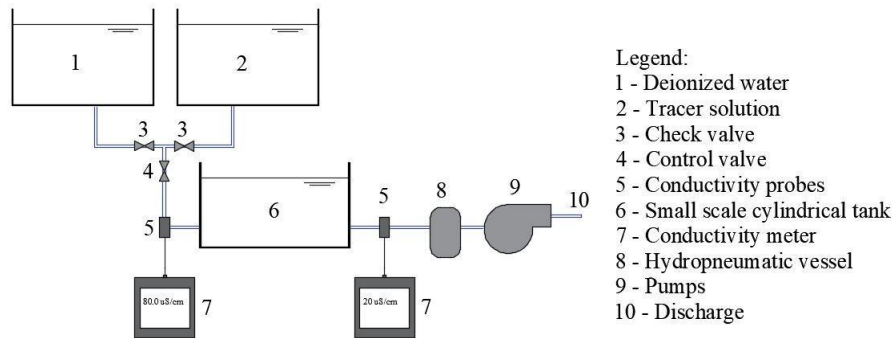


Figure 4.1 – Schematic of the experimental facility.

The small-scale tanks used are 1:100 cylindrical tanks prototypes of acrylic with 392 mm diameter and a maximum water-depth-to-tank-diameter ratio of 0.15. The tank dimensions were determined by down-scaling sizes and shapes of drinking water storage tanks common in Portugal (Monteiro et al. 2021) for the 1:100 geometric scale.

Three different inlet/outlet pipe configurations were tested (internal diameter = 4 mm). In all tested configurations, an inlet pipe was located 14 mm above the maximum water level (70 mm). Configuration A has an outflow pipe at the opposite side of the tank, aligned with the inlet pipe, and located 4 mm above the bottom (Figure 4.2a). In Configuration B, the outlet pipe is near the inlet pipe, with a circumference arc length of 30 mm and 4 mm above the bottom (Figure 4.2b). In Configuration C, the inlet/outlet pipes location was the same as in Configuration B, but an acrylic baffle of 75% of the tank diameter and 4 mm of thickness was included (Figure 4.2c).

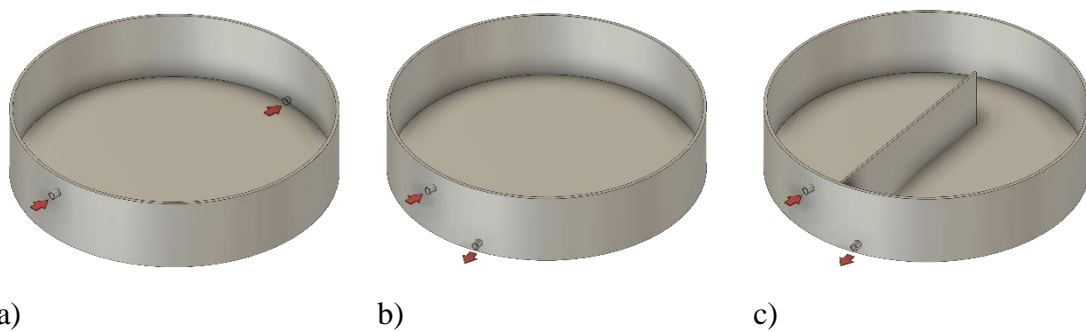


Figure 4.2 – Tested small-scale tanks: a) Configuration A; b) Configuration B; c) Configuration C.

### 4.2.2 Experimental procedure

Three configurations were tested under two different operational modes: mode 1 at steady-state conditions with a fixed water level and four flow rates; and mode 2 with fill-and-draw cycles with different operational levels and flow rates. The operational conditions of all experimental tests are presented in Table 4.1. The tests consisted of a step injection of NaCl in the tank and on the monitoring of its concentration in the outflow.

In operational mode 1, deionized water was introduced into the small-scale tank to the set height (60 mm) and both inlet and outlet were set at the same flow rate. The system was run for 30 minutes, allowing the flow within the small-scale tank to reach a steady-state. Then, the feed was changed to the tracer solution. The experiments lasted until the conductivity in the effluent differed from that in the inflowing water by less than 5%, which took between 4 to 6 hours, depending on the flow rate. The flow rates used were grouped into four categories: Q1 ranging from 5.1 to 5.4 Lh<sup>-1</sup>; Q2 from 7.3 to 7.4 Lh<sup>-1</sup>; Q3 from 9.1 to 9.4 Lh<sup>-1</sup>; and Q4 11.6 Lh<sup>-1</sup> (Table 4.1). In this operating mode, 12 tests were carried out in triplicate. To visualize flow paths and tracer distribution under mode 1 conditions, tracer tests were also performed with Rhodamine WT 20% at a 1:50 000 dilution. A video camera (GoPro) was installed over the tank for image acquisition during the tests.

The operational mode 2 mimics the most common operation scheme of storage tanks in water supply systems, with successive fill-and-draw cycles. In this mode, a variable outflow pattern with four steps (Figure 4.3) was adopted as a proxy of the daily demand cycle of a water distribution system. In this mode, a constant inflow rate was applied until defined water level was reached (filling period). Tank filling was resumed when a set minimum water level was attained. During this fill-and-draw mode, the water was continuously drawn out via the outlet pipe at variable flow rates according to the consumption pattern. The experimental procedure for these tests started by running one fill-and-draw cycle with deionized water only. Tracer injection started at the beginning of the filling period and three minimum water levels were tested (20%, 50% and 80% of the maximum water level) which corresponded to volume variations of 80%, 50% and 20%, respectively. Each experimental test lasted between 7 and 10 hours. In operating



mode 2, three tests were carried out in triplicate, with the fill and draw rates listed in Table 4.1.

Table 4.1 – Operational conditions tested.

Parameters	Operational conditions	
	Mode 1	Mode 2
Flow rate (L/h)	Q1 (5.1 or 5.4); Q2 (7.3 or 7.4); Q3 (9.1 or 9.4); Q4 (11.6)	Inlet: 9.0 Outlet: 1.5, 3.0, 4.5
Water level (mm)	60	Maximum: 70 Minimum: 14, 35, 56
Tracer solution conductivity ( $\mu\text{S}/\text{cm}$ ) at 25°	80 – 300	280 – 310
Inflow and outflow water temperature difference (°C)	0 – 1	0 – 2
Water temperature variation over time for each test (°C)	0.4 – 2.2	0.4 – 1.5
Jet flow Reynolds number	446 – 1 007	788
Jet momentum flux, $M = u \times Q$ ( $\text{m}^4/\text{s}^2$ )	$1.6 \times 10^{-7} - 8.1 \times 10^{-7}$	$5.0 \times 10^{-7}$

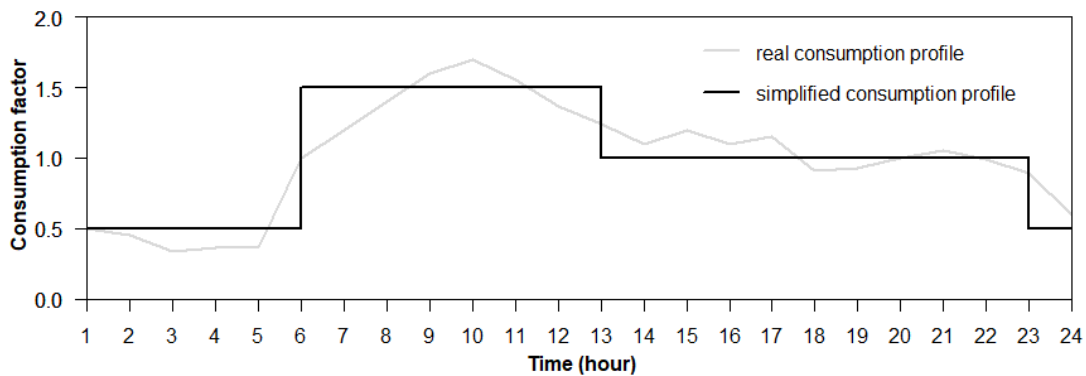


Figure 4.3 – Daily water consumption profile.

### 4.2.3 Data treatment and analysis

#### 4.2.3.1 Residence time distribution and hydraulic indexes

The tracer concentration in the outlet pipe  $C(t)$  was normalized to obtain the non-dimensional cumulative distribution function  $F(t)$  (Eq. 2.5), where  $C_0$  is the tracer concentration in the inlet pipe. The residence time distribution function,  $E(t)$ , was calculated by differentiating  $F(t)$  (Fogler 2016) (Eq. 2.6).

The RTD function,  $E(t)$ , represents the time spent by the different fluid elements inside the tank;  $E(t)$  is the distribution of ages of the fluid elements that comprise the effluent stream, which has been inside the tank for different time periods, depending on the pathway they took inside the tank. The area under the  $E(t)$  curve, at any time  $t$ , is the percentage of fluid elements that remained in the tank for a period of less than  $t$ .

In operational mode 1, both  $F(t)$  and  $E(t)$  were calculated, whereas, in operational mode 2, only  $F(t)$  was determined because of the variable water volume in the tank.

To compare the RTD calculated for different operating conditions,  $F(t)$  and  $E(t)$  can also be described as a function of the normalized time,  $\theta$ , defined as follows (Eq. 4.1):

$$\theta = \frac{t}{\tau} \quad \text{Eq. 4.1}$$

where  $\tau$  is the theoretical residence time given by the ratio between the effective volume of fluid inside the tank,  $V$ , and the flow rate,  $Q$  (Eq. 4.2).

$$\tau = \frac{V}{Q} \quad \text{Eq. 4.2}$$

Functions  $F(\theta)$  and  $E(\theta)$  are also determined for an ideal continuous stirred tank reactor (CSTR) of the same volume (see 4.2.3.2), to allow for a comparison of the results with the complete mixing assumption.

To characterize each RTD, its moments are also determined. The first moment of the RTD function,  $t'$ , is the mean residence time spent in the tank by the effluent fluid elements (Eq. 4.3).

$$t' = \int_0^{\infty} tE(t)dt \quad \text{Eq. 4.3}$$

In fully mixed tanks, the mean residence time equals the theoretical residence time ( $t' = \tau$ ).

The variance, or the second moment of the RTD,  $\sigma^2$ , is a measure of the dispersion of the distribution (Eq. 4.4).

$$\sigma^2 = \int_0^{\infty} (t - t')^2 E(t) dt \quad \text{Eq. 4.4}$$

Other hydraulic indexes extracted from RTD functions are used to assess short-circuiting and mixing in water tanks (Teixeira and Siqueira 2008). In the present work, the short-circuiting indicator used is time  $t_{10}$  which refers to the time needed for 10% of the injected tracer particles to leave the tank. This indicator is related to the advection of the tracer front and to the amount of fluid that leaves the tank through preferential paths. Very short  $t_{10}$  values (less than 20% of the theoretical residence time) indicate that 10% of the fluid reaches the exit very quickly without effective mixing and denotes short-circuiting.

Regarding mixing indexes, the dispersion and the Morrill indexes are used. Mixing indexes are intended to represent the random spreading of the fluid elements in the tanks, whether due to advection or to other effects that can cause the spreading or the retention of the tracer, (e.g., recirculation and dead zones) and, thus, the mixing indexes are measures of the dispersion of the RTD.

The dispersion index,  $\bar{\sigma}$ , is the ratio between the temporal variance of the RTD function,  $\sigma^2$ , and the squared mean residence time  $t'^2$ . This index takes the value of 1 in completely mixed tanks and the value of 0 in close to plug flow conditions. The dispersion index has been recommended for assessing mixing, because it is closely related to the physical phenomenon it represents and for its wide use in kinetic reaction models, although it presents high variability for low mixing levels (Teixeira and Siqueira 2008). The Morrill index is defined as the ratio between  $t_{90}$  and  $t_{10}$ , i.e., the ratio between the time needed for 90% and 10% of the injected tracer particles to leave the tank. The Morrill index is approximately 22 for a CSTR and 1 for a plug flow reactor. The Morrill index is particularly useful in situations with very low mixing, avoiding misleading conclusions from the analysis of the dispersion index only (Teixeira and Siqueira 2008).

To estimate the time required for the water stored inside a tank to be completely replaced by fresh water, the turnover coefficient,  $\alpha$ , is used (Eq. 4.5).

$$\alpha = 1 - \frac{C(t)}{C_0} = 1 - F(t) \quad \text{Eq. 4.5}$$

The time for total water replacement (turnover time),  $t_T$ , was assumed as the time for which the turnover coefficient  $\alpha$  becomes less than 0.05 (i.e., the time to have  $F(t) = 0.95$ ). Turnover times were estimated for the three tanks operated in the two modes.

#### 4.2.3.2 Ideal reactor residence time distribution and indexes

Tanks operated at steady-state conditions (constant water level) can be compared to ideal CSTR. In a CSTR, the fluid entering the reactor completely mixes with the fluid that is on the inside. That is, some of the fluid elements entering the CSTR leave it almost immediately, while others remain in the reactor almost forever. This is because the fluid elements are never removed from the reactor at one time. Many fluid elements leave the reactor after spending a period of time close to the mean residence time.

The cumulative distribution function,  $F(t)$ , and the residence time distribution function,  $E(t)$ , for an ideal CSTR are known and given by the following equations (Fogler, 2006):

$$F(t) = 1 - e^{-t/\tau} \quad \text{Eq. 4.6}$$

$$E(t) = \frac{1}{\tau} e^{-t/\tau} \quad \text{Eq. 4.7}$$

where  $\tau$  is the theoretical residence time, given by  $V/Q$  (i.e., obtained by dividing the reactor volume,  $V$ , by the volumetric flow rate,  $Q$ ). The normalized forms of  $F(t)$  and  $E(t)$  functions are given by:

$$F(\theta) = 1 - e^{-\theta} \quad \text{Eq. 4.8}$$

$$E(\theta) = \tau E(t) = e^{-\theta} \quad \text{Eq. 4.9}$$

$F(t)$  function can be computed from Eq. 4.6, for a time range, once known the theoretical residence time in the tank. From  $F(t)$  values, the indexes  $t_{10}$  and  $t_{90}$  can be obtained, as these correspond to the time it takes for  $F(t)$  to reach 0.10 and 0.90, respectively. Then,  $E(t)$  values can be computed over time by Eq. 4.9.

For an ideal CSTR, the theoretical residence time ( $\tau$ ) is also the mean residence time ( $\bar{t}$ ). The variance of  $E(t)$ ,  $\sigma^2$ , which is a measure of the spread of the residence time distribution, is equal to the square of the theoretical residence time ( $\sigma^2 = \tau^2 = \bar{t}^2$ ).

The dispersion index,  $\bar{\sigma}$ , which is a measure of the mixing in reactors, is defined as the ratio between the temporal variance of the RTD function,  $\sigma^2$ , and the squared mean residence time,  $t^2$ . Thus, it takes the value of 1 in a fully mixed CSTR. On the opposite, the dispersion index takes a value of 0 in a plug flow reactor (PFR), where there is no variance in the residence time distribution, as all fluid elements spend exactly the same time in the reactor. The closer to the dispersion index is, the closer a tank is to a fully mixed regime.

The *Morrill* index, defined as the ratio between  $t_{90}$  and  $t_{10}$ , i.e., the ratio between the time needed for 90% and 10% of the injected tracer particles to leave the tank, is also a measure of the dispersion of the RTD. The *Morrill* index is approximately 22 in fully mixed CSTR, that is,  $t_{90}$  is approximately 22 times  $t_{10}$ . In a reactor with close to plug flow conditions, the  $F(t)$  curve is steeper,  $t_{90}$  and  $t_{10}$  values are closer and the ratio  $t_{90}/t_{10}$  approaches to unity.

#### 4.2.3.3 Preliminary data treatment

A preliminary data treatment was carried out using R Studio software. First, a temperature correction was applied to conductivity time series, using a non-linear correction to 25°C (ISO 7888, 1985). Conductivity time series were converted to NaCl concentrations series through standard curves. Then, the reproducibility of the results for the three repetitions of each test was verified. Cumulative functions were then determined for every repetition. A single cumulative distribution function was then calculated for each test using median values. Kernel regression technique (Nadaraya-Watson kernel regression) was applied to  $F(t)$  to remove the noise from the experimental data. Three different values of smoothing parameter “bandwidth” in the Nadaraya-Watson estimator were tested. The application of various bandwidth values (2, 4 and 6) did not result in significant changes in the values of  $t'$  or  $t_{10}$ , so the intermediate value was chosen. This value was applied to all data sets. Figure 4.4 presents an example of the data treatment applied to the experimental results.

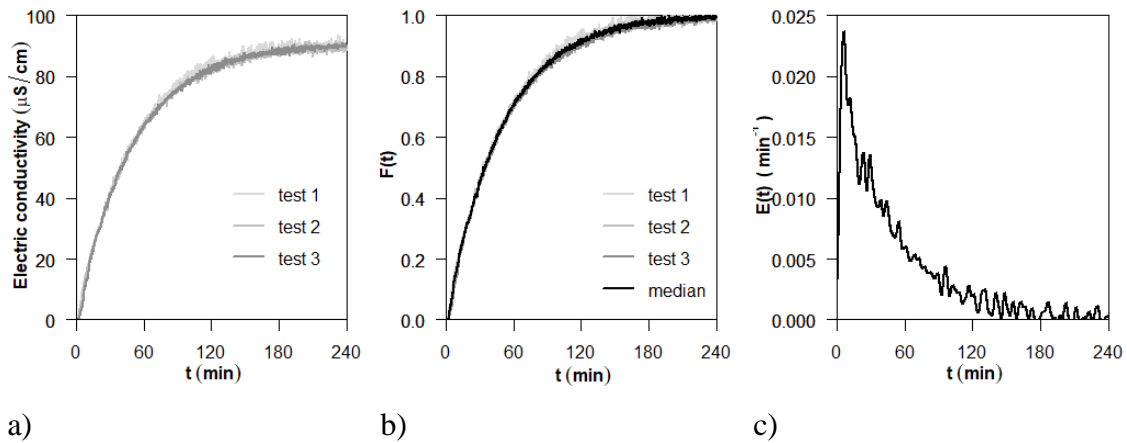


Figure 4.4 – Data treatment sequence: a) electric conductivity measured at the outflow pipe; b) cumulative distribution curves for all tests and median curve; c) obtained residence time distribution curve. Presented results are for Configuration A at Mode 1 and  $Q3$ .

### 4.3 Results

#### 4.3.1 Qualitative assessment of preferential flow paths

Recorded images of the movement of dye tracer solution provided a general qualitative understanding of the preferential flow paths within the three small-scale tanks in mode 1. Figure 4.5 shows the evolution of the dye tracer at three instants after the beginning of the injection (1, 5, and 10 minutes) for the three tested configurations. These images depict different slow mix zones that contain low tracer concentrations over time. When mixing is poor, then areas with low concentration coexist with others with higher concentration.

The structural symmetry of the Configuration A develops a symmetrical flow with two plumes close to the sides of the tank and a return of part of the fluid through the central zone forming two water pockets that mix slowly with the inflow tracer solution. The proximity of the inlet and outlet pipes in Configuration B creates an asymmetry in the flow. Part of the fluid entering the tank is directed to the outflow, not mixing with the existent water in the tank. In Configuration C, the existence of a baffle separating the inlet and outlet pipes causes longer flow paths inside the tank. This baffle promotes recirculation in the first half of the tank, thus delaying the dye from reaching the second half and the outflow pipe. These results allow a better understanding and interpretation of tracer tests with NaCl but offer limited information since only the top water layer is observed.

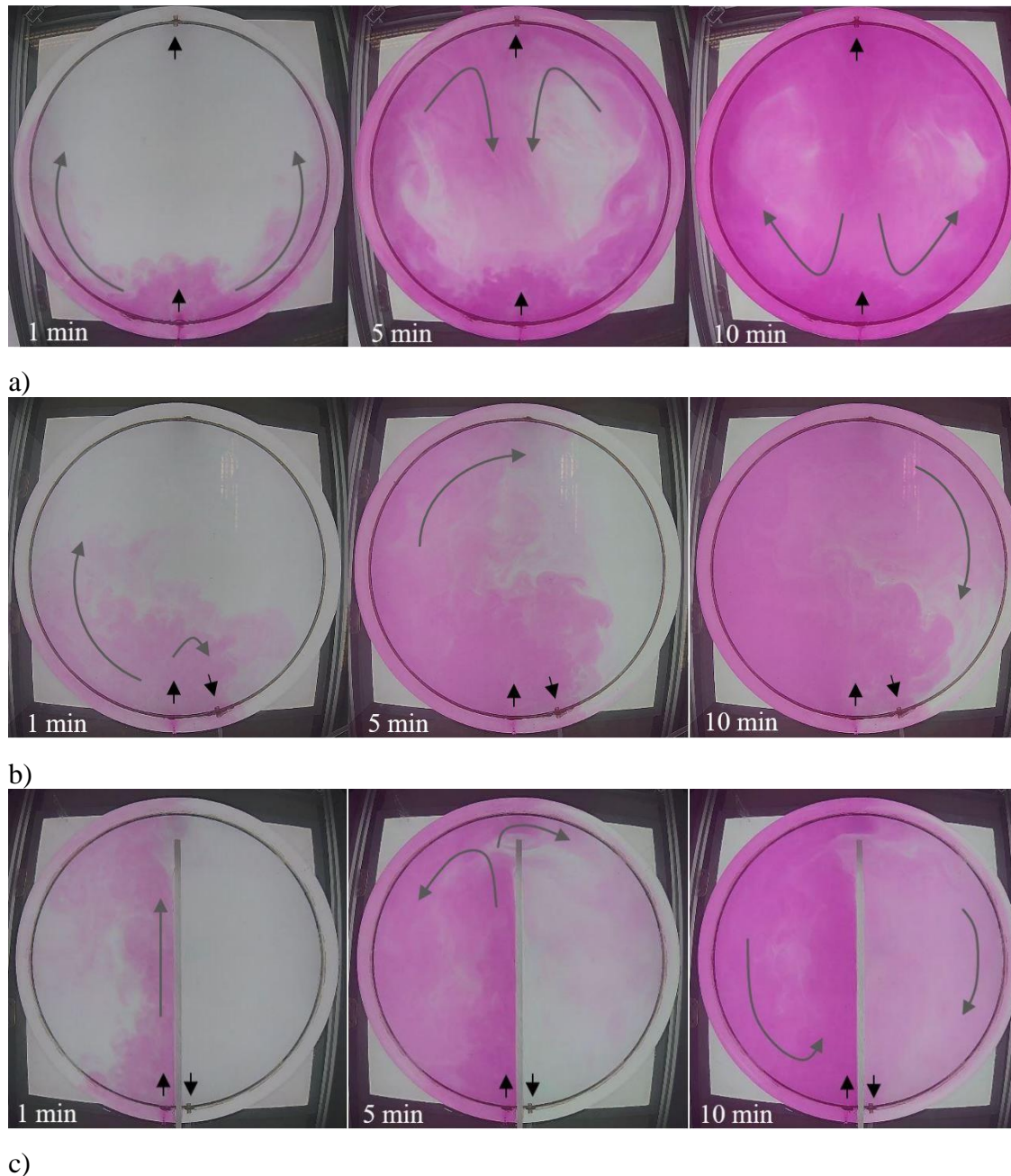


Figure 4.5 – Rhodamine dispersion within the three configurations at 1, 5, and 10 min after injection (constant water level, flow rate  $Q3$ ): a) Configuration A; b) Configuration B; c) Configuration C.

### 4.3.2 Mixing at steady-state conditions

#### 4.3.2.1 Residence time distribution

The cumulative distribution  $F(\theta)$  and the residence time distribution  $E(\theta)$  were determined for the tanks of Configurations A, B and C operated at mode 1 conditions and for the four tested flow rates ( $Q1$  to  $Q4$ ) (Figure 4.6). Overall, differences in  $F(\theta)$  and  $E(\theta)$  profiles are observed, showing that the tank configuration affects the residence time

distribution in the tanks. Also,  $F(\theta)$  profiles present a similar trend to that of a completely mixed tank, with observable deviations at the initial and final stages of the tracer injection, indicating different degrees of short-circuiting and of stagnation, respectively (Figure 4.6a, c, e, g). Those deviations from ideal mixed conditions are clearer in the bumpy  $E(\theta)$  profiles (Figure 4.6b, d, f, h).

The baffled tank (Configuration C) presents the highest deviation from the completely mixed conditions, as expected. The delayed and sharp increase in  $F(\theta)$  at initial times denotes a some-what close to plug flow regime in the tank. This fast increase in  $F(\theta)$  is also observed in  $E(\theta)$  as a single and narrow peak in the first minutes of the tracer tests. The peak also means that many tracer molecules reach the outlet at the same time in Configuration C. The baffle prevents the inflowing jet to mix with half of the water in the tank that is on the other side of the wall, promoting the formation of two compartments within the tank that hardly mix.

For the tank with the closely located inlet and outlet pipes (Configuration B),  $F(\theta)$  shows that poor mixing and stagnation occurs at all flow rates tested, as  $F(\theta)$  curve is under the CSTR one at times above the theoretical residence time ( $\theta > 1$ ). Also, it takes more time for  $F(\theta)$  to reach close to one values in Configuration B than for any other. In some tests, this is never reached, meaning that part of the initial water volume in the tank was not completely replaced by the tracer solution. This suggests that pockets of older water remain in the tank. In a full-scale tank operated under similar conditions, this means that dead zones of aged water and very different disinfectant concentrations are likely to be found within the tank. At the highest flow rates ( $Q4$ ),  $F(\theta)$  increases faster than the cumulative function for the completely mixed tank, particularly at the beginning of the tracer test ( $\theta < 1$ ), showing that the injected tracer reaches the outlet pipe quickly, without effective mixing. This  $F(\theta)$  feature, which results in the first peak in  $E(\theta)$ , is an indicator of a high short-circuiting in the tank. The second peak in  $E(\theta)$  and the following are likely associated with the release of the entrapped tracer in internal circulation zones (Figure 4.5b).



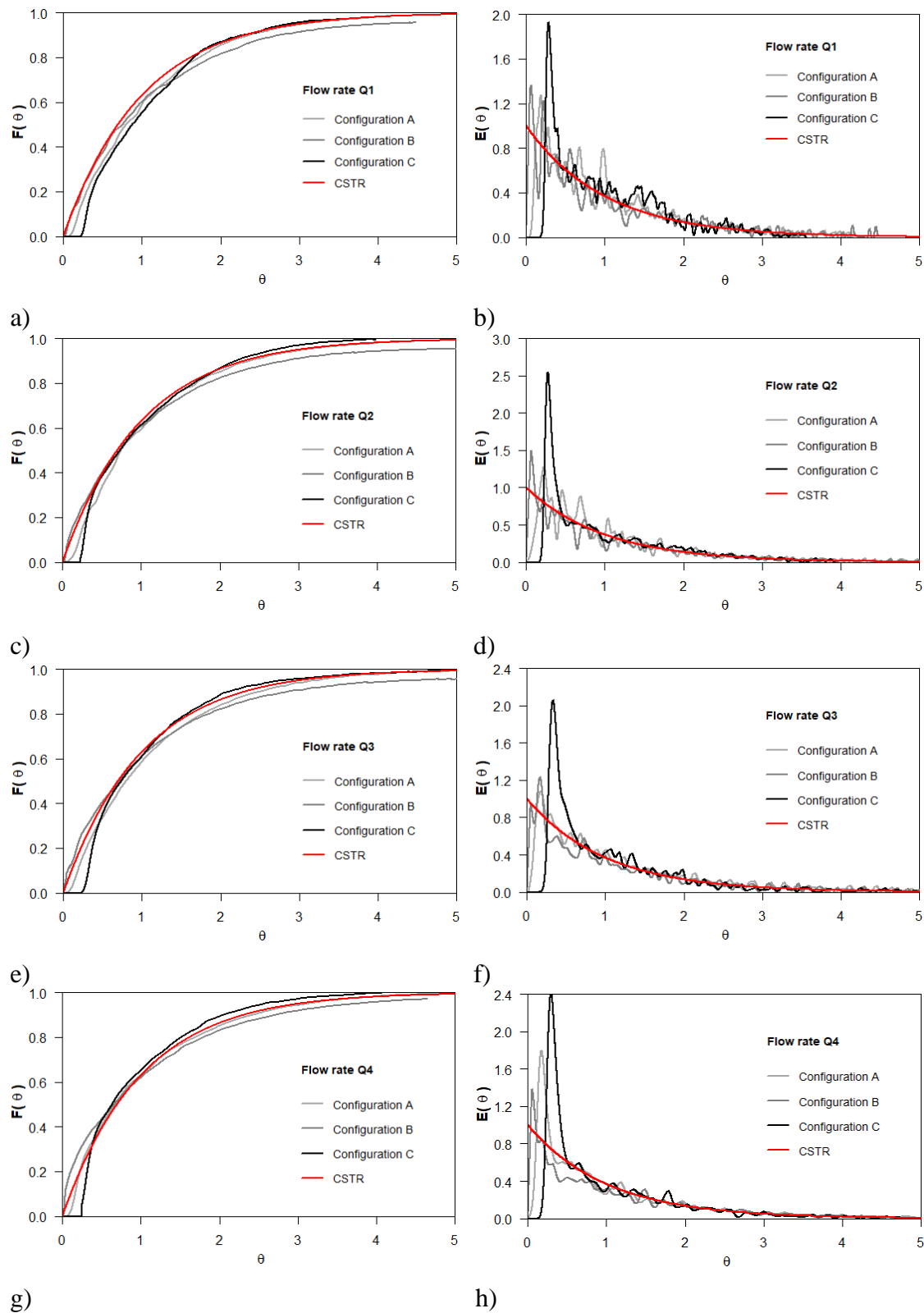


Figure 4.6 – Normalized cumulative distribution and residence time distribution for the three storage tank configurations at steady-state conditions and flow rate: (a and b)  $Q1$ ; (c and d)  $Q2$ ; (e and f)  $Q3$ ; (g and h)  $Q4$ . Plots (a,c,e, and g) show the normalized cumulative distribution, and plots (b,d,f, and h) show the residence time distribution.

The tank with the inlet and outlet pipes at opposite walls (Configuration A) presents a mixing behaviour similar to completely mixed tank, even if it has no active mixing devices and relies only on the inlet jet momentum. At  $\theta$  higher than 2,  $F(\theta)$  curves for Configuration A are similar to those for Configuration C and water renewal in both tanks is reached almost simultaneously, despite the different flow paths.

The effect of inflow momentum flux on mixing in each tank is assessed by comparing the distribution curves (Figure 4.7) and the mean residence times ( $t'$ ) for flow rates  $Q1$  to  $Q4$  (Table 4.2). The normalized RTD functions at different inlet flow rates present similar profiles, showing that the tested momentum flux range did not significantly change mixing within the tanks, except for Configuration A (Figure 4.7b) where the first peak increases with the flow rate. In this configuration, because of the opposite locations of the inlet and outlet pipes, a higher jet momentum flux may direct the inlet flow further into the tank and closer to the outlet pipe, promoting the tracer exit and reducing mixing in the tank. Increasing the flow rates makes the mean residence time ( $t'$ ) to approach the theoretical residence time ( $\tau$ ) (Table 4.2), because of diminished dispersion effects (Fogler 2016). Comparing  $t'$  obtained experimentally with the theoretical value  $\tau$ , differences are observed for all configurations and flow rates tested. In the case of Configuration A,  $t'$  values are higher than  $\tau$ , most probably because of the swirl movement observed (Figure 4.5a) that results in longer flow paths and, thus, in higher residence times. In contrast, in Configuration B, a large part of the fluid entering the tank leaves almost immediately, which results in a mean residence time lower than  $\tau$ . Similar observations in a cylindrical tank suffering from short-circuiting are described by Montoya-Pachongo et al. (2016). In the baffled tank (Configuration C), the mean and the theoretical values are very similar, showing that dispersion effects are negligible.

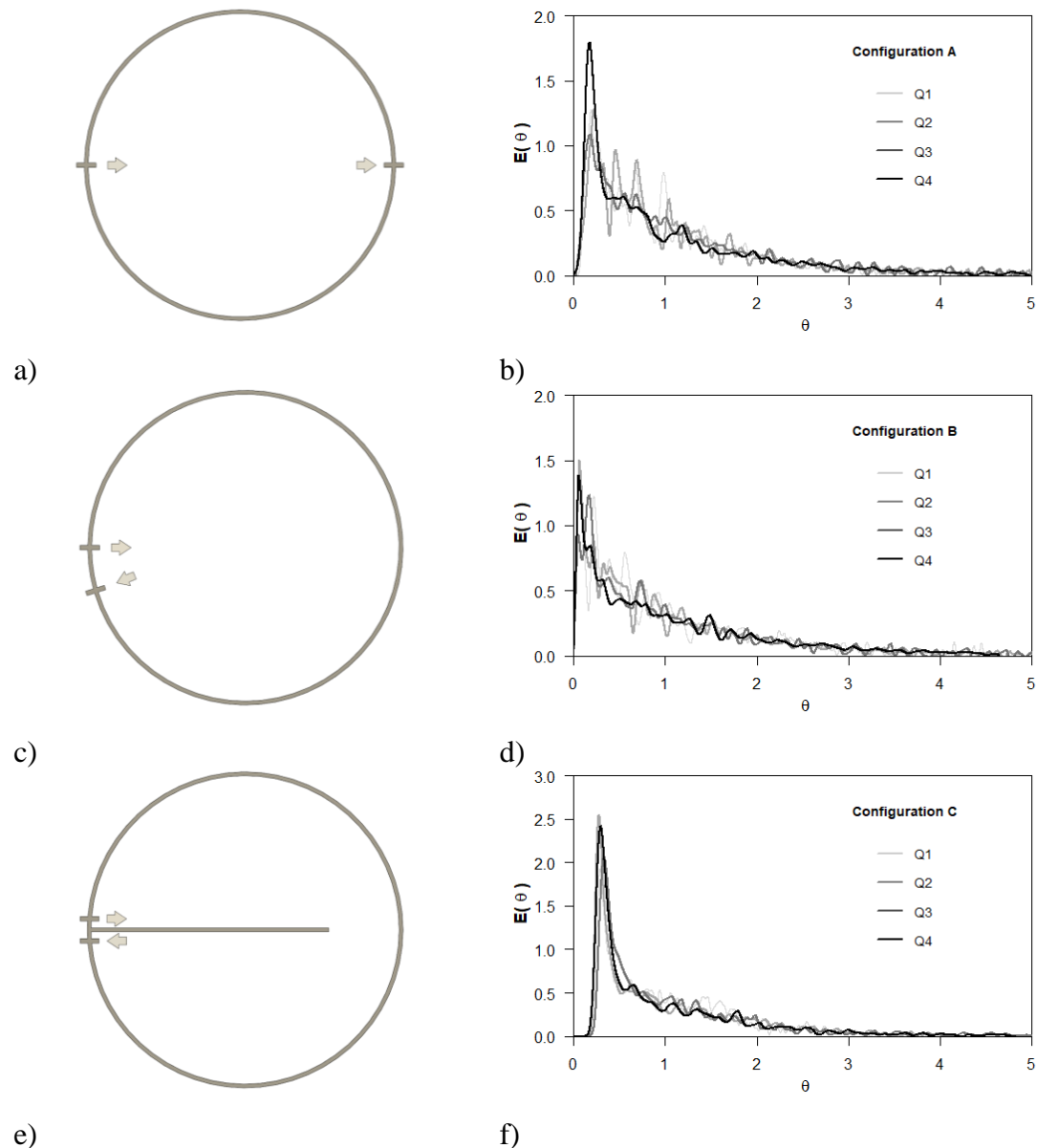


Figure 4.7 – Normalized residence time distribution for each configuration and different flow rates tested: (a and b) Configuration A; (c and d) Configuration B; (e and f) Configuration C. Plots (a, c, and e) show the small-scale tanks plan view, and plots (b, d, and f) show the normalized residence time distribution.

#### 4.3.2.2 Short-circuiting and mixing

Short-circuiting and mixing indexes for the three tanks at steady-state conditions are presented in Table 4.2. Configuration B exhibits the lowest  $t_{10}$  values compared with the other configurations. In this tank, 10% of the injected tracer reaches the outlet pipe very quickly, in less time than needed for the same amount of tracer to leave a CSTR, denoting short-circuiting. For the higher flow rates tested ( $9.2$  and  $11.6 \text{ Lh}^{-1}$ ),  $t_{10}$  is about half or less of that of a completely mixed tank, in agreement with Boulos et al. (1996) observations in a full-scale cylindrical tank of identical configuration. The low  $t_{10}$  values

( $\theta_{10} \leq 0.1$ ) are also in agreement with those obtained by Moncho-Esteve et al. (2015) for a simulated rectangular tank with similar pipe configuration and steady-state conditions. For Configuration A,  $t_{10}$  is higher than for the CSTR, because of recirculation within the tank. This short-circuiting index presents the highest values for the baffled tank, much higher than those for the completely mixed tank, denoting the delayed exit of the tracer from the tank.

The spread of the RTD for Configuration B, assessed through  $\bar{\sigma}$ , is also the highest observed (Table 4.2), which indicates that flow paths within the tank are quite diverse. This is probably the result of internal recirculation and the formation of stagnation zones, promoted by the relative position of the inlet and outlet pipes. The dispersion index  $\bar{\sigma}$  presents values close to 1, which is a characteristic of a CSTR and could suggest that close to perfect mixing conditions can be found in tanks of Configuration B. However, all other indexes indicate that mixing in Configuration B is far from perfect, namely  $t_{10}$ ,  $t_{95}$  and  $Mo$  (Table 4.2). Morrill values (27 to 70) even surpass those of a perfectly mixed tank (22), which does not indicate that a more than perfectly mixed regime is achieved, instead, it shows that bypassing and stagnation phenomena are severe, increasing the spread of the residence time distribution. These results demonstrate that the effluent water of cylindrical storage tanks with inlet and outlet pipes located very closely is composed of fluid elements that have spent very different residence times within the tank. In addition, the results indicate that mixing assessment in the tanks should not rely on a single mixing index to avoid misleading conclusions, as previously stated by Teixeira and Siqueira (2008).

The tank with the inlet and outlet pipes in opposite walls exhibits high dispersion indexes, reaching values close to 1 and, thus, close to perfect mixing, at the highest flow rate (Table 4.2).  $Mo$  values range from 11 to 18, which is below but close to the ideal value of 22. For such tanks, both mixing indexes indicate that close to ideal mixing conditions can be achieved with an adequate inlet flow rate. Configuration C presents the lowest  $\bar{\sigma}$  and, thus, the lowest degree of mixing, particularly at the lower flow rates. The Morrill index also shows that a lower degree of mixing is achieved in the tank with the baffle (Configuration C) than in the one without the baffle (Configuration A), as  $Mo$  values are lower for tank C. These results agree with previous observations of lower  $\bar{\sigma}$  and  $Mo$  in baffled tanks, than in non-baffled tanks (Angeloudis et al. 2014).

Table 4.2 – Hydraulic indexes for the three configurations in steady-state conditions.

Config.	$Q$ (L/h)	$\tau$ (min)	$t'$ (min)	$t_{10}$ (min) [ $\theta_{10}$ ]	$t_{95}$ (min)	$\bar{\sigma}$ (-)	$Mo$ (-)	$t_{10}$ CSTR (min)	$t_{95}$ CSTR (min)
<b>A</b>	5.1	85.2	87.7	16.5 [0.19]	264	0.7	12	9.0	255
	7.4	58.7	61.1	12.3 [0.21]	180	0.8	11	6.2	176
	9.4	46.2	47.3	8.5 [0.18]	147	0.8	18	4.9	138
	11.6	37.5	37.7	6.1 [0.16]	116	0.9	15	4.0	112
<b>B</b>	5.4	80.5	76.4	8.0 [0.10]	328	0.9	27	8.5	241
	7.4	58.7	54.7	4.4 [0.08]	258	1.0	36	6.2	176
	9.2	47.2	44.1	2.6 [0.06]	211	1.1	46	5.0	141
	11.6	37.5	33.9	1.4 [0.04]	140	1.1	70	4.0	112
<b>C</b>	5.2	83.6	83.4	24.7 [0.30]	240	0.5	8	8.8	250
	7.3	59.5	59.0	16.2 [0.27]	162	0.6	8	6.3	178
	9.1	47.7	48.8	15.3 [0.32]	132	0.7	7	5.0	143
	11.6	37.5	36.2	10.3 [0.27]	96	0.8	7	4.0	112

#### 4.3.2.3 Turnover time

Turnover time was determined from  $F(t)$  as the time needed to reach 95% of water renewal. Results show that turnover time decreases with increasing flow rate (Table 4.2), which contributes to the renewal process. Configuration C presents lower turnover times because of the high uniformity of the water pathways and low dispersion within the tank. Higher turnover times in Configuration B are due to the high spread of the residence time distribution. Configuration A presents turnover time values very similar to those obtained for a completely mixed tank. Since the water renewal in the tanks is associated with the mixing mechanisms, a relationship between the turnover time and the parameters in the mixing time formula of Rossman and Grayman (Eq. 2.1) was assessed. Figure 4.8 shows that the turnover time in the three configurations operating at a constant inflow and outflow rate is a linear function of  $V^{2/3}M^{-1/2}$ , as the mixing time in tanks during the filling period.

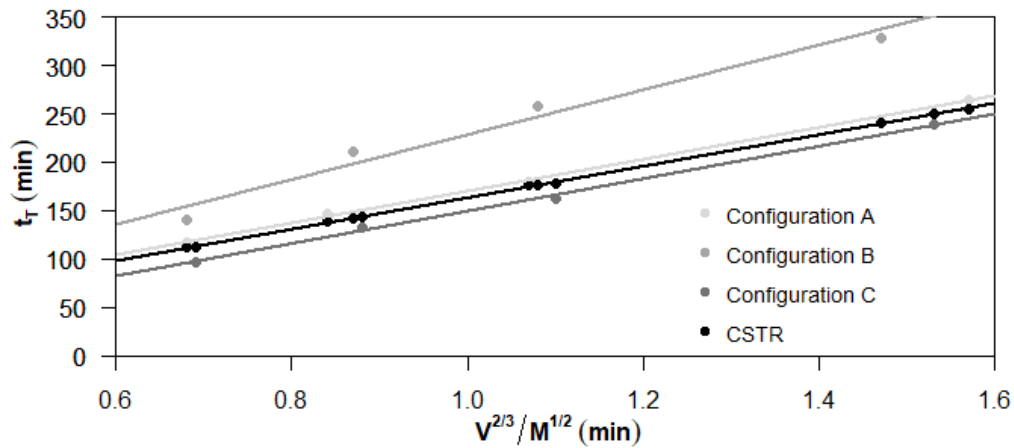


Figure 4.8 – Fit of Rossman and Grayman formula for turnover time for each configuration.

The estimated dimensionless constants  $k$  are much higher than 10 (Table 4.3), the dimensionless mixing time in Rossman and Grayman formula, which is in accordance with the increased time needed to renew the water inside the tanks. For Configurations A and C, the estimated values (169 and 152, respectively) are similar to that of a CSTR, while Configuration B presents a higher dimensionless turnover time. These results allow for the estimation of the turnover time for cylindrical water storage tanks with water-depth-to-tank-diameter ratios in order of 0.15 and operated with close to a constant level with the following formula:

$$t_T = \frac{kV^{2/3}}{M^{1/2}} \quad \text{Eq. 4.10}$$

where  $k$  is an empirical constant configuration-dependent, whose values are presented in Table 4.3.

Table 4.3 – Estimated dimensionless constant ( $k$ ) for each configuration.

Conf.	$k$ (-)	$R^2$
A	169	0.998
B	229	0.965
C	152	0.987
CSTR	163	0.999

### 4.3.3 Mixing at variable water levels

Tracer tests were carried out in the same tanks operated at variable water levels. Three levels of variation in tank volumes were tested (20%, 50% and 80%) and an outflow

pattern was used (Figure 4.3) to simulate real water storage tanks conditions. The inflow rate was either  $9.0 \text{ Lh}^{-1}$ , during the filling period, or null, while the water level was decreasing.

#### 4.3.3.1 Residence time distribution

Cumulative distribution functions show that the higher the water volume exchanged in each cycle, the fewer cycles are needed to renew the water inside the tanks (Figure 4.9b,d,f), regardless of the tank configuration, as expected. Results show that for 80% of volume variation, only two cycles are needed to replace completely the water inside the tanks with tracer solution (Figure 4.9e,f). Nine fill and draw cycles are needed to renew the water in the tanks when only 20% of the total volume is exchanged in each cycle.

In the first minutes after tracer injection,  $F(t)$  for the three configurations exhibit similar trends to those observed at steady-state conditions, which indicates that the same preferential flow paths prevail (Figure 4.9). After that,  $F(t)$  profiles at the variable water level are very different from the previous ones, increasing when there is inflowing water to the tank (water level rising) and remaining nearly constant or slightly decreasing when there is only outflow. Instead of a smooth increase over time,  $F(t)$  functions at variable water levels show a bumpy profile because of the intermittent inflow.

In general,  $F(t)$  curves for Configuration C are smoother than those of Configurations A and B (Figure 4.10). The  $F(t)$  profile is very similar for configurations A and B, although a peak in tracer concentration is observed at the beginning of the filling periods in Configuration B, which is likely because of the short-circuiting. This is particularly observed when the volume variation in each cycle is small (20%). After some fill and draw cycles, the difference between the inflowing concentration and the one in the tank becomes lower and the peak fades. For all configurations, a decrease in  $F(t)$  curve is observed in the emptying period, particularly in the first fill and draw cycle, when the exchange volume is small. This decrease in  $F(t)$  indicates that volumes of water of lower tracer concentration are reaching the outlet pipe, which demonstrates that the mixing promoted by the inlet jet during the filling period was insufficient, not ensuring a homogeneous tracer concentration.

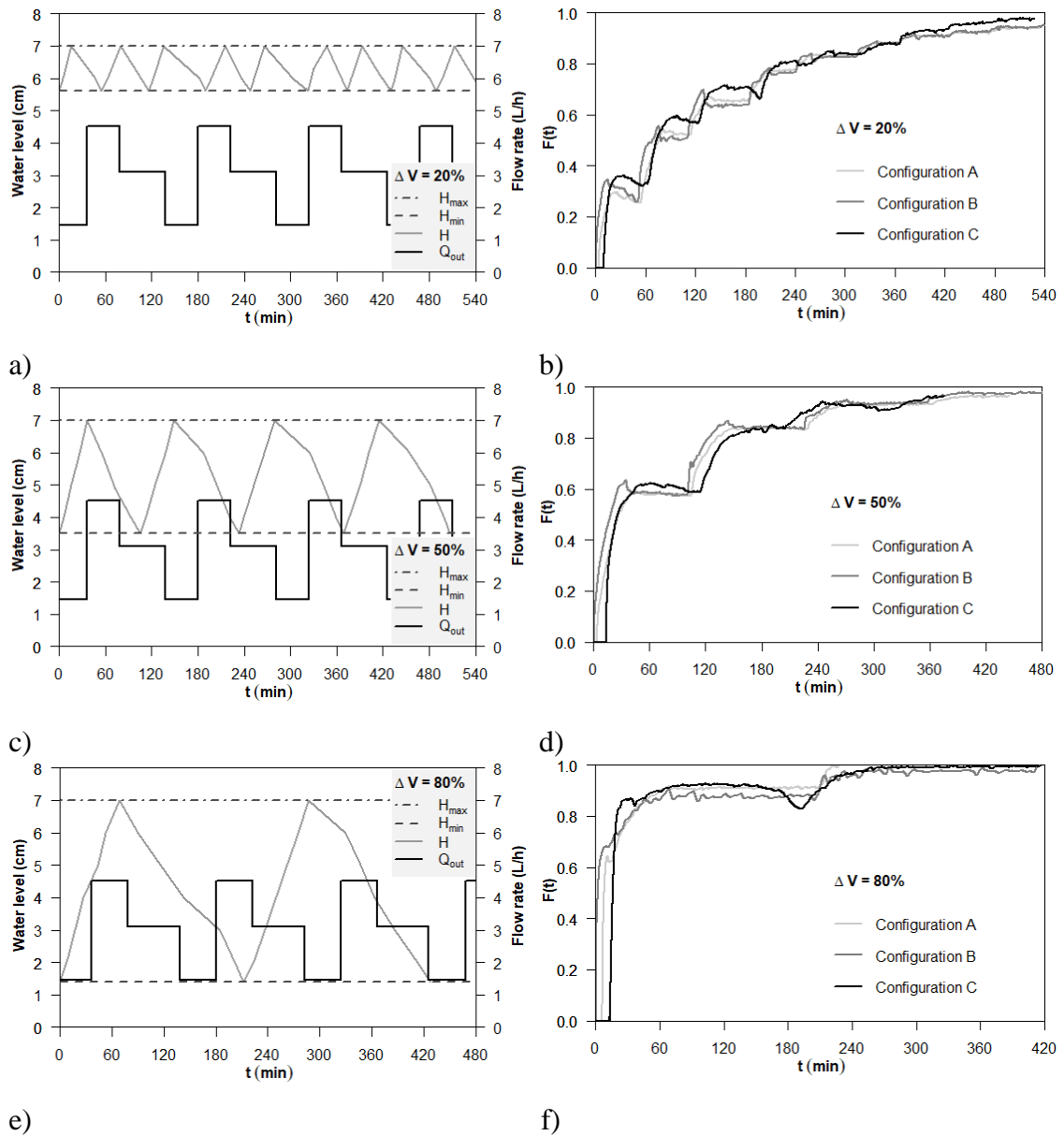


Figure 4.9 – Results of tracer tests at variable water level: (a, c, and e) water level and outflow rate variations; (b, d, and f) cumulative distribution curves.



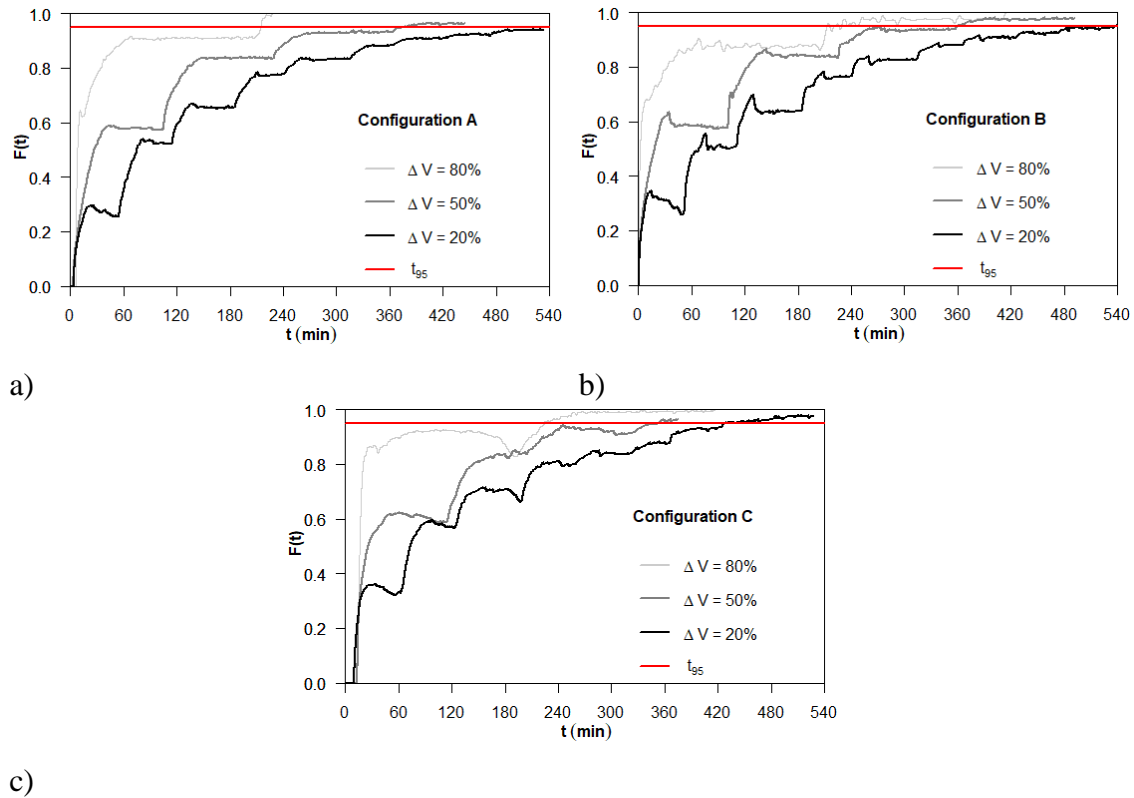


Figure 4.10 – Cumulative distribution curves obtain for each configuration operated at variable water level: a) Configuration A; Configuration B; c) Configuration C.

#### 4.3.3.2 Short-circuiting and mixing

The short-circuiting index  $t_{10}$  does not significantly vary with the volume exchange in each cycle and confirms the strongest short-circuiting effect in Configuration B (Table 4.4). When comparing  $t_{10}$  values with those estimated for steady-state conditions at  $Q3$  (which is similar to the inflow rate in the variable water level tests) (Table 4.2), a slight decrease in  $t_{10}$  is observed. It must be highlighted that  $t_{10}$  values are within the time range of the filling time of the first cycle (Table 4.4), which started at the lowest water level. In such conditions, the tracer was injected into a water volume that is smaller than that at the beginning of the steady-state tests. This apparently assisted the tracer in reaching the outlet pipe, even though the outflow rate at the beginning of the tests ( $1.5 \text{ Lh}^{-1}$ ) was less than that at the steady-state conditions (Table 4.1). These results suggest that operating the tanks at variable water levels can intensify existing short-circuiting effects, compared with what is observed in steady-state tests.

Table 4.4 – Hydraulic indexes for the three configurations at variable water level.

Config.	Volume variation $\Delta V$ (%)	Mixing Time (min)	Filling time (min)	10% arrival time $t_{10}$ (min)	Turnover time $t_{95}$ (min)	Morrill index $Mo$ (-)
<b>A</b>	20	8.6	15	5.6	610	69
	50	6.3	36	5.0	386	51
	80	3.4	70	6.5	230	35
<b>B</b>	20	8.6	15	1.5	555	254
	50	6.3	36	1.1	370	223
	80	3.4	70	1.0	235	215
<b>C</b>	20	8.6	15	11.3	436	33
	50	6.3	36	13.9	357	16
	80	3.4	70	14.3	229	15

Mixing times, obtained through Eq. 2.1, are smaller than the filling times in all tests, meaning that well-mixed conditions are likely to have been achieved in all tanks operated at 20 to 80% of exchange volume per fill and draw cycle (Table 4.4). The Morrill index increased for all configurations operated at variable water levels (Table 4.4), in comparison with the steady-state conditions (Table 4.2). Such increase in  $Mo$  is due to much higher  $t_{90}$  and lower  $t_{10}$  values when the tanks operate at variable water level. Though these conditions are different from the steady-state ones, it seems reasonable to assume that a  $t_{90}/t_{10}$  ratio of 22, as in a CSTR, would be the target value for  $Mo$  of a homogeneously mixed tank. For all configurations, the high  $Mo$  values decrease as the percentage of exchange volume increases. That is, the deviation from the ideal mixing condition is higher when the water level variation is small and mixing is enhanced when the exchange volume in each cycle increases. This suggests that it is preferable to widely vary the water volume in the tank, as it will promote mixing more than filling very often. That is, for the same inflowing jet momentum flux, better mixing is attained when the water volume in the tank at the beginning of the filling period is smaller.

Mixing levels in the tank of Configuration A with 80% exchange volume per cycle show a small deviation from the ideal mixing, indicating that it might be possible to achieve good mixing conditions in these tanks, depending on the inflow and outflow patterns and flow rates, if a high percentage of exchange volume occurs. For Configuration B,  $t_{90}$  values, and thus  $Mo$ , are exceptionally high, because of recirculation and of the formation of stagnation zones that are apparently promoted when the tank is operated at variable

water level. The large  $Mo$  values indicate a strong deviation from the ideal mixing conditions. In contrast, for Configuration C, increasing the exchange volume in each cycle diminishes  $Mo$  to values that approach 1, that is, it promotes plug flow conditions in the tank instead of mixing.

#### 4.3.3.3 Turnover time

Operating the tanks at variable water levels resulted in a high increase of the turnover times, for all tested configurations, due to the lower outflow rates. When water volume variation within one cycle is high (80%), all storage tank configurations present similar turnover times, ranging only from 229 to 235 min (Table 4.4), suggesting little effect of the tank configuration on water renewal (Figure 4.11). However, when volume variation within one cycle is low (20%), which is frequent in daily operation of storage tanks of water supply systems, the turnover time is significantly different for the three tanks configurations, ranging from 436 min (Configuration C) to 610 min (Configuration A). For the smaller volume variations (20 to 50%), Configuration C promotes faster water replacement compared to the other two configurations and Configuration A presents the longest turnover times. That is, the typical tank Configuration A, which has the potential to achieve good mixing levels, when the water level varies widely, has also the potential to have the longest water retention times, if inadequately operated.

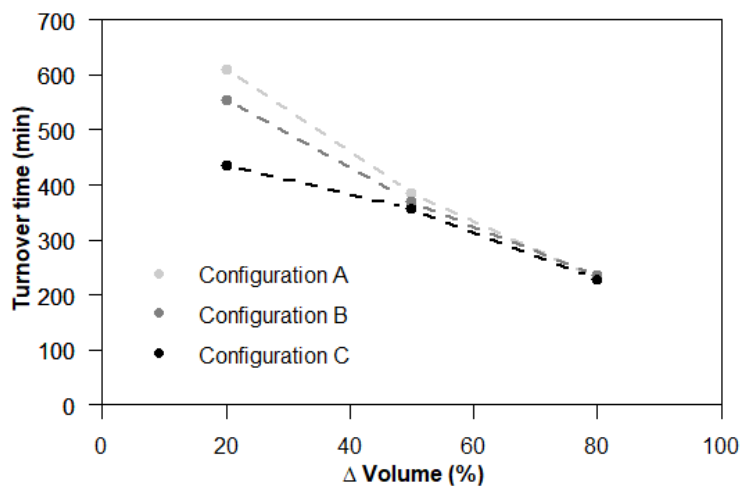


Figure 4.11 – Turnover time for each configuration and volume variation.

#### 4.4 Discussion

The presented results generally agree with those in similar studies, although the diversity of tested conditions (e.g., tank geometry; inlet and outlet location, size and number; variable or constant water level) and approaches used (e.g., analysis of velocity fields, of the mixing time or the RTD) hamper the comparison.

The short-circuiting and recirculation observed in Configuration B, either by the visual assessment of the rhodamine dispersion or by  $E(t)$  profile and the short-circuiting index  $t_{10}$ , at steady-state conditions, are in agreement with the observations of Montoya-Pachongo et al. (2016) on the RTD and on the velocity profiles obtained by numerical modelling of a circular tank with inlet and outlet pipes very closely located. Moncho-Esteve et al. (2015) also observed recirculation zones and short-circuiting in a rectangular tank with a similar inlet/outlet pipes configuration. This suggests that this configuration, although widely implemented, should not be used in the design of new tanks, as it promotes stagnation zones and possible water quality degradation. Improvement measures are necessary for the actual tanks.

Including of baffles (Configuration C), though effectively reducing short-circuiting, does not promote mixing. Instead, it leads to a close to plug-flow regime. Comparable low values of the mixing indicators  $Mo$  and  $\bar{\sigma}$  are found in hydraulic studies of baffled contact tanks for water disinfection (Angeloudis et al. 2014), where plug flow regimes are preferred over fully mixed ones.

The deviations from the fully mixed regime, observed in all configurations at different levels, were also observed by (Crowther and Dandy 2012) when modelling a circular tank with inlet/outlet pipes configuration somewhere in between those of Configurations A and B. Those authors could model the tank with acceptable accuracy using a two-compartment model, but not with a simple CSTR model, which agrees with the observed deviations to the fully mixed conditions in both tanks A and B.

The results of the present work show that mixing in the tanks is diminished and by-passing (if existent) is increased, when these tanks are operated at variable water levels, compared to what is observed at steady-state conditions with similar inflow rates. This suggests that observations from CFD modelling at steady-state conditions may not represent the hydrodynamics and the mixing conditions in full-scale storage tanks operated at variable

water levels. Previous studies have focused on the filling period only (Grayman et al. 2004; Tian and Roberts 2008) or have considered daily flow patterns without simultaneous inflow and outflow (Nordblom and Bergdahl, 2004; Zhang et al., 2013b). Thus, the results presented in this work cannot be compared with previous ones. Because of the importance of such findings in the operation of real storage tanks, further studies are required to assess the effect of different inflow and outflow patterns on mixing in the tanks.

#### **4.5 Conclusions**

A comprehensive assessment of mixing, ageing and water renewal in cylindrical small-scale water storage tanks is presented in this chapter. Tracer experiments, with no buoyancy effects, were carried out in tanks of three typical inlet/outlet pipes configurations, operated at steady-state and under variable water level conditions. Residence time distributions and hydraulic indexes were determined for appraising mixing and short-circuiting in the water tanks.

Mixing in cylindrical water tanks, with inlet and outlet pipes placed at opposite sides, can be close to that of a fully mixed reactor, depending on the inlet flow momentum and on the water level variation in fill-and-draw cycles. Higher inflowing rates and water volume variations within each cycle can cause good mixing levels in such tanks. From the operational point of view, wide variations in water level are, thus, preferred over frequent, but small, variations in water level of the storage tanks.

Tanks with inlet and outlet pipes located closely suffer from short-circuiting and promote the formation of water pockets of very high residence time. Mixing in these tanks is far from the fully mixed condition assumed in water quality simulators. Placing a baffle in such tanks changes the predominant flow paths and decreases the spread of residence times, although it does not promote mixing. This tank configuration should be avoided in the design of new water storage tanks.

In general, stronger short-circuiting effects occur in the storage tanks operated at variable water levels than in steady-state conditions. Under fill-and-draw mode, the establishment of water pockets of higher residence time is promoted in all tank's configurations, particularly if small water level variation occurs in each cycle. Even when the filling periods are longer than the theoretical mixing time, mixing in the tanks operated with

small volume variation in each cycle is far from complete. Consequently, despite results from CFD and tracer small-scale tests at steady-state conditions providing good insights on the hydrodynamics in the tanks, care must be taken when inferring results for full-scale tanks operated at variable water levels.

This chapter demonstrates that the turnover time in cylindrical tanks of  $H/D$  ratio in the order of 0.15, operated at close to constant water level, can be accurately estimated by the Rossman and Grayman (1999) formula for mixing time, provided that the adequate dimensionless constant is used. Dimensionless turnover times for the three tested configurations are proposed.

# Chapter 5

---

## **Rectangular storage tanks: small-scale versus field tests**

This chapter is based on the following scientific publication already submitted to a peer-review journal:

**Pinheiro, A.,** Monteiro, L., Almeida, M.C., Covas, D. (2021) Water mixing in rectangular storage tanks: small-scale versus field tests. *Journal of Hydraulic Research* (submitted in September 2021).

## 5.1 Introduction

The current chapter aims at the experimental study of the influence of the baffle structures and the operating conditions on water mixing and renewal in rectangular cross-section tanks through tracer tests carried out in laboratory and full-scale conditions. Tracer tests allow the calculation of the residence time distribution and a set of mixing, renewal, and short-circuiting indexes. Small-scale tests are carried out for constant water level (steady-state conditions) and for variable water level to simulate fill-and-draw cycles created by daily water demand variation. Full-scale tracer tests are carried out at three measurement sections in a real-life rectangular tank with baffles. Results are compared with those for circular cross-section tanks presented in chapter 4 (Pineiro et al. 2021). Mixing and renewal conditions are thoroughly analysed and discussed.

This chapter innovatively presents: i) the experimental study of mixing conditions in small-scale rectangular cross-section storage tanks with and without baffle structures, not previously analysed in laboratory conditions; ii) the analysis of the effect of the fill-and-draw cycles on the water mixing and renewal both in small-scale and full-scale conditions; and iii) the comparison of mixing, renewal and short-circuiting indexes for different tank configurations and operating conditions.

## 5.2 Materials and methods

### 5.2.1 Small-scale tests

Two different small-scale tank configurations were constructed and tested in the Laboratory of Hydraulics of Instituto Superior Técnico, Universidade de Lisboa. Configuration A corresponds to a tank without a baffle structure and Configuration B to a similar tank with a baffle (Figure 5.1). Tank dimensions were determined by downscaling the principal dimensions of a full-scale water tank for the 1:77 geometric scale (Configuration B). The material of the tanks is acrylic; both have a square cross-section ( $350 \times 350 \text{ mm}^2$ ), allowing a maximum water depth of 70 mm (corresponding to a maximum depth-width ratio of 0.2). The inlet and outlet pipes have an internal diameter of 4 mm. In both configurations, the inlet pipe is 14 mm above the maximum water level (70 mm) and the outlet pipe at 4 mm above the bottom of the tank. Configuration A is a tank without baffles with pipes in two opposite corners (Figure 5.1a). Configuration B has internal baffles that force the flow through a series of  $90^\circ$  and  $180^\circ$  turns (Figure 5.1b).



The resulting width of each channel (because of the baffles) is 55 mm; the total length of the water path is approximately 2.2 m. For structural simplification, the small-scale tanks have an inlet pipe perpendicular to the tank wall and above the maximum water height, and the outlet pipe lies above the tank floor.

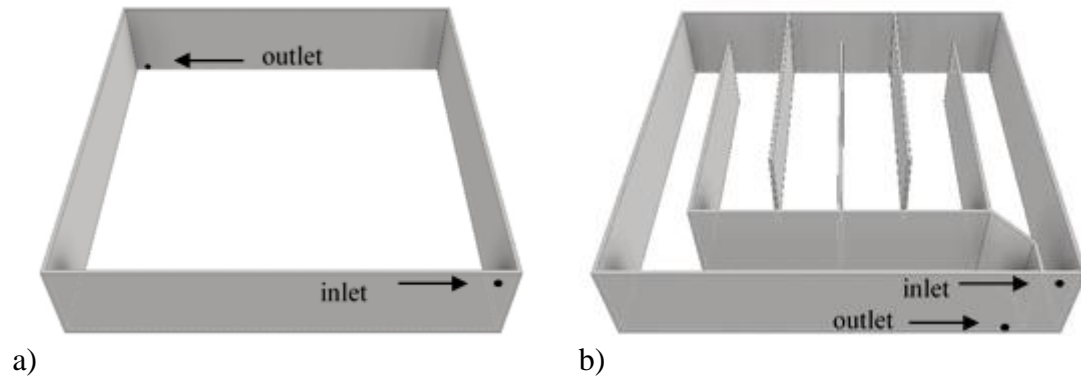


Figure 5.1 – Small-scale tanks tested: a) Configuration A; b) Configuration B.

The experimental procedure description is in Pinheiro et al. (2021). Experiments were carried out for two different operating conditions: mode 1 for steady-state flow with a constant water level, repeated for three different flow rates, and mode 2 for variable water level conditions (fill-and-draw cycles) with different operational levels and flow rates. Operating modes parameters are in Table 5.1 and photos of the experimental facility in Figure 5.2.

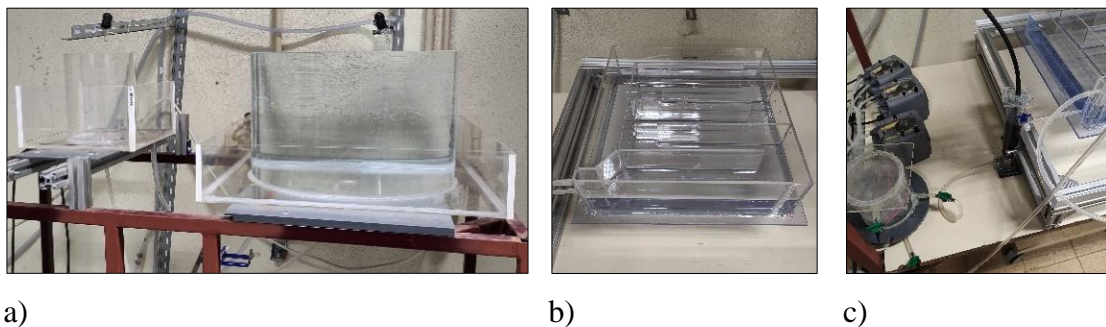


Figure 5.2 – Tracer tests facility pictures: a) deionized and tracer solution tanks; b) small-scale tank; c) conductivity probe, hydropneumatic tank and peristaltic pumps.

The tracer used in the tests was rhodamine WT 20% at a 1:50 000 dilution to visualize flow patterns and tracer distributions in mode 1. Two video cameras were installed above and on the side of the tanks for image acquisition during dye tracer tests.

Table 5.1 – Operational conditions tested in laboratory.

	<b>Mode 1</b>	<b>Mode 2</b>
<b>Flow rate [L/h]</b>	Q1 (7.4); Q2 (9.1); Q3 (11.5)	Inlet: 9.0 Outlet: 1.5, 3.0, 4.5
<b>Water level [mm]</b>	60	Maximum: 70 Minimum: 14, 35, 56
<b>Tracer solution conductivity [<math>\mu\text{S}/\text{cm}</math>] at 25°</b>	221 – 286	228 – 274
<b>Inflow and outflow water temperature difference [°C]</b>	0 – 1	0 – 1
<b>Water temperature variation over time for each test [°C]</b>	0.4 – 2.0	0.4 – 1.4

### 5.2.2 Full-scale tests

The full-scale tank selected to undertake the tests is an aboveground square cross-section structure made of concrete belonging to Águas do Algarve, the water utility responsible for the water supply and wastewater transport in the South of Portugal. This tank receives treated water directly from a Water Treatment Plant (WTP) and delivers it to two distribution networks. The configuration and size of this tank were considered the reference for the construction of a small-scale tank tested in laboratory conditions as Configuration B with the baffle structure.

The tank has a capacity of about 3 450 m<sup>3</sup>, with an inner side with of 26.6 m, and corridors 5.5 m wide. An inlet pipe, with a 0.8 m diameter, enters the tank near the bottom of the structure, and an elbow with an upward angle directs the flow to the opening at 4.5 m height (Figure 5.3b). The outlet pipe, also with 0.8 m diameter, is located inside a ditch, 1.5 m below the tank floor. This tank features internal baffles that force the flow through a series of 90° and 180° turns between inlet and outlet, and the total length of the water path is approximately 160 m.

This type of tank configuration, a rectangular cross-section with internal baffles, is very common in large tanks in Portugal (Monteiro et al. 2021). To identify the effects of operating a full-scale tank on the water renewal time and on the time required for the stored water to be completely renewed, a tracer test was carried out. Because of drinking water safety constraints, it was not possible to add a tracer to the flow at the inlet to the tank. Thus, the adopted solution was the change of the water source that fed the water treatment plant (WTP). The change of water from underground sources to surface

reservoir allowed an  $80 \mu\text{Scm}^{-1}$  increase in conductivity between the water stored and new water entering the tank.

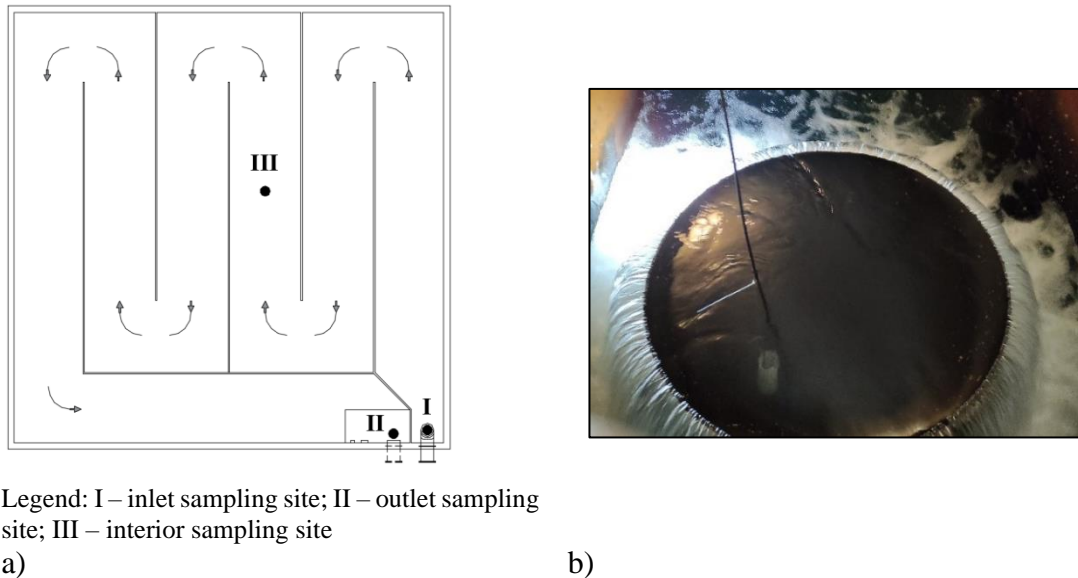


Figure 5.3 – Full-scale tank: a) layout and location of monitoring equipment; b) inlet pipe upper view.

The locations of the monitoring equipment are shown in Figure 5.3a: I) at 1 m inside the inlet pipe (Figure 5.3b); II) inside the ditch and 1 m below the floor of the tank next to the outlet pipe; and III) in the middle of the third corridor and 2.8 m from the floor of the tank. Three conductivity probes were installed at each sampling site (two YSI Pro 30 and one YSI 556 MPS) and used to monitor the conductivity and the temperature during the test at 10-minutes intervals.

The test comprised the application of the step tracer method (Fogler, 2006), in which the inflow water with a higher conductivity enters the tank filled with water with lower conductivity. The test started when the intended conductivity was achieved in the WTP (about 3 km from the tank). Inflow and outflow rates respond to the needs of the distribution systems, allowing for a minimum volume variation (ca. 20%). The test lasted until the conductivity between inflowing water and the outflowing differed by less than 5%.

### 5.2.3 Data treatment and analysis

The methodology used for data treatment and analysis is presented in Pinheiro et al. (2021). In operational mode 1, both cumulative distribution curve,  $F(t)$ , and residence

time distribution curve,  $E(t)$ , are obtained, however, in operational mode 2, only  $F(t)$  is determined because of variable water volume in the tank. The treatment and analysis of the field tests are the same applied for tests with operational mode 2, given the inability to keep the water level constant and, thus, not allowing to get the  $E(t)$ . Tracer tests in small-scale and full-scale tanks allow to calculate water mixing and renewal indexes extracted from  $F(t)$  and  $E(t)$  functions and are used to assess water short-circuiting and mixing inside the tank.

In the current work, the short-circuiting indicator used is time  $t_{10}$ , which refers to the time needed for 10% of the injected tracer particles to leave the tank. The dispersion index and the Morrill index are used to assess mixing conditions. The dispersion index,  $\bar{\sigma}$ , is the ratio between the temporal variance of the  $E(t)$  function and the squared mean residence time, which is one for completely mixed tanks (Fogler, 2006). The Morrill index is defined as the ratio between  $t_{90}$  and  $t_{10}$ , that is the ratio between the time needed for 90% and 10% of the injected tracer particles to leave the tank, respectively (Teixeira and Siqueira 2008). The time for total water renewal (turnover time),  $t_T$ , proposed in Pinheiro et al. (2021) and corresponding to  $F(t) = 0.95$ , is also estimated.

## 5.3 Results and discussion

### 5.3.1 Laboratory results

#### 5.3.1.1 Steady-state conditions

A general understanding of the preferential flow paths within the two configurations is extracted from the recorded video images of the dye tracer movement. Figure 5.4 shows the evolution of the dye tracer at four instants after the injection of a solution (0.5, 5, 20 and 40 min), with a plan view and a lateral view.

Configuration A has no baffle structures inside the tank and the fluid spreads close to the sidewalls, forming two fronts that surround the stored fluid. This is because of the Coanda effect in which the fluid emerging from an orifice follows an adjacent flat surface, remaining attached to it and mixing with its surroundings as it flows away from a nozzle. This is observed in all depths of the tank wall and in both walls near the nozzle. One front reaches first the outlet pipe (see Figure 5.4a at  $t = 5$  min). The fluid behaviour creates a

central zone with lower speeds and a slower mixing between the stored and the entering water (Figure 5.4a).

In Configuration B, the baffles create corridors that separate the inlet and the outlet of the tank, inducing a plug-flow effect in which the fluid that enters first leaves first (Figure 5.4b). However, this type of test does not allow to identify the occurrence of older water pockets trapped at low-speed or stagnation zones. Tracer tests with NaCl will be important to verify the existence of these pockets.

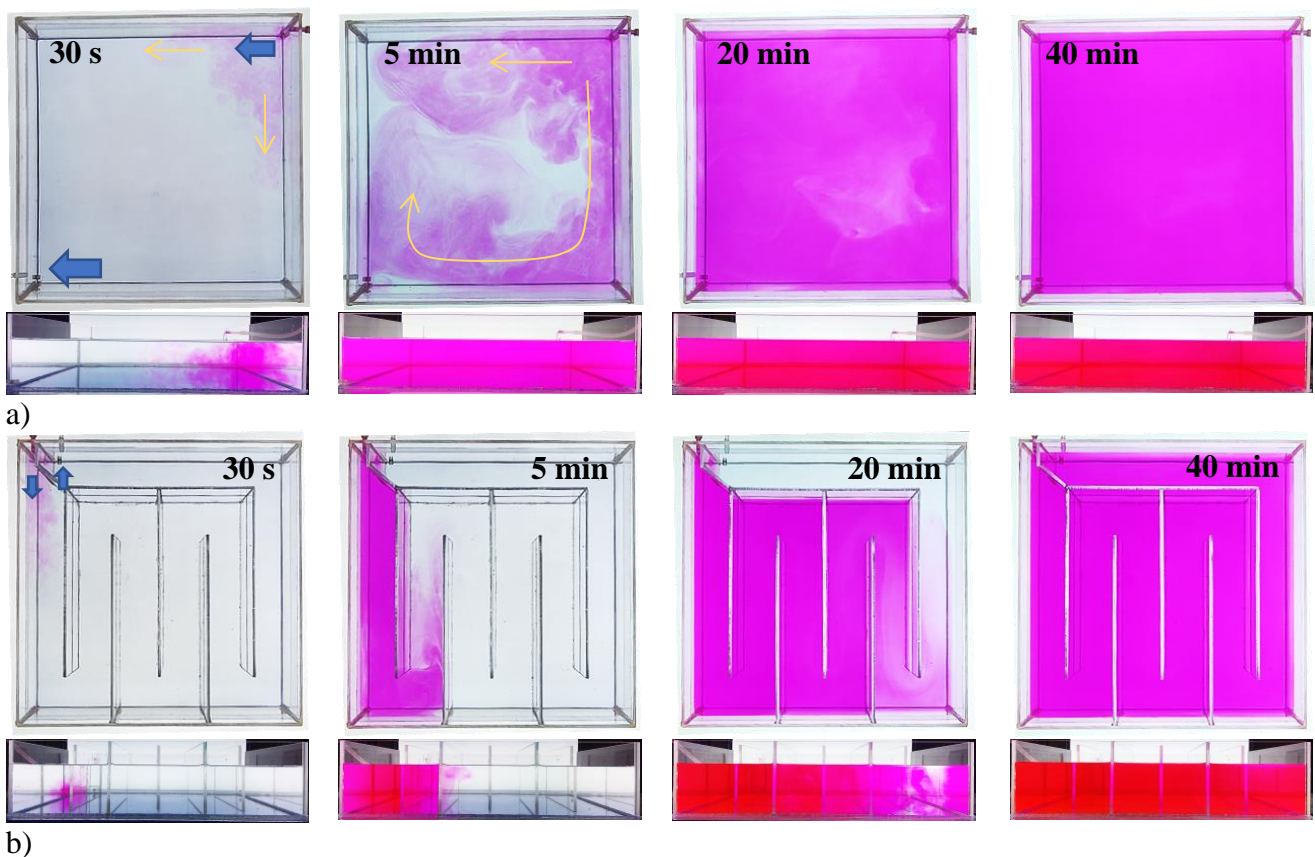


Figure 5.4 – Rhodamine dispersion within the two configurations at 0.5, 2, 10 and 15 min after injection (constant water level, flow rate  $9.1 \text{ Lh}^{-1}$ ): a) Configuration A; b) Configuration B.

The cumulative distribution  $F(t)$  and the residence time distribution  $E(t)$  are determined for the two configurations A and B with mode 1 and three flow rates (Figure 5.5). The  $F(t)$  increases in the beginning of the test in Configuration A (fully open) (Figure 5.5a), highlighting the existence of short-circuiting phenomena which is corroborated by the peak in the  $E(t)$  initial moments (Figure 5.5c). Configuration B (baffled tank) presents a delayed and sharp increase in  $F(t)$  at initial times, evidencing the effect similar to a plug flow regime (Figure 5.5b). This fast increase in  $F(t)$  is also observed in  $E(t)$  as a single and narrow peak (Figure 5.5d), in the first minutes of the tracer tests. The peak also shows

many tracer molecules reaching the outlet at the same time in Configuration B. The fact is that baffles prevent the inflowing jet to mix with older water stored in the tank and push older water to the outlet pipe.

The increase in flow rate contributes to a decrease in the mean residence time,  $t'$ . While Configuration A tends to approach theoretical residence time values,  $\tau$ , Configuration B, conversely, presents lower values of  $t'$ .

Short-circuiting and mixing indexes for the two tanks at steady-state conditions are presented in Table 5.2. Configuration A exhibits the lowest  $t_{10}$  values compared with the other configuration. In this tank, 10% of the injected tracer reaches the outlet pipe quickly denoting a short-circuiting effect. The higher the flow rate is, the lower the  $t_{10}$  value for both configurations. This short-circuiting index presents the highest values for the baffled tank, denoting the delayed exit of the tracer from the tank.

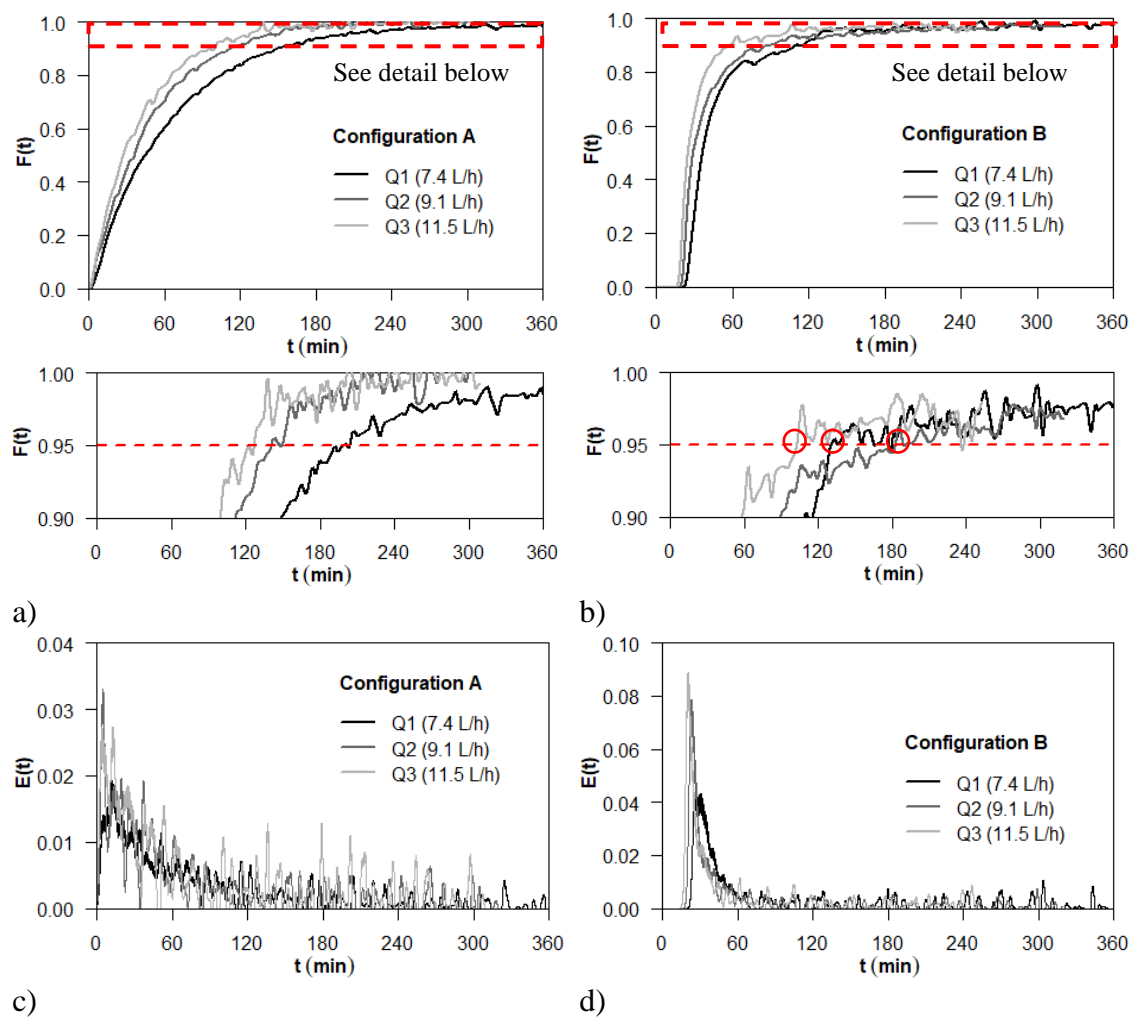


Figure 5.5 –  $F(t)$  and  $E(t)$  for the two configurations at steady-state conditions and for three flow rates: (a,c) Configuration A; (b,d) Configuration B.

The dispersion index,  $\bar{\sigma}$ , indicates the spread of the  $E(t)$  for Configuration A. This index has also the highest observed values for Configuration A (Table 5.2), which show that flow paths within the tank are quite diverse. This is probably the result of internal recirculation and the formation of stagnation zones, promoted by the relative position of the inlet and outlet pipes. Typically, high values of the  $\bar{\sigma}$  suggest close to perfect mixing conditions. However, in the current case, the other indexes indicate that Configuration A water mixing is far from perfect, namely  $t_{10}$ ,  $t_{95}$  and  $Mo$  (Table 5.2).

The Morrill index values for Configuration A range from 15.6 to 19.5, which are lower but close to the ideal value of 22, corresponding to an ideal continuous stirred tank reactor (CSTR). The low Morrill index values observed for Configuration B (between 3.0 and 4.3) are close to the unit value, characteristic of a plug flow reactor (PFR), suggesting that flow dynamics inside the tank with baffles tends to a plug flow.

Turnover time ( $t_{95}$ ) is also determined from  $F(t)$ , as the time needed to reach 95% of water renewal. Results for Configuration A show that turnover time decreases with increasing flow rate (Table 5.2), which contributes to the renewal process. However, Configuration B has a significant influence of older water pockets that are identified at the outflow tracer over time. This phenomenon is detected by the instability of the  $F(t)$  for values close to 0.95.  $F(t)$  equal to 0.95 occurs several times, being necessary to identify the first instant and the last time the curve crosses the  $t_{95}$ . Assuming that  $t_{95}$  corresponds to the last instant, Configuration B has a faster renewal for lower flow rates. As the flow rate increases, water pockets tend to be trapped for a longer time next to the tanks corners, tending to be released later (see also Figure 5.5b).

Table 5.2 – Hydraulic indexes for the two configurations at steady-state conditions.

Config.	$Q$ (Lh <sup>-1</sup> )	$\tau$ (min)	$t'$ (min)	$t_{10}$ (min)	$t_{95}$ (min) [1 <sup>st</sup> , last]	$\bar{\sigma}$ (-)	$Mo$ (-)
<b>A</b>	7.4	59.6	61.5	9.6	204	0.86	15.6
	9.1	48.5	49.9	5.7	145	0.92	19.5
	11.5	38.3	38.9	5.4	127	0.70	18.5
<b>B</b>	7.4	59.6	49.1	26.1	130, 180	0.60	4.3
	9.1	48.5	40.5	22.0	175, 183	0.73	4.1
	11.5	38.3	33.7	19.2	103, 238	0.83	3.0

The results from the rectangular tank without baffles (Configuration A) can be compared with those presented in Pinheiro et al. (2021) for the circular cross-section with an outlet pipe located at the opposite side, though aligned with the inlet pipe, given the similar

operating conditions in which the tests were carried out (volume, flow rates and inflow/outflow velocities). Short-circuiting and mixing indexes for these two tanks at steady-state are presented in Table 5.3. The rectangular and circular cross-section tanks show many similarities in the values of hydraulic indexes. It should be noted that the short-circuiting effect is slightly greater in the rectangular tank; this can be explained by the geometry of the tank and the alignment of the inlet and outlet pipes. In the circular tank, the inflowing fluid is divided into two fronts of similar portions that run along the sides of the tank until the outlet pipe, while in the rectangular tank, the fluid divides into two fronts, but one travels faster along a larger section (Figure 5.4a). The fastest front is aligned with the outlet pipe, creating a favourable flow in the outlet region in this direction, being this the reason for the earlier particles' arrival to the outlet end. In terms of water renewal, circular tanks have better results (lower  $t_{95}$ ), even with slightly worse mixing indexes (lower  $\bar{\sigma}$  and  $Mo$ ).

Table 5.3 – Comparison of hydraulic indexes between circular cross-section (Pinheiro et al. 2021) and rectangular cross-section tank (Configuration A) for steady-state conditions.

Config.	$V$ ( $m^3$ )	$Q$ ( $Lh^{-1}$ )	$\tau$ (min)	$t'$ (min)	$t_{10}$ (min)	$t_{95}$ (min)	$\bar{\sigma}$ (-)	$Mo$ (-)
<b>Circular cross-section tank</b>	0.00724	7.4	58.7	61.1	12.3	180	0.8	11
		9.4	46.2	47.3	8.5	147	0.8	18
		11.6	37.5	37.7	6.1	116	0.9	15
<b>Rectangular cross-section tank (Conf A)</b>	0.00735	7.4	59.6	61.5	9.6	204	0.9	16
		9.1	48.5	49.9	5.7	145	0.9	20
		11.5	38.3	38.9	5.4	127	0.7	19

### 5.3.1.2 Variable water conditions

The influence of variable water levels is analysed for the two configurations through tracer tests. Three levels of variation in tank volumes are tested (20%, 50% and 80%) and an outflow pattern is used to simulate a real water consumption. Inflow rate is  $9.0 Lh^{-1}$ , during the filling period, and null, when the water level is decreasing (Figure 5.6).



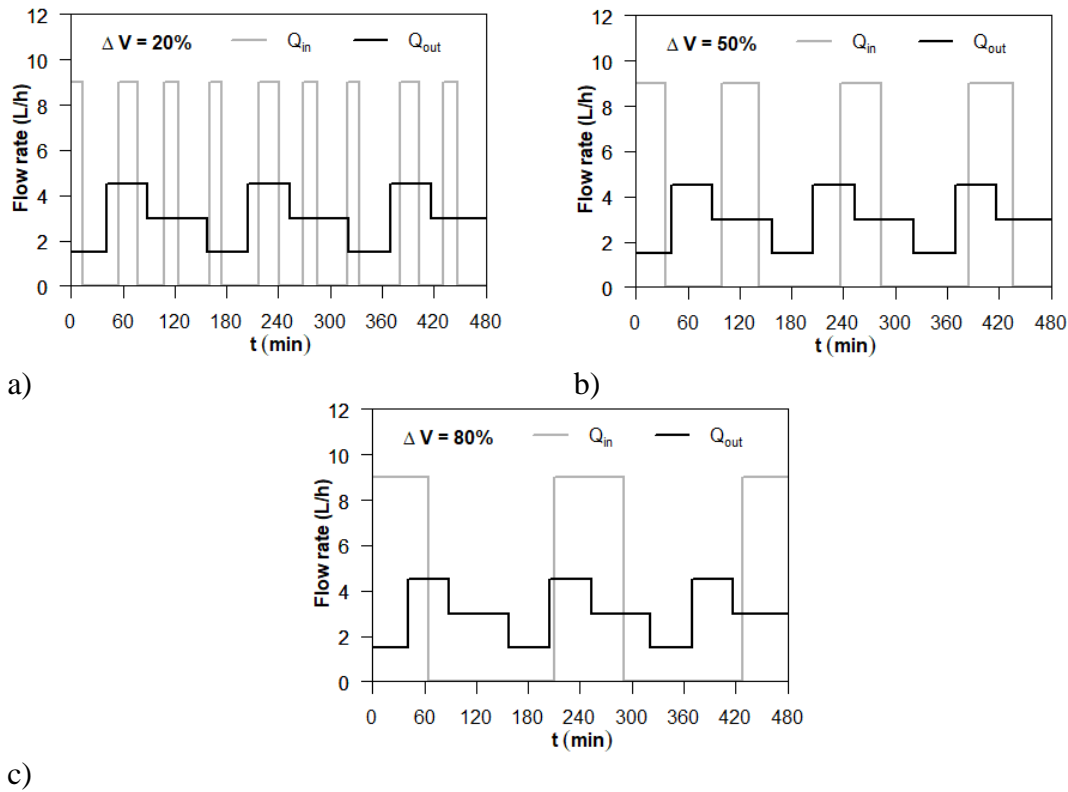


Figure 5.6 – Inflow and outflow rate variations at mode 2: a) 20%; b) 50%; and c) 80%.

The resulting  $F(t)$  curves are presented in Figure 5.7. The analysis of these functions shows: (i) the higher the water volume exchanged in each cycle is, the fewer cycles are needed to renew the water inside the tank (Figure 5.7a,c,e), regardless of the tank configuration (A or B); (ii) the  $F(t)$  curves from Configuration B present sudden drops that show older water pockets that come over time, as in to the steady-state conditions results; these pockets result in the  $F(t)$  curve oscillation, instead of a smooth increase over time similar to the one obtained for Configuration A (Figure 5.7a,c,e). These drops in  $F(t)$  curves occurring during the emptying stage correspond to periods only with outflow and no inflow. In Configuration A, the emptying periods attenuate these effects and to smooth the  $F(t)$  curve until the water entering promotes mixing and  $F(t)$  increases again. Assuming the turnover time is given by the last  $t_{95}$ , the higher the water volume variation in the tank, the lower water renewal times are for both configurations (Figure 5.7b,d,f and Table 5.4). For 80% volume variation, at least two filling periods are needed to renew completely the water inside the tank, whilst nine to ten fill-and-draw cycles are necessary to renew the water when only 20% of the total volume is exchanged in each cycle for both Configurations A and B.

In terms of short-circuiting index,  $t_{10}$ , the greater the volume exchange, the lower the indicator and the faster the short-circuiting occurs. Short-circuiting in Configuration B has shown a greater delay than in Configuration A because of plug flow created by the baffle structure.

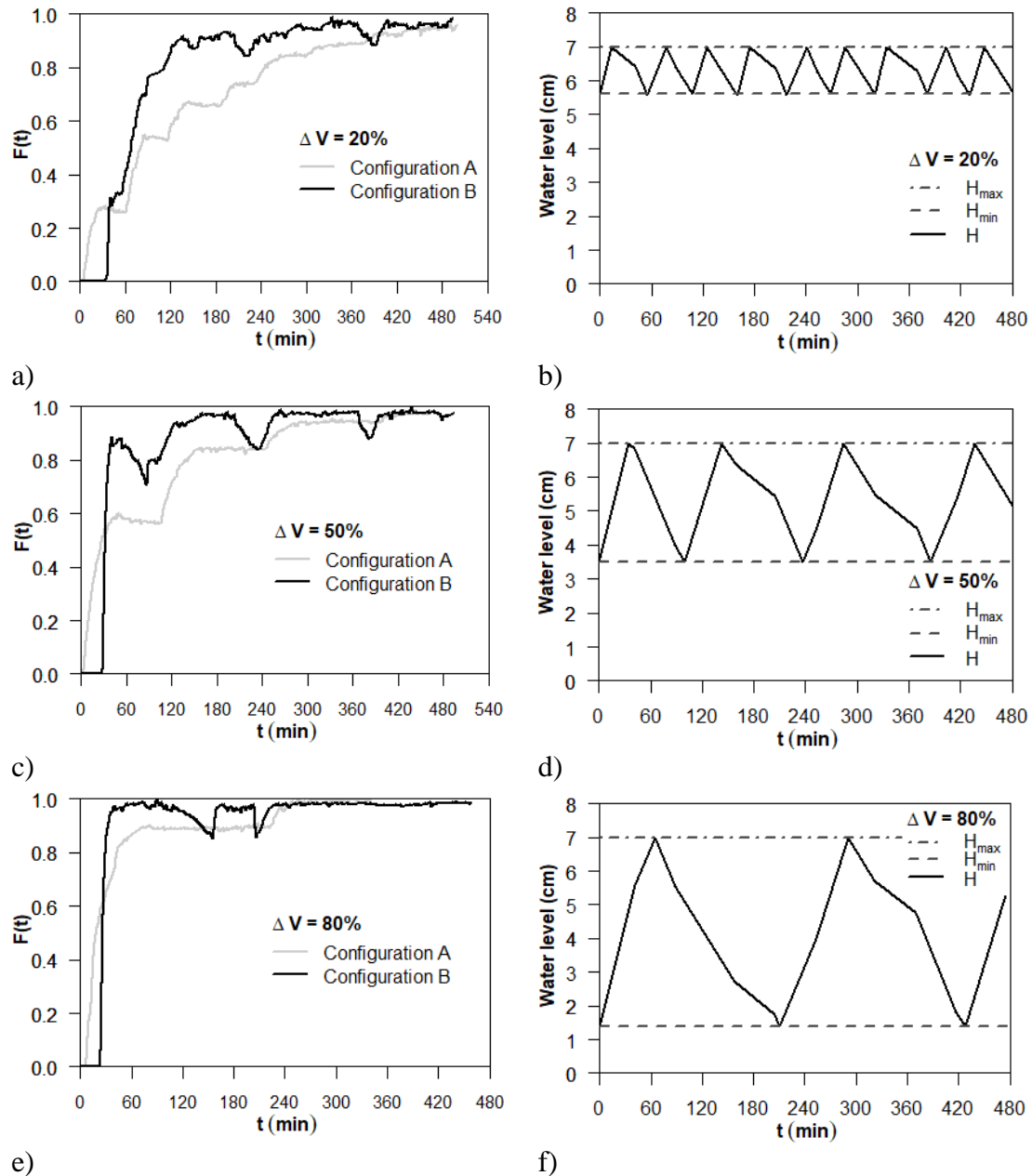


Figure 5.7 – Variable water level results: a) cumulative distribution curves; b) water level variations.

Operating the tanks with variable water levels according to the daily demand pattern has showed that larger variations in the water level allow a faster renewal of the stored water (Figure 5.8). However, the results of the  $F(t)$  show that Configuration B accumulates pockets of older water that, as the tank fills and empties, will end up leaving over time

(Figure 5.8b). These older water pockets can be trapped in the tank for a long time and contribute to the localized accumulation of older water. When the water volume variation is 80%, both tanks present similar turnover times. However, Configuration B reaches for the first time  $t_{95}$  at 37 min, but only stabilizes (the last  $t_{95}$ ) at 220 min, whereas Configuration A only reaches the turnover time at 231 min (i.e.,  $t_{95}$  occurs only once) (Table 5.4). When the volume variation is low (20%) in Configuration B, the turnover time stabilizes earlier than in Configuration A (compare  $t_{95}$  values: 447 and 498 min).

Overall, although in Configuration B, because of the plug flow effect, the renewal of the stored water is faster, there will always be pockets of older water that will come out over time, regardless of the volume variation. This effect is minimized when the volume variation is higher (80%).

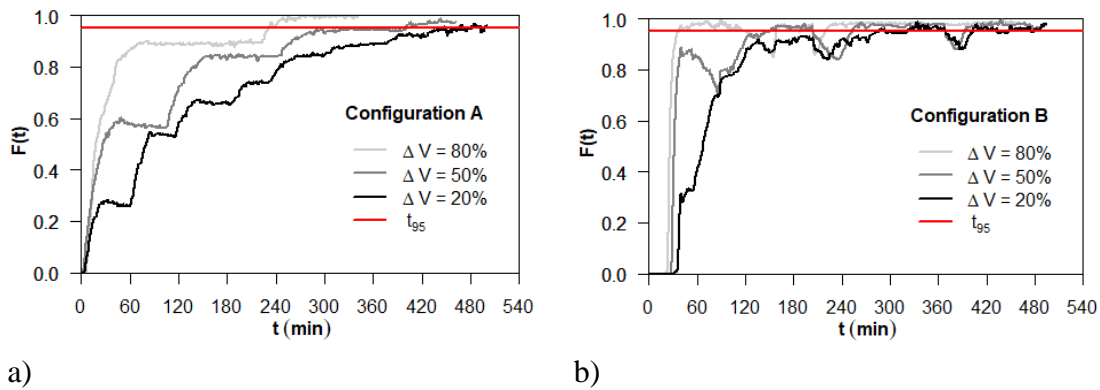


Figure 5.8 –  $F(t)$  curves obtain for each configuration and the respective volume variation: a) Configuration A; b) Configuration B.

Table 5.4 – Hydraulic indexes for the three configurations at variable water level.

Config.	$\Delta V$ (%)	$t_f$ (min)	$t_{10}$ (min)	$t_{95}$ (min) [1 <sup>st</sup> , last]	$Mo$ (-)
<b>A</b>	20	14	9.5	466, 498	40.2
	50	34	5.9	334, 400	44.1
	80	64	8.5	231	24.7
<b>B</b>	20	14	37.0	285, 447	3.8, 10.7
	50	34	28.7	150, 393	4.1, 13.5
	80	64	23.5	37, 220	1.4, 9.0

The rectangular tank without baffles (Configuration A) can be compared with the circular tank presented in Pinheiro et al. (2021), given the similar operating conditions (volume, flow rates and inflow/outflow velocities). Short-circuiting and mixing indexes for both tanks under steady-state conditions are presented in Table 5.5. The comparison of results between the two tanks shows that: (i) the filling time is very similar in both tanks because

the volume and the operating conditions are the same; (ii) the  $t_{10}$  has lower values in the circular tanks because of a shorter water path near the wall between the inlet and outlet pipe for equal mean velocities (in the circular tank, this is half of the perimeter, 63 cm; in the rectangular tank, this is the length of two sides, 70 cm); (iii) the turnover times are identical in both tanks, except for the lowest volume variation (20%) in which it is higher in the circular tank since water travels faster and takes longer to mix.

Table 5.5 – Comparison of hydraulic indexes between circular cross-section (Pinheiro et al. 2021) and rectangular cross-section tank (Configuration A) for variable water level conditions.

Config.	$\Delta V$ (%)	$t_f$ (min)	$t_{10}$ (min)	$t_{95}$ (min) [1 <sup>st</sup> , last]	$Mo$ (-)
<b>Circular cross-section tank</b>	20	15	5.6	610	69
	50	36	5.0	386	51
	80	70	6.5	230	35
<b>Rectangular cross-section tank (Conf A)</b>	20	14	9.5	466, 498	40.2
	50	34	5.9	334, 400	44
	80	64	8.5	231	25

### 5.3.2 Field results

The operation of a tracer test in an actual storage tank is a major challenge because of the difficulty in controlling all operating conditions (e.g., the valves opening, and closure are not instantaneous). Monitoring the water conductivity at three different locations in the tank allowed measuring the evolution of this parameter during a 24-h period and assessing the water renewal and mixing in actual operating conditions. The beginning of the test took place when the inlet and outlet pipes were opened. Initially, the stored water was at rest to guarantee the sudden variation in water conductivity between the stored water and the new entering water. The inlet and outlet flow rates during the test are shown in Figure 5.9. Despite the 24-h test, after six hours, the turnover time was reached, thus, only results over this period are presented. During these six hours, the inflow was practically constant (1 000 Ls<sup>-1</sup>); the outflow varied between 665 and 945 Ls<sup>-1</sup> (Figure 5.9a) and the water level varied between 3.6 and 4.5 m (Figure 5.9b), which corresponds to a volume variation of 20%.

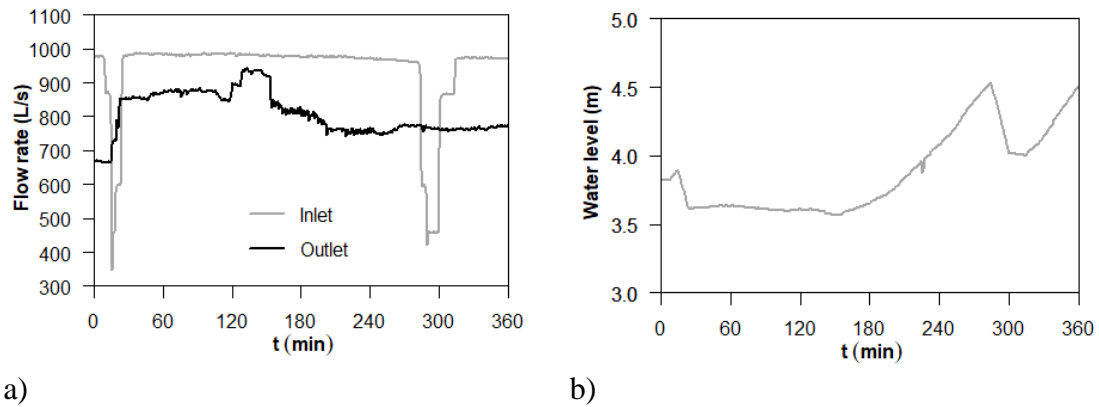


Figure 5.9 – Collected field data: a) flow rate; b) water level.

The electric conductivity evolution at the three monitoring sites is presented in Figure 5.10a. Even though the water was leaving the WTP with a constant conductivity (ca.  $402 \mu\text{Scm}^{-1}$ ), it still took approximately 30 minutes for the inflow conductivity to stabilize, and during that period new water was already arriving at the sampling point in the middle of the tank. Since it was not possible to generate a sudden conductivity increase (step method) between the incoming water and the stored water, a sudden jump was assumed for the subsequent analysis. Before obtaining the cumulative distribution function, it was necessary to remove data outliers, namely, output conductivity values higher than those observed in the input conductivity. The analysis of the time series of water conductivities at the exit of the WTP during the previous seven days allowed to verify that there was no treated water with conductivities higher than  $402 \mu\text{Scm}^{-1}$  that could justify accumulated old water.

Cumulative distribution curves,  $F(t)$ , show a rapid increase even in the outlet pipe (Figure 5.10b). Only after 40 minutes it is possible to start noticing the newer water reaching the outlet pipe. After 46 min, the 10% inflow conductivity was reached at the outlet point ( $t_{10}$ ) and the complete renewal was attained at the intermediate monitoring point ( $t_{95}$ ); after 1 h 41 min, the water in the tank was completely renewed (Table 5.6). Even with the plug flow created by the existing baffle structure, the high flow rates allowed a rapid renewal of the stored water. Some older water pockets come out later and, after 6 hours, the renovation is almost complete.

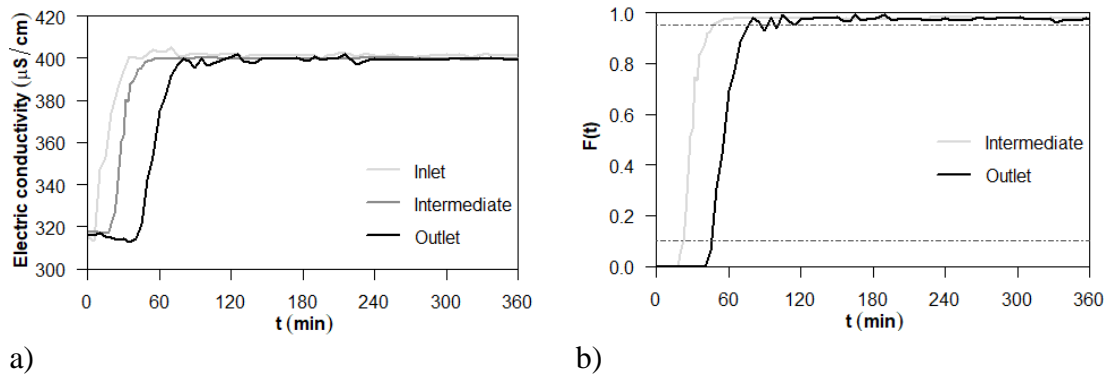


Figure 5.10 – Full-scale results: a) electric conductivity measured at the three sampling sites; b) cumulative distributions curves for the intermediate and outlet sampling sites.

Temperature can have a substantial effect on the water tank mixture (Olson and Deboer 2008) since significant temperature differences between stored water and filling water can generate water stratification with different temperatures and densities inside the tank. The water temperature was also monitored during the field tests at the three sampling sites and the maximum observed difference with time was  $0.4^{\circ}\text{C}$ . As the temperature difference is negligible, the possibility of having stratified water layers in the tank is not considered.

The Reynolds number of the filling jet is also calculated to determine whether inflows are turbulent or laminar. These Reynolds numbers vary between 945, for the minimum flow rate was  $350 \text{ L s}^{-1}$ , which occurred for a short period (cf. Figure 5.9a) and  $1.6 \times 10^6$  for  $1\,000 \text{ L s}^{-1}$ , with a median value of  $1.5 \times 10^6$  and being most of the time a turbulent flow. Turbulent jets have sufficient momentum to establish strong mixing patterns inside the tank.

Table 5.6 – Hydraulic indexes for intermediate and outlet sampling sites.

Sampling sites	$t_{10}$ (min)	$t_{95}$ (min) [1 <sup>st</sup> , last]	$Mo$ (-)
Intermediate	22	46	1.9
Outlet	46	75, 101	1.5

To compare the experimental turnover time values with those gathered in the field tests, this parameter should be normalized. The normalized turnover time can be defined as the ratio between  $t_{95}$  and  $\tau$ , where  $\tau$  is the theoretical residence time given by the ratio between the volume of fluid inside the tank,  $V$ , and the flow rate,  $Q$ . Two approaches are considered to calculate the theoretical residence time  $\tau$  in variable water level tests, namely: a) the ratio between the average volume and average flow rate (Figure 5.11a); b)

the ratio between the maximum volume and the flow rate (Figure 5.11b). The flow rate is given by the average inlet and outlet flow rates during the tests.

Results show that, independently of the approach used to calculate theoretical residence time, the normalized turnover time decrease with the increase of volume variation in the tank, suggesting that operating the tank varying the full stored volume improves water renewal, however, it does not necessarily mean that it improves water mixing conditions as lower velocity zones still exist and the plug flow phenomena are significant. Normalized turnover time values for 20% volume variation are lower in the field tests than in the laboratory since the operating flow rates were higher in actual conditions.

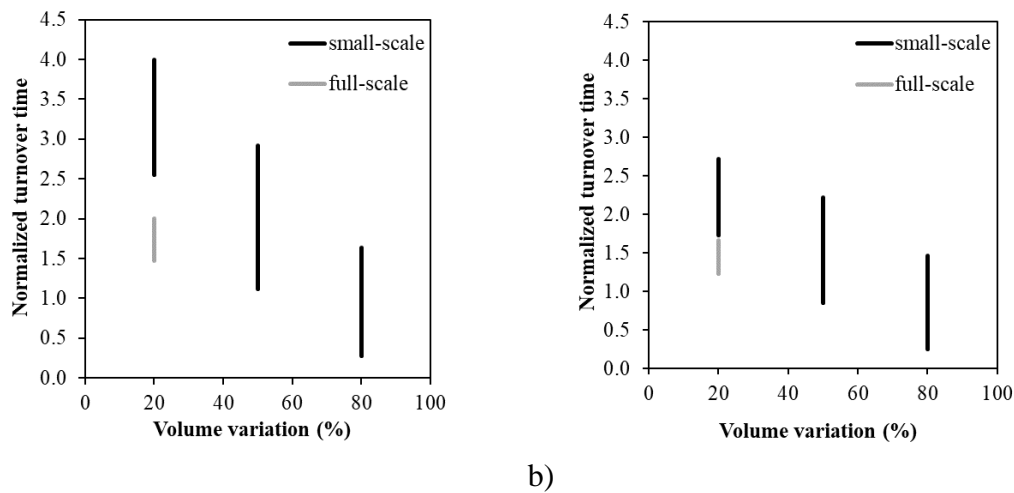


Figure 5.11 – Normalized turnover time as a function of volume variation and according to two approaches: a) the ratio between the average volume and average flow rate; b) the ratio between the maximum volume and the flow rate.

#### 5.4 Discussion of water mixing and renewal conditions

Results from the experimental tests carried out in small-scale circular and rectangular tanks with different configurations<sup>1</sup>, schematically represented in Figure 5.12, and for steady-state conditions and for different volume variations (20%, 50%, 80%) are compared in terms of normalised turnover time ( $t_{95}/\tau$ ), dispersion and Morrill indexes ( $\bar{\sigma}$ ,  $Mo = t_{90}/t_{10}$ ) (mixing indexes) and normalized short-circuit index ( $t_{10}/\tau$ ) in Figure 5.13, Figure 5.14 and Figure 5.15.

<sup>1</sup> Three configurations were analysed in circular cross-section storage tanks (Chapter 4), being Configuration A similar to the one used in the rectangular cross-section tank, Configuration B with inlet and outlet pipes located in the same side of the tank wall and Configuration C corresponding to a tank with a baffle with a length of 75% of tank diameter.

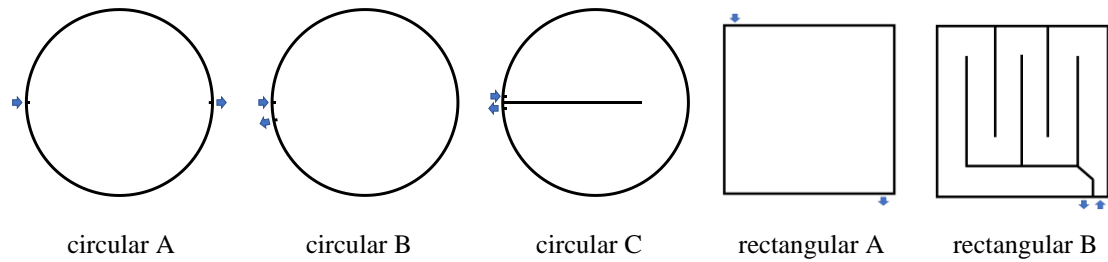


Figure 5.12 – Schematics for circular and rectangular small-scale tanks.

#### 5.4.1 Morrill index

For steady-state conditions, the best water mixing conditions ( $Mo = 22$ , ideal reactor) are observed in Configuration A for both circular ( $Mo = 11-18$ ) and rectangular ( $Mo = 16-19$ ) tanks with very similar renewal times (i.e.,  $t_{95}/\tau = 3.0-3.4$ ) (Figure 5.13a). This is because the inlet and the outlet pipes are on opposite sides of the tank, promoting a higher water mixing. The increase of the flow rate contributes to higher jet momentum and to higher turbulence and a better water mixing. Conversely, tanks with baffles – circular C ( $Mo = 7-8$ ) and rectangular B (3–4) – approximate to a plug flow reactor ( $Mo = 1$ ), because of the water circulation along the created pathway between the inlet and the outlet pipes. This plug flow is clearer in the rectangular tank because of the several baffles creating a longer and narrower water path. In tanks with baffles, the flow rate strongly influences the turnover conditions in the rectangular tank, in which higher flow rates result in lower renewal times. Finally, the tank with the inlet and outlet pipes on the same side and close to each other (circular B with  $Mo = 27-70$ ) generates a bypass and water short-circuiting in a localized area, between the inlet and outlet pipes, and several low-velocities and stagnation zones in remaining volume of the tank. The short-circuiting phenomenon increases with the increase in flow rate. In this tank, renewal times (i.e.,  $t_{95}/\tau = 3.7-4.7$ ) are of the same order as those in the other tanks, despite having a significant variation in the flow rate.

For fill-and-draw conditions which attempt to simulate the actual tank operation, results show that (Figure 5.13b): (i) circular tank B has worse mixing conditions ( $Mo = 215-254$ ) than for steady-state, far from the ideal reactor, having higher renewal times for lower level variations; (ii) circular and rectangular tanks A have higher Morrill index values ( $Mo = 25-69$ ) than for steady-state conditions; (iii) tanks with baffles (circular C and rectangular B) have significant improvements in mixing conditions when the tank is operated with a variable water level, in particular, the circular tanks that approach the



ideal reactor for the three variations; (iv) the full-scale tank, operated with approximately 20% level variation, has a behaviour that approaches the plug flow conditions ( $Mo = 1.5$ ).

It should be highlighted that, for water level variations of 50% and 80%, the normalized turnover times are practically independent of the tank configuration ( $t_{95}/\tau = 1.63\text{--}1.75$ ) and that the fill-and-draw cycles in the rectangular tank B significantly reduce the renewal times.

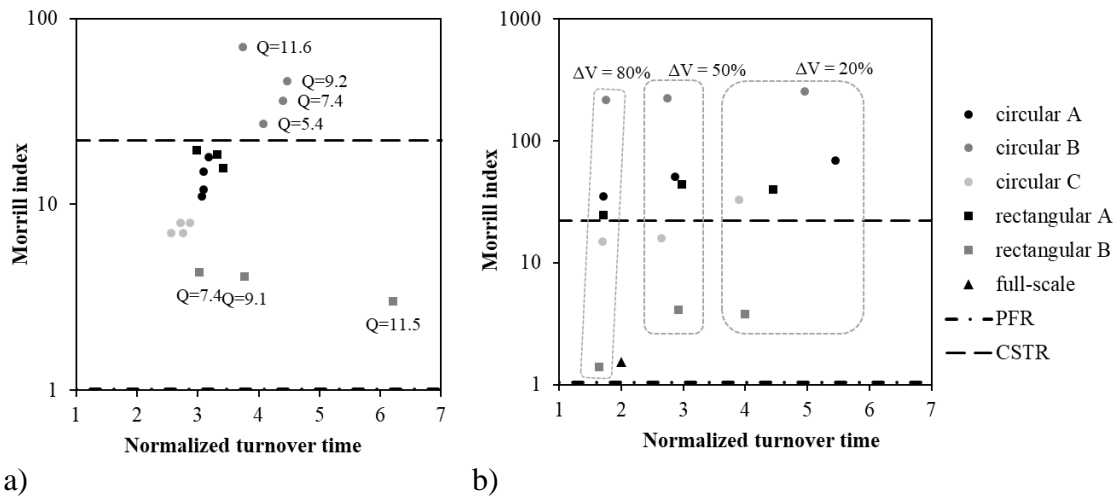


Figure 5.13 – Assessment of mixing and renewal conditions in storage tanks for: a) steady-state; b) fill-and-draw conditions. Normalized turnover time vs Morrill index.

### 5.4.2 Dispersion index

Values of the dispersion index are only calculated for the steady-state conditions (Figure 5.14). The circular tank B behaviour (the one with the inlet and outlet pipes on the same side) approaches  $\bar{\sigma} = 1$  (completely mixed tanks) (Figure 5.14); however, the high values of  $Mo$  show that water mixing is far from complete as a short-circuiting and many stagnation zones are created. Indeed, results from the dispersion index must be analysed jointly with those of other indicators to avoid misinterpretation of the results. In all the other tank configurations, the dispersion index increases with the flow rate, given the higher momentum associated. Tanks with configuration A have better mixing conditions than those with baffles for the same flow rate.

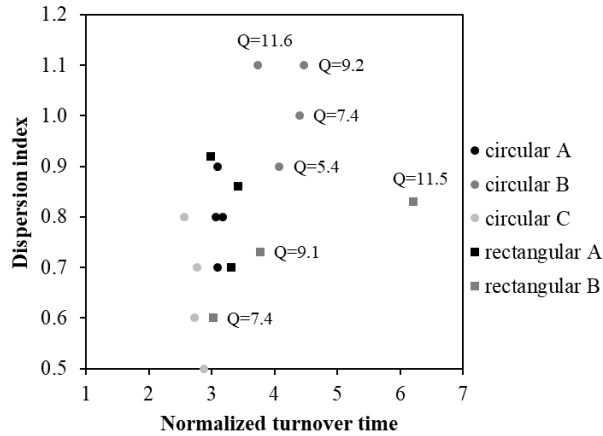


Figure 5.14 – Assessment of mixing and renewal conditions in storage tanks for steady-state. Normalized turnover time vs dispersion index.

### 5.4.3 Short-circuiting index

The resulting values for the short-circuiting index (Figure 5.15) corroborate previous conclusions. For steady-state conditions, there is a higher short-circuiting in circular tank B ( $t_{10}/\tau < 0.1$ ), followed by configurations A in the rectangular ( $t_{10}/\tau = 0.11\text{--}0.16$ ) and circular ( $t_{10}/\tau = 0.16\text{--}0.21$ ) tanks. Tanks with baffles (circular C and rectangular B) have a higher short-circuiting value ( $t_{10}/\tau > 0.25$ ). In the variable level operation, the short-circuiting effect is much higher (lower values) than in steady-state conditions and this effect hardly varies with the exchanged volume for each tank; the volume variation significantly affects the turnover time.

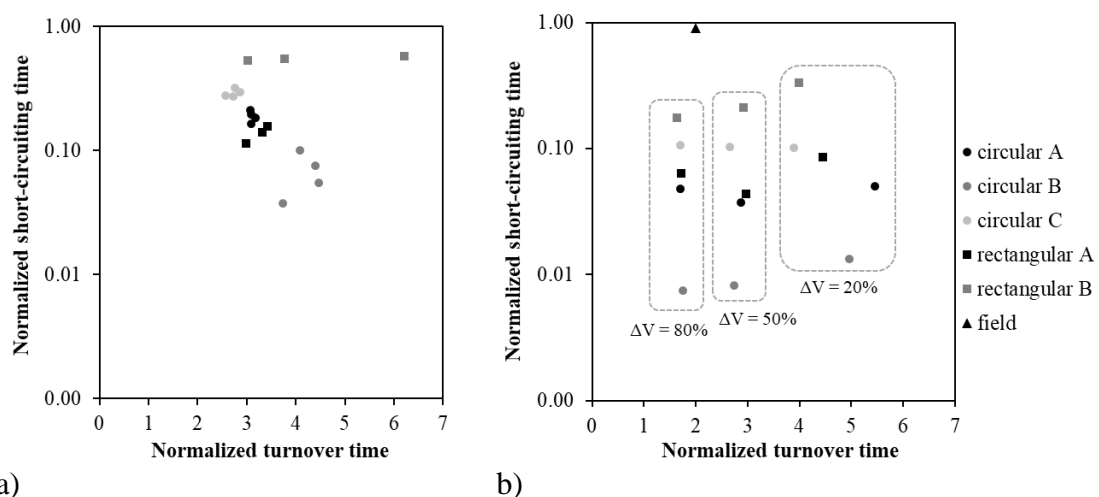


Figure 5.15 – Assessment of short-circuiting and renewal conditions in storage tanks for: a) steady-state; b) fill-and-draw conditions. Normalized turnover time vs Normalized short-circuiting time.

Overall, the best tank configurations for the renewal times are those with baffles, i.e., circular C and rectangular B (with baffles) when operated with constant or with a minor variation (e.g., up to 20%) of the water volume variation. For high fill-and-draw cycles (50-80% volume), the tank configuration has a minor effect on the renewal time, and the mean values of normalized turnover times are  $t_{10}/\tau = 1.75$  for 80%  $\Delta V$  and 2.8 for 50%  $\Delta V$ . The configurations with better results for the water mixing, are those without baffles and with the inlet and outlet pipes opposite to each other (i.e., circular A and rectangular A), for operation with constant water level, and circular C tanks with operation with variable volume. The fill-and-draw cycles were found to improve the mixing and renewal.

## 5.5 Conclusions

Tracer tests, with no buoyancy effects, were carried out in two small-scale tanks rectangular cross-section, operated at steady-state and at variable water level conditions, and in a full-scale tank in normal operating conditions. Cumulative distribution function, residence time distribution and hydraulic indexes were determined to assess mixing and short-circuiting in these water storage tanks.

Water mixing and renewal are key factors to assess water quality in storage tanks. Typically, the tanks are operated with water levels close to the maximum, with minor variations in water level to improve system reliability in case of an emergency. Using internal baffles allows to direct and control the flow through the tank and to promote the plug flow conditions. However, these structures can foment the appearance of badly agitated areas at the corners with poor connection with the mainstream flow, a situation that can last for a long time. These water pockets with high residence times can be gradually released if the flow rate increases and the water level changes.

In rectangular tanks operated with a relatively constant water level, higher flow rates increase the water renewal in open tanks (Configuration A). However, the opposite effect is observed in tanks with interior walls (baffles structures) (Configuration B). When operating the rectangular tanks at variable water levels, the higher the water volume variation in each fill-and-draw cycle, the faster the renewal of stored water becomes, with slightly better results in Configuration B despite the worse mixing conditions. For high-volume variations (50 to 80%), the renewal times are very similar in the two

configurations; for a 20% volume variation, Configuration B promotes a faster water renewal.

The comparison between tanks with circular and rectangular cross-sections shows that the use of baffles or physical structures to direct the flow allows reaching lower renewal times, especially in the configuration circular C (for a constant level operation) or the configuration circular C and rectangular B for 20% volume variations. For volumes variations between 50% and 80%, the configuration of the tank has a minor effect on the turnover time. For mixing, configurations without baffles allow better results, either for a constant level operation (circular A and rectangular A) or for an operation with a variable level (circular A, rectangular A and circular C).

The introduction of baffles in water storage tanks inhibits mixing between older and new water and promotes the creation of localized stagnant and poor mixing zones. Optimum baffles configuration can be difficult to determine, as different operating conditions can have different effects in terms of mixing and renewal conditions.

# Chapter 6

---

## **Flow dynamics in storage tanks using particle image velocimetry**

This chapter is based on the following scientific publication already submitted to a peer-review journal:

**Pinheiro, A.,** Ricardo, A., Monteiro, L., Almeida, M.C., Covas, D. Understanding flow dynamics in storage tanks using particle image velocimetry. *Journal of Experiments in Fluids* (to be submitted in February 2022).

## 6.1 Introduction

The current chapter aims at a better understanding of the flow dynamics inside circular cross-section storage tanks based on the measurement of instantaneous 2D velocities fields acquired with a particle image velocimetry (PIV) system. The description of the experimental facility, the used instrumentation, and the data collection methodology are presented. Measurements are carried out in horizontal planes at three water heights in small-scale tanks with different configurations and inlet/outlet pipe arrangements.

This chapter innovatively presents: i) the experimental study of flow dynamics conditions using PIV technology in small-scale storage tanks; ii) the analysis of the effect of tank configuration on velocity fields inside the tanks; iii) the identification of areas of stagnation and the characterization of turbulence intensities.

## 6.2 Particle image velocimetry

Particle image velocimetry (PIV) technology has been used to study flow dynamics in many engineering processes, such as the erosion of channels with vegetation (Ricardo et al. 2018), the velocity profile inversion in hydraulic transients in pressurized pipes (Brito et al. 2016) and the interaction between density driven flow and a stationary object (Ferreira et al. 2021). PIV is an optical measuring technique for fluid velocity, which utilizes captured images to produce quasi-instantaneous vector measurements. It calculates the displacement of added tracer particles in a fluid by taking two images shortly after one another using a video camera installed outside the water volume. These recorded images are processed using a specific software that analyses the movement of particles in subsections of the PIV images through cross-correlation techniques. The result produces a particle-image displacement pattern after taking into consideration of image magnification and time delay. The resulting flow fields can be post-processed to derive additional characteristics to describe local flow characteristics and structures (Raffel et al. 2007).

PIV has many advantages over other velocity measurements techniques. It is an almost non-intrusive measuring technique and does not cause fluid flow disturbances, which is only limited to the injection of the solid targets (seeding) in the flow. The use of PIV avoids the need of using intrusive flow measurement probes in the analysed flow region. However, PIV has some limitations, namely, the particles might not exactly follow the

motion of the fluid due to their immense density if the user does not choose the adequate seeding particles. The characteristics of seeding particles, namely their size and weight (to ensure neutrally buoyancy) and their non-toxicity, make this material very expensive. Other disadvantages, such as, the high cost of instrumentation, the time-consuming and complex data processing and the dangers of dealing with lasers can be a setback in the use of this technology. Although the acquisition of raw data is relatively simple, PIV data processing needs the use of specific software and involves a large processing time for converting the acquired images into instantaneous velocity fields adequately calibrated (Adrian 2005; Lavoie et al. 2007). Despite PIV having been used for studying flow and mixing conditions in stirred water tanks (Sheng et al. 1998), this technique has never been applied to measure velocity fields and to characterize the flow dynamics inside water storage tanks.

### **6.3 Data collection and analysis**

#### **6.3.1 Experimental setup description**

Experimental tests were carried out in small-scale tanks assembled at the Laboratory of Hydraulics and Environment of the Instituto Superior Técnico. These tanks consisted of 1:100 acrylic cylindrical tanks with a 392 mm inner diameter, with three different inlet/outlet pipe configurations (with an internal diameter of 4 mm) and a maximum water-depth-to-tank-diameter ratio of 0.15. The tank dimensions were determined by downscaling the most common sizes, shapes and cross-section configurations of drinking water storage tanks in Portugal (Monteiro et al. 2021). Similar tank configurations were tested and analysed in terms of water mixing and renewal in Chapter 4.

Three tank configurations were tested (A to C), in which the inlet pipe was located 14 mm above the water level (located 60 mm above the tank bottom). Configuration A presents an outlet pipe located at the opposite side of the tank, aligned with the inlet pipe, but located 4 mm above the bottom (Figure 6.1a). Configuration B has the outlet pipe located near the inlet pipe, with a circumference arc length of 30 mm and 4 mm above the bottom (Figure 6.1b). In Configuration C, the inlet/outlet pipes location is the same as in Configuration B, but with an acrylic baffle, with a length of 75% of the tank diameter and 4 mm of thickness, used to simulate an inner tank wall (Figure 6.1c).

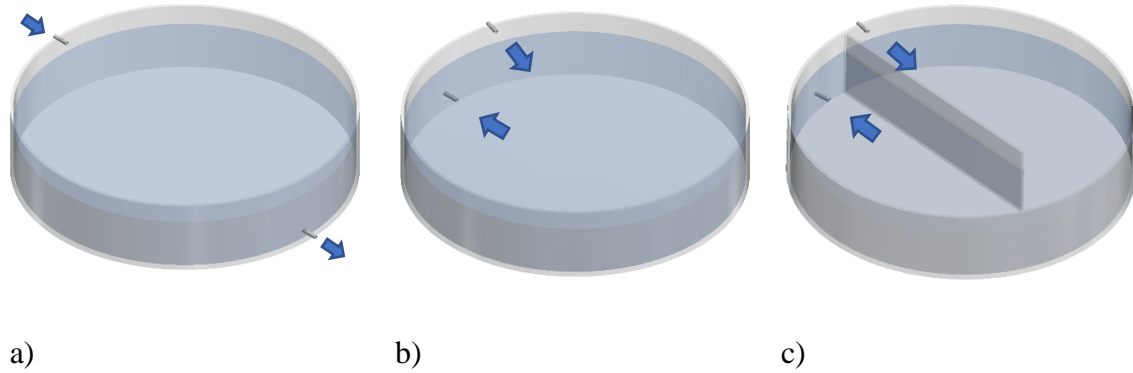


Figure 6.1 – Tested small-scale tanks: a) Configuration A; b) Configuration B; c) Configuration C.

The tested small-scale tank is gravity fed from a tank located at a higher level with a constant flow rate of  $9 \text{ L h}^{-1}$  regulated with an upstream valve (Figure 6.2). The outflow is controlled by three peristaltic pumps operating in parallel (FWT Model VPER Type 4-3, Ariccia, Italy), located after a hydropneumatic vessel (0.3 L) that is used to damp the pulsation of pumps in the small-scale tank. A second tank is used as an intermediate storage tank between the small-scale one and the feed tank, installed to receive the surplus water, overflowing from the feed tank. A stirring mechanism is installed in the feed tank to mix the PIV seeding particles and to homogenize the inflow water.

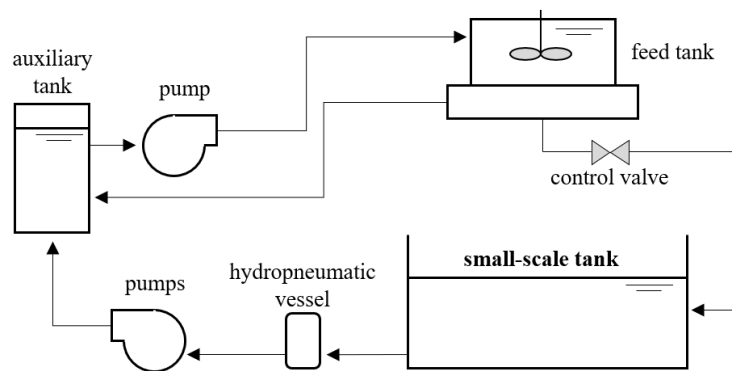


Figure 6.2 – Schematic representation of the experimental flow circuit.

The experimental PIV system, schematically represented in Figure 6.3 is composed of a laser head and lens, emitting a pulsed laser beam optically transformed into a 2-mm-thick laser sheet, a power supply or laser beam generator, a digital camera, a timing unit and an acquisition and control software.



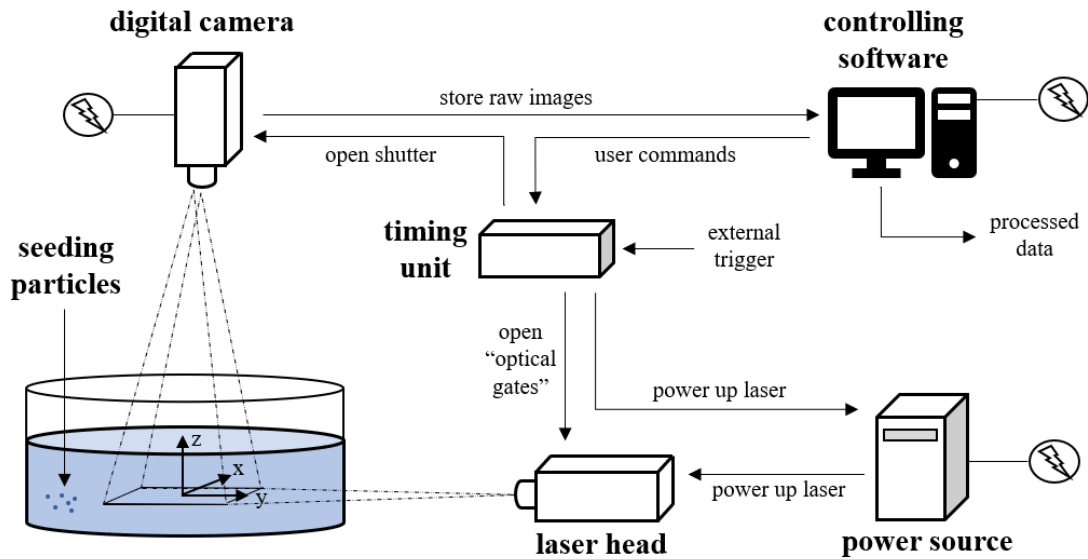


Figure 6.3 – Schematic representation of the PIV instrumentation.

Polyamid Seeding Particles (PSP-50 9080A5011 Dantec Dynamics®, Denmark) with a mean particle diameter of 50  $\mu\text{m}$  are used as seeding material in the current tests. The particles with round shape are small enough for a good tracking of the flow and, at the same time, have good light scatters (refractive index of 1.5).

A cylindrical lens producing the laser sheet is used and installed in a small cylindrical box attached to the laser head allowing the orientation of the light sheet. The 2D-PIV can only measure the projection of the velocity into the plane of the light sheet. This may result in some uncertainty in flow measurements, due to the existence of a secondary circulation in storage tanks since the out-of-plane velocity is lost and in-plane components are affected by perspective transformation (Raffel et al. 2007). The timing unit ensures the synchronization between the light emission by the laser head and the image acquisition by the CCD camera. The laser beam generator controls the power and the production of the laser light. The laser source used is a double-cavity neodymium-doped *Yttrium Aluminium Garnet* (Nd:YAG) model, which generates a pulse of energy of 30 mJ. The output laser beam is green with 532 nm of wavelength (Ferreira 2011). The whole system is controlled by DynamicStudio software.

The complete schematic representation of the experimental facility is presented in Figure 6.4. Further photos of the facility components assembled in the laboratory are presented in Figure A.2 in Appendix A.

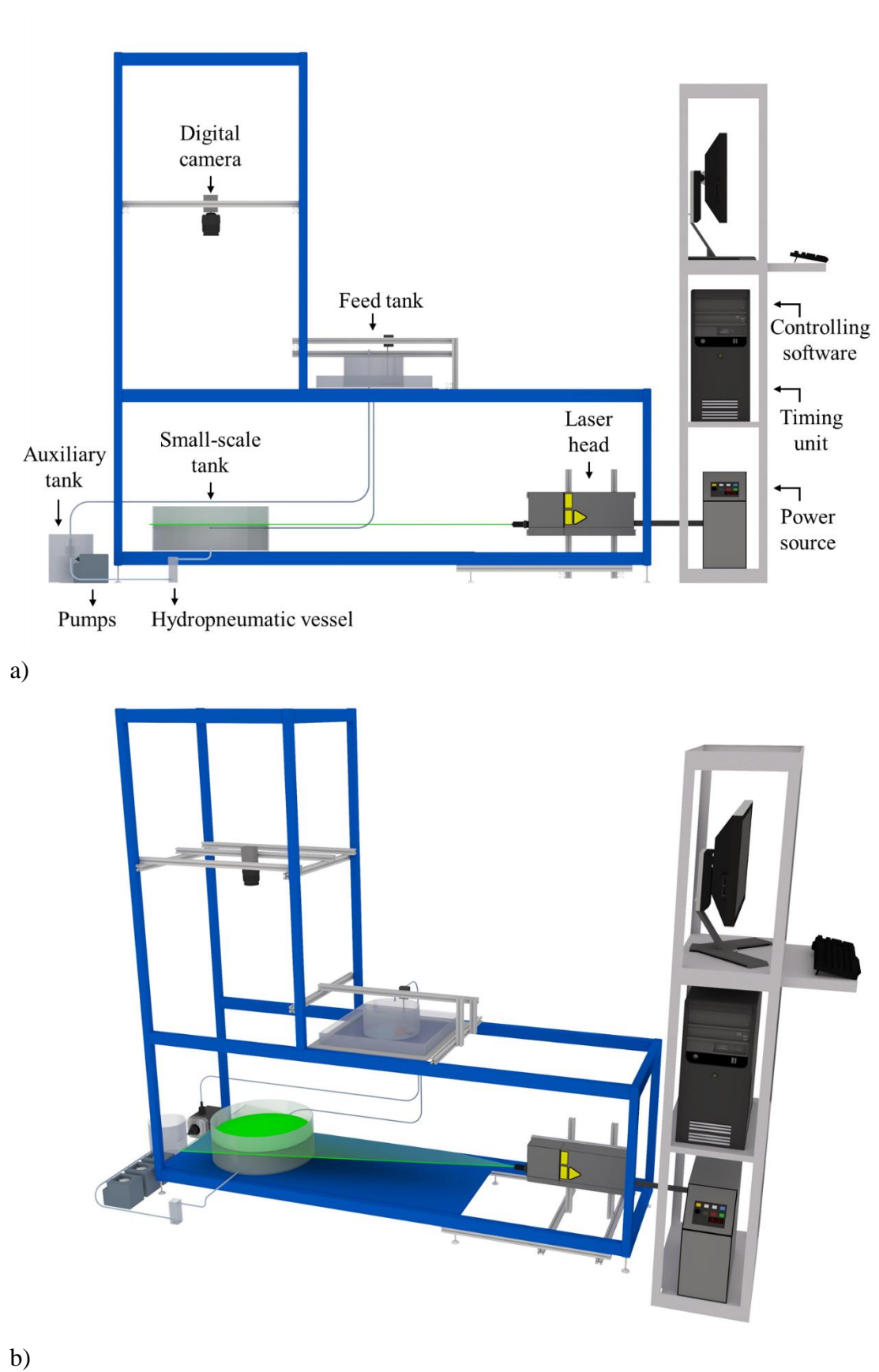


Figure 6.4 – Schematic view of the experimental facility: a) lateral view; b) axonometric view.

The synchronization between the light emission by the laser head and the image acquisition by the CCD camera (8-bit,  $1600 \times 1200 \text{ pix}^2$ ) is ensured by the timing unit. The CCD camera is positioned perpendicularly to the laser sheet to acquire images of the region lightened by the laser minimizing the distortion effects. The CCD sensors operate with photoelectric effect at each pixel, converting light into electric charge. The sensor is only sensitive to light intensity, that is to the amount of energy (Raffel et al. 2007). To maximize the contrast between the bright illuminated particles and the black background in the recorded images, the small tank is covered with black fabrics in order to prevent the entry of light from other sources.

In this work, the PIV system is operated between 0.5 and 15 Hz sample frequency. In each measuring gap, horizontal PIV velocity maps ( $u$  and  $v$ ) are acquired at three water heights, namely, at 0.010, 0.030 and 0.055 m from the tank bottom. Each horizontal plane was composed of the 9 or 12 small sections with 9.5 cm long and 12.5 cm wide. For each acquisition, approximately, 15 minutes of consecutive data are collected.

The local coordinates of measurement plane  $xy$  are aligned with the center of the small-scale tank. The PIV systems used in this work was commercialized by Dantec®. The control, acquisition and processing of raw data are carried out using the software DynamicStudio®.

### **6.3.2 Data processing**

As referred, the PIV is a non-intrusive technique that allows the determination of instantaneous velocity fields through the measurement of the small displacement of seeding particles being transported in the water flow. These displacements are determined through the photographic record of the seeding particles position in two consecutive instants of time. This technique allows to obtain the two components of velocity in the plane illuminated by the laser beam. By using seeding particles with density close to that of water density, the particles follow the water motion without affecting the flow characteristics. The recorded images are divided into small areas, referred as interrogation areas (IA). The displacements of the illuminated particles are obtained through the particles initial and final position within a given IA and for a given time between two consecutive images. The instantaneous velocity maps are obtained from the following approximation of the velocity components definition:

$$u(x, y) \cong \frac{(x + \Delta d_x) - x}{\Delta t} \quad \text{Eq. 5.1}$$

$$v(x, y) \cong \frac{(y + \Delta d_y) - y}{\Delta t} \quad \text{Eq. 5.2}$$

where  $u$  and  $v$  are longitudinal and lateral components of the instantaneous velocity in the horizontal plane (i.e., along  $xx$  and  $yy$  axes, respectively),  $\Delta d_x$  and  $\Delta d_y$  are the seeding particles displacement in the  $x$  and  $y$  directions within an IA, and  $\Delta t$  is the time interval between two consecutive images. The mean displacements in each IA are determined by adaptive correlation algorithm. For this correlation, a large IA is firstly employed and subjected to a simple cross correlation. The obtained correlation peak is used to re-centre (offset) a smaller IA and was again subjected to correlation. The process is repeated while there is enough illuminated seeding particles in the IA. This process is repeated for all IA of the image pair resulting in a complete displacement vector map in the units of the camera (pixel). The acquired data are processed with adaptive correlation and a validation method based on the median of the neighbour vectors was applied. The instantaneous velocity field exported from the PIV software is expressed in image units ( $\text{px s}^{-1}$ ), thus, a conversion to metric units ( $\text{ms}^{-1}$ ) is applied. A simple linear transformation is considered since the field of view is small enough so that it became possible to neglect circular camera distortions. For each acquired plane and before carrying out the velocity measurements, a circular acrylic sheet, with 1 cm quadrangular grid, is installed on the measurement plane and an image is recorded to allow the computation of the calibration coefficient. Herein, the size of the IA is chosen to start at  $128 \times 128 \text{ px}^2$  and to finished at  $16 \times 16 \text{ px}^2$  after three iterations on the correlation process. This choice aims to maximize the spatial resolution of the velocity field. A 50% overlap of the IA is considered.

After choosing the IA size, a sensitivity analysis is carried out to establish the frequency of acquisition. According to the displacements from each section (approximately 25% of the IA size), the sample frequency ranges from 0.5 (lower velocities) to 15 Hz (higher velocities). At last, the quantity of seeding is adjusted to have enough seeding particles for the chosen IA size (Figure 6.5). The quality of the velocity maps acquired with PIV technique depends on three correlated parameters: the frequency of acquisition, the quantity of seed particles and the IA size. Combinations between these three parameters are weighted for each tank section. Since the camera view field included parts that are not

inside the small-scale tank (Figure 6.5a), the original velocity maps are masked out to eliminate those parts (see white areas in Figure 6.5b).

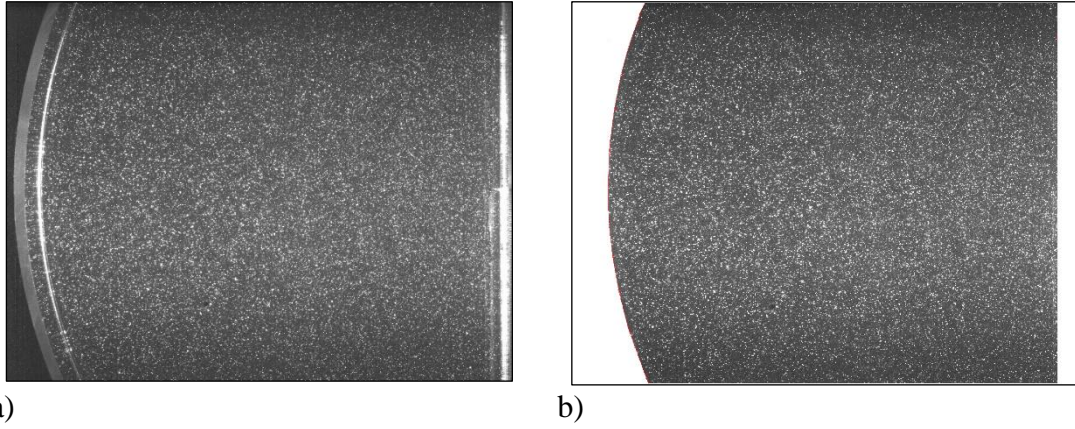


Figure 6.5 – Seeding particles illuminated and recorded from a section of the water storage tank: a) acquired (original) image; b) treated image.

The longitudinal  $u$  and lateral  $v$  velocities consist of time-average components,  $\bar{u}$  and  $\bar{v}$ , and fluctuating velocities,  $u'$  and  $v'$ , respectively, described by  $u = \bar{u} + u'$  and  $v = \bar{v} + v'$ . The longitudinal and lateral time-averaged velocities are obtained by:

$$\bar{u}(x, y) = \frac{1}{N_a} \sum_{i=1}^{N_a} u_i(x, y) \quad \text{Eq. 5.3}$$

$$\bar{v}(x, y) = \frac{1}{N_a} \sum_{i=1}^{N_a} v_i(x, y) \quad \text{Eq. 5.4}$$

where  $u_i$  and  $v_i$  are the velocities at  $i^{th}$  time and  $N_a$  are the number of acquired samples during established interval. In steady-state incompressible flow, the time-averaged normal turbulent stresses in  $xy$  plane are defined as

$$\overline{u'u'}(x, y) = \frac{1}{N_a} \sum_{i=1}^{N_a} [u_i - \bar{u}]^2(x, y) \quad \text{Eq. 5.5}$$

$$\overline{v'v'}(x, y) = \frac{1}{N_a} \sum_{i=1}^{N_a} [v_i - \bar{v}]^2(x, y) \quad \text{Eq. 5.6}$$

and the time-averaged shear stress in  $xy$  plane as

$$\overline{u'v'}(x, y) = \frac{1}{N_a} \sum_{i=1}^{N_a} [u_i - \bar{u}][v_i - \bar{v}](x, y) \quad \text{Eq. 5.7}$$

The normal turbulent stresses are typically used to calculate the components of turbulent intensities, defined as

$$I_x = \frac{\sqrt{\overline{u'u'}}}{V} \quad \text{Eq. 5.8}$$

$$I_y = \frac{\sqrt{\overline{v'v'}}}{V} \quad \text{Eq. 5.9}$$

being  $V$  the mean value of velocity. Since the velocity in the  $z$  direction is not obtained.

## 6.4 Experimental results

### 6.4.1 PIV velocity maps

The time-averaged velocity fields, obtained based on instantaneous velocity measurements, are presented in Figure 6.6 for each tank configuration (A, B and C) and for each horizontal plan (i.e., water heights of 0.01, 0.03 and 0.055 m). The colormaps represent the horizontal velocity magnitude,  $V_h=(u + v)^{1/2}$ , and the vector plots correspond the time-averaged velocity field. This velocity field allows a qualitative characterization of the flow within small-scale tank for each plane. The qualitative time-averaged velocity analysis for three configurations shows that each horizontal plane is characterized by zones of low velocity and others of high velocity. The flow patterns identified through the velocity fields obtained by the PIV technique corroborate the colour tracer data (Figure 4.5) observed in Pinheiro et al. (2021), as explained in the following paragraphs. Regions with no measurements near the tank wall and near the baffle structure are represented with white colour in Figure 6.6.

In Configuration A, since the flow is symmetrical, velocity field measurements are only carried out in half cross-section area of the tank and mirrored to the other half (Figure 6.6a,b,c). As the inlet jet falls into the surface of the water volume, it creates a three-dimensional flow with a very significant vertical component, not measured, but that can be inferred through the velocity components directions in the horizontal planes. The plunging jet sinks into the water surface (Figure 6.6c), is reflected in the tank bottom and rises again in nearby region (Figure 6.6a). Afterwards, the water travels along the tank walls and returns backwards through the central zone of the tank, mainly in the upper layers; this flow pattern forms two symmetrical vortical structures with lower velocity

zones in its centre (Figure 6.6a,b,c). Higher horizontal velocities are observed in the upper layer ( $z=0.055$  m) near the jet sink and, also, near the tank walls (Figure 6.6c).

In Configuration B, the observed phenomenon inlet region of the tank is similar to that in Configuration A: the jet sinks into the water surface and rises again; however, the flow tends to go along the tank wall nearer the inlet pipe and to travel back along the opposite wall to the outlet pipe (Figure 6.6d,e,f). This flow has a zone of very low velocities, especially in the lower layers in the centre of the tank (Figure 6.6d,e).

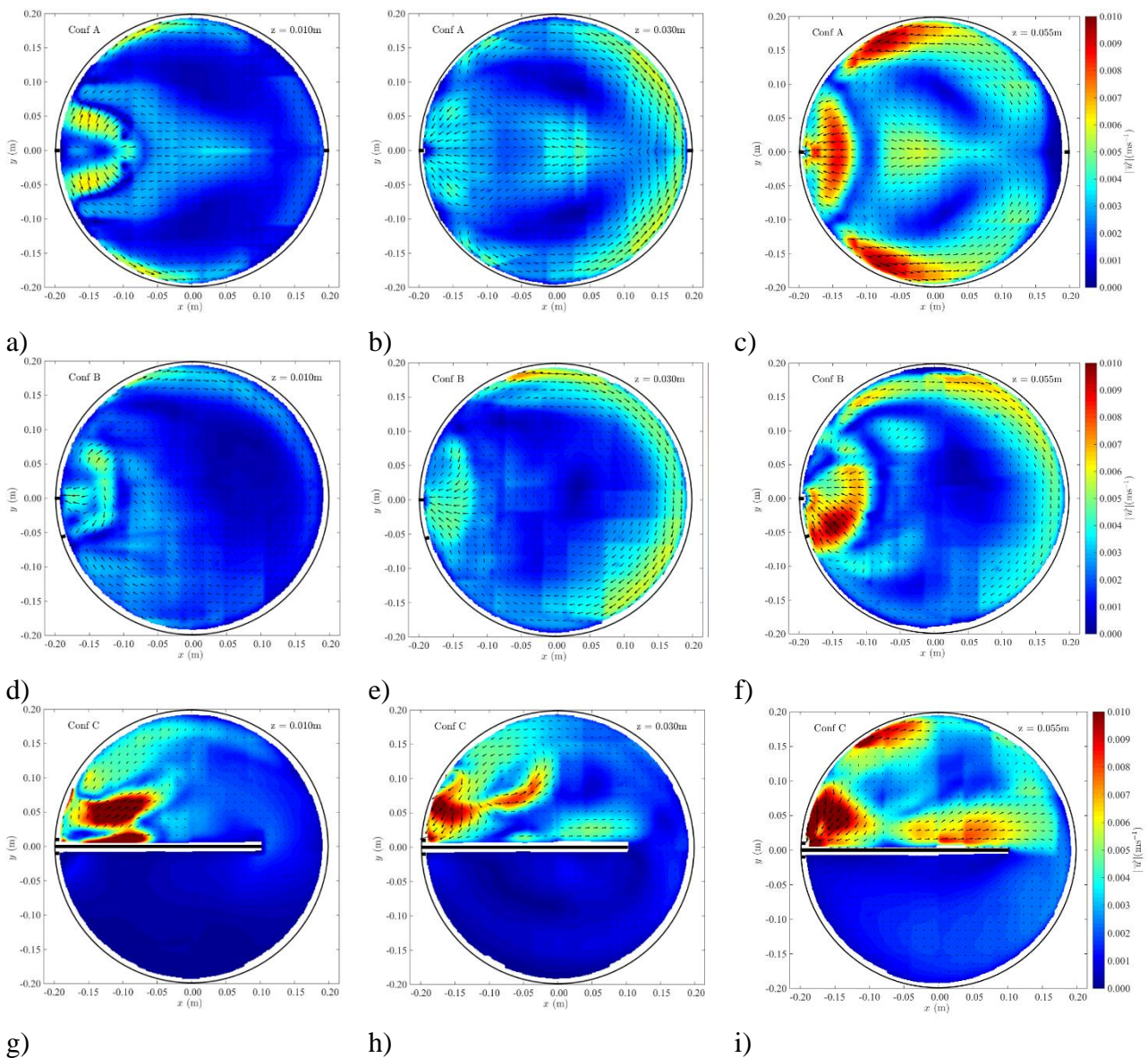


Figure 6.6 – Time-averaged velocity maps at each configuration and horizontal plane. The colormap represents the velocity magnitude and the arrow is the scale of the vector plot.

In Configuration C, the baffle structure with the size of 75% of the tank diameter contributes to faster inlet-side flow, with high velocity gradients near the plunging jet and

higher velocities in the upper layers and, also, to significantly lower and more uniformly distributed velocities after the baffle structure, particularly in lower water layers. (Figure 6.6g,h,i).

The time-averaged velocity fields allow the representation of the streamlines inside the tank for the different tank configurations and for the three horizontal planes, as depicted in Figure 6.7. Regions with no measurements are represented in dark colour. Low velocity regions (i.e., quasi-stagnant areas) are represented with grey colour; these regions correspond to points with average velocity in  $xy$  plane below  $0.001 \text{ ms}^{-1}$ .

In Configuration A, the flow travels along the walls since the tank inlet until the outlet and part of the flow reverses, as it reaches the outlet pipe, forming two symmetrical vortices. The centre of these vortices corresponds to lower velocity regions, particularly evident for lower water depths (Figure 6.7a,b). Low velocities are also observed near the outlet section in the upper water levels (Figure 6.7c).

In Configuration B, the flow travels in the clockwise direction from the inlet to the outlet pipe, along the tank walls, forming one single vortex in the centre of the tank. Lower velocity regions are located in the tank bottom (Figure 6.7d) and in the centre of the vortex in the upper water layers (Figure 6.7e,f).

In Configuration C, as the inlet flow reaches the water body, it pulls the water down and water travels along the baffle structure until the outlet region, tending create a reverse flow along the tank wall in the same side of the tank. Then, the flow continues to the second half of the tank along the tank walls with higher velocities in the upper layer ( $z=0.055 \text{ m}$ ). Low velocities regions are predominant after the baffle structure, except in some areas of the referred upper layer (Figure 6.7g,h,i).



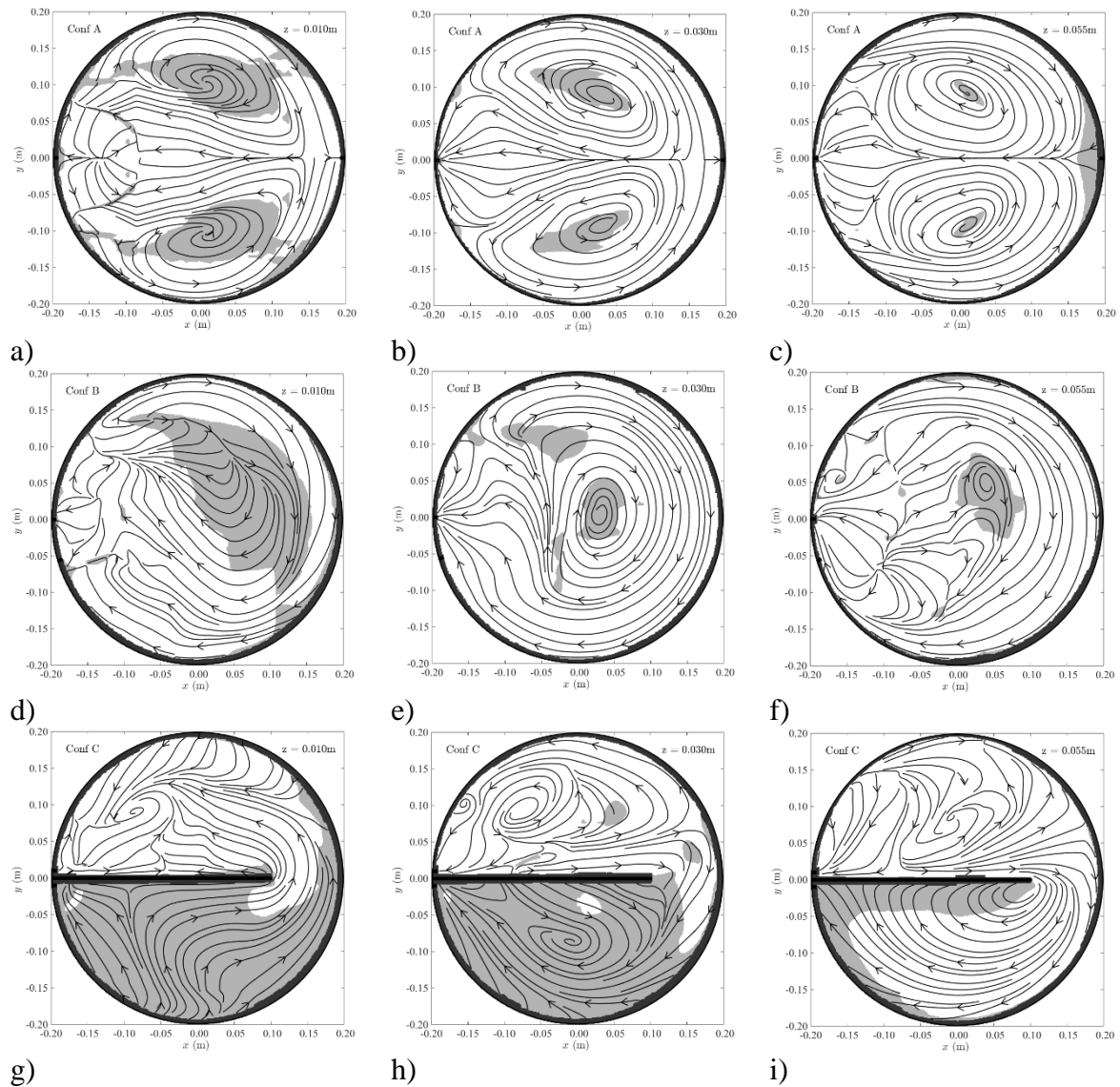


Figure 6.7 – Flow streamlines for each tank configuration and horizontal plane. The grey colour represents low velocity regions.

The distribution of the absolute velocity values, calculated only with  $x$  and  $y$  velocity components, for each tank configuration and in the three horizontal planes is depicted in Figure 6.8. These values correspond to ca. 120 000 observation points in each plane, covering almost 100% the tank cross-section, being represented in  $x$  axis as the percentage of the tank cross-section area,  $p$ .

The upper water layer ( $z=0.055$  m) has the highest velocities, and the lower layer has the lowest velocities for the three tank configurations. This shows the effect of the boundary conditions: the *no-slip condition* in the tank bottom creates high velocity gradients and slows down the flow; and the *quasi-non-air resistance* in the water surface allows the flow to have higher velocity values in the upper water layers.

The velocity distribution in intermediate layers strongly depends on the tank configuration: the configurations with no baffle structure (A and B) have decreasing velocities from the top to the bottom (Figure 6.8a,b); the tank with the baffle (configuration C), with a predominantly plug flow, has higher velocities in the upper layer, except in the inlet region (corresponding to less than 10% of total area), and has similar velocity distributions in the intermediate and the lower layers (Figure 6.8c).

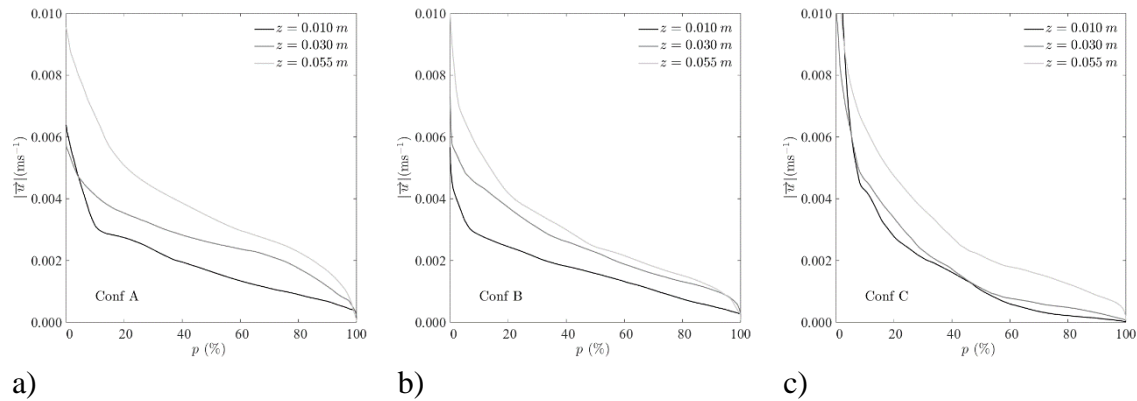


Figure 6.8 – Spatial distribution of time-averaged velocity (absolute velocity) values for: a) Configuration A; b) Configuration B; c) Configuration C.

#### 6.4.2 Turbulence analysis

Regarding the data from horizontal planes, instantaneous velocity series are used to analyse the turbulence in the three planes of each of the three configurations tested. The turbulent intensities in  $x$  and  $y$  directions ( $\overline{u'u'}$  and  $\overline{v'v'}$ ) and the Reynolds shear stress ( $\overline{u'v'}$ ) distributions in the tank cross-section area are presented in Figure 6.9 for the three configurations of the tank.

In general terms, the turbulent intensities are negligible in approximately 80% of the tank cross-section area independently of the tank configuration. Configurations A and B have higher turbulence in the intermediate layer of the tank, while the turbulence in Configuration C is higher in the layer near the bottom of the tank.

The associated momentum fluctuation (Reynolds stress) shows, in the same way, that most of the tank flow is characterized by smooth and constant fluid motion and a small area tends to have chaotic eddies, vortices and other flow instabilities.

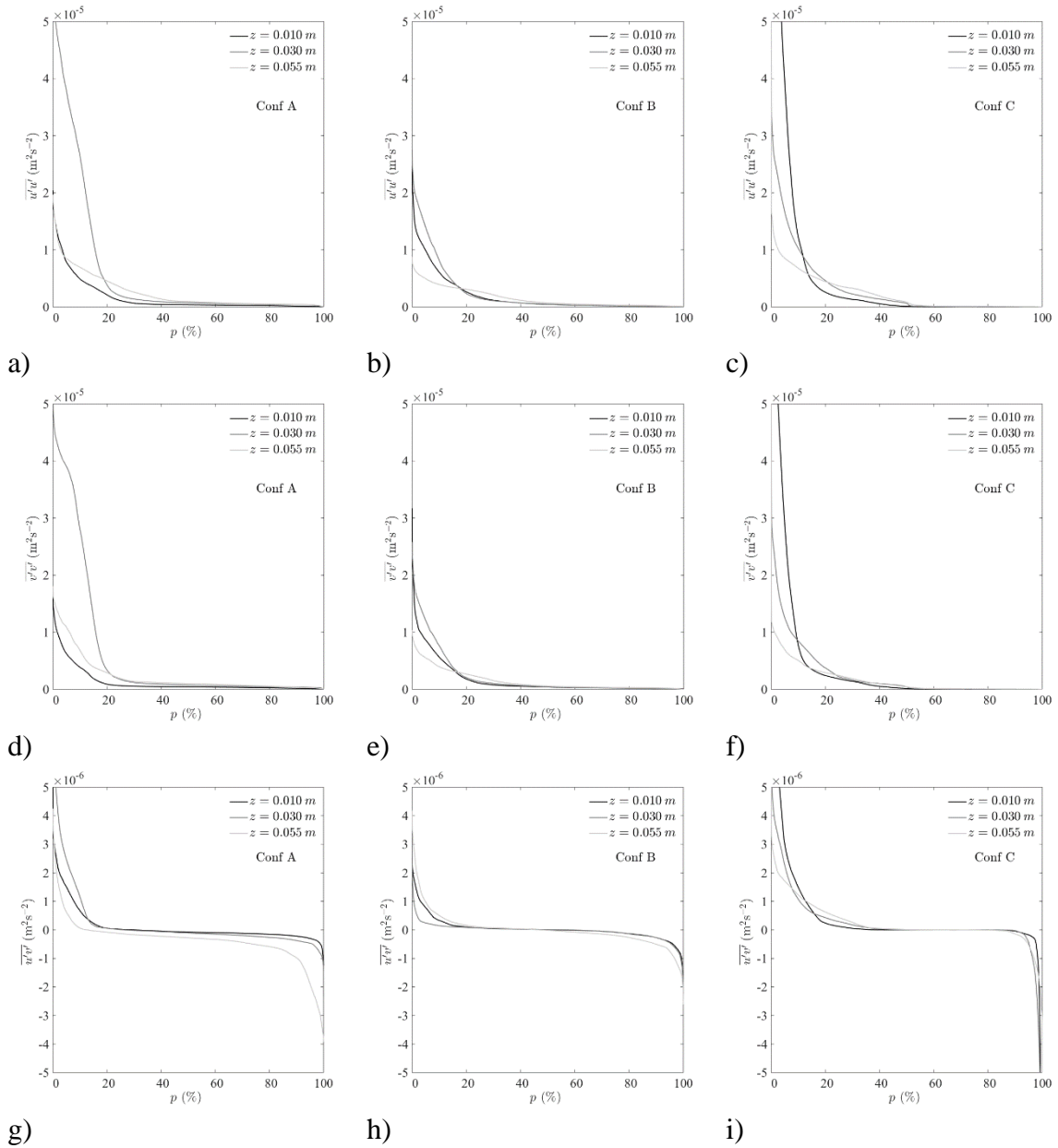


Figure 6.9 –Longitudinal ( $\overline{u'u'}$ ), lateral ( $\overline{v'v'}$ ) and Reynold’s shear stresses distributions for the three configurations.

The turbulent intensity maps ( $\overline{u'u'}$  and  $\overline{v'v'}$ ) and the shear stress map ( $\overline{u'v'}$ ) for Configuration A are presented in Figure 6.10 and for Configurations B and C are depicted in Figure B.1 and Figure B.2. Appendix B. These maps show that the intensity of lateral and of longitudinal turbulence tends to have particular expression near the water inlet zone for all tank configurations. It should be noted that shear stresses are significantly lower (10 times lower) than normal turbulent stresses and the latter are of the same order of magnitude in  $x$  and  $y$  directions (compare Figure 6.10a,b with Figure 6.10c). This means that the turbulence in most of the tank tends to be isotropic, that is independent of the axis direction in the horizontal plane (i.e., equal in all directions of the  $xy$  plane), since

shear stresses are almost null and normal stresses have similar values; this is typical of large tanks in which most flow has very low velocities. However, these measurements do not allow taking conclusions of the turbulence intensity in the vertical direction.

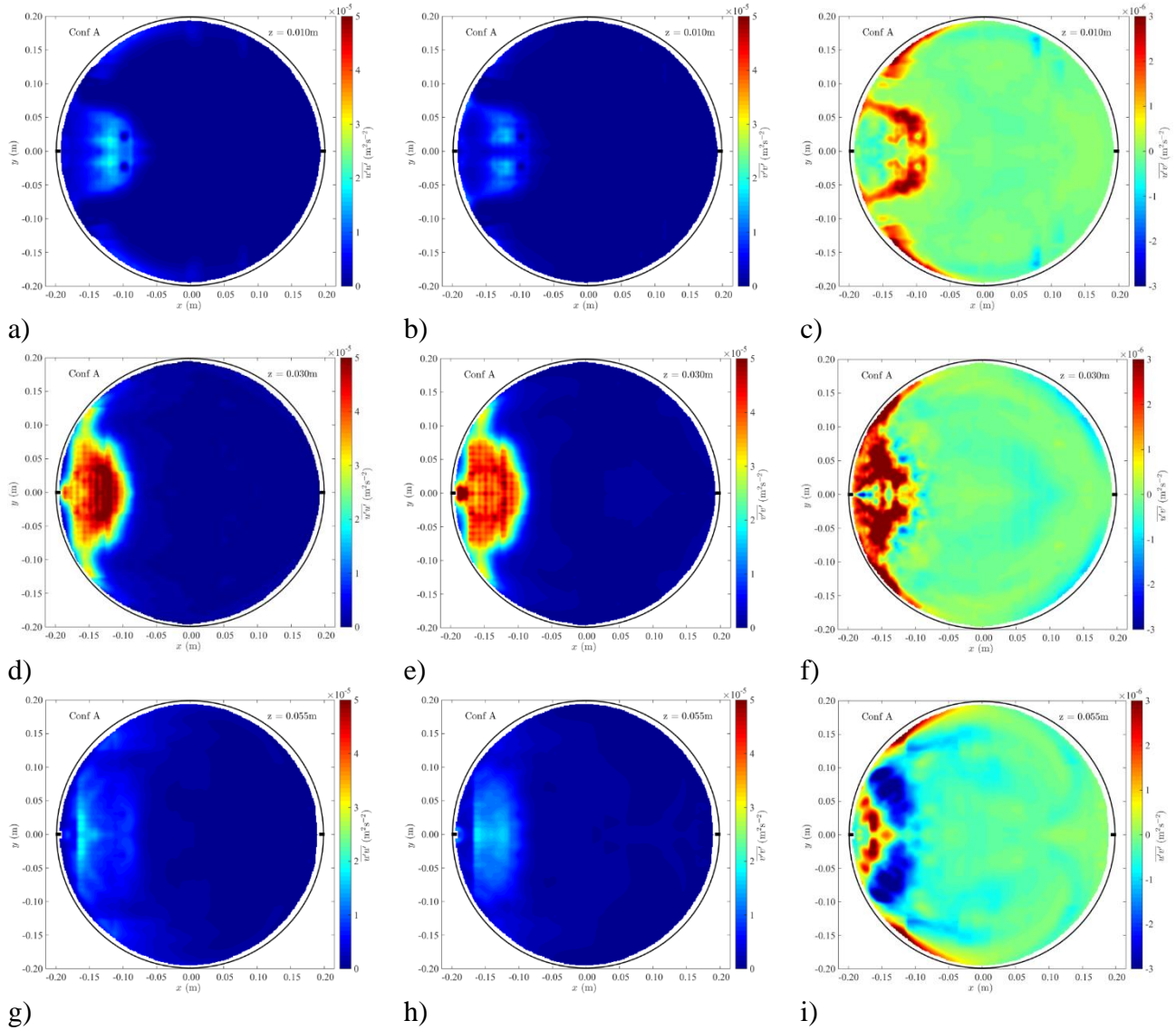


Figure 6.10 –Longitudinal ( $\overline{u'u'}$ ) and lateral ( $\overline{v'v'}$ ) stresses and time-averaged shear stress ( $\overline{u'v'}$ ) for each horizontal plane in Configuration A.

## 6.5 Discussion

Obtained velocity fields, streamlines and turbulence intensity maps show different flow patterns for each tank configuration, though with some similar features and flow trends. The first common feature is the high water mixing near the tank inlet region in the three configurations, which is typical of this type of tank with the inlet pipe above the water surface forming a plunging jet that sinks into the water surface and creates a vertical flow from the top to the bottom that is, then, reflected and moves upwards again; the jet

momentum moving downwards and upwards strongly promotes water mixing in this region. The second feature is the established flow paths along the tank walls: in Configuration A, the flow travels along the two walls from the inlet towards the outlet region, located in the opposite side of the tank, creating two symmetrically vortices, whereas, in the other two configurations, the flow travels in the clockwise direction along the outside wall until the outlet pipe, located close the inlet pipe. The third similarity is the low velocity regions formed in the centre of the vortices in Configurations A and B and after the flow passing the baffle in Configuration C. These promote the formation of stagnation zones with particle sedimentation, the loss of disinfectant residual and the microorganisms' growth, compromising the safe water supply.

Most common circular tanks in Portugal correspond to Configurations B and C. The former (B) tends to have lower velocity regions in lower layers (except at the inlet region) and a short-circuiting near the inlet/outlet pipes given the proximity between them, being expected to have poor water mixing conditions in the remaining parts of the tank, particularly in the centre, as well as, high particle sedimentation. As such, Configuration B is clearly not the most adequate for promoting water mixing and renewal, requiring more frequent cleaning works.

Several measures can be taken to improve these poor mixing conditions, such as constructing a baffle structure in the middle of the tank (Configuration C) to increase velocities and to promote the plug-flow, that, despite having a lower velocity after the baffle, assures a faster water renewal. Another improvement measure can be extending the inlet pipe downwards along the tank wall and then, along the tank floor until the opposite side with a nozzle at the extreme end. These measures will be further analysed and discussed in Chapter 7.

## **6.6 Conclusions**

This chapter analyses the flow dynamics inside three different water storage tanks configurations by measurements of velocities using a 2D PIV in steady-state conditions. The measured velocity fields obtained for three horizontal planes (near the bottom, at half height and close to the surface of the water) demonstrate that there is a significant variation of velocities throughout the water depth and between the configurations of the tanks. Additionally, the flow patterns observed using the PIV technique are identical to

those observed through the recorded images of the movement of dye tracer solution in Chapter 4. However, the velocity maps at the three water depths show that the flow is not identical throughout the water column. Independently of the tank configuration, lower velocity regions are more pronounced near the bottom of the tank (due to the *non-slip condition* in the tank bottom) and higher velocities are observed near the water surface (due to the *quasi-non-air* resistance).

The three configurations have very different flow patterns. Configuration A develops two symmetrical vortices in which the water moves onwards along the tank walls and returns in the central zone. Configuration B, given the proximity of the inlet and outlet pipes, enhances the short-circuiting flow path with poor mixing in most of the tank, since part of the incoming fluid is directed to the outlet without mixing with the stored water. Also, the region with lower velocities is located in the central zone of the tank and with higher expression near the tank bottom. In Configuration C, the baffle reduces the short-circuiting and promotes de recirculation and mixing in the first half of the tank, delaying the new water from reaching the outlet pipe. Reynold's shear stresses and longitudinal and lateral turbulent intensities show the existence of larger intensities differences across the tank, with regions farther away from the inlet with negligible turbulent intensity.

This chapter innovatively presents the first PIV-based study of steady-state flows in small-scale water tanks with an inflow jet above the water level as well as new experimental results for the validation of computational fluid dynamics models. The application of PIV technique has allowed a better understanding of the flow dynamics inside small-scale water storage tanks, however 2D PIV can only measure the projection of the velocity into the plane of the light sheet that is in horizontal planes. However, these 2D measurements do not allow to fully characterize the complex three-dimensional mixing phenomenon as that observed in water storage tanks since the out-of-plane velocity is lost, and in-plane components are affected by perspective transformation (Raffel et al. 2007). Thus, future velocity measurements should be carried out in vertical planes, correcting collected images according to the curvature effect of the tank wall, to allow the full three-dimensional characterization of the flow. Finally, further research should be carried out in rectangular cross-section tanks and with submerged inlet pipes and inlet pipes with multiple nozzles, in order to allow the establishment of operational and infrastructural improvement measures more appropriate to each particular case.

# Chapter 7

---

## **Water mixing improvement measures**

## 7.1 Introduction

The current chapter investigates the effect of different types of measures (structural and operational) on water mixing in circular cross-section tanks. Three structural improvement measures are analysed, namely: the inlet pipe diameter reduction; the use of multiple nozzles; and the use of baffles with different lengths. One operational improvement measure already analysed in Chapter 3 – the time-variation of water volume inside the tank is further discussed. Tests are carried out for the inlet pipe located above the surface of the water volume. This condition is based on the typical characteristics of the inlet pipes in existing water storage tanks in Portugal. Likewise, the use of filling and emptying cycles is based on typical consumption patterns in Portugal.

This chapter presents: i) the innovative analyses of several improvement measures of water mixing and renewal in small-scale storage tank; ii) the assessment of measures effectiveness through three hydraulic indexes; and iii) the identification of the most adequate measures for different circular cross-section tanks.

## 7.2 Review of existing measures

Extensive research has been developed and knowledge attained on design methods for ensuring a better water mixing and renewal inside water storage tanks to comply with water quality standards. These design practices have been widely used and have been validated by field sampling and monitoring. Some studies are limited in their application and tested conditions, but they have given some signs on how to improve the quality of the stored water. It is indisputable that water mixing and ageing are two related phenomena that affect the water quality in storage tanks (Grayman et al. 2004). Although a completely mixed flow is preferred for its minimal potential loss of disinfectant, it is usually not achievable for a full-scale tank because of the (large) size, and the limited mixing energy provided by the inflow momentum. In the case of nonuniform mixing, water may stay for a long time in stagnant zones, which can result in diminished disinfectant (e.g., chlorine) concentration and in higher bacterial regrowth.

Water storage tanks are generally operated without active mixing devices, such as turbines or impellers (specially in Portugal), being the inflow momentum the only driving force for mixing the new water with the stored one. The number, the position and the orientation of the inlet pipes are important factors that affect the degree of mixing inside



the tank. About 92% of the tanks in Portugal have only one water inlet pipe and 5% have two inlet pipes (as reported in 3.3).

According to Grayman et al. (2004) and Lemke and Deboer (2013), the inlet pipes must be positioned to avoid stagnation regions inside the tank and to promote the water mixing. The water jet formed by the inflow should have sufficient momentum to promote the effective circulation of the stored water. However, this very much depends on the diameter of the pipe as well as on the flow rate value and time-variation. Turbulent flows lead to a better mixing than laminar flows (Grayman et al. 2004).

The effect of the location and orientation of the inlet pipes on mixing effectiveness has been widely studied (Grayman et al. 2004; Okita and Oyama 1963; Tian and Roberts 2008; Zhang et al. 2014). Okita and Oyama (1963) show that jets are useful for mixing water within the confined geometry of storage tanks, particularly when a vertical jet reaches the water surface or when a horizontal jet reaches the opposite wall and the water reverses its direction. Grayman et al. (2004) experimentally analysed several inlet pipes' configurations for a constant water level tank, observing that some may cause poor mixing inside the circular cross-section tanks: the tangential inlet can lead to swirling flow, which may result in a stagnation area in centre of the tank; the inlet pipe extension and directed at the wall and to deflectors do not allow jet to completely develop, which may result in incomplete mixing or long mixing times; and large diameter inlet pipes may lead to low inlet velocity and momentum, which increase mixing times.

Tian and Roberts (2008a) studied the influence of different inlet configurations on mixing conditions, during the tank filling cycle. The authors carried out experiments in which the quantity, location and direction of the jet were combined. The results show that a higher number of jets is usually better when considering the same direction and that horizontal jets lead to better mixing conditions than vertical or 45° angle jets.

Both Grayman et al. (2004) and Tian and Roberts (2008a) studied the influence of submerged jets on the mixing conditions, however, it is not clear how the influence of a jet would be on the surface of the stored water volume, nor the flow patterns resulting from this phenomena. The location of the outlet pipe relative to the inlet pipe can also affect the mixing inside the tank. The existing of an outlet close to the inlet pipe can promote the short-circuiting phenomena, leading to newer water leaving the tank before

the water already stored. This dynamics in the flow can lead to the formation of older water pockets inside the tank that have more difficulty getting out. Studies conducted considering both inflow and outflow simultaneously and considering filling and drawing cycles are scarce (Pinheiro et al., 2021; Zhang et al., 2013b).

According to Mahmood et al. (2005b) the inlet pipe diameter and orientation must be carefully designed to provide adequate mixing within the filling period. Zhang et al. (2013b) applied computational fluid dynamics to simulate the flow patterns and water age distributions of a rectangular cross-section tank considering a fill-and-draw cycle condition. The results show that, depending on the cycle phase, the flow pattern changes. This means that it is important to consider both the outlet pipe position and the inlet. The same study only considers the submerged inflow. Due to the large dimensions of the tanks and limited mixing energy provided by the inflow momentum, completely mixed flows are usually not achievable and stagnation zones tend to be formed (Grayman et al., 1996). One way to provide a higher inlet momentum is by increasing the flow rate, whenever possible. Other way is by decreasing the inlet pipe diameter. The reduction of the diameter allows to increase the flow velocity and, consequently, the jet momentum. Based on the experiments of small-scale cylindrical tanks, other researchers (Rossman and Grayman 1999; Tian and Roberts 2008) reported that the mixing time was inversely proportional to the square root of inflow momentum. Reducing the nozzle cross sectional area by half will (theoretically) reduce the mixing time by up to 50%.

Some water utilities have started to develop solutions in which the inlet pipe is extended and has several horizontal and/or vertical flexible nozzles. These nozzles allow to optimize the jet velocity at all flow rates unlike fixed diameter pipes. Figure 7.1 presents some of these solutions of pipes with multiple nozzles.

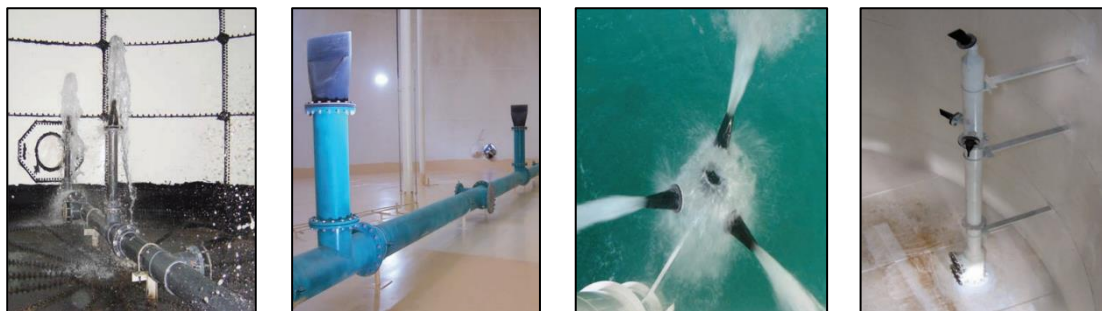


Figure 7.1 – Inlet pipe with several flexible nozzles.

The combination of an elaborate passive system of pipes inside the tank and multiple nozzles can be something to consider given its effectiveness, if well designed, however it can entail high construction costs. These multiport systems can mix the tanks up to 50% faster than a single inlet pipe, because of the inlet flow momentum is distributed through the tank instead of being concentrated in the inlet area (Duer 2011). Properly designed passive mixing systems require knowledge of jet-induced mixing characteristics as a function of tank shape, flow rate, turnover time, jet momentum and water density differences to determine the proper location, elevation, spacing, discharge angle and jet velocity of inlet and outlet pipes to achieve complete mixing (Duer 2011).

For tanks that have extremely low turnover, one way to mix water is to use an active mixing system that can operate 24 hours/day, if necessary. The application of active mixing devices, such as electric submersible mechanic mixers, solar powered mechanical mixers and air bubblers (Zhang et al., 2013b), are not common measures, given the high costs of the equipment and of operation and maintenance. However, these solutions can be effective, when properly sized, designed and tested. Some are actually used for disinfectant injection.

The application of structures, like tank inner walls (baffles), aims to direct the water flow inside the tank. These structures are common in contact tanks in water treatment plants since they promote plug-flow regimes needed to assure the long and precise contact time between the water and the disinfectant (e.g., ozone or chlorine in primary disinfection). In Portugal, the use of baffles in water storage tanks is also common. In circular cross-section tanks, the use of baffles allows to separate the tank in two half circles and the gap between these two parts tends to be between 25% and 50% of the tank diameter (Figure 7.2a). However, the existence of baffles is more frequent in rectangular cross-section tanks and, particularly, for larger volumes (Figure 7.2b).

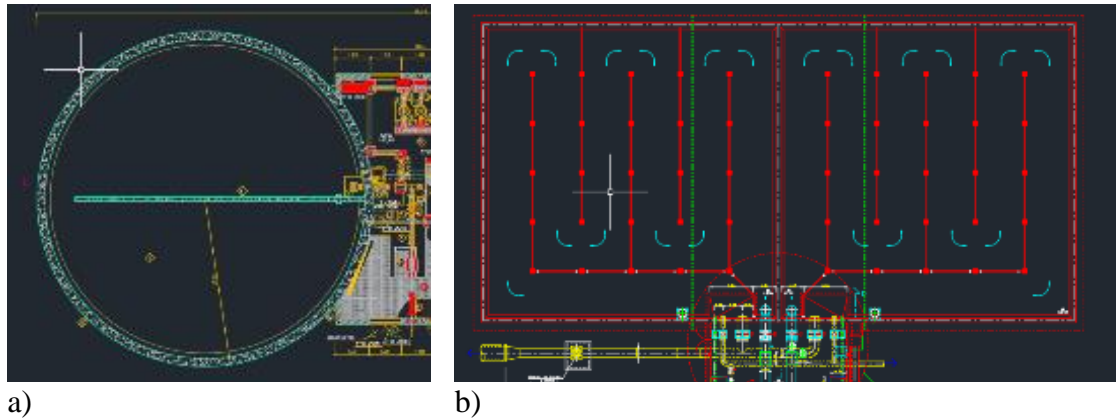


Figure 7.2 – Examples of water storage tanks with baffles in Portugal with: a) circular cross-section; b) rectangular cross-section.

In water storage tanks, the inflow contains a residual concentration of a disinfectant, usually chlorine in Portugal, necessary to prevent the deterioration of the stored water. To avoid the loss of this disinfectant residual, regimes close to complete mixing operation are preferable (i.e., the water enters the tank and is automatically mixed with the existing water). In a plug-flow operation, like the one promoted in a tank with baffles, the disinfectant concentration is higher at inlet region and lower at the exit region (depending on the operation, this may be a problem). Some authors recommend not using baffles in water storage tanks since they lead to poorer mixing conditions (Grayman et al., 2004; Zhang et al., 2012; Gualtieri, 2009; WHO, 2004). However, the application of baffles may not result on worse results in terms of the time needed to replace the water that is in the tank compared to fully open tanks (see Chapter 4).

Variable tank levels have shown to be an important operational mechanism to minimize the water age inside water storage tanks. The required amount of turnover varies depending on the system, but a common turnover goal is 3-5 days, or 20-33% daily fluctuation. However, tanks can have a significant localized increase in water age when they short-circuit and are not completely mixed, even if they are fluctuated 20-33%. Often, the increased water age and all associated water quality problems are specifically attributed to the inlet and outlet pipes (Duer 2003). The influence of a fill-and-draw mode is analysed in Chapter 3, and it should be highlighted that, for water level variations of 50% and 80%, the necessary time to renew the water inside the tank is practically independent of the tank configuration.

In the last two decades, studies started to be developed in the context of water supply tanks to try to determine the causes of water quality problems and improve the design and

operation of these tanks. However, little is known about the effect of various structural and operational conditions on the flow dynamics inside the tanks and only for specific conditions. Also, there is no quantification of the effects of structural and operational measures on tanks with the characteristics similar to those existing in Portugal.

This chapter presents an experimental study to analyse the effect of different structural measures (i.e., changes in the characteristics of the inlet pipe through the number of nozzles, the size and orientation; use of baffles with different dimensions) and of operational changes (variation in storage volume; flow rates) on water mixing and renewal.

### **7.3 Materials and methods**

#### **7.3.1 Experimental tests**

Water mixing improvement measures in the three circular cross-section water storage tanks are analysed by means of the development of dye and of conductivity tracer tests on a small-scale model. The methodology used for data acquisition, treatment and analysis is similar to that presented in Chapter 4. Dye experiments are carried out to identify the predominant flow patterns and the most important low velocity regions (almost stagnation areas) for each tank configuration. The application of a dye tracer allows a better understanding of the mixing phenomenon that occurs inside the tank. For each configuration tested in dye experiments, the top view is recorded by a GoPro camera. Conductivity step tracer experiments are carried out according to two tank operating modes: constant water level and variable water level (as described in 4.2.2.) allowing the quantification of mixing (Morrill index), short-circuiting ( $t_{10}$ ) and turnover ( $t_{95}$ ) characteristics that are used to assess each tested improvement measure.

#### **7.3.2 Tested structural measures**

The effect of several structural measures on circular cross-section tanks is analysed, namely the change of the inlet pipe diameter, the use of baffles and the use of multiple nozzles in the inlet pipe, as explained in the following paragraphs.

Two inlet pipe diameters are tested and compared: the initially tested 4 mm pipe (as described in Chapter 4) and a 2 mm pipe, corresponding to a 50% reduction. Tested flow

rate values are grouped in three categories since it was very difficult to experimentally control such low flows rates:  $Q1$  ranging from 5.0 to 5.4  $\text{Lh}^{-1}$ ;  $Q2$  from 7.2 to 7.4  $\text{Lh}^{-1}$ ; and  $Q3$  from 9.1 to 9.4  $\text{Lh}^{-1}$ .

Two baffles' sizes (Configuration C) are tested and compared to study the influence of the size of the baffle. The first baffle corresponds to the one studied in Chapter 4 which has an inner wall with a total length of 75% of the tank diameter (Figure 7.3a). The second case is a baffle of 50% of the tank diameter (Figure 7.3b). Both cases are compared with the no baffle configuration (Configuration A). Tested flow rates are grouped in four categories:  $Q1$  with 5.3  $\text{Lh}^{-1}$ ;  $Q2$  with 7.3  $\text{Lh}^{-1}$ ;  $Q3$  with 9.2  $\text{Lh}^{-1}$ ; and  $Q4$  with 11.8  $\text{Lh}^{-1}$ .

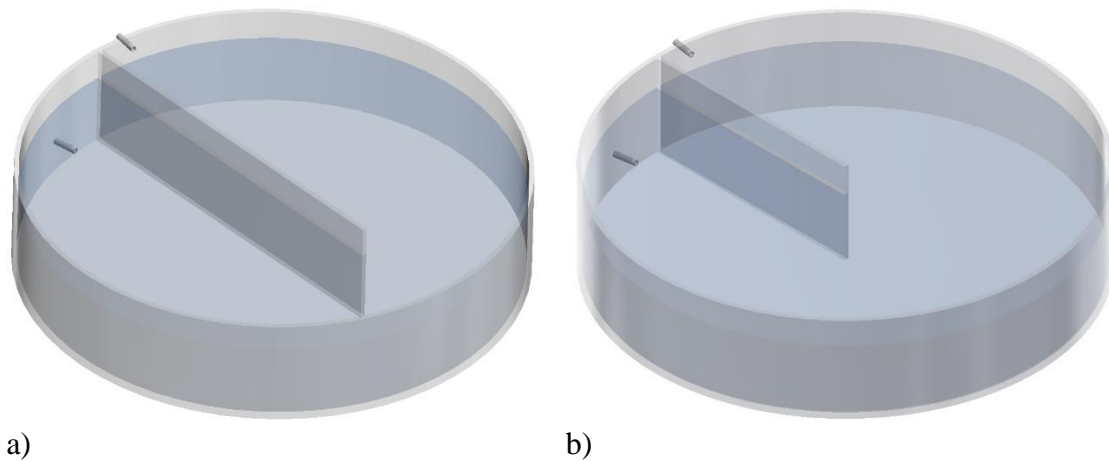


Figure 7.3 – Baffle influence: a) baffle with 75% of tank diameter (Configuration C); b) baffle with 50% of tank diameter.

Three multiple nozzle solutions are analysed for the tank configurations A and B. The main objectives of these solutions are: i) to increase the jet momentum by reducing the diameter of each nozzle (1 mm) with respect to the original inlet pipe diameter (4 mm); and ii) to guide the flow to multiple directions. In both tank configurations (A and B), the inflow pipe with multiple nozzles is submerged, as opposed to the initial conditions analysed in Chapter 4 in which the pipe was above the water level.

In Configuration A, two solutions, A1 and A2, are studied with nozzles with an angle of  $45^\circ$  and one solution, A3, with nozzles parallel to the bottom of the tank (Figure 7.4a). Since the inlet pipe is submerged and to prevent the formation of a jet directly into the outlet pipe, the nozzles are only directed towards the sides of the tank (Figure 7.5a). According to Grayman et al. (2004), this inlet orientation can promote a poor mixing condition inside the tank, however the authors' experimental conditions did not include

the influence of an outflow or nozzles with the proposed orientations. Additionally, the study of the thermal stratification effect (as carried out by those authors) is not the scope of study in this chapter, but it may have an influence on the obtained results, especially between the solutions with nozzles oriented at 45° and the solution with nozzles oriented at 0°. If stratification is likely to occur, solution A3 can aggravate mixing conditions.

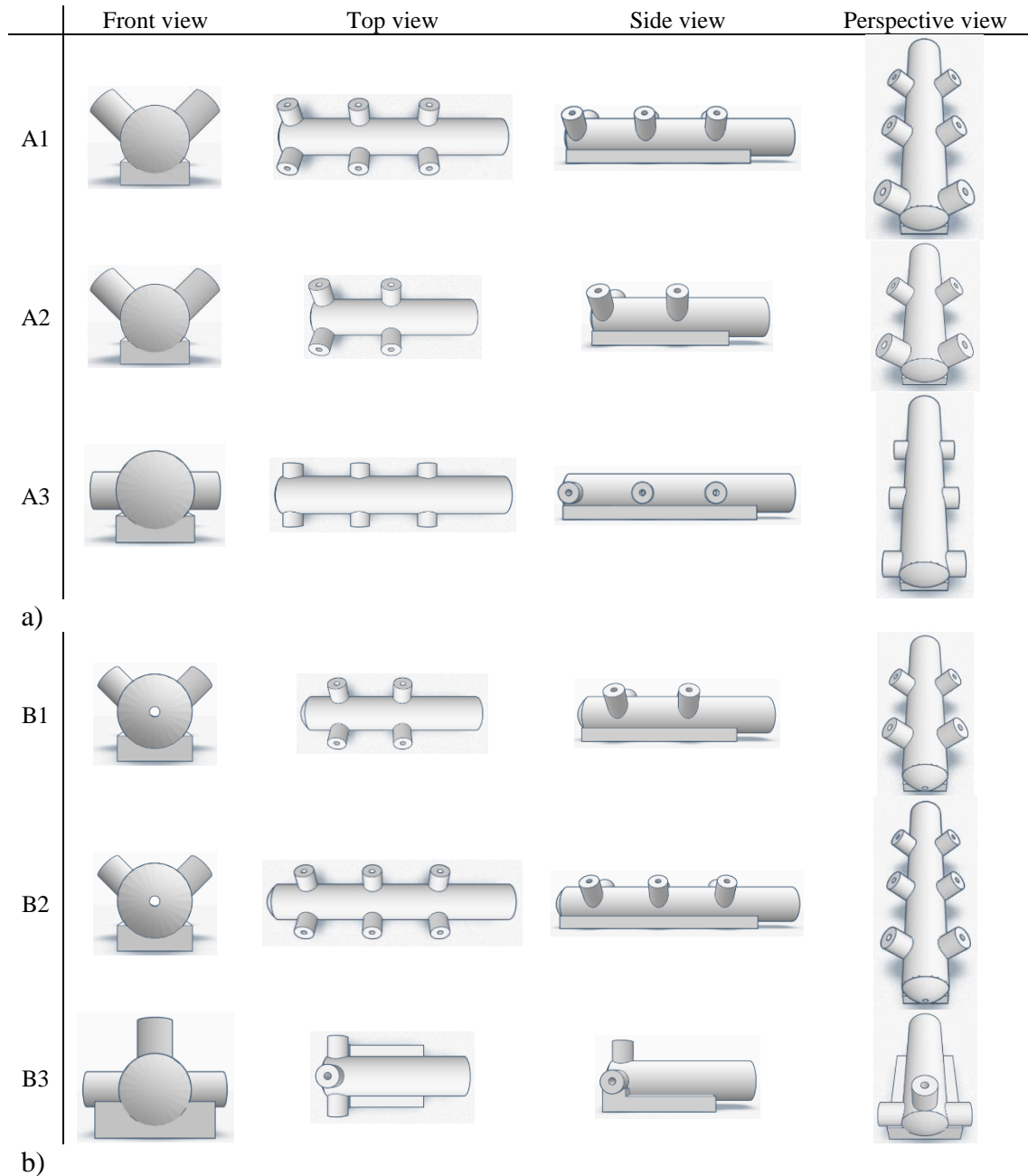


Figure 7.4 – Several views of the tested inlet pipe nozzles for tank: a) Configuration A; b) Configuration B.

In Configuration B, the objective is to locate the inlet pipe as far as possible from the outlet pipe, to reduce the short-circuiting effect, which is particularly relevant in this

configuration (Figure 7.5). For this purpose, an extension of the inlet pipe near the bottom of the tank is assembled and aligned with the outlet pipe, located 3 cm from the opposite wall of the tank (Figure 7.5b). The nozzle directed towards the tank wall is intended to avoid creating low velocities in that zone of the tank.

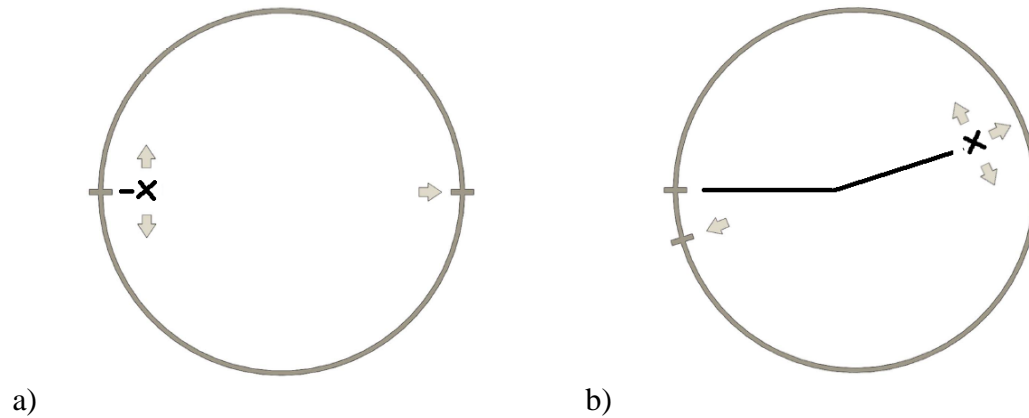


Figure 7.5 – Inlet diffusers locations: a) Configuration A; b) Configuration B.

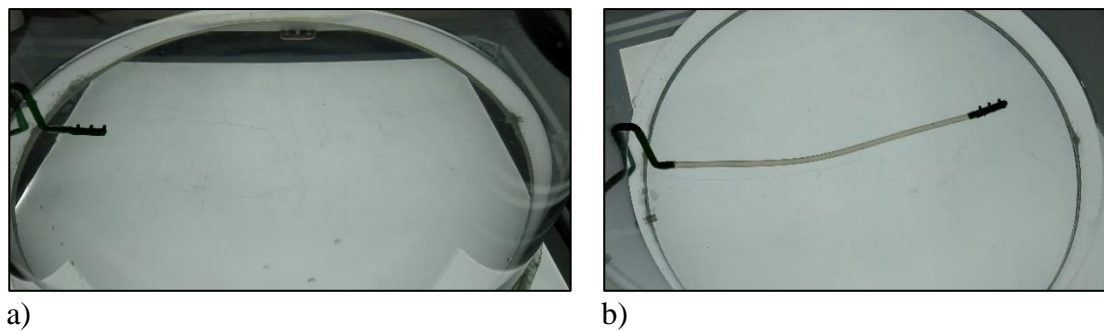


Figure 7.6 – Tracer tests with inlet diffusers: a) Configuration A; b) Configuration B.

### 7.3.3 Tested operational measures

The tested operational measures aim to simulate the most common operation schemes of storage tanks in water supply systems, with successive fill-and-draw cycles. In this mode (see 4.2.2.), a variable outflow pattern with four steps is used, as a proxy of the daily demand cycle of a water distribution system.

In this mode, a constant inflow rate is applied until a predefined water level is reached (filling period). Tank filling is resumed when a set minimum water level is attained. During this fill-and-draw mode, the water is continuously drawn out through the outlet pipe at variable flow rates, according to the consumption pattern. Three minimum water levels are tested (20%, 50% and 80% of the maximum water level) which correspond to volume variations of 80%, 50% and 20%, respectively.



## 7.4 Analysis of the results

### 7.4.1 Effects of the inlet pipe diameter

The momentum (force) of the inlet jet is used to stir the water inside the tank. The inlet pipe orientation and dimension with respect to the tank size and geometry determines the effectiveness of the resulting water mixing. Reducing the diameter of the inlet pipe is a passive method used to promote water mixing since it allows to increase the flow velocity and the kinetic energy of the inflow. Considering the steady-state conditions analysed for the three circular cross-section tanks presented in Chapter 4, the reduction in the internal diameter of the inlet pipe is explored considering the water mixing (Morrill index –  $Mo$ ), the normalized short-circuiting time ( $\theta_{10}$ ) and the normalized turnover time ( $\theta_{95}$ ).

Water mixing in the tank with the inlet and outlet pipes located at opposite side walls (Configuration A) when reducing the inlet pipe diameter has shown improvements in mixing indicators, for all tested flow rates (Figure 7.7a,b). Both Morrill index and dispersion index values approach those of a perfectly mixed tank, 22 and 1, respectively. Also, Configuration A leads to lower  $\theta_{10}$  values when the diameter is reduced, which means that 10% of the injected tracer reaches the outlet pipe faster and shows that turnover time increases (Figure 7.7c). According to these results, reducing the inlet pipe diameter for steady-state operation (for constant water level) and, consequently, increasing the flow velocity may not have conclusive results. The fact is that in terms of water mixing, this reduction of diameter is beneficial, but in terms of the time taken to renew stored water it is not.

For the tank with closely located inlet and outlet pipes (Configuration B), this diameter reduction contributes for better results in terms of mixing inside the tank. Both Morrill and dispersion indexes approximate the values of a CSTR (Figure 7.7d,e). The increase of inlet velocity allows the water jet to reach further way from the inlet and slightly reduces the short-circuiting effect, which is one of the problems in tanks in which the inlet and outlet pipes are very close (Figure 7.7f). Results show that turnover time significantly decreases with this structural measure especially for higher flow rates (Figure 7.7).

The baffled tank (Configuration C) shows improvements in the mixing indexes ( $Mo$  and  $\bar{\sigma}$ ) compared to the initial conditions (Figure 7.7g,h). However, the increase in the inflow

momentum boosts the short-circuiting effect, specifically for the lower flow rates (Figure 7.7i) and considerably increases the time necessary for the renewal of the stored water.

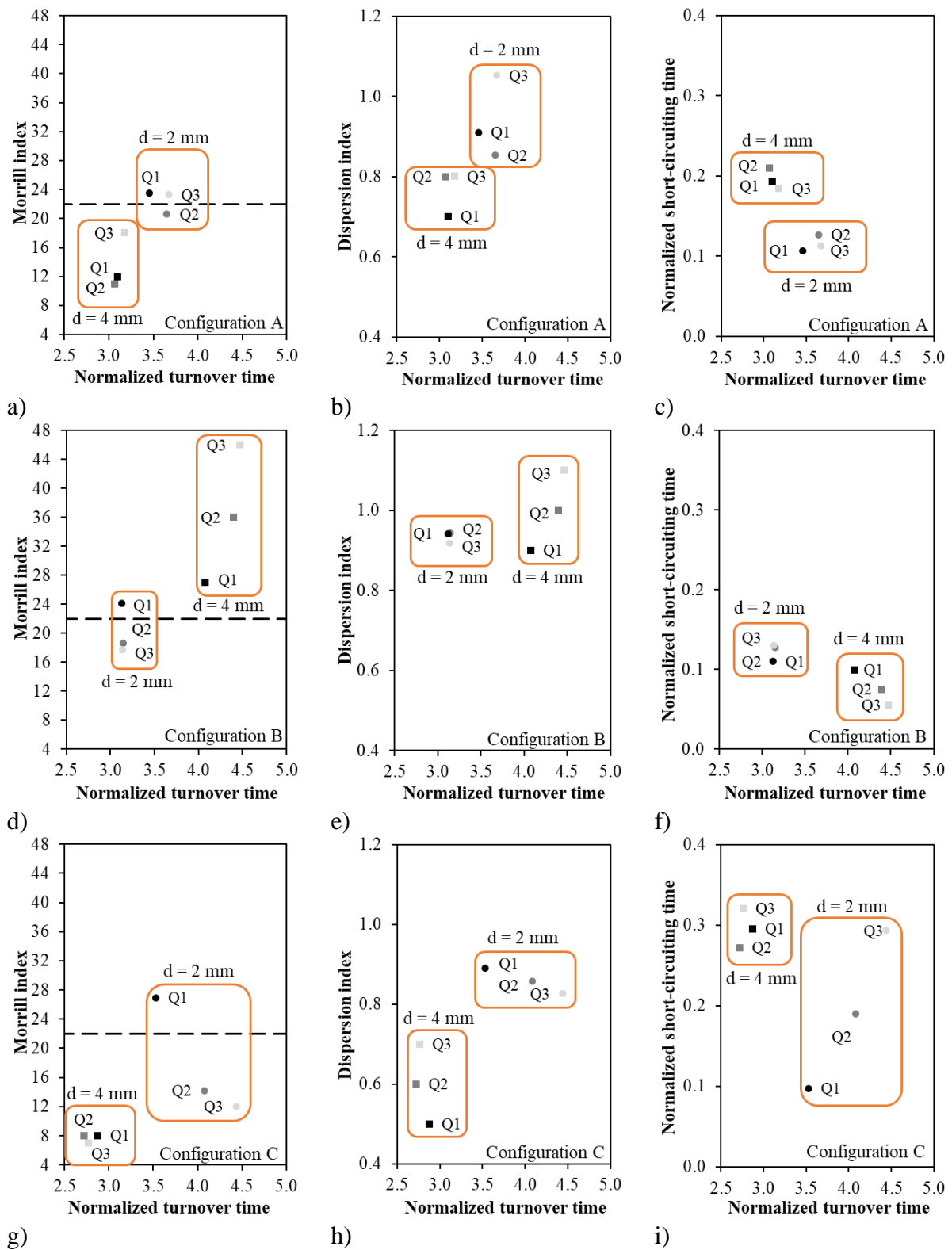


Figure 7.7 – Hydraulic indexes for the three configurations in steady-state conditions with different inlet pipe diameter: (a-c) Configuration A; (d-f) Configuration B; (g-i) Configuration C. The dashed line corresponds to the Morrill index value for a CSTR.

#### **7.4.2 Effect of inlet pipe nozzles**

The installation of oriented inlet pipes with several nozzles is tested for tank Configurations A and B in order to study whether the use of this type of structure improves the water mixing and renewal conditions in existing tanks. This solution consists of extending the pipe from the inlet located above the water level along the wall until the bottom of the tank and then along the tank floor, instead of extending and fixing the pipe in the tank ceiling (a solution often used).

In Configuration A, three pipes with four to six nozzles each are tested. Figure 7.8 and Figure 7.9 show the evolution of the dye tracer at three instants after the beginning of the injection (1, 5, and 10 min) for the three diffusors tested for each configuration.

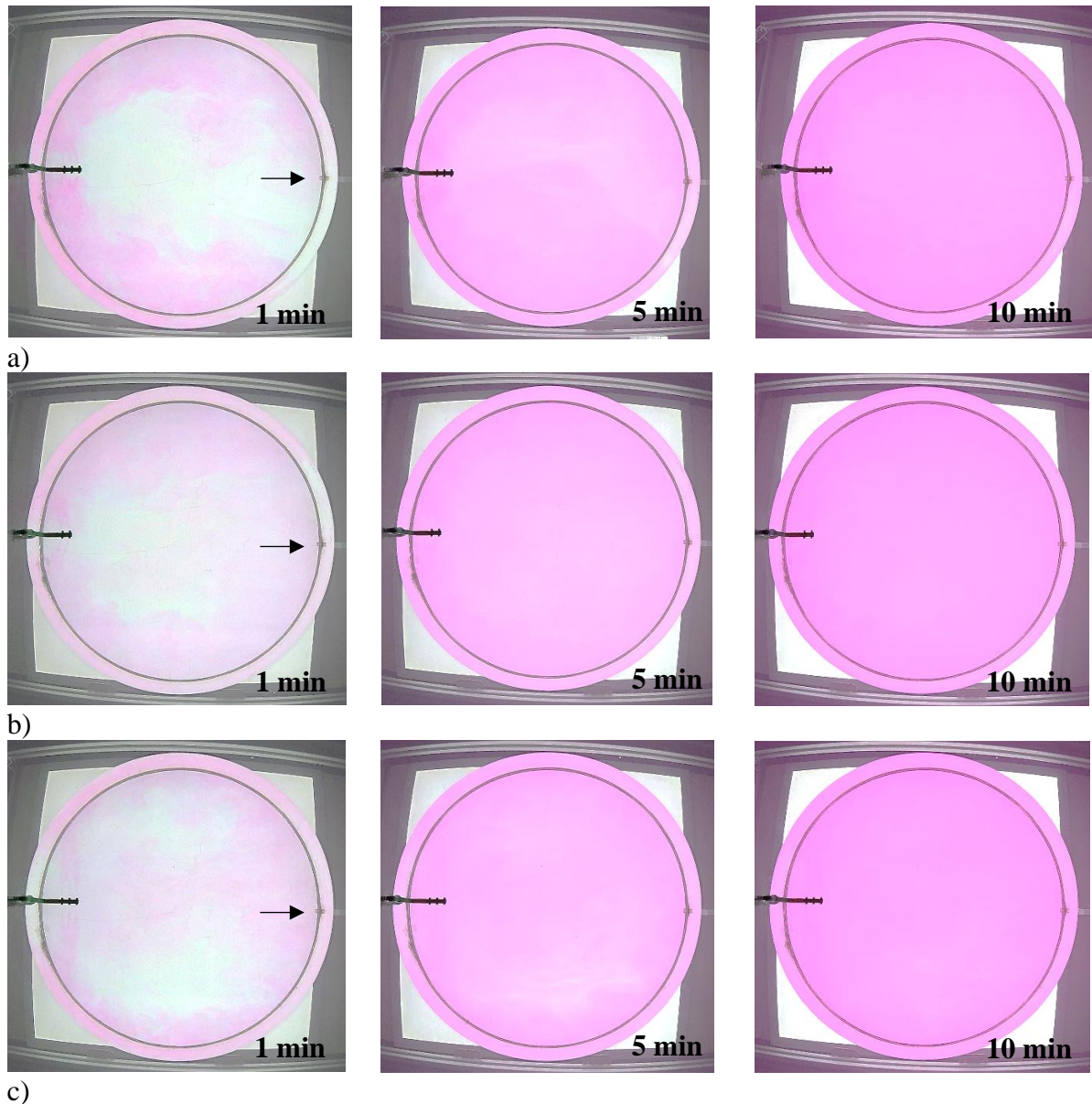


Figure 7.8 – Rhodamine dispersion within Configuration A at 1, 5, and 10 min after injection (constant water level, flow rate Q3): a) A1; b) A2; c) A3.

These images show the flow pattern and the slow mixing zones that contain low tracer concentrations over time. Tangential water velocities at the inlet pipes tend to promote a flow path along the perimeter of the tank, resulting in a stagnant zone in the centre (AWWA, 2006), however Configuration A with and without diffusors tends to form two lateral currents that when they meet on the opposite side of the tank return to the entrance area through the middle of the tank, forming two symmetrical vortices.

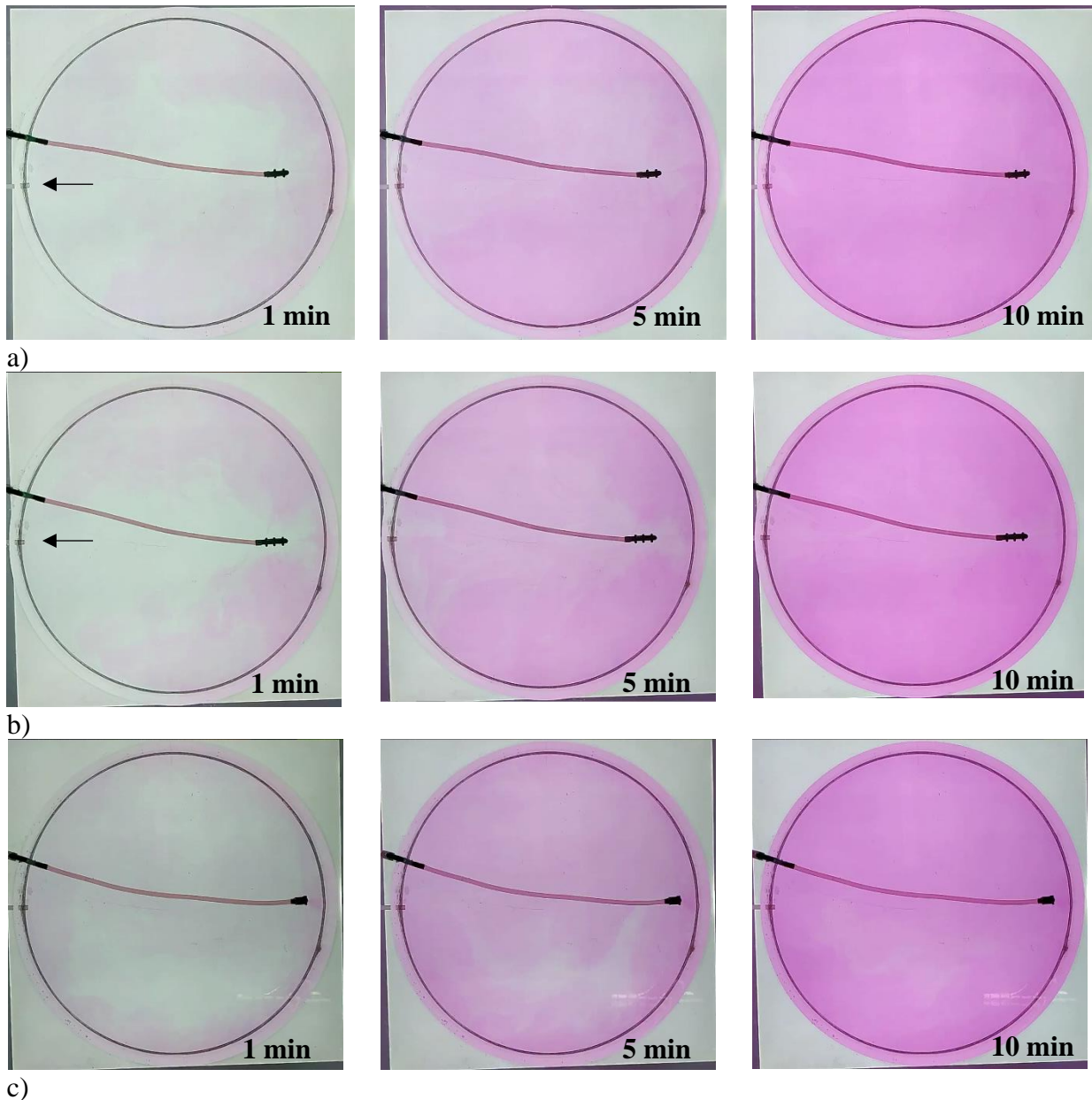


Figure 7.9 – Rhodamine dispersion within Configuration B at 1, 5, and 10 min after injection (constant water level, flow rate  $Q_3$ ): a) B1; b) B2; c) B3.

In Configuration A, the tested diffusers slightly improve the results in terms of mixing,  $Mo$  and  $\bar{\sigma}$  (Figure 7.10a,b). These also somewhat increase the short-circuiting effect, especially the A3 diffuser (Figure 7.10c). Regarding the time required for water renewal, only the A2 diffuser presents slightly worse results.

On the contrary, in Configuration B, the use of the diffusers leads to significant improvements in the mixing indexes (Figure 7.10d,e) and also minimizes the short-circuiting effect, especially the B1 diffuser (Figure 7.10f). The three diffusers allow to achieve lower turnover times, with the B3 diffuser being the one with the best results.

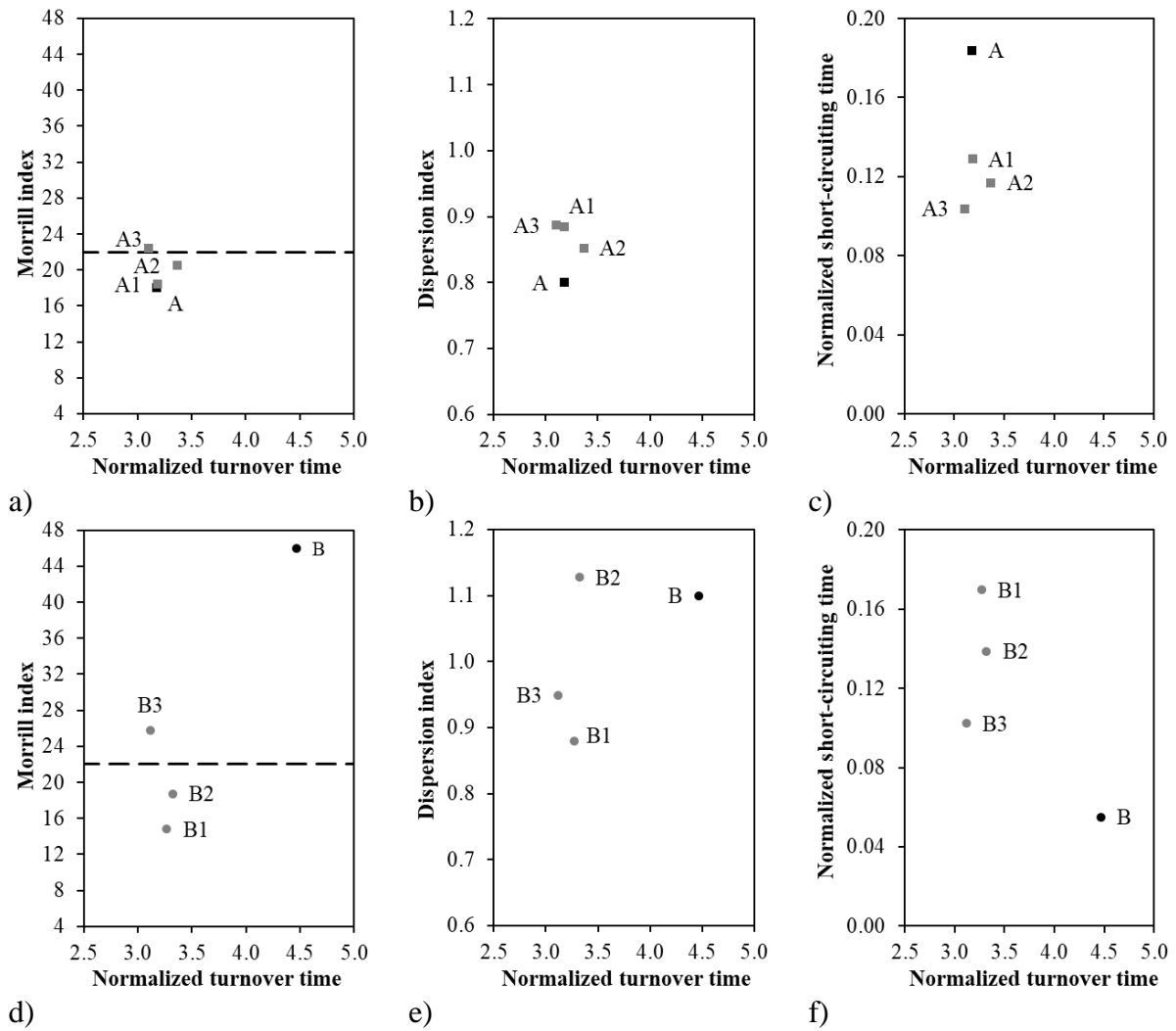


Figure 7.10 – Morrill index, dispersion index and normalized short-circuiting time vs normalized turnover time: (a-c) Configuration A and inlet nozzles solutions; (d-f) Configuration B and inlet nozzles solutions. The dashed line corresponds to the Morrill index value for a CSTR.

### 7.4.3 Effect of baffle structures

Building baffles in tanks can direct water through regions of a tank that would otherwise have poor turnover conditions, thus eliminating short-circuiting flow. Optimal configurations can be difficult to determine. Generally, in Portugal, the circular cross-section tanks have a baffle wall which can have between 50% and 75% of the tank diameter. Configuration C with two baffles sizes is tested (50% and 75% of diameter) to understand the effect of the size of the baffle on the water mixing and renewal conditions.

Figure 7.11 depicts the evolution of the dye tracer at three instants after the beginning of the injection (1, 5, and 10 min) for the two baffled circular cross-section tanks. The existence of a baffle separating the inlet and outlet pipes causes longer flow paths inside

the two tanks. These baffles promote recirculation in the first half of the tank, thus delaying the dye from reaching the second half and outlet pipe.

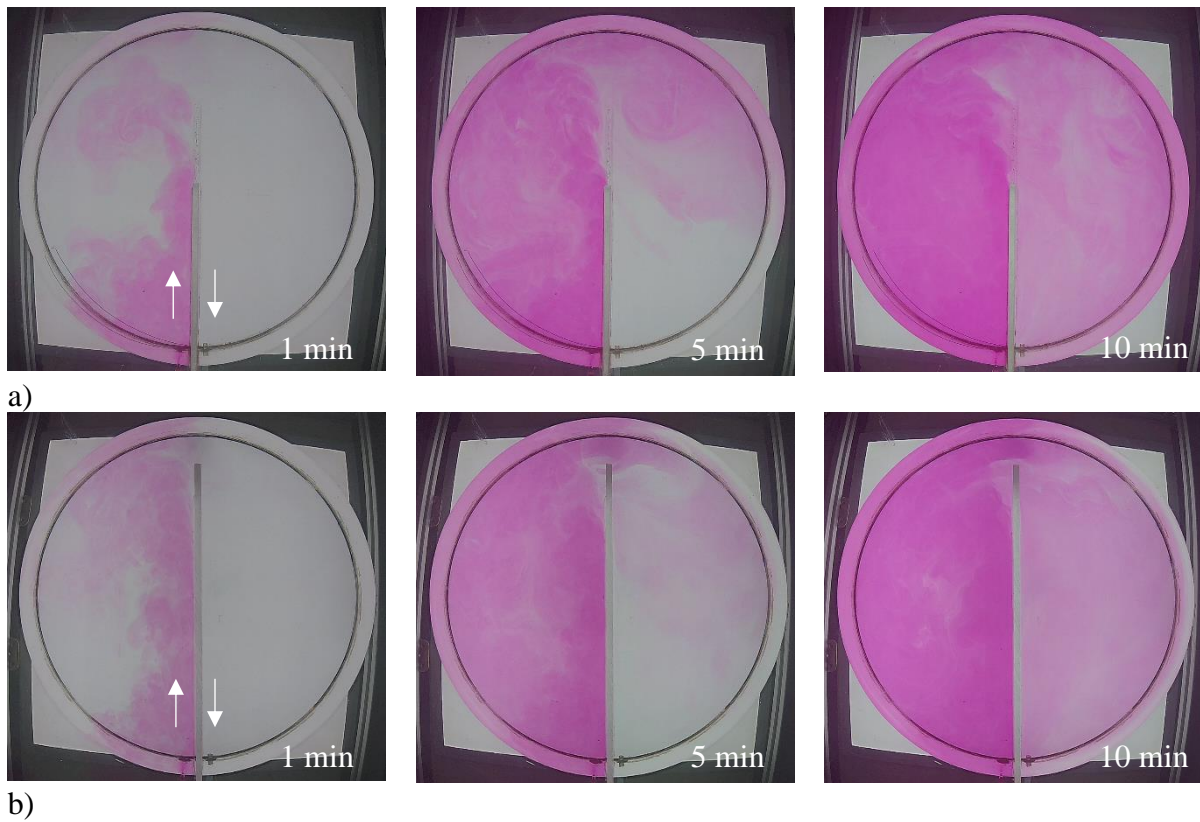


Figure 7.11 – Rhodamine dispersion within the two baffled configurations at 1, 5, and 10 min after injection (constant water level, flow rate  $Q_3$ ): a) baffle 50% tank diameter; b) baffle 75% tank diameter (Configuration C).

In terms of mixing, the tank with a 50% baffle gives better results especially for lower flow rates ( $Mo$ ), whereas the tank with a 75% baffle is closer to a PFR ( $Mo = 1$ ) (Figure 7.12a,d). As expected, the short-circuiting effect is smaller for the larger baffle since the flow has a longer path (Figure 7.12c,f). In terms of renewal times, the results are considerably better for the 75% baffle regardless of flow rate.

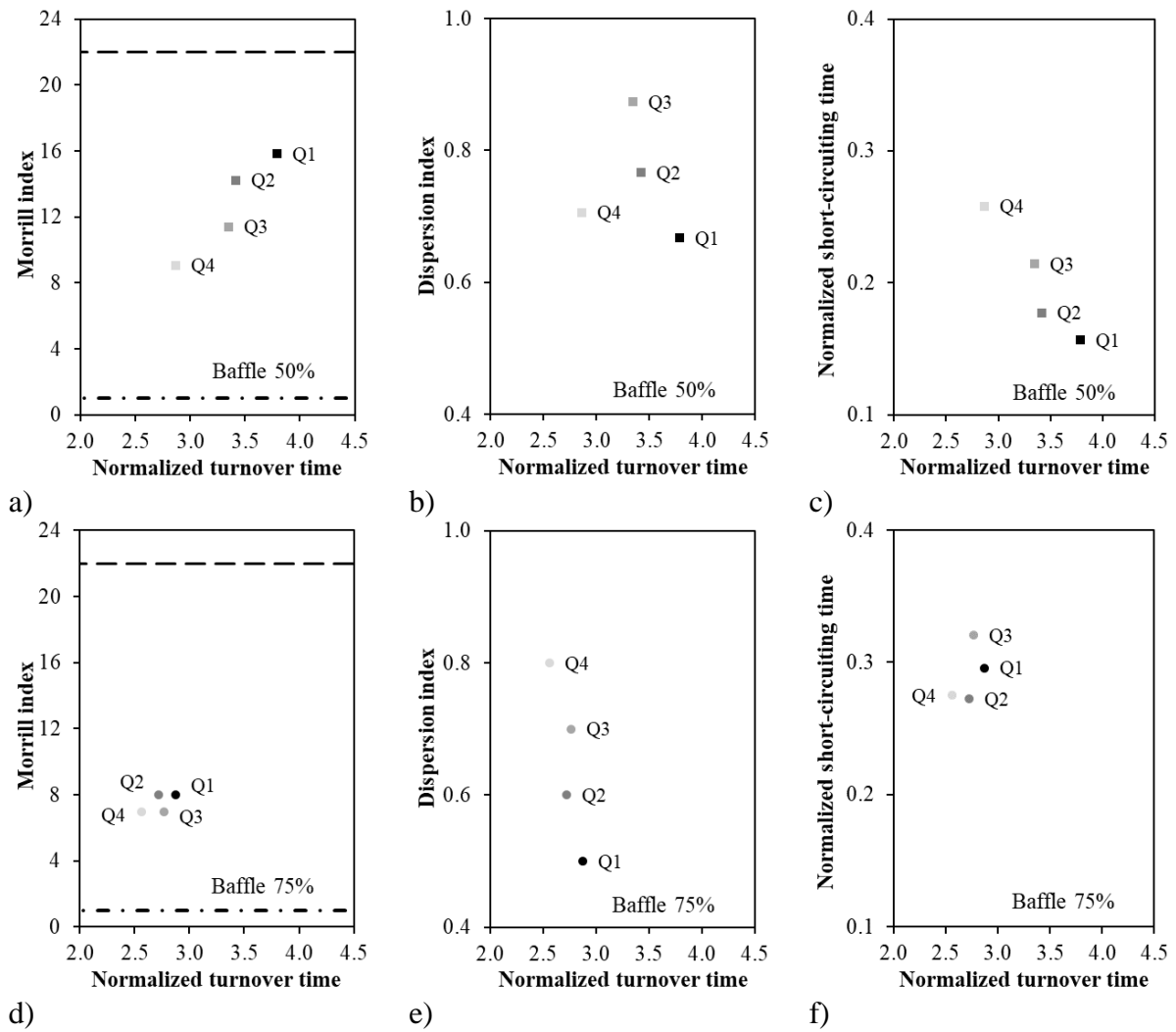


Figure 7.12 – Morrill index, dispersion index and normalized short-circuiting time vs normalized turnover time: (a-c) baffle with 50% of the tank diameter; (d-f) baffle with 75% of the tank diameter (Configuration C). The dashed line corresponds to the Morrill index value for a CSTR and the dotted line corresponds to a PFR.

#### 7.4.4 Effects of operational measures

Tracer tests are carried out in the three circular cross-section tanks operated at variable water levels (see Chapter 4). Three levels of variation in tank volumes are analysed (20%, 50% and 80%) and an outflow pattern is used to simulate the real daily water consumption and storage tanks operating conditions.

The short-circuiting index  $\theta_{10}$  does not significantly vary with the volume exchange and confirms the strongest short-circuiting effect in Configuration B (Figure 7.13b). These results suggest that operating the tanks at variable water levels can intensify existing short-circuiting effects, compared with what is observed in steady-state tests. The Morrill index increases for all configurations operated at variable water levels (Figure 7.13a), in



comparison with the steady-state conditions. Such increase in  $Mo$  is due to much higher  $\theta_{90}$  and lower  $\theta_{10}$  values when the tanks operate at variable water level. Though these conditions are different from the steady-state ones, it seems reasonable to assume that a  $\theta_{90}/\theta_{10}$  ratio of 22, as in a CSTR, would be the target value for  $Mo$  of a homogeneously mixed tank. For all configurations, the high  $Mo$  values decrease as the percentage of exchange volume increases. This suggests that the deviation from the ideal mixing condition is higher when the water level variation is small and that increasing the exchange volume in each cycle enhances mixing.

Mixing levels in the tank of Configuration A with 80% exchange volume per cycle show a small deviation from the ideal mixing, indicating that it might be possible to achieve good mixing conditions in these tanks, depending on the inflow and outflow patterns and flow rates, if a high percentage of exchange volume occurs. For Configuration B,  $t_{90}$  values and, thus,  $Mo$  are exceptionally high, as a result of recirculation and of the formation of stagnation zones that are apparently promoted when the tank is operated at variable water level. The large  $Mo$  values indicate a strong deviation from the ideal mixing conditions. Contrarily, for Configuration C, increasing the exchange volume in each cycle diminishes  $Mo$  to values that approach 1, that is, it promotes plug flow conditions in the tank instead of mixing.

When water volume variation within one cycle is high (80%), all storage tank configurations present similar turnover times suggesting a small effect of the tank configuration on water renewal (Figure 7.13). However, when volume variation within one cycle is low (20%), which is frequent in daily operation of storage tanks of water supply systems, the turnover time is significantly different for the three tanks configurations. For the smaller volume variations (20 to 50%), Configuration C promotes faster water replacement compared to the other two configurations and Configuration A presents the highest turnover times. That is the typical tank Configuration A, which has the potential to achieve good mixing levels, has also to potential to have the longest water retention times, due to the low mixing levels, if inadequately operate.

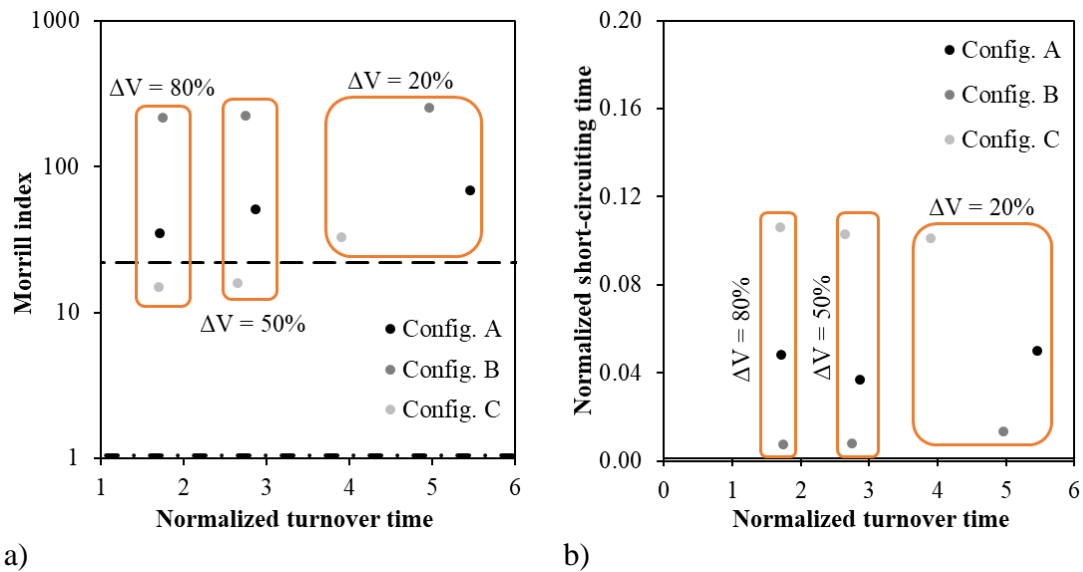


Figure 7.13 – Hydraulic indexes for the three configurations in variable water level operation: a) Morrill index vs normalized turnover time; b) normalized short-circuiting time vs normalized turnover time. The dashed line corresponds to the Morrill index value for a CSTR, and the dotted line corresponds to a PFR.

## 7.5 Discussion

Based on the three most common tank configurations in Portugal (Configuration A, B and C), structural and operational measures and their influence on the conditions of mixing and renewal of water are analysed. In structural terms, the reduction in the diameter of the inlet pipe, the inclusion of baffles and the use of diffusers to guide the flow are tested. The main hydraulic indexes calculated based on RTD functions, which are used to assess the short-circuiting and the water mixing in these water storage tanks, are summarised in Table 7.1, Table 7.2 and Table 7.3.

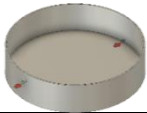
The recommendations presented herein will be analysed according to two aspects: mixing and turnover time. As identified in previous chapters, there are tanks that may have better mixing conditions than others, but that have much higher times to renew the stored water. In the literature, there is a tendency to give a lot of importance to mixing and hardly any studies are carried on water renewal. Depending on the disinfection conditions of the water, this may, or not, be a relevant issue.

The comparison of different improvement measures for tank Configuration A, considering the operation close to steady-state condition (i.e., with the tank almost full), is presented in Table 7.1. The effect of each measure is classified using a colour-scale for a better understanding of the results.

Decreasing the inlet pipe diameter in Configuration A is a simple way to increase the mixing efficiency inside the tank, regardless of the flow rate in which the tank is operated (see close to 22 values of Morrill index results in Table 7.1). Likewise, the diffusers A2 and A3 are good options to increase the mixing conditions. However, since the turnover time is also important, it should be noted that reducing the diameter will increase the renewal time by 11% to 19%, while the diffuser A2 increases it by 6%. The short-circuiting effect seems to increase by any of the analysed measures, since the inlet flow jet tends to reach faster (given the higher velocities due to the inlet diameter reduction) or to be located closer (nozzles) to the outlet pipe; thus, both reducing the diameter and using diffusers increase the short-circuiting effect.

Overall, considering a balance between the three hydraulic indexes, the diffuser A3 demonstrates to be the best compromise solution, since both indexes  $Mo$  and  $\theta_{95}$  have improved –  $Mo = 22$  is similar to ideal mixing conditions and the renewal time has a 2% reduction – despite the increase of the short-circuiting effect that is quite similar in all measures analysed.

Table 7.1 – Structural improvement measures tested for Configuration A and the corresponding hydraulic indexes.



	Inlet pipe (mm)	Flow rate (-)	Morrill index $Mo$ (-)		Short-circuiting index $\theta_{10}$ (-)			Turnover time $\theta_{95}$ (-)		
			$Mo$ (-)		$\theta_{10}$ (-)	Variation		$\theta_{95}$ (-)	Variation	
<b>Configuration A</b> (Initial conditions)	4	Q1	12		0.19			3.10		
	4	Q2	11		0.21			3.07		
	4	Q3	18		0.18			3.18		
	4	Q4	15		0.16			3.10		
<b>Inlet diameter reduction</b>	2	Q1	23	●	0.11	- 45 %	●	3.45	+ 11 %	●
	2	Q2	21	●	0.13	- 39 %	●	3.65	+ 19 %	●
	2	Q3	23	●	0.11	- 39 %	●	3.67	+ 15 %	●
<b>Diffusers</b>	A1	6 × 1	18	●	0.13	- 30 %	●	3.18	0 %	●
	A2	4 × 1	20	●	0.12	- 36 %	●	3.36	+ 6 %	●
	A3	6 × 1	22	●	0.10	- 44 %	●	3.10	- 2 %	●


Note: ● positive effect; ● identical effect; ● negative effect

The comparison of different improvement measures for tank Configuration B is presented in Table 7.2. In Configuration B, a simple solution to increase water mixing efficiency is to reduce the diameter of the inlet pipe or to use diffusers, like those analysed herein. The construction of baffles with 50% or 75% of the tank diameter will only enhance the plug flow effect and move away from the ideal mixing conditions of a CSTR. In terms of

turnover time, any of the solutions demonstrates improvements ranging from 12% to 42%.

Overall, considering the balance between the hydraulic indexes, the reduction of the diameter of the inlet pipe and the installation of diffusers are the best compromise solutions to improve water mixing and reduce renewal times.

Table 7.2 – Structural improvement measures tested for Configuration B and the corresponding hydraulic indexes.

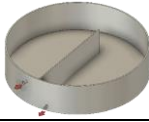


	Inlet pipe (mm)	Flow rate (-)	Morrill index $Mo$ (-)	Short-circuiting index			Turnover time		
				$\theta_{10}$ (-)	Variation		$\theta_{95}$ (-)	Variation	
<b>Configuration B</b> (Initial conditions)	4	Q1	27	0.10			4.29		
	4	Q2	36	0.08			4.72		
	4	Q3	46	0.06			4.78		
	4	Q4	70	0.04			4.13		
<b>Inlet diameter reduction</b>	2	Q1	24 ●	0.11	+ 10 % ●		3.12	- 27 % ●	
	2	Q2	19 ●	0.13	+ 63 % ●		3.15	- 33 % ●	
	2	Q3	18 ●	0.13	+ 117 % ●		3.13	- 34 % ●	
<b>Diffusers</b>	B1	5 × 1	Q3	15 ●	0.17	+ 183 % ●		3.27	- 32 % ●
	B2	7 × 1	Q3	19 ●	0.14	+ 133 % ●		3.32	- 31 % ●
	B3	3 × 1	Q3	26 ●	0.10	+ 67 % ●		3.12	- 35 % ●
<b>Baffle 50%</b>	4	Q1	16 ●	0.16	+ 60 % ●		3.79	- 12 % ●	
	4	Q2	14 ●	0.18	+ 125 % ●		3.42	- 28 % ●	
	4	Q3	11 ●	0.21	+ 250 % ●		3.35	- 30 % ●	
	4	Q4	9 ●	0.26	+ 550 % ●		2.87	- 31 % ●	
<b>Baffle 75%</b> (Configuration C)	4	Q1	8 ●	0.30	+ 200 % ●		2.87	- 33 % ●	
	4	Q2	8 ●	0.27	+ 238 % ●		2.72	- 42 % ●	
	4	Q3	7 ●	0.32	+ 433 % ●		2.76	- 42 % ●	
	4	Q4	7 ●	0.27	+ 575 % ●		2.56	- 38 % ●	

Note: ● positive effect; ● identical effect; ● negative effect

The comparison of different measures for Configuration C is presented in Table 7.3. The mixing conditions in tanks with a baffle with 75% of the tank diameter show improvements when the inlet diameter is reduced (from 4 to 2 mm) and, also, when the baffle size is reduced to 50%. However, these structural measures will increase by 12% to 61% the time required for water renewal. Thus, these two measures should be avoided in tanks with Configuration C.

Table 7.3 – Structural improvement measures tested for Configuration C and the corresponding hydraulic indexes.



	Inlet pipe (mm)	Flow rate (-)	Morrill index $M_o$ (-)	Short-circuiting index			Turnover time		
				$\theta_{10}$ (-)	Variation		$\theta_{95}$ (-)	Variation	
<b>Configuration C</b> (initial conditions)	4	Q1	8	0.30			2.87		
	4	Q2	8	0.27			2.72		
	4	Q3	7	0.32			2.76		
	4	Q4	7	0.27			2.56		
<b>Inlet diameter reduction</b>	2	Q1	27	●	0.10	- 67 % ●	3.53	+ 23 % ●	●
	2	Q2	14	●	0.19	- 30 % ●	4.08	+ 50 % ●	●
	2	Q3	12	●	0.29	- 8 % ●	4.44	+ 61 % ●	●
<b>Baffle 50%</b>	4	Q1	16	●	0.16	- 47 % ●	3.79	+ 32 % ●	●
	4	Q2	14	●	0.18	- 35 % ●	3.42	+ 26 % ●	●
	4	Q3	11	●	0.21	- 33 % ●	3.35	+ 21 % ●	●
	4	Q4	9	●	0.26	- 6 % ●	2.87	+ 12 % ●	●

Note: ● positive effect; ● identical effect; ● negative effect

The comparison of different fill-and-draw cycles for the three tank configurations (A, B, C) is presented in Table 7.4. Each fill-and-draw cycle is characterized by a volume variation of 20%, 50% and 80% of the total water volume. The comparison is made with the smallest volume variation (20%).

The mixing conditions in the three tanks show improvements when the volume variation is higher, especially in Configuration A and C. The short-circuiting effect is increased in Configuration B due to the proximity of the inlet and outlet pipes. Regarding the water renewal time, there is a significant improvement for the three configurations with improvements between 18% and 62%.

For the three configurations, higher inflow rates (Q3 and Q4) and higher water volume variations in each cycle can result in good mixing levels in such tanks. Thus, from the operational point of view, larger variations in water level are better for improving water mixing and renewal than smaller and more frequent water level variations Table 7.4.

Table 7.4 – Operational measures tested and the corresponding hydraulic indexes.

Configuration	Volume variation (%)	Morrill index $Mo$ (-)	Short-circuiting index			Turnover time	
			$t_{10}$ (min)	Variation		$t_{95}$ (min)	Variation
A	20 %	69	5.6			610	
	50 %	51 ●	5.0	- 11 % ●		386	- 37 % ●
	80 %	35 ●	6.5	+ 16 % ●		230	- 62 % ●
B	20 %	254	1.5			555	
	50 %	223 ●	1.1	- 27 % ●		370	- 33 % ●
	80 %	215 ●	1.0	- 33 % ●		235	- 58 % ●
C	20 %	33	11.3			436	
	50 %	16 ●	13.9	+ 23 % ●		357	- 18 % ●
	80 %	15 ●	14.3	+ 27 % ●		229	- 47% ●

Note: ● positive effect; ● identical effect; ● negative effect

## 7.6 Conclusions

Different water mixing and renewal improvement measures are analysed in a small-scale storage tank model, that is three structural solutions (i.e., the reduction of the inlet pipe diameter, the use of submerged diffusers, the use of baffles) and one operation measure (i.e., operating the tank with fill-and-draw cycles). The effectiveness of each measure is assessed and compared with reference situations by means of three hydraulic indexes (Morrill index, short-circuiting index and turnover time) calculated based on RTD results for the three circular-cross section tank configurations (A, B and C).

When operating the tanks with quasi-constant water level, the most effective improvement solutions are the following:

- i) the diffuser A3 with nozzles jet parallel to the tank bottom (Figure 7.5a), for tanks with inlet and outlet pipes located at opposite side walls (Configuration A), since this solution improves the water mixing in lower velocity regions (near the tank bottom), leading to a water mixing in the whole tank close to ideal reactor conditions ( $Mo = 22$ ) and reducing slightly (2%) the renewal time.
- ii) the inlet pipe diameter reduction, the installation of diffusers or the use of baffles in tanks with the inlet and the outlet pipes located at the same side wall (Configuration B), since the first two solutions deliver the jet further away from the outlet and the third one promotes a plug-flow, thus, improving water mixing and renewal and minimizing the short-circuiting effect.

- iii) the use of smaller size baffles (i.e., 50% of the diameter, instead of 75%) and inlet pipe diameter reduction is more efficient for improving mixing conditions in tanks with baffles (Configuration C), however it makes it necessary to have more time to renew the stored water.

When operating tanks with fill-and-draw cycles, the larger the water volume variation is, the better the mixing conditions and the shorter the renewal time become. Thus, operating tanks with fill-and-draw cycles is preferable to operating the tanks with quasi-constant water level or with minor but frequent variations of the water level, which is the current practice of many water utilities to increase the global reliability of the distribution system in case of supply disruption upstream the storage tank.





# Chapter 8

---

## **Modelling chlorine decay in water storage tanks**

## 8.1 Introduction

The current chapter presents a study on the chlorine residual decay modelling in circular cross-section tanks. The residence time distributions obtained experimentally for circular cross-section tanks (Chapter 4) are used to develop analytical models that describe the water mixing in storage tanks. Two circular cross-section tanks models are developed: Configuration A and C (Figure 4.2a,c). Several tank mixing models are tested by fitting the calculated cumulative distribution curve to the results obtained experimentally being the quality of the adjustment assessed by the root-mean-square error. The two configurations are modelled for steady-state conditions with a fixed water level and for the flow rate of  $9.44 \text{ L h}^{-1}$ . The experimental tests used to collect data consisted of a step injection of NaCl at the tank inlet pipe and the measurement of this tracer concentration at the outlet pipe (see 4.2.2). The chlorine decay modelling inside the tanks is carried out by combining the calibrated tank models with the disinfectant decay first order reaction. This chlorine model can be incorporated in hydraulic simulators of water distribution networks to better describe the disinfectant decay along the system.

The novel contributions of this chapter are: i) the development of water mixing models for two circular cross-section tanks; ii) the calibration of these models by using experimental data; and iii) the combination of these models with the disinfectant first order reaction to describe the chlorine decay inside the tank.

## 8.2 Residence time distribution models

The development of a tank flow model based on experimental RTD data consisting of finding the mathematical function, or combination of predefined functions, that better describes collected data. The flow model attempts to quantitatively describe the hydrodynamics characteristics of the transport material (the fluid). The model helps to understand the transport process and to predict it for other operating conditions. The flow model consists of the arrangement in series or in parallel of basic flow elements with known mathematic functions.

The applied methodology herein is the following: (i) to obtain a set of elementary reactors describing the basic phenomena of fluid flow; (ii) to use typical rules for combining these elementary models; (iii) to apply an optimization method to fit the model parameters to experimental data and to assess the fitting quality by the root-mean-square-error (RMSE).

In general terms, a real reactor can be modelled by the composition of different regions interconnected in different ways. These regions can be represented by plug flow reactors (PFR), continuous stirred tank reactors (CSTR), CSTR battery, dead volumes, poorly mixed volumes, among other elements, and the interconnections can represent situations of bypass, recirculation and cross flow (Lemos et al. 2014).

After the construction of the model, it has to be calibrated by fitting the respective  $E(t)$  to the experimental data. This consists of calculating the values of the parameters for which the best agreement between the experimental and the model is attained. This adjustment can also be done through the cumulative distribution function,  $F(t)$ .

### 8.3 Experimental data

The cumulative distribution and the residence time distribution are determined for the small-scale tanks. Since the step input tracer injection technique implies differentiation of the data to obtain the  $E(t)$ , which can lead to large errors, it is only presented the  $F(t)$  results and the following analyses will be based on this distribution.

The cumulative distribution function,  $F(t)$ , for the two configurations (A and C) of the circular-cross section tanks are presented in Figure 8.1. Significant differences in the two  $F(t)$  are observed, indicating that the tank configuration strongly affects the respective cumulative distributions and, consequently, should be described by a different mixing model.

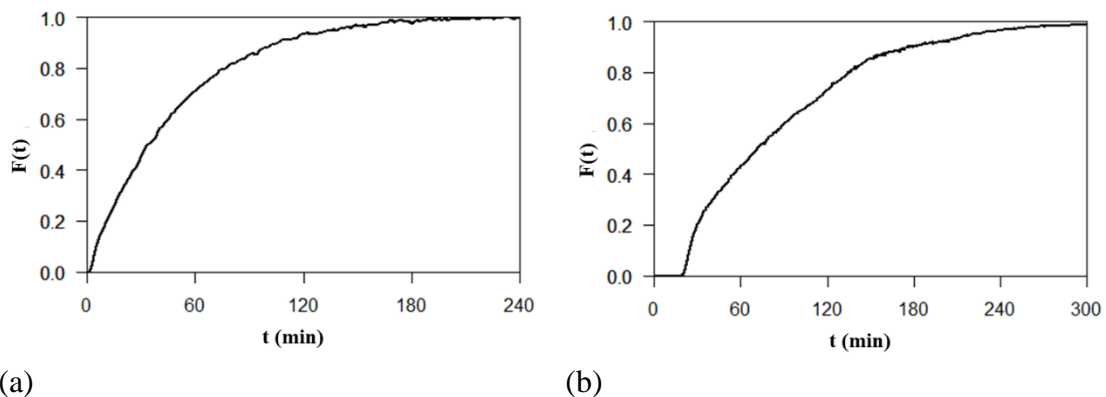


Figure 8.1 – Cumulative distribution functions,  $F(t)$  for the two storage tank configurations: a) Configuration A; b) Configuration C.

The mean residence times,  $\theta$ , obtained experimentally for configuration A and C are 47.3 and 48.8 min, respectively (see 4.2.3.2). These values are slightly higher than those

expected based on the ideal reactor volume and the flow rate which corresponds to 46.0 min. Higher mean residence times may be the indication of a bypass in the tank. Thus, further analyses are necessary to find the best combination of elementary models that describes the flow behaviour in each tank configuration.

#### 8.4 Model development

The model development consists of two stages: model construction and model parameters' calibration. The model construction requires a preliminary analysis of the cumulative distribution function experimentally obtained. Some assumptions are generally considered in the model development:

- The sum of all elementary reactors volumes equals the total volume of the small-scale tank.
- The flow rate between elementary reactors corresponds to a fraction of the experimental flow rate.

Calibration process involves comparing model predictions with experimental measurements and then adjusting model parameters to improve the fit between predicted and observed data. This can be carried out by a trial-and-error procedure or by using an optimization algorithm. The root-mean-square error (RMSE) is generally used to compare the model results with the experimental data, that is to assess the quality of the fitting. RMSE statistics provides information about the short-term performance of a model by allowing a term-by-term comparison of the actual difference between the estimated and the measured value.

In a first approach, the experimental cumulative distribution curves for configurations A and C are compared to the results calculated for an ideal continuous stirred-tank reactor (CSTR), as presented in Figure 8.2. Further details on the mathematical model that describes the CSTR model are presented in Appendix C. The tank with the inlet and the outlet pipes located at opposite-side walls (Configuration A) presents a mixing behaviour that is quite similar to that of a completely mixed tank (CSTR) with small deviations along the curve. This occurs even though there has no active mixing devices and the water mixing relies only on the inlet jet momentum. For this elementary model (i.e., the CSTR model), where the volume and flow rate correspond to the experimental values, the RMSE is 0.012797.

The baffled tank (Configuration C) presents a major deviation from the completely mixed conditions (CSTR model). The delayed and sharp increase of  $F(t)$  at initial times denotes a close to plug flow regime in the tank. In fact, the baffle prevents the inflowing jet to mix with the water that is on the other side of the baffle, promoting the formation of two compartments inside the tank that hardly mix with each other.

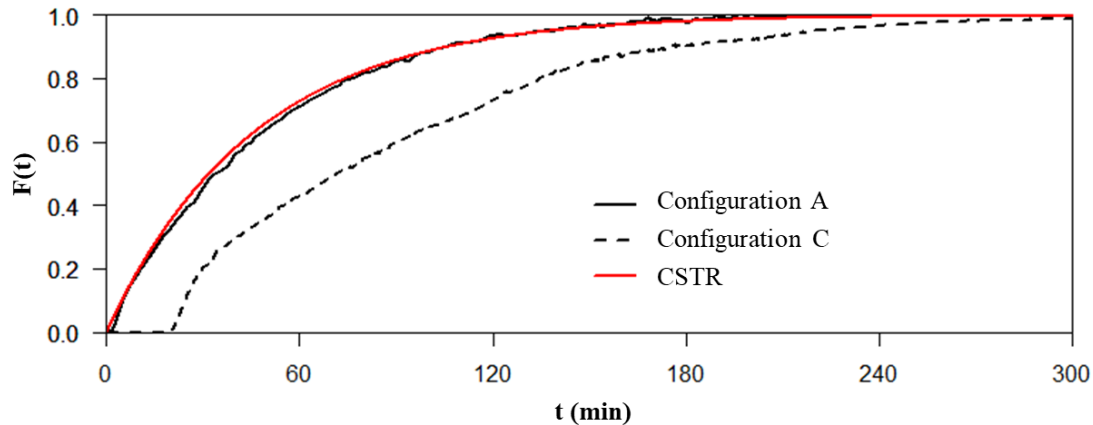


Figure 8.2 – Cumulative distribution functions,  $F(t)$ . Comparison between the ideal CSTR model and experimental data for Configurations A and C.

The comparison between the cumulative distribution of an ideal CSTR and configuration A shows that there may be a slight plug flow phenomenon at the beginning and some influence of poorly mixing zones in the tank that explain the deviations over time.

The model developed for Configuration A (Model 1) consists of a combination of a PFR in series with two CSTR with portions of poorly mixed volumes (Figure 8.3). The mathematical equations of  $F(t)$  and  $E(t)$  obtained for this model are described in Appendix C.

The numerical and the experimental cumulative distribution curves,  $F(t)$ , are presented in Figure 8.4. The developed model (Figure 8.3) has six parameters ( $V_1$ ,  $V_a$ ,  $V_2$ ,  $V_b$ ,  $Q_1'$  and  $Q_2'$ ), that have been calibrated by an optimization algorithm. The calibrated values minimize the squared deviations between the  $F(t)$  values of the model and the respective experimental points are presented in Table 8.1. While RMSE for the initial model CSTR is 0.012797, the RMSE for this new model is 0.006720, showing an excellent data fitting.

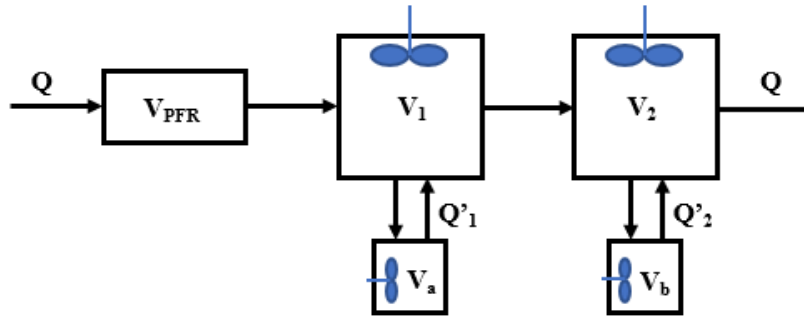


Figure 8.3 – Schematic representation of the Model 1 developed for Configuration A.

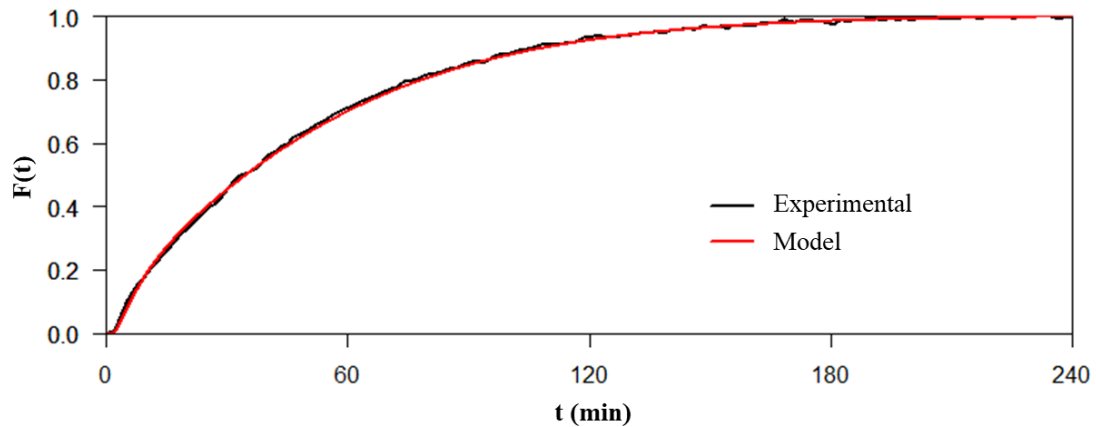


Figure 8.4 – Cumulative distribution functions,  $F(t)$ . Comparison between experimental data and results of Model 1 developed for Configuration A.

Table 8.1 – Calibrated parameters for Model 1 developed for Configuration A.

Reactor	Volume [L] (% total)	Flow rate [L h <sup>-1</sup> ] (% total)
<i>PFR</i>	$V_{PFR} = 0.217$ (3.0)	$Q = 9.44$ (100.0)
<i>First CSTR</i>	$V_1 = 2.382$ (32.9) $V_a = 2.289$ (31.6)	$Q'_1 = 9.31$ (99.0)
<i>Second CSTR</i>	$V_2 = 0.412$ (5.7) $V_b = 1.942$ (26.8)	$Q'_2 = 7.05$ (75.0)

The same model is applied to Configuration B, though it did not allow obtaining a good curve fit. A second model (Model 2) is developed for Configuration C. This model includes two branches in parallel and each branch has a battery of reactors in series (Figure 8.5). The mathematical equations of  $F(t)$  and  $E(t)$  for this model are described in Appendix C.

The numerical and the experimental cumulative distribution curves,  $F(t)$ , are presented in Figure 8.6. This model contains 11 parameters ( $V_1, V_a, V_2, V_b, V_3, V_m, V_4, Q_1, Q_1', Q_2'$  and

$\alpha$ ), whose calibrated values are presented in Table 8.2. While RMSE for the model CSTR is 0.012797, the RMSE for this model is 0.008394, demonstrating a good data fit.

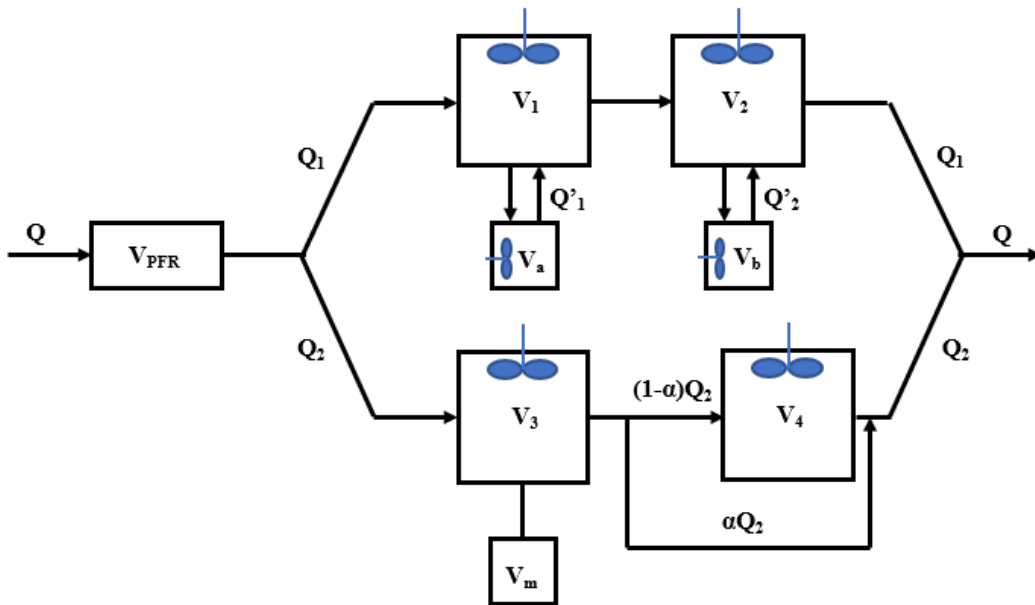


Figure 8.5 – Schematic representation of the Model 2 developed for Configuration C.

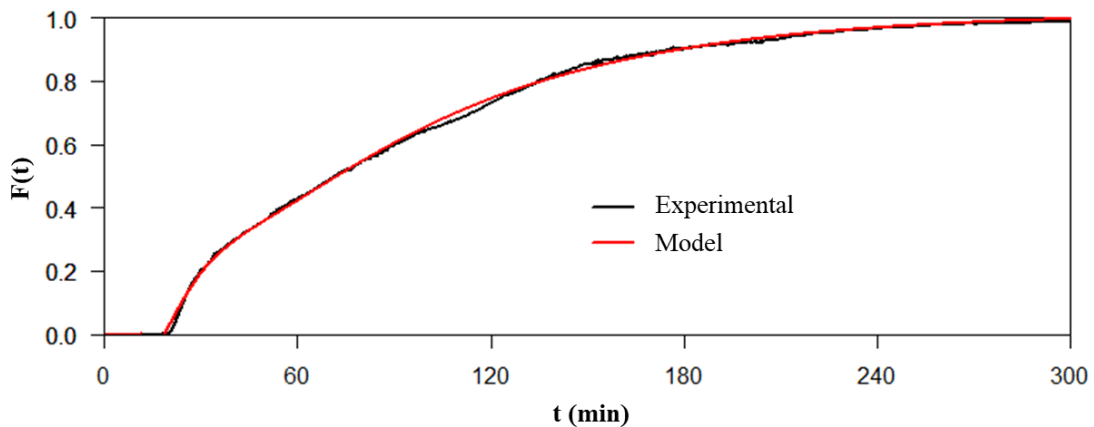


Figure 8.6 – Cumulative distribution functions,  $F(t)$ . Comparison between experimental data and results calculated by Model 2 developed for Configuration C.

Table 8.2 – Calibrated parameters for the Model 2 developed for Configuration C.

Reactor	Volume [L] (% total)	Flow rate [L h <sup>-1</sup> ] (% total)
<i>PFR</i>	$V_{PFR} = 1.741$ (24.0)	$Q = 9.44$ (100.0)
<i>First CSTR</i>	$V_1 = 1.404$ (19.4)	$Q_1 = 0.497Q = 4.69$
	$V_a = 1.272$ (17.6)	$Q'_1 = 0.344Q_1 = 1.61$
<i>Second CSTR</i>	$V_2 = 1.559$ (21.4)	$Q_1 = 0.497Q = 4.69$
	$V_b \approx 0$ (0.1)	$Q'_2 = 7.05$ (75.0)

<i>Third CSTR</i>	$V_3 = 0.558$ (7.7) $V_m = 0.341$ (4.7)	$Q_2 = 4.75$
<i>Fourth CSTR</i>	$V_4 = 0.365$ (5.0)	$(1 - \alpha)Q_2 = 2.61$ $\alpha Q_2 = 2.14$ (bypass) where $\alpha = 0.45$

### 8.5 Chlorine decay in storage tanks

Assuming that chlorine decay is governed by a first order reaction, the conversion obtained in the reactor is independent of the degree of micromixing. The prediction of the chlorine decay behaviour inside the tank can then be carried out by the technique that assumes total segregation at the microscopic level, without loss of precision. Assuming that the chlorine feed is started at time  $t = 0$ , with a concentration of  $1 \text{ mg L}^{-1}$ , the evolution of the chlorine concentration at the outlet can be obtained by calculating the integral of the product of the two functions – the first order kinetics,  $C^*(t)$ , and the residence time distribution resulting from the model,  $E(t)$  – as described Eq. 2.8. Chlorine concentration at the tank outlet can be determined using the residence time distribution by numerically integrating the function  $C^*(t).E(t)$ .

Considering the referred bulk decay rate coefficient, the disinfectant concentration at the outflow for the two configurations (A and C) are presented in Figure 8.7. The evolution of  $C_a(t)$  for Configuration A shows a less pronounced increasing trend than that obtained for Configuration C, though starts earlier. On the other hand, the disinfectant concentration calculated for Configuration C takes longer to reach the tank outlet, but the evolution is more accelerated at the beginning. The chlorine consumption in configurations A and C are 7.9% and 5.9%, respectively.



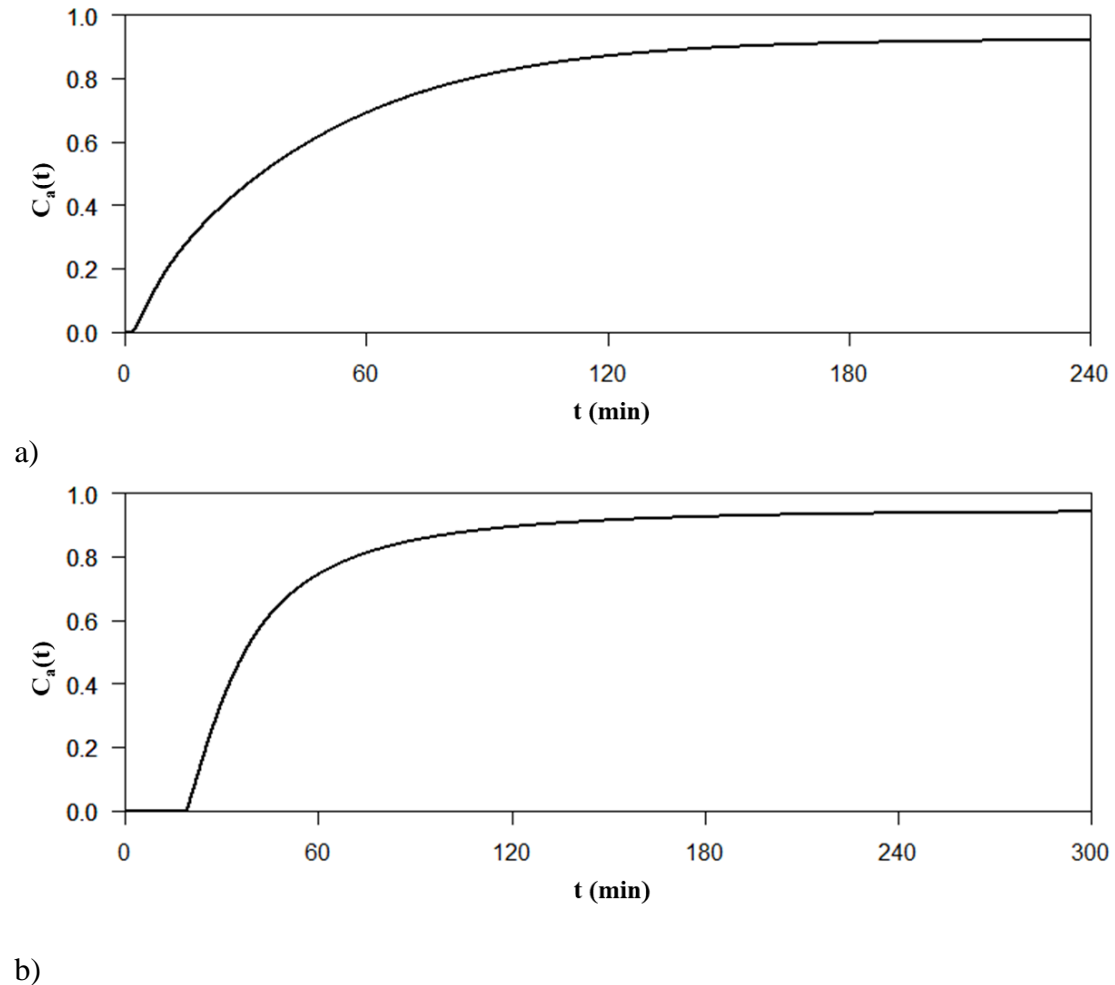


Figure 8.7 – Predicting the behaviour of the model obtained for the total segregation method: a) Configuration A; b) Configuration C.

## 8.6 Conclusions

Water mixing mathematical models are developed for two circular cross-section small-scale tanks operated at steady-state conditions, based on the experimental cumulative distribution curves.

Ideal reactors are used to develop these models to best describe the observed tank behaviour. Configuration A model consists of three elementary-models with six calibration parameters, while the configuration B model is composed of five elements with eleven parameters.

The calculated values of cumulative distribution curves are compared with the experimental data, being obtained RMSE of 0.006720 and 0.008394 for Configuration A and C models, respectively.

The knowledge of the residence time distribution for these two tanks is used to simulate the chlorine decay inside these tanks. Considering a first order reaction and the principle of total segregation, the conversions of disinfectant to other forms of disinfectant by-products for configuration A and C are 5.9% and 7.9%, respectively.

Water storage tanks tend to be large infrastructures that, depending on their operation, can hold large volumes of water for several days. Poor water mixing and the existence of stagnation zones with long residence times make storage tanks potential sites for deterioration of water quality and increase the risk of drinking water contamination. Modelling chlorine decay in water storage tanks is an important tool to develop a strategy capable of disinfecting a water supply system and, at the same time, preserving water quality until the point of use, without using more disinfectant than necessary.

# Chapter 9

---

## **Conclusions and further research**

## 9.1 Research overview

This research aims to apply and to contribute to the knowledge on the flow dynamics in water storage tanks to find structural and operational measures to improve water mixing and to reduce water retention time. For this purpose, experimental research was developed combining physical modelling with the use of recent technology to support the gathering of information. The research problem, and the main novel contributions to be achieved in this research are identified in Chapter 1. A state-of-the-art review in the context of water mixing in water storage tanks, including the identification of knowledge gaps, is presented in Chapter 2. The characterization of water storage tanks in Portugal, focusing on the main physical characteristics and operational conditions that mostly affect their performance regarding water mixing and renewal is carried out in Chapter 3. An extensive experimental analysis to assess the water mixing and renewal conditions in small-scale circular cross-section tanks is carried out for three tank configurations and several operating conditions – constant/variable water level and different flow rates (Chapter 4). A similar analysis is carried out for rectangular cross-section tanks in Chapter 5. A methodology for developing tracer tests in full-scale tanks is developed and applied to real-life tank (Chapter 5). The application of the particle image velocimetry technique to obtain measurements of instantaneous 2D velocities fields to assess flow dynamics inside circular cross-section storage tanks is carried out in Chapter 6. The analysis of the effects of different types of water mixing and renewal improvement measures (structural and operational) in circular cross-section tanks is developed (Chapter 7). The chlorine residual decay modelling is described and applied for circular cross-section tanks using experimental data for model calibration (Chapter 8). The research overview and the main scientific contributions of each study are summarized in this section. Finally, recommendations for future research addressing questions that remain unsolved are suggested.

## 9.2 Main scientific findings

In Portugal, the existing water storage tanks present several configurations and dimensions. Rectangular and quadrangular cross-sections are more frequent in tanks with larger volumes, and circular cross-section shapes are often used for smaller to medium tank volumes. Typically, tanks are operated close to full, being the level variation small in a fill-and-draw cycle, with  $H_{min}/H_{max}$  ratio between 60% and 70%. The estimated

mixing times for tanks in Portugal, predominantly varying between 1 to 2 h (27%). In more than 70% of the tanks, the volume of water entering the tank in each filling cycle suffices to mix completely the incoming water with that already stored. However, in many of these tanks, this mixing is only possible when the water level varies between the minimum and the maximum operational level in a single filling cycle. The survey also demonstrated that some water utilities are unaware of the structural and operational characteristics of their tanks. This emphasizes the need to create and to maintain up-to-date databases with records of the main tank characteristics.

Water mixing and renewal are key factors to assess water quality in storage tanks. The present work contributes to assess these conditions in circular and rectangular cross-section small-scale water storage tanks. Tracer experiments, with no buoyancy effects, carried out in tanks operated at steady-state and under variable water level conditions show that the tank configuration has an important influence on water mixing and renewal. The main conclusions achieved are summarised in the following paragraphs.

For circular cross-section tanks:

- The configuration with inlet and outlet pipes close to each other promotes the increased short-circuiting effects and promotes the formation of water pockets with very high residence time. Although widely used, this configuration is not recommended in the design of new tanks.
- The use of internal baffles allows to direct and to control the flow through the storage tank and decreases the spread of water residence times, although it does not promote water mixing. The baffles lead to a close to plug-flow inside the tank.
- When the tanks are operated at variable water levels, wide variations in water level are preferred over frequent, but small, variations in water level of the storage tanks.
- The water mixing in these tanks is far from fully mixed condition, as assumed in hydraulic and water quality models.

For rectangular cross-section tanks:

- When operated with a relatively constant water level, higher flow rates increase the water renewal in tanks without baffles, however, the opposite effect is observed in tanks with baffles (corridor effect).

- When operating at variable water levels, the higher the water volume variation in each fill-and-draw cycle is, the faster the renewal of stored water becomes, with slightly better results in tanks without baffles, despite worse mixing conditions being observed. For high-volume variations (50% to 80%), the renewal times are very similar in tanks with or without baffles; for a 20% volume variation, the baffled tank promotes a faster water renewal.
- The baffles prevent mixing between older (stored) and newer (inflow) water and promotes the creation of localized stagnant pockets and poor mixing zones. Optimum baffles configuration can be difficult to define, as different operating conditions can have different effects in terms of mixing and renewal conditions.

The velocity fields measured for three horizontal planes show that there is a significant variation in velocities throughout the water depth for all three circular cross-section configurations tested. Additionally, the flow patterns observed using the PIV are identical to those observed through the recorded images of the movement of dye tracer solution. The three configurations of circular cross-section tanks tested revealed very different flow patterns with lower velocity regions more pronounced near the bottom of the tank and higher velocities near the water surface. The laboratory experiments showed that:

- In Configuration A, two symmetrical vortices, in which the water moves onwards along the tank walls and returns backwards in the central zone, are developed.
- In Configuration B, given the proximity of the inlet and outlet pipes, the short-circuiting phenomenon is very pronounced with poor mixing in most of the tank, since part of the incoming fluid is directed to the outlet without mixing with the stored water. Moreover, lower velocities are observed in the central zone of the tank, with higher expression near the tank bottom.
- In Configuration C, the baffle reduces the short-circuiting phenomenon (observed in Configuration B) and promotes de recirculation and water mixing in the first half of the tank, delaying the fresh water from reaching the outlet pipe.
- Reynold's shear stresses and time-averaged longitudinal and lateral turbulent intensities show the existence of larger intensities differences across the tank, with regions further away from the inlet with negligible turbulent intensity.

The assessment of the effect of different types of measures (structural and operational) to improve the water mixing and renewal in circular cross-section tanks were investigated.

Three structural improvement measures are analysed, namely: the inlet pipe diameter reduction; the use of multiple nozzles; and the use of baffles with different lengths. The operational measure – the water volume variation inside the tank – is further discussed.

When operating the tanks with quasi-constant water level, the most effective improvement solutions are the following:

- In Configuration A, the tank with inlet and outlet pipes located at opposite side walls, the diffuser A3 with nozzles parallel to the tank bottom promotes the water mixing in lower velocity regions (near the tank bottom), leading to a water mixing close to ideal reactor conditions and reducing slightly the renewal time.
- In Configuration B, the tank with the inlet and outlet pipes located at the same wall, the inlet pipe diameter reduction, the installation of diffusers or the use of baffles shows that the first two solutions deliver the jet further away from the outlet and the third one promotes a plug-flow, thus, promoting water mixing and renewal and minimizing the short-circuiting effect.
- The use of smaller-size baffles (i.e., 50% of the diameter, instead of 75%) is more efficient for improving mixing conditions in tanks in close inlet/outlet pipes (Configuration C).

When operating tanks with fill-and-draw cycles the larger the water volume variation is, the better the mixing conditions and the shorter the renewal time become. Thus, operating tanks with fill-and-draw cycles is preferable to operating the tanks with quasi-constant water level or with minor but frequent variations of the water level, which is the current practice of many water utilities to increase the global reliability of the distribution system in case of supply disruption upstream the storage tank.

Water mixing mathematical models are developed for two circular cross-section small-scale tanks operated at steady-state conditions, based on the experimental cumulative distribution curves. The knowledge of the residence time distribution for these two tanks can be used to simulate the chlorine decay inside these tanks.

### **9.3 Recommendations for future work**

The scope of the present research work is vast and can be particularly useful to support water utilities in the design and operation of new and existing water storage tanks.

Although a considerable amount of research has been carried out, the questions are still numerous and the practical applications, sought by water utilities, are not fully answered yet. Some recommendations for future work are suggested and explained in the following paragraphs.

The first recommendation is to extend the proposed water mixing and renewal assessment approach to other water storage tank configurations (e.g., inlet and outlet pipe location; different inlet nozzles configuration; other  $H/D$  ratio) and operating conditions (e.g., different demand profiles) not considered in this study. The location of the inlet pipe depending on its position, submerged or above the waterline, significantly influences the flow dynamics within the tank. In Portugal, water storage tanks have a predominance of inlet pipes above the water level (80%) and, therefore, the present study had a greater focus on these cases. The tested circular cross-section tanks had a water-depth-to-tank-diameter ratio of 0.15 which is a main characteristic for larger capacity tanks. The effect of these higher ratios in tanks with similar characteristics existing tanks in Portugal (i.e., the same inlet and outlet pipe configurations as tested in this research) on the water mixing and renewal conditions should be further explored.

The second recommendation is to extend the experimental methodology to assess the influence of temperature differences between the inflow and the stored water considering variable water level and the typical configurations tested. Water stratification promotes zones where the water stagnates or moves slower, leading to an increase in the residence time of the stored water and changing the flow dynamics inside the tank. This condition should be further investigated.

The third recommendation is to extend the methodology for assessing mixing conditions based on temperature and conductivity measurements in full-scale tanks to other water storage tanks with different configurations and operational conditions. The assessment of the tank performance should also be explored contributing to more informed decision-making.

The fourth recommendation is to improve the PIV experiments results by collecting particles displacement data to determine velocity fields in vertical planes. These plans obtained in well-defined areas would allow to understand the flow path along the water



column, especially near the water inlet, and in the central zone, where for whatever the configuration the water velocity is lower.

The last recommendation is to develop numerical models of the flow dynamics and compare with the experimental results obtained. The most suitable intervention alternatives for these tanks, with a view to improving mixing conditions, should be studied in the future, for example, through the use of advanced computational fluid dynamics models.



---

## References

- Adrian, R. J. (2005). "Twenty years of particle image velocimetry." *Experiments in Fluids*, 39(2), 159–169.
- Angeloudis, A., Stoesser, T., and Falconer, R. A. (2014). "Predicting the disinfection efficiency range in chlorine contact tanks through a CFD-based approach." *Water Research*, Elsevier, 60, 118–129.
- AWWA. (2002). "Finished Water Storage Facilities." *Epa*, 24.
- AWWA. (2006). *Formation and decay of disinfection by-products in the distribution system*. Denver, USA.
- Blokker, E. J. M., Vreeburg, J. H. G., Buchberger, S. G., and van Dijk, J. C. (2008). "Importance of demand modelling in network water quality models: a review." *Drinking Water Engineering and Science Discussions*, 1(1), 1–20.
- Boulos, P. F., Grayman, W. M., Bowcock, R. W., Clapp, J. W., Rossman, L. A., Clark, R. M., Deininger, R. A., and Dhingra, A. K. (1996). "Hydraulic mixing and free chlorine residual in reservoirs." *American Water Works Association*, 88(7), 48–59.
- Brito, M., Sanches, P., Ferreira, R. M. L., Asce, A. M., and Covas, D. I. C. (2016). "Experimental Study of the Transient Flow in a Coiled Pipe Using PIV." *Journal of Hydraulic Engineering*, 143(3).
- Chambers, K., Creasey, J., and Forbes, L. (2004). "Design and Operation of Distribution Centres." *Safe Piped Water: Managing Microbial Water Quality in Piped Distribution Systems*, World Health Organization, ed., IWA Publishing.
- Chambers, K. et al. (2004). *Design and Operation of Distribution Networks, In Safe Piped Water: Managing Microbial Water Quality in Piped Distribution Systems by Richard Ainsworth (ed.)*. *Safe Piped Water: Managing Microbial Water Quality in Piped Distribution Systems*, (E. L. Ainsworth, R., ed.), IWA Publishing.
- Clark, R. M., Abdesaken, F., Boulos, P. F., and Mau, R. E. (1996). "Mixing in distribution system storage tanks: Its effects on water quality." *Journal of Environmental Engineering*, 122(9), 814–821.
- Codina, R., Principe, J., Muñoz, C., and Baiges, J. (2015). "Numerical modeling of chlorine concentration in water storage tanks." *International Journal for Numerical Methods in Fluids*, 79, 84–107.
- Crowther, J. M., and Dandy, G. C. (2012). "Model comparisons for tracer experiments at a clear water storage tank." *Australasian Journal of Water Resources*, 15(2), 145–156.
- Danckwerts, P. V. (1953). "Continuous flow systems." *Chemical Engineering Science*, 2(1), 1–13.
- Deborde, M., and von Gunten, U. (2008). "Reactions of chlorine with inorganic and organic compounds during water treatment—Kinetics and mechanisms: A critical review." *Water Research*, 42(1–2), 13–51.
- Duer, M. (2011). "Passive Mixing Systems Improve Storage Tank Water Quality." *Opflow*, 37(8), 20–23.
- Duer, M. J. (2003). "The science of mixing and maintaining water quality in water storage tanks."

- ERSAR. (2018). *Recomendação ERSAR n.º 01/2018 INSPEÇÃO, LIMPEZA E HIGIENIZAÇÃO DE RESERVATÓRIOS DESTINADOS AO ARMAZENAMENTO DE ÁGUA PARA CONSUMO HUMANO.*
- Fard, M. A., and Barkdoll, B. D. (2018). “Stagnation Reduction in Drinking Water Storage Tanks through Internal Piping with Implications for Water Quality Improvement.” *Journal of Hydraulic Engineering*, 144(5), 05018004.
- Ferreira, R. M. L. (2011). “Turbulent flow hydrodynamics and sediment transport: Laboratory research with LDA and PIV.” *Experimental Methods in Hydraulic Research*, Springer, 67–111.
- Ferreira, R. M. L., Gymnopoulos, M., Prinos, P., Alves, E., and Ricardo, A. M. (2021). “Drag on a Square-Cylinder Array Placed in the Mixing Layer of a Compound Channel.” *Water*, 13(22), 3225.
- Fisher, I., Kastl, G., Sathasivan, A., and Jegatheesan, V. (2011). “Suitability of Chlorine Bulk Decay Models for Planning and Management of Water Distribution Systems.” *Critical Reviews in Environmental Science and Technology*, 41(20), 1843–1882.
- Fisher, I., Sathasivan, A., Chuo, P., and Kastl, G. (2009). “Effects of stratification on chloramine decay in distribution system service reservoirs.” *Journal of Water Research*, Elsevier Ltd, 43(5), 1403–1413.
- Fogler, H. S. (2016). *Elements of chemical reaction engineering. Bioprocess Engineering*, Prentice Hall, Philadelphia, PA.
- Graham, N. (2011). *Guidelines for Drinking-Water Quality, 4th Ed. WHO.*
- Grayman, W. M., Deininger, R. A., Green, A., Boulos, P. F., Bowcock, R. W., and Godwin, C. C. (1996). “Water quality and mixing models for tanks and reservoirs.” *American Water Works Association*, 88(7), 60–73.
- Grayman, W. M., Rossman, L. A., Arnold, C. N., Deininger, R. A., Smith, C. D., Smith, J. F., and Schniphe, R. (2000). “Water quality modeling of distribution storage facilities.” *American Water Works Association Research Foundation*, Denver, USA.
- Grayman, W. M., Rossman, L. A., Deininger, R. A., Smith, C. D., Arnold, C. N., and Smith, J. F. (2004). “Mixing and aging of water in distribution system storage facilities.” *American Water Works Association*, 96(9), 70–80.
- Ho, C. K., Christian, J. M., Ching, E. J., Slavin, J., Ortega, J., Murray, R., and Rossman, L. A. (2016). “Sediment resuspension and transport in water distribution storage tanks.” *Journal - American Water Works Association*, 108(6), E349–E361.
- Hua, P., Oliveira, K. R. F., Cheung, P., Gonçalves, F. V., and Zhang, J. (2018). “Influences of model structure and calibration data size on predicting chlorine residuals in water storage tanks.” *Science of the Total Environment*, Elsevier B.V., 634, 705–714.
- Jayanti, S. (2001). “Hydrodynamics of jet mixing in vessels.” *Chemical Engineering Science*, 56(1), 193–210.
- Kennedy, M. S., Moegling, S., Sarikelle, S., and Suravallo, K. (1993). “Assessing the effects of storage tank design on water quality.” *Journal American Water Works Association*, 85(7), 78–88.

- Kizilaslan, M. A., Demirel, E., and Aral, M. M. (2019). "Efficiency Enhancement of Chlorine Contact Tanks in Water Treatment Plants: A Full-Scale Application." *Processes*, 7(9), 551.
- Laín, S., and Aliod, R. (2000). "Deduction and validation of an Eulerian-Eulerian model for turbulent dilute two-phase flows by means of the phase indicator function - disperse elements probability density function." *Chinese Journal of Chemical Engineering*, 8, 189–202.
- Lavoie, P., Avallone, G., De Gregorio, F., Romano, G. P., and Antonia, R. A. (2007). "Spatial resolution of PIV for the measurement of turbulence." *Experiments in Fluids*, 43(1), 39–51.
- Lemke, A., and Deboer, D. E. (2013). *Effect of Storage Tank Mixing on Water Quality*. Water and Environmental Engineering Research Reports. 3.
- Lemos, F., Lopes, J. M., and Ribeiro, F. R. (2014). *Reactores Químicos*. IST Press.
- Liu, M. (2012). "Age distribution and the degree of mixing in continuous flow stirred tank reactors." *Chemical Engineering Science*, Elsevier, 69(1), 382–393.
- Mahmood, F., Pimblett, J. G., Grace, N. O., and Grayman, W. M. (2005a). "Evaluation of water mixing characteristics in distribution system storage tanks." *Journal American Water Works Association*, 97(3).
- Mahmood, F., Pimblett, J. G., Grace, N. O., and Grayman, W. M. (2005b). "Evaluation of water mixing characteristics in distribution system storage tanks." *Journal American Water Works Association*.
- Martel, K. D., Kirmeyer, G. J., Murphy, B. M., Noran, P. F., Kirby, L., Lund, T. W., Anderson, J. L., Medhurst, R., and Caprara, M. (2002). "Preventing water quality deterioration in finished water storage facilities." *Journal American Water Works Association*, 94(4), 139–148.
- Mau, R. E., Boulos, P. F., and Bowcock, R. W. (1996). "Modelling distribution storage water quality: An analytical approach." *Applied Mathematical Modelling*, 20(4), 329–338.
- Van Der Merwe, V., Duvenage, S., and Korsten, L. (2013). "Comparison of biofilm formation and water quality when water from different sources was stored in large commercial water storage tanks." *Journal of Water and Health*, 11(1), 30–40.
- Moncho-Esteve, I. J., Palau-Salvador, G., Brevis, W., Vaas, M. O., and López-Jiménez, P. A. (2015). "Numerical simulation of the hydrodynamics and turbulent mixing process in a drinking water storage tank." *Journal of Hydraulic Research*, 53(2), 207–217.
- Monteiro, L., Carneiro, J., and Covas, D. I. C. (2020). "Modelling chlorine wall decay in a full-scale water supply system." *Urban Water Journal*, 17(8), 754–762.
- Monteiro, L., Pinheiro, A., Carneiro, J., and Covas, D. (2021). "Characterization of drinking water storage tanks in Portugal." *Ingeniería del agua*, 25(1), 49–58.
- Monteiro, L. S. P. P., Viegas, R. M. C., Covas, D. I. C., and Menaia, J. A. G. F. (2017). "Assessment of Current Models Ability to Describe Chlorine Decay and Appraisal of Water Spectroscopic Data as Model Inputs." *Journal of Environmental*

- Engineering*, 143(1), 04016071.
- Monteiro, L., Viegas, R. M. C., Covas, D. I. C., and Menaia, J. (2015). "Modelling chlorine residual decay as influenced by temperature." *Water and Environment Journal*, 29(3), 331–337.
- Montoya-Pachongo, C., Laín-Beatove, S., Torres-Lozada, P., Cruz-Vélez, C. H., and Escobar-Rivera, J. C. (2016). "Effects of water inlet configuration in a service reservoir applying CFD modelling." *Ingenieria e Investigacion*, 36(1), 31–40.
- Nordblom, O. (2004). "Mixing and stagnation in drinking water storage tanks." *Doktorsavhandlingar vid Chalmers Tekniska Hogskola*, (2129), 49–57.
- Nordblom, O., and Bergdahl, L. (2004). "Initiation of Stagnation in Drinking Water Storage Tanks." *Journal of Hydraulic Engineering*, 130(1), 49–57.
- Okita, N., and Oyama, Y. (1963). "Mixing characteristics in jet mixing." *Chemical engineering*, 27(4), 252–260.
- Olson, C. T., and Deboer, D. E. (2008). *The effects of tank operation and design characteristics on water quality in distribution system storage tanks*. Regional Water System Research Consortium.
- Pasha, M. F. K., and Lansey, K. (2010). "Effect of parameter uncertainty on water quality predictions in distribution systems-case study." *Journal of Hydroinformatics*, 12(1), 1–21.
- Pinheiro, A., Monteiro, L., Carneiro, J., Céu Almeida, M., and Covas, D. (2021). "Water mixing and renewal in circular cross-section storage tanks as influenced by configuration and operational conditions." *Journal of Hydraulic Research*.
- Raffel, M., Willert, C. E., Wereley, S. T., and Kompenhans, J. (2007). *Particle Image Velocimetry. A Practical Guide*. Springer Berlin Heidelberg, Berlin, Heidelberg.
- Rauen, W. B., Angeloudis, A., and Falconer, R. A. (2012). "Appraisal of chlorine contact tank modelling practices." *Water Research*, 46(18), 5834–5847.
- Ricardo, A. M., Grigoriadis, D. G. E., and Ferreira, R. M. L. (2018). "Numerical simulations of turbulent flows within an infinite array of randomly placed cylinders." *Journal of Fluids and Structures*, 80, 245–261.
- Richardson, S. D., Plewa, M. J., Wagner, E. D., Schoeny, R., and DeMarini, D. M. (2007). "Occurrence, genotoxicity, and carcinogenicity of regulated and emerging disinfection by-products in drinking water: A review and roadmap for research." *Mutation Research - Reviews in Mutation Research*, Elsevier, 636(1–3), 178–242.
- Roberts, P. J. W., Tian, X., Sotiropoulos, F., and Duer, M. (2006). *Physical modeling of mixing in water storage tanks*. AWWA Research Foundation.
- Rossman, L. A. (2000). *Epanet 2 users manual*. (U.S. Environmental Protection Agency, ed.), U S Environmental Protection Agency.
- Rossman, L. A., Clark, R. M., and Grayman, W. M. (1994). "Modeling Chlorine Residuals in Drinking-Water Distribution Systems." *Journal of Environmental Engineering*, 120(4), 803–820.
- Rossman, L. A., and Grayman, W. M. (1999). "Scale-model studies of mixing in drinking

- water storage tanks.” *Journal of Environmental Engineering*, (125), 755–761.
- Shang, F., Uber, J. G., and Rossman, L. A. (2008). “Modeling Reaction and Transport of Multiple Species in Water Distribution Systems.” *Environmental Science & Technology*, 42(3), 808–814.
- Sheng, J., Meng, H., and Fox, R. O. (1998). “Validation of CFD simulations of a stirred tank using particle image velocimetry data.” *The Canadian Journal of Chemical Engineering*, 76(3), 611–625.
- Simard, A., Pelletier, G., and Rodriguez, M. (2011). “Water residence time in a distribution system and its impact on disinfectant residuals and trihalomethanes.” *Journal of Water Supply: Research and Technology-Aqua*, 60(6), 375–390.
- Singer, P. C. (2006). “DBPs in drinking water: Additional scientific and policy considerations for public health protection.” *Journal - American Water Works Association*, 98(10), 73–80.
- Taylor, Z. H., Carlston, J. S., and Venayagamoorthy, S. K. (2015). “Hydraulic design of baffles in disinfection contact tanks.” *Journal of Hydraulic Research*, Taylor & Francis, 53(3), 400–407.
- Teixeira, E. C., and Siqueira, R. do N. (2008). “Performance assessment of hydraulic efficiency indexes.” *Journal of Environmental Engineering*, 134(10), 851–859.
- Tian, X., and Roberts, P. J. (2008). “Mixing in Water Storage Tanks. I: No Buoyancy Effects.” *Journal of Environmental Engineering*, 134(12), 974–985.
- USEPA. (2002). *Finished Water Storage Facilities*. United States Environmental Protection Agency, Washington DC.
- Van der Walt, J. J. (2002). “The modelling of water treatment process tanks.” Rand Afrikaans University.
- Wilson, J. M., and Venayagamoorthy, S. K. (2010). “Evaluation of hydraulic efficiency of disinfection systems based on residence time distribution curves.” *Environmental Science and Technology*, 44(24), 9377–9382.
- Xavier, M. L. M., and Janzen, J. G. (2017). “Effects of inlet momentum and orientation on the hydraulic performance of water storage tanks.” *Applied Water Science*, 7(5), 2545–2557.
- Zhang, J.-M., Khoo, B. C., Lee, H. P., and Teo, C. P. (2013a). “Numerical simulation and assessment of the effects of operation and baffling on a potable water service reservoir.” *Journal of Environmental Engineering*, 139(3), 341–348.
- Zhang, J.-M., Khoo, B. C., Lee, H. P., Teo, C. P., Haja, N., and Peng, K. Q. (2012). “Effects of Baffle Configurations on the Performance of a Potable Water Service Reservoir.” *Journal of Environmental Engineering*, 138(5), 578–587.
- Zhang, J.-M., Khoo, B. C., Teo, C. P., Haja, N., Tham, T. K., Zhong, L., and Lee, H. P. (2013b). “Passive and active methods for enhancing water quality of service reservoir.” *Journal of Hydraulic Engineering*, 139(7), 745–753.
- Zhang, J., C. Pierre, K., and E. Tejada-Martínez, A. (2019). “Impacts of Flow and Tracer Release Unsteadiness on Tracer Analysis of Water and Wastewater Treatment Facilities.” *Journal of Hydraulic Engineering*, American Society of Civil Engineers,



145(4), 4019004.

Zhang, J. M., Khoo, B. C., Teo, C. P., Haja, N., Tham, T. K., Zhong, L., and Lee, H. P. (2013c). "Passive and Active Methods for Enhancing Water Quality of Service Reservoir." *Journal of Hydraulic Engineering*, 139(7), 745–753.

Zhang, J. M., Lee, H. P., Khoo, B. C., Peng, K. Q., Zhong, L., Kang, C.-W., and Ba, T. (2014). "Shape effect on mixing and age distributions in service reservoirs." *Journal - American Water Works Association*, 106(11), E481–E491.



---

# Appendix A



Figure A.1 – Experimental facility designed for developing tracer tests in small-scale storage tanks and determining the water residence time distribution. Tracer tests facility pictures: a) deionized water system; b) tracer solution and deionized auxiliary tanks; c) tracer solution and deionized feeder tanks (above) and small-scale tank (below); d) control valves; e) small-scale tank; (f,g) conductivity probe, hydropneumatic vessel and peristaltic pumps; h) conductivity datalogger; i) controlling software.

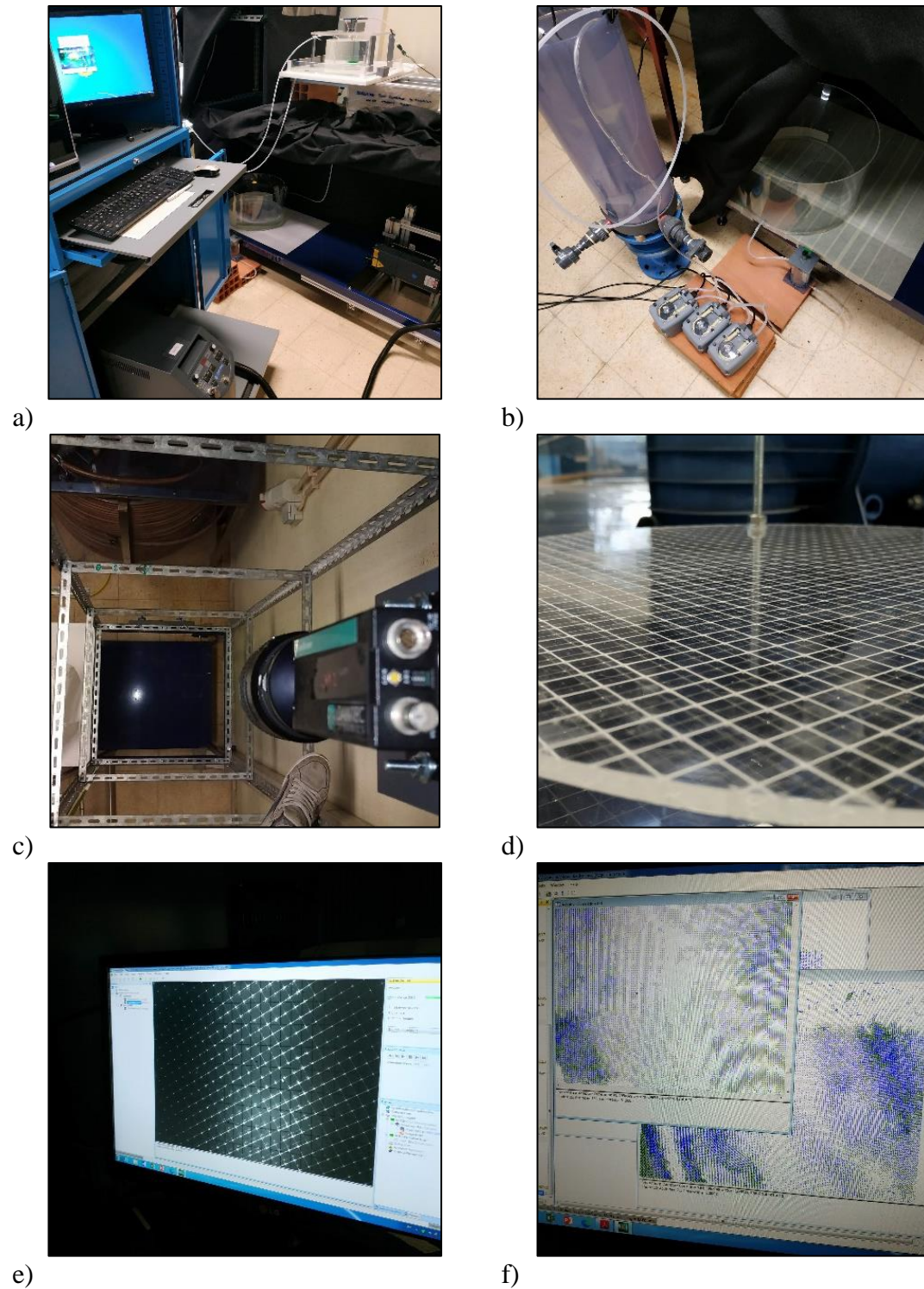


Figure A.2 – Experimental facility designed for developing the particle image velocimetry technique in small-scale storage tanks: a) facility overview; b) part of the outflow system that includes the hydropneumatic vessel, pumps and auxiliary tank; c) digital camera; d) circular acrylic sheet with quadrangular grid; e) laser and camera calibration process; f) velocity fields.



---

## **Appendix B**

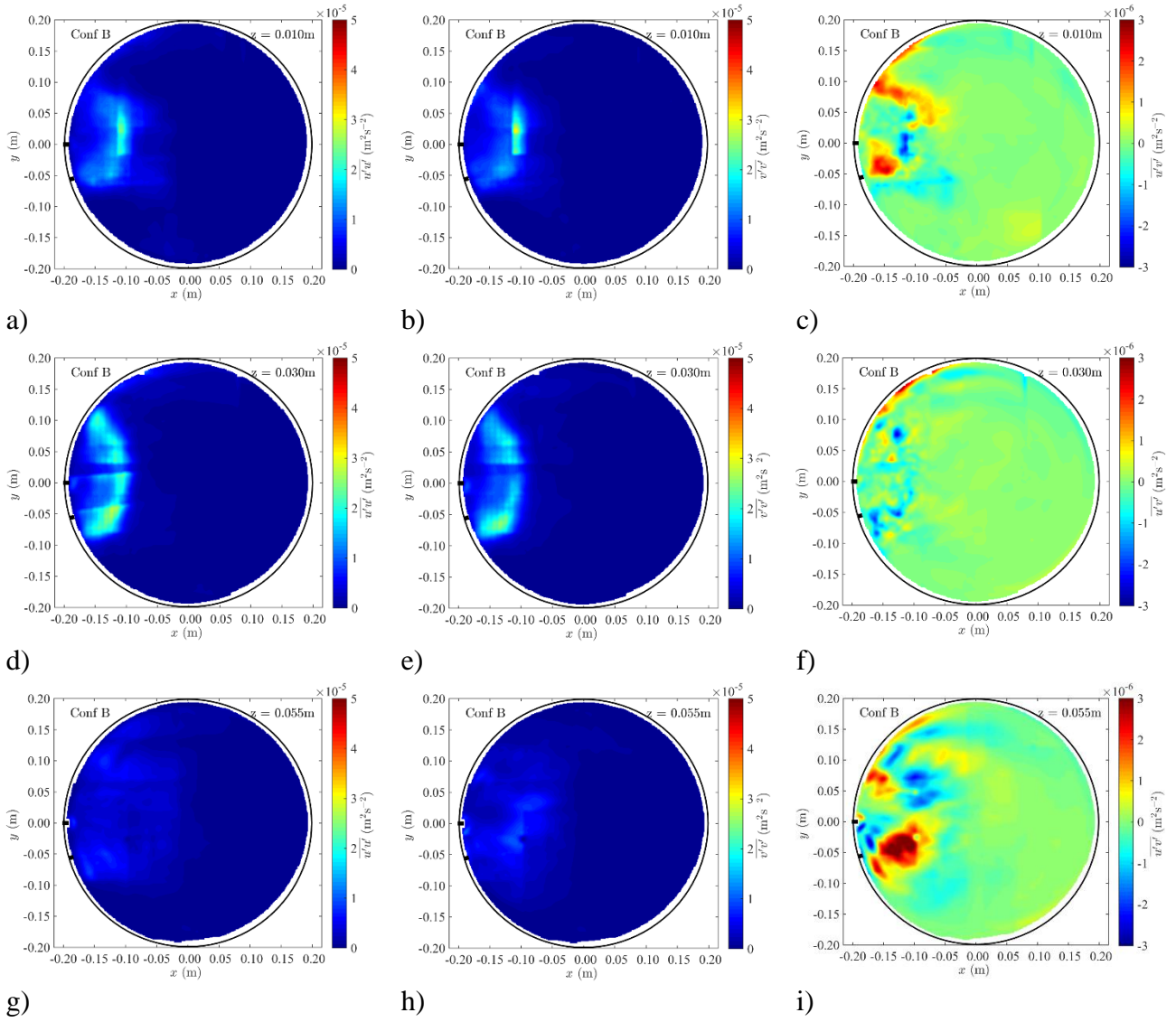


Figure B.1 – The turbulent intensity maps  $\overline{u'u'}$  and  $\overline{v'v'}$  and the turbulent shear stress map  $\overline{u'v'}$  for Configurations B.



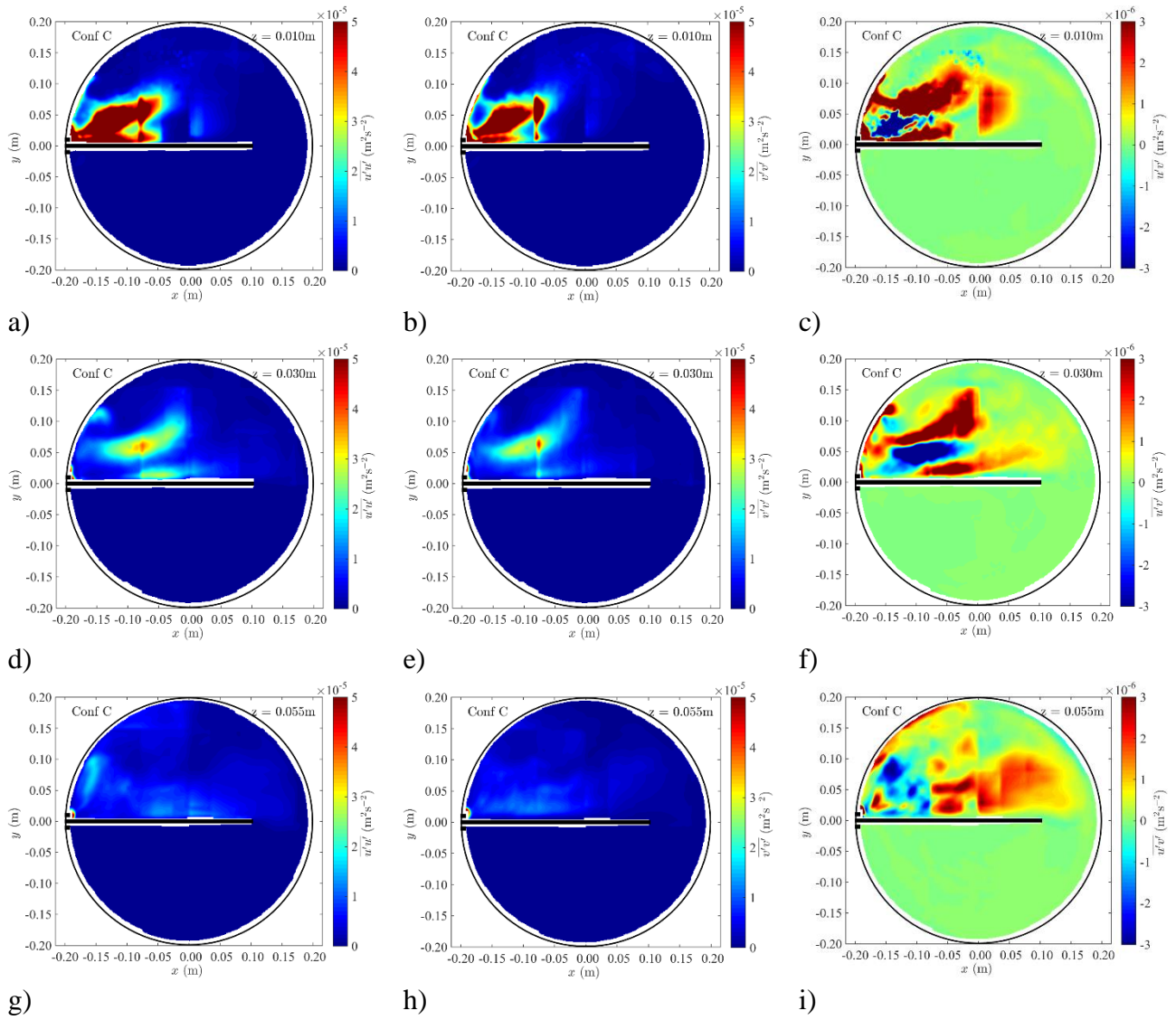


Figure B.2 – The turbulent intensity maps  $\overline{u'u'}$  and  $\overline{v'v'}$  and the turbulent shear stress map  $\overline{u'v'}$  for Configurations C.



---

## **Appendix C**

### Residence Time Distribution (RTD) for ideal and non-ideal reactors

This appendix presents the equations used to obtain the cumulative distribution and residence time distribution functions, respectively  $F(t)$  and  $E(t)$ .

#### *CSTR model (ideal reactor)*

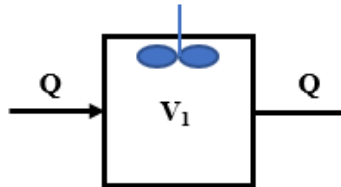


Figure C.1 – CSTR scheme.

Considering the step injection method, the mass balance for a CSTR corresponds to:

$$V \frac{dC_1}{dt} = QC_e - QC_1 \quad \text{Eq. C.1}$$

where  $C_1$  is the outlet concentration,  $C_e$  is the inlet concentration,  $Q$  is the flow rate and  $V$  is the reactor volume and the initial conditions are:

$$t = 0, C_1 = 0, C_e = \text{constant}$$

The resulting  $F(t)$  and  $E(t)$  functions are given by Eq. 4.6 and Eq. 4.7.

#### *CSTR with poorly mixed volume*

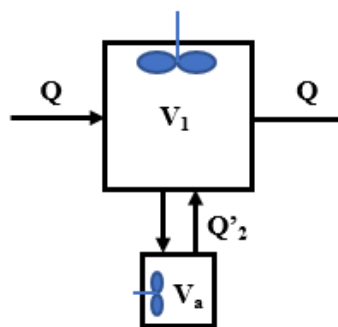


Figure C.2 – CSTR with poorly mixed volume scheme.

Considering the step injection method, the mass balances for a CSTR with a poorly mixed volume is given by:

$$V_1 \frac{dC_1}{dt} = QC_e + Q'C_a - QC_1 - Q'C_1 \quad \text{Eq. C.2}$$

$$V_a \frac{dC_a}{dt} = Q'C_1 - Q'C_a \quad \text{Eq. C.3}$$

where  $C_1$  is the concentration in the well-mixed volume,  $C_a$  is the concentration in the volume poorly mixed and  $Q'$  is the exchange flow rate between these two volumes.

This set of ordinary differential equations can be solved by order elevation and elimination. Thus, they can be converted into the following linear and non-homogeneous 2<sup>nd</sup> order differential equation:

$$\frac{d^2C_1}{dt^2} + \frac{dC_1}{dt} \left( \frac{Q'}{V_a} + \frac{Q}{V_1} + \frac{Q'}{V_1} \right) + \frac{Q'Q}{V_1V_a} C_1 = \frac{Q'Q}{V_1V_a} C_e \quad \text{Eq. C.4}$$

With the following initial conditions:

$$t = 0, C_1 = C_2 = 0, C_e = \text{constant}$$

The  $F(t)$  and  $E(t)$  functions are given by:

$$F(t) = \frac{Ae^{tx_1} + Be^{tx_2}}{C_e} + 1 \quad \text{Eq. C.5}$$

$$E(t) = \frac{A}{C_e} x_1 e^{tx_1} + \frac{B}{C_e} x_2 e^{tx_2} \quad \text{Eq. C.6}$$

where

$$A = \frac{C_e \left( x_2 + \frac{Q}{V_1} \right)}{(x_1 - x_2)} \quad \text{Eq. C.7}$$

$$B = \frac{C_e \left( x_2 + \frac{Q}{V_1} \right)}{(x_1 - x_2)} - 1 \quad \text{Eq. C.8}$$

$$x_1 = \frac{1}{2} \left( - \sqrt{\frac{(Q'V_1 + Q'V_a + QV_a)^2}{V_1^2 V_a^2} - \frac{4Q'Q}{V_1 V_a} - \frac{Q'}{V_1} - \frac{Q'}{V_a} - \frac{Q}{V_1}} \right) \quad \text{Eq. C.9}$$

$$x_2 = \frac{1}{2} \left( \sqrt{\frac{(Q'V_1 + Q'V_a + QV_a)^2}{V_1^2 V_a^2} - \frac{4Q'Q}{V_1 V_a} - \frac{Q'}{V_1} - \frac{Q'}{V_a} - \frac{Q}{V_1}} \right) \quad \text{Eq. C.10}$$

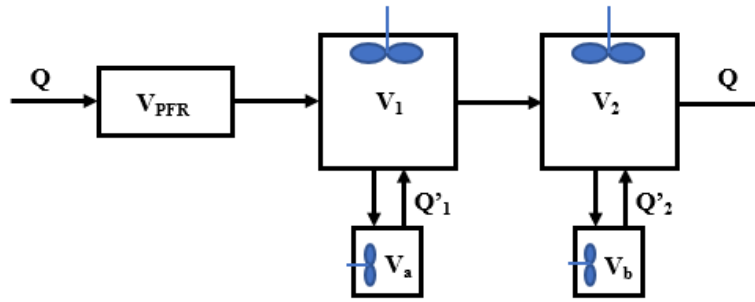
**Model 1 – Configuration A**

Figure C.3 – Model 1 scheme.

The  $E(t)$  for this model can be achieved using the methodology for obtaining associations of reactors in series (Lemos et al. 2014) or from the numerical resolution of mass balances for each reactor. The  $F(t)$  and  $E(t)$  for the first reactor was determined above (Eq. C.5 and Eq. C.6). Considering the step injection method, the mass balances for the second reactor with poorly mixed volume is given by:

$$V_2 \frac{dC_2}{dt} = QC_1 + Q'_2 C_b - QC_2 - Q'_2 C_2 \quad \text{Eq. C.11}$$

$$V_b \frac{dC_b}{dt} = Q'_2 C_2 - Q'_2 C_b \quad \text{Eq. C.12}$$

where  $C_2$  is the concentration in the volume well-mixed in the second reactor,  $C_b$  is the concentration in the volume poorly mixed and  $Q'_2$  is the exchange flow rate between these two volumes.

This set of ordinary differential equations can be solved by order elevation and elimination. Thus, they can be converted into the following linear and non-homogeneous 2<sup>nd</sup> order differential equation:

$$\begin{aligned} \frac{d^2 C_2}{dt^2} + \frac{dC_2}{dt} \left( \frac{Q'_2}{V_1} + \frac{Q}{V_2} + \frac{Q'_2}{V_2} \right) + \frac{Q'_2 Q}{V_2 V_b} C_2 \\ = \frac{Q}{V_2} (Ax_1 e^{tx_1} + Bx_2 e^{tx_2}) \\ + \frac{Q'_2 Q}{V_2 V_b} (Ae^{tx_1} + Be^{tx_2} + C_e) \end{aligned} \quad \text{Eq. C.13}$$

The combination of each residence time distribution function for this two CSTR with poorly mixed volumes is given by:

$$\begin{aligned}
 E(t) = \frac{1}{\theta_1 \theta_2} & \left( \frac{e^{(-A_1 - B_1)t}}{(-A_1 - B_1 + A_2 + B_2)} - \frac{e^{(-A_2 - B_2)t}}{(-A_1 - B_1 + A_2 + B_2)} \right. \\
 & + \left( \frac{Q + Q'_2}{2V_2 B_2} - \frac{A_2 + B_2}{2B_2} \right) \alpha \\
 & + \left( \frac{Q + Q'_1}{2V_1 B_1} - \frac{A_1 + B_1}{2B_1} \right) \beta \\
 & \left. + \left( \frac{Q + Q'_1}{2V_1 B_1} - \frac{A_1 + B_1}{2B_1} \right) \left( \frac{Q + Q'_2}{2V_2 B_2} - \frac{A_2 + B_2}{2B_2} \right) \gamma \right)
 \end{aligned}
 \tag{Eq. C.14}$$

where,

$$A_1 = \left( \frac{Q + Q'_1}{V_1} + \frac{Q'_1}{V_a} \right) / 2
 \tag{Eq. C.15}$$

$$B_1 = \sqrt{\left( \frac{Q + Q'_1}{V_1} + \frac{Q'_1}{V_a} \right)^2 - \frac{4QQ'_1}{V_1 V_a}} / 2
 \tag{Eq. C.16}$$

$$\theta_1 = \frac{V_1}{Q}
 \tag{Eq. C.17}$$

$$A_2 = \left( \frac{Q + Q'_2}{V_2} + \frac{Q'_2}{V_b} \right) / 2
 \tag{Eq. C.18}$$

$$B_2 = \sqrt{\left( \frac{Q + Q'_2}{V_2} + \frac{Q'_2}{V_b} \right)^2 - \frac{4QQ'_2}{V_2 V_b}} / 2
 \tag{Eq. C.19}$$

$$\theta_2 = \frac{V_2}{Q}
 \tag{Eq. C.20}$$

$$\begin{aligned}
 \alpha = & \frac{e^{(-A_1 - B_1)t}}{(-A_1 - B_1 + A_2 + B_2)} - \frac{e^{(-A_2 - B_2)t}}{(-A_1 - B_1 + A_2 + B_2)} \\
 & - \frac{e^{(-A_1 - B_1)t}}{(-A_1 - B_1 + A_2 - B_2)} \\
 & + \frac{e^{(-A_2 - B_2)t}}{(-A_1 - B_1 + A_2 - B_2)}
 \end{aligned}
 \tag{Eq. C.21}$$

$$\begin{aligned}
 \beta = & \frac{e^{(-A_1 - B_1)t}}{(-A_1 - B_1 + A_2 + B_2)} - \frac{e^{(-A_2 - B_2)t}}{(-A_1 - B_1 + A_2 + B_2)} \\
 & - \frac{e^{(-A_1 - B_1)t}}{(-A_1 + B_1 + A_2 + B_2)} \\
 & + \frac{e^{(-A_2 - B_2)t}}{(-A_1 + B_1 + A_2 + B_2)}
 \end{aligned}
 \tag{Eq. C.22}$$

$$\begin{aligned}
 Y = & \frac{e^{(-A_1-B_1)t}}{(-A_1 - B_1 + A_2 + B_2)} - \frac{e^{(-A_2-B_2)t}}{(-A_1 - B_1 + A_2 + B_2)} \\
 & - \frac{e^{(-A_1-B_1)t}}{(-A_1 - B_1 + A_2 - B_2)} \\
 & + \frac{e^{(-A_2+B_2)t}}{(-A_1 - B_1 + A_2 - B_2)} \\
 & - \frac{e^{(-A_1-B_1)t}}{(-A_1 + B_1 + A_2 + B_2)} \\
 & + \frac{e^{(-A_2-B_2)t}}{(-A_1 + B_1 + A_2 + B_2)} \\
 & + \frac{e^{(-A_1+B_1)t}}{(-A_1 + B_1 + A_2 - B_2)} \\
 & - \frac{e^{(-A_2+B_2)t}}{(-A_1 + B_1 + A_2 - B_2)} \\
 & - \frac{e^{(-A_1+B_1)t}}{(-A_1 + B_1 + A_2 - B_2)}
 \end{aligned}
 \tag{Eq. C.23}$$

Considering a PFR in series with these two reactors, the  $E(t)$  expression for this model will be the expression of the  $E(t)$  previously calculated with a delay equal to the PFR mean residence time ( $\theta_{PFR}$ ) and valid only for times greater than this delay.

$$E(t) = \begin{cases} \text{Eq. C. 14} & \text{para } t > \theta_{PFR} \\ 0 & \text{para } t < \theta_{PFR} \end{cases}
 \tag{Eq. C.24}$$

where  $\theta_{PFR}$  is given by the ratio between the PFR volume,  $V_{PFR}$ , and the flow rate,  $Q$ .

The cumulative distribution is obtained integrating  $E(t)$  between time  $t = 0$  and time,  $t$ .

**Model 2 – Configuration C**

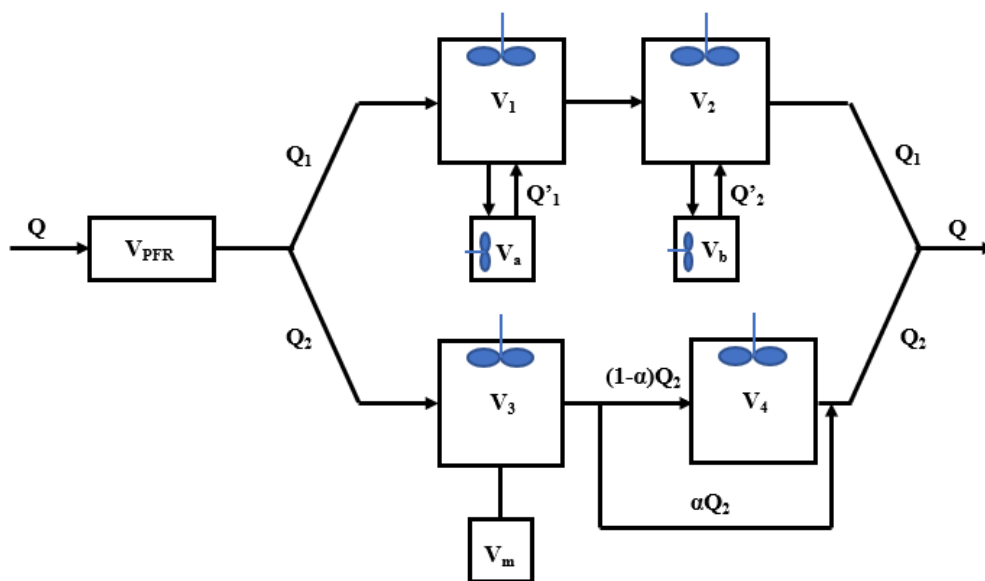


Figure C.4 – Model 2 scheme.



This model consists of a battery of reactors in parallel and in series. The battery first branch (top) was previously obtained. The second branch includes a reactor with a dead volume in series with a reactor which presents a bypass. The  $E(t)$  for this branch is given by:

$$E(t) = \alpha \frac{1}{\theta_3} e^{-\frac{t}{\theta_3}} + \frac{1 - \alpha}{\theta_4 - \theta_3} \left( e^{-\frac{t}{\theta_4}} - e^{-\frac{t}{\theta_3}} \right) \quad \text{Eq. C.25}$$

where  $V_m$  is the dead volume,  $\alpha$  is the fraction of bypass, and

$$\theta_3 = \frac{V_3}{Q_2} \quad \text{Eq. C.26}$$

$$\theta_4 = \frac{V_4}{Q_2} \quad \text{Eq. C.27}$$

Applying the methodology for association of reactors in parallel (Lemos et al. 2014), the resulting RTD will be given by:

$$E(t) = \frac{Q_1}{Q} E_1(t) + \frac{Q_2}{Q} E_2(t) \quad \text{Eq. C.28}$$

Where  $E_1(t)$  corresponds to Eq. C.14 and  $E_2(t)$  corresponds to Eq. C.25. In similarity to the previous model, where is used a PFR before the battery, the  $E(t)$  will be given by:

$$E(t) = \begin{cases} \text{Eq. C. 25} & \text{para } t > \theta_{PFR} \\ 0 & \text{para } t < \theta_{PFR} \end{cases} \quad \text{Eq. C.29}$$

The cumulative distribution is obtained integrating  $E(t)$  between time  $t = 0$  and time,  $t$ .